A Nonlinear Dynamical Model of Borehole Spiraling

A DISSERTATION
SUBMITTED TO THE FACULTY OF THE GRADUATE SCHOOL
OF THE UNIVERSITY OF MINNESOTA
BY

Julien Marck

IN PARTIAL FULFILLMENT OF THE REQUIREMENTS
FOR THE DEGREE OF
Doctor of Philosophy

ADVISER
Emmanuel Detournay

December, 2015

Acknowledgements

A successful experience in graduate school relies in great part on finding the right adviser. I could not have asked for more. Emmanuel has always been supportive and available. He has steered my work and progress into the right direction, while giving me the freedom to manage them on a daily basis. (If this dissertation is acceptably readable, it is mainly due to his incessant effort to improve my writing skills.) The bond that has been created between us goes far beyond the normal advisor-advisee relationship; it extends out of the academic sphere and hopefully will resist time.

My first years (and winters) in Minneapolis were particularly enjoyable thanks to my two Belgian mates, Alexandre Huynen and Luc Perneder, as well as Catalina Pena (and her amazing desserts). I am also thankful to other graduate students of the department for their friendship: Jeff, Paolo, Roman, Ganesh, Panos, Kaixiao, Eduardo, and many others, who made working underground more bearable. I do not forget all my friends from Perth, especially Masood, Behnaz, Amir, Antoine, Luis and Luiz.

The last fours years would not have been the same without Karsta Sunne and her family. Not only did they accept me among them in spite of my terrible French accent, they also introduced me to the Minnesotan way of life. Karsta has always been particularly supportive and caring and patiently put up with my atypical work schedule.

Finally, a final thought goes to my family back in Belgium, especially to my parents, who despite the distance have always been encouraging. They visited me twice here in Minneapolis and joined me as soon as they could on many trips in Europe and around the world; home never seemed really far away.

I can never satisfy myself until I can make a mechanical model of a thing.

If I can make a mechanical model, I can understand it.

As long as I cannot make a mechanical model all the way through I cannot understand.

Baron William Thomson Kelvin

Abstract

With the emergence of new measurement devices, the non-smooth nature of the borehole geometry has been comprehended more accurately. In many happenstances, the borehole has been seen taking the shape of a corkscrew or helix. Referred to as micro-tortuosity, or more commonly spiraling, this drilling dysfunction correlates with lower-than-expected rates of penetration, increased shocks and vibrations, damage to components and tools, and smaller drift diameters.

In this dissertation, the relevant mechanism and parameters leading to borehole spiraling are identified and studied. Spiraling is predicted by conducting a stability analysis of the linearized delay differential equations governing the borehole propagation. These evolution equations, expressed in terms of the borehole inclination and azimuth, are obtained from considerations involving: (a) a bit/rock interaction law that relates the force and moment acting on the bit to its penetration into the rock; (b) kinematic relationships that describe the local borehole geometry in relation to the bit penetration; and (c) a beam model for the bottom-hole assembly (BHA) that expresses the force and moment at the bit as functions of the external loads applied on the BHA and the geometrical constraints arising from the stabilizers conforming to the borehole geometry.

The analytical nature of the propagation equations makes it possible to conduct a systematic stability analysis in terms of a key dimensionless group that controls the directional stability of the drilling system. This group depends on the downhole weight on bit (WOB), on properties of the BHA, on the bit bluntness, and on parameters characterizing the steering response of the bit. The directional stability of a particular system then is assessed by comparing the magnitude of this group to a critical value representing a Hopf bifurcation of stability, which depends only on the BHA configuration and the bit walk. If this group is less than the critical value, the system is referred to as being directionally unstable and borehole spiraling is likely. Stability curves for an idealized BHA with two stabilizers show that the bit walk tends to make drilling systems more prone to spiraling. The influence of the design of push-the-bit rotary steerable

systems (RSS) on the onset of spiraling is also discussed, as well as the ability of the stabilizers to tilt freely or not.

For directionally unstable systems, the resulting limit cycle, corresponding to the spiral, has been captured by the introduction of the relevant nonlinearity: a saturation of the bit tilt. This nonlinearity enables to characterize further the influence of the directional stability on the borehole geometry and illustrates how the amplitude of the spiral also depends on the borehole inclination and the RSS force.

Applications to field cases are discussed and model predictions are tested against actual spiraled-hole data. Simulations conducted by integrating the equations of borehole propagation also are presented. For unstable systems, the model predicts spiraled boreholes with a pitch comparable to what generally is observed in the field. The general good agreement between the model predictions and the field data suggests potential direct implementations. It could lead to model-based control algorithms limiting micro-tortuosity or to better bit and BHA designs, if complemented with field campaigns aiming at refining the model parameters.

Contents

List of Tables

List of Figures

Nomenclature

Greek

α	Characteristic roots
α_{rm}	Rightmost complex-conjugate characteristic roots
$\boldsymbol{\gamma}$	Relative deflection of the bit around the stationary trajectory
$\Delta\boldsymbol{\gamma}$	Relative deflection respective to the bit around the stationary trajectory
$\boldsymbol{\Gamma}$	Scaled imposed RSS force
$\boldsymbol{\Gamma}_*$	Scaled RSS force at full saturation of the tilt without other influence
Γ_2, Γ_3	Scaled components of the RSS force
Γ_t	Scaled instantaneous RSS force
δ	Bit pseudo-azimuth
$\boldsymbol{\Delta}$	Scaled relative deflection of the BHA at the RSS pads
Δ	Pseudo-azimuth
$\boldsymbol{\Delta}_r$	Scaled relative deflection of reference of the BHA at the RSS pads
ε	Ratio of the angular and lateral steering resistances
ζ	Stretched coordinate in the boundary layer
ζ, ζ', ζ''	Coefficients of the bilinear single-cutter/rock interaction law
η	Bit lateral steering resistance
$\eta\Pi\big\vert_s$	Critical value of dimensionless group $\eta\Pi$ at bifurcation of stability
$\eta\Pi\big\vert_\Gamma$	Value of $\eta\Pi$ for which Γ does not influence the borehole trajectory
$\eta W_a\big\vert_s$	Unscaled version of $\eta\Pi\big\vert_s$
θ	Bit inclination

$\hat{\theta}$	Bit inclination for the inner solution
Θ	Borehole inclination
Θ_0	Initial borehole inclination
Θ_i	Borehole inclination at the level of stabilizer i
$\langle\Theta\rangle$	Averaged inclination of the BHA
$\langle\Theta\rangle_i$	Inclination of the i^{th} section of the BHA
ι	Rock intrinsic specific energy
$\boldsymbol{\kappa}_s$	(Quasi-)stationary curvature
κ_{2s}, κ_{3s}	Components of the (quasi-)stationary curvature
λ_i	Scaled length of the i^{th} section of the BHA
Λ	Relative position of the RSS pads
μ	Scaled lateral stiffness of the RSS pads
ξ	Scaled curvilinear coordinate along the borehole
ξ_i	Scaled position of stabilizer i behind the bit
Π	Scaled active weight
ϖ	Bit walk
ϖ_*	Critical bit walk
σ_*	Maximum contact stress at the cutter wearflat
ς	Bit flip
τ	Scaled rigidity in tilt of the stabilizers
τ_F	Relative orientation of the lateral force at the bit
τ_ϖ	Relative orientation of the bit tilt
τ_{max}	Largest delay of a delay differential equation
υ	Friction coefficient at the rock/cutter interface
Υ	Scaled weight of the BHA
ϕ	Phase between the pseudo-inclination and pseudo-azimuth
ϕ	Bit azimuth
Φ	Borehole azimuth
Φ_0	Initial borehole azimuth

Φ_i	Borehole azimuth at the level of stabilizer i
$\langle\Phi\rangle_i$	Azimuth of the i^{th} section of the BHA
$\boldsymbol{\varphi}$	Angular penetration vector
φ_2, φ_3	Components of the angular penetration vector
χ	Bit angular steering resistance
ψ_c	Saturation value of the bit tilt
ψ_s	(Quasi-)stationary tilt
ψ_{2s}, ψ_{3s}	Components of the (quasi-)stationary tilt
ψ_2, ψ_3	Small angles defining the bit tilt
$\boldsymbol{\omega}$	Spin vector
$\boldsymbol{\Omega}$	Angular velocity of the bit

Latin

A	Amplitude of the prescribed ripple/spiral
$\mathcal{A}, ..., \mathcal{H}$	Coefficients for the propagation equation
$\mathcal{A}_\theta, ..., \mathcal{H}_\theta$	Coefficients for the bit inclination
$\mathcal{A}_\Theta, ..., \mathcal{F}_\Theta$	Coefficients for the borehole inclination for $\varepsilon = 0$
$\mathcal{A}_{\Xi\Xi}, ..., \mathcal{F}_{\Xi\Xi}$	Coefficients for the borehole inclination and (pseudo-)azimuth
$\mathcal{A}_{F_2}, ..., \mathcal{H}_{F_2}$	Coefficients for the lateral force at the bit
$\boldsymbol{C}$	Torque on bit
$\mathcal{C}_1$	Chord delimited by the bit and the first stabilizer
$\mathcal{C}_i$	Chord delimited by stabilizers $i-1$ and i
$\boldsymbol{d}$	Penetration vector
d_1	Axial penetration per revolution
d_2, d_3	Lateral penetrations per revolution
($\boldsymbol{e}_x$,$\boldsymbol{e}_y$,$\boldsymbol{e}_z$)	Cartesian system of reference
f_n, f_w	Components of the force on a single cutter
$\boldsymbol{F}$	Reaction force at the bit
F_1	Axial reaction force opposite to weight on bit

F_2, F_3	Lateral components of the force at the bit
F_*	Characteristic force
$\boldsymbol{F}_c$	Minimum lateral force at the bit for tilt saturation
$\breve{\boldsymbol{F}}$	RSS force
$\breve{F}_2$, $\breve{F}_3$	Components of the RSS force
$\boldsymbol{\mathcal{F}}$	Generalized-force vector
$\mathcal{F}_i$	Coefficients of influence for the lateral force at the bit
G_1	Part of the weight on bit mobilized in contact forces
G_i	Independent terms in the bit/rock interaction law
H_i	Coefficients of the bit/rock interaction law
$(\boldsymbol{i}_1,\boldsymbol{i}_2,\boldsymbol{i}_3)$	Reference system attached to the bit
$(\boldsymbol{I}_1,\boldsymbol{I}_2,\boldsymbol{I}_3)$	Reference system attached to the borehole axis
$(\hat{\boldsymbol{I}}_1,\hat{\boldsymbol{I}}_2,\hat{\boldsymbol{I}}_3)$	Reference system attached to the first chord of the BHA
$(\tilde{\boldsymbol{I}}_1,\tilde{\boldsymbol{I}}_2,\tilde{\boldsymbol{I}}_3)$	Reference system attached to the (quasi-)stationary solution
K	Lateral stiffness of the RSS pads
l	Length of the cutter wearflat
$\tilde{\ell}$	Wavelength of the prescribed oscillations
ℓ_1	Distance between the bit and the first stabilizer
ℓ_i	Length of the i^{th} section of the BHA
L	Current length of the borehole
$\boldsymbol{\mathcal{L}}$	Tensorial operator encapsulating the bit/rock interaction law
$\boldsymbol{M}$	Moment at the bit
M_1	Axial component of the moment, opposite to the torque on bit
M_2, M_3	Components of the orthogonal moment at the bit
$\boldsymbol{M}^e$	Moment at the last modeled stabilizer
$\mathcal{M}_i$	Coefficients of influence for the moment at the bit
n	Number of stabilizers
p	Depth of cut of a single cutter
p_*	Critical depth of cut for the change of regime

$\boldsymbol{\mathcal{P}}$	Generalized-penetration vector
$\boldsymbol{r}$	Vector position for the BHA axis
$\boldsymbol{R}$	Vector position for the borehole axis
R	Rotation matrix between ($\boldsymbol{e}_x$,$\boldsymbol{e}_y$,$\boldsymbol{e}_z$) and ($\boldsymbol{i}_1$,$\boldsymbol{i}_2$,$\boldsymbol{i}_3$)
s	Curvilinear coordinate along the BHA
S	Curvilinear coordinate along the borehole axis
$\mathcal{S}$	Switch signal
$\mathcal{S}_i$	Coefficients for the 3D stationary solution
T	Rigidity in tilt of the stabilizers
$\boldsymbol{V}$	Velocity of the single cutter
w	Linear weight of the BHA
W	Weight on bit
W_a	Active weight
$\boldsymbol{y}$	Relative deflection of the BHA at the RSS pads
$\boldsymbol{y}_r$	Relative deflection of reference of the BHA at the RSS pads

Chapter 1

Introduction

1.1 General Context

Access to oil resources has been pivotal to many historical events: World War II, the Korean War or the Suez crisis, for example, are all connected to oil and the capacity of the different actors to cope with meeting their own domestic needs (Yergin, 2011). This concern is still central to geopolitics and to the competition between oil- and gas-importing powers for extending their spheres of influence and securing access to crucial resources (Kaplan, 2011).

The history of oil can be seen as a succession of periods of surpluses and shortages loosely regulated by a relentless struggle between oil companies, exporting countries, and importing powers, which all have different, and often contradictory, motives and objectives. The Oil and Gas Industry has been recently caught in such turmoil, following the abrupt drop in oil and gas market prices in the aftermath of the 2009 economic crisis.

This collapse of the oil price is the consequence of political decisions, paralleled with lower-than-anticipated demand and record production, particularly in the United States. Years 2013 and 2014 were characterized by the two highest domestic production surges of liquid fuels in American history, due to the gas-shale revolution. During these two years, domestic supply increased by about 3 million barrels per day (Mb/d) for a total output of 14 Mb/d. These numbers are compared to domestic and worldwide demand, respectively at about 20 and 94

Mb/d in 2015[1] (BP, 2015; EIA, 2015). Over the second half of 2015, the global oversupply is estimated at about 2.3 Mb/d (EIA, 2015). After the historic nuclear agreement with Iran in mid-2015 and the slow rehabilitation of Iraq and Libya, these historic producers are back on the market and should maintain some pressure on oil and gas prices in the short-term (EIA, 2015).

Demand for oil and gas should keep increasing, however, over at least the next 20 years, pushed by demographic growth and by large-scale industrialization of emerging countries, led by China and India (EIA, 2014; BP, 2015). These two giants – comprising close to a third of the world population – will, indeed, massively import fossil fuels to funnel their growth and meet the new needs and expectations of their emerging middle-class population. Even within the OECD-countries, with their tendency to switch progressively to more sustainable sources of energy, the *most likely* scenario still anticipates a constantly rising demand for fossil fuels, especially natural liquefied gas (NLG), that will help in the transition between high-CO_2-emitting coal power stations and wind or solar plants (BP, 2015).

Combined with the progressive depletion of active wells and the slowing development rate of new production capacities, it is expected that demand should get closer to supply within the next few years (EIA, 2014, 2015). Consequently, oil and gas production will remain a central, growing industry for the decades to come and be still in need of technological and fundamental advances to drill and complete boreholes always longer, deeper, and cheaper in an extremely competitive environment.

1.2 A Short History of Drilling...

Centuries before the current era, several-hundred-feet-deep wells had already been dug in Egypt and China. Some of them, used to produce brine, were mentioned by Confucius in 600 BC. In about 450 BC, Herodotus referred to a well producing some mix of asphalt, soil, and oil; this is virtually the first written record of hydrocarbon production. The Chinese even reached depths larger than 2000 ft back in the 17^{th} century, more than two hundred years before the beginning of large-scale oil production in the United States (Moor, 1977).

[1] The US, with only about 4.5% of total world population, consumes more than a fifth of worldwide oil production.

The first wells drilled with the sole objective to produce oil date from the mid-18$^{\text{th}}$ century in Eastern France. Basic drilling technology is already alluded to in the Encyclopedia of Diderot and d'Alembert in 1751 (Kopey, 2007). These wells only reached shallow depths as oil was easily accessible and the demand still trickling. By progressively improving their technique, Italian and French engineers were able to reach depths of about 1900 ft by 1841 for geothermal and water-production applications, without any mechanical power; animals were used to rotate the drill pipe (Moor, 1977).

Large-scale oil production in the US started in the mid-19$^{\text{th}}$ century, when kerosene, one of the products of crude oil refinement, was discovered to produce a high-quality light when burnt and became increasingly consumed as an illumination source. Manufacture of kerosene was patented in 1854 and in 1859, the first *oil rush* started in Titusville, Pennsylvania, when "Colonel" Drake was able to produce oil from a drilled well after almost two years of unsuccessful attempts (Yergin, 2011). That well was 69 ft deep only but what it meant in terms of economic success and access to underground untapped reserves of *rock oil* gave a big thrust to the emerging oil industry. This achievement on American soil occurred, however, more than a decade after the first modern oil well – coincidentally also 69 ft deep – was drilled in Baku in 1846 (Kopey, 2007). Baku was then the pioneering industrial center for oil production. That region, now located in Azerbaijan, went on to produce more than half of the world supply by the early 20^{th} century, led by Nobel's and Rothschild's industrial interests (Yergin, 2011).

Despite the technological progress achieved in France and Italy in previous centuries, rotary techniques were not directly adopted in the oil patch: The first oil drillers relied on so-called cable-tool technology. This percussive-drilling technique is based on the rig repeatedly lifting and dropping a thin rod at the end of which lies a heavy drilling bit that progressively pulverizes the rock.

Though older in concept[2], rotary drilling was only progressively implemented in the US following the "discovery" of the Baker brothers who, in the late 19$^{\text{th}}$ century, designed a drilling method in which a drill bit would sit at the end of a continuously rotating pipe (Moor, 1977). By applying an axial force, the bit continuously scraps and shears the rock. Cleaning of the

[2] Rotary tools were already sketched by Leonardo da Vinci in 1517 (Moon, 2007).

bottom-hole is performed by circulating water from inside and around the rotating pipe. (Water was later replaced by *mud*, a complex fluid consisting of water or oil products mixed with many chemicals working as thickening, lubricating, or weighting agents.)

Cable-tool drilling was commonly chosen up to the late 1940s for its better performances in hard-rock formations even though it was already outperformed by rotary drilling in soft-rock applications. The introduction of mechanical power to rotate the drillstring and circulate the cleaning mud as well as progressive improvements in drill bits, such as self-cleaning teeth or hard-alloy materials, finally provided rotary drilling a definitive advantage in most environments. The final blow was hammered by Phillips Petroleum Co. in 1958 when it drilled economically a 25,000-ft well using only a modest-size rotary rig. For comparison, the deepest cable-tool well had reached *only* 7,759 ft back in 1925. Nowadays, rotary drilling is virtually the only technique used in the Oil and Gas Industry; percussive drilling is still widely used, however, for large-diameter water wells (Moor, 1977).

With developments in measurement-while-drilling (MWD) technologies, telemetry, and trajectory control, borehole depths and horizontal reaches keep beating records. The deepest well, the Kola Superdeep Borehole in Russia, completed in 1989 for scientific purposes, attained the depth of 40,230 ft (Kozlovsky, 1984). It is still the deepest artificial point on Earth. In 2008, it has been surpassed in terms of the so-called measured depth, *i.e.*, the borehole total length, by the Al Shaheen BD-04A well in Qatar, with a total length of 40,318 ft (for a horizontal reach of 35,770 ft). With the development of the Sakhalin-1 project, this distance has been surpassed a few times: 9 of the 10 world's longest wells now belong to that consortium. The current record is detained since April 2015 by the Chayvo O-14 well with a measured depth of 44291 ft and a horizontal reach of 39,478 ft.

1.3 Directional Drilling

In the early days of large-scale production, oil was extracted from multiple vertical wells reaching shallow reservoirs. With the development of borehole survey instruments in the 1910s and 1920s came the realization that most "vertical" wells were actually *crooked* (Muller, 1924; Lahee, 1929; Eastman, 1937). Drilling engineers first considered this deviation from the planned, vertical

trajectory as a dysfunction that needed to be corrected (Muller, 1924; Lahee, 1929) but some of them gradually understood that many advantages could be achieved if well trajectories could be controlled effectively (Hughes, 1935; Close, 1939; Weaver, 1946): directional drilling was born. Directional drilling is defined as "the art and science involved in the deflection of a wellbore in a specific direction in order to reach a pre-determined objective below the surface of the Earth" (Inglis, 1987); with time, the *science* component has become predominant.

The rise of directional drilling originates from the need to tackle increasingly challenging field situations, as reservoirs progressively become more difficult to reach. The ability of controlling borehole trajectories makes possible, indeed, a new range of applications (Inglis, 1987; Downton et al., 2000): (a) sidetracking to circumvent obstructions at the bottom of the hole, if a pipe or tool gets stuck for example; (b) avoiding troublesome geological formations such as salt domes; (c) controlling borehole verticality when needed; (d) drilling beneath inaccessible or difficult-to-access locations such as lakes or cities; (e) drilling different wells from a same location for either offshore drilling or limited land disturbance; and (f) drilling relief wells in emergencies such as blowouts.

Horizontal and extended-reach drillings are direct extensions of directional drilling. They provide increased drainage for a unique well or improved productivity in fractured reservoirs by intersecting several (vertical) faults. Directional drilling is also used in geothermal applications, in the mining industry for core samples, or in shale-gas and oil exploitation for which compact, low-conductivity reservoirs are stimulated by fractures hydraulically initiated from a horizontal well in the shale layer.

Current expertise in trajectory control is best illustrated by the relief borehole drilled to *kill* the leaking Macondo well that had blown out following an explosion on the Deepwater Horizon platform in the gulf of Mexico in 2010. Directional drillers successfully intersected the 10-inch-wide target, at a depth close to 18,000 ft under sea level, to seal the well by pumping cement into it[3].

A typical rotary directional drilling system is sketched on Fig. 1.1. At the ground level, operations are managed from a rig. From there, the main drilling parameters are controlled,

[3] This leak led to the largest maritime oil spill in history with an estimate of 4.9 million barrels released in the Gulf of Mexico (Cleveland et al., 2010).

such as the hookload, *i.e.*, the axial force applied at the top of the drillstring, the rotary speed, and the mud flow. The rig also facilitates the handling of the drillstring.

The drillstring is a long shaft composed of circular about-30-foot-long hollow pipes, whose main mechanical function is to transmit the torque and the axial load from the rig to the bit. Most of the drillstring is in tension to avoid buckling but as a compressive thrust is required at the bit (the so-called weight on bit), its lower part, called the bottom-hole assembly (BHA), works in compression and is composed of thicker pipes called drill collars.

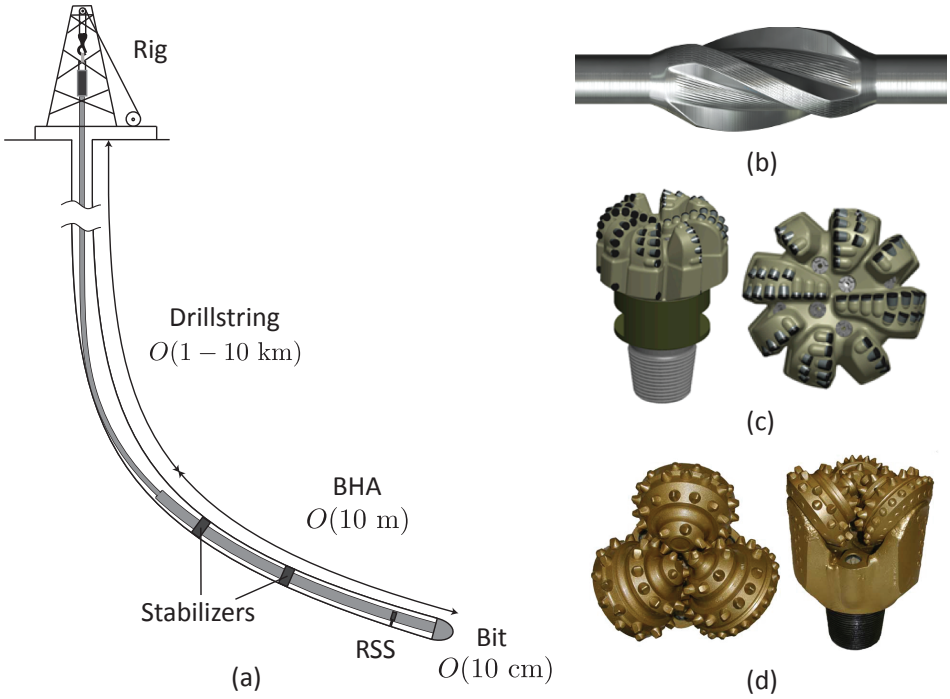

Figure 1.1: (a) Typical rotary drilling system equipped with a push-the-bit RSS [adapted from Perneder (2013)], (b) stabilizer (www.hunting-intl.com), (c) PDC bit, characterized by its complex distribution of cutters along several blades (model SHARC MDSi813 from Smith Bits), and (d) roller-cone bit, recognizable to its three moving parts, the cones, which progressively crush the rock (www.moabbit.com).

The geometry and design of the BHA is crucial for the general behavior and directional properties of the system. It is indeed along it that most of the sensitive drilling equipment is placed. First, short thick elements, the stabilizers, are placed to help center and limit the

deflection of the BHA in the borehole[4] (Fig. 1.1b). Measurement- and logging-while-drilling devices are also located on the BHA to be as close to the bit as possible. Some measurement tools are able to transmit information to the surface through mud pulses; however transmission rates usually remain rather low, $O(10$ bits/s).

For directional applications, instruments to deviate the borehole are also present along the BHA. In the present research, a push-the-bit rotary steerable system (RSS) is considered. This last generation of steering devices emerged in the mid-1990s and revolutionized directional drilling (Downton et al., 2000). These servo-controlled downhole robots impose on the BHA either a controlled lateral force (the push-the-bit RSS used in this research) or a kink (the so-called point-the-bit RSS), generally a few feet behind the bit, to steer it toward the desired direction. In the case of push-the-bit systems, the force is generated by actuated pads, rotating or not with the BHA, which directly push on the borehole wall.

Rotary steerable systems are the last evolution of a series of directional tools and technical developments. As early as the 1890s, whipstocks were used to intentionally sidetrack boreholes at the bottom of which a tool was stuck (Brantly, 1971; Inglis, 1987) but it was only in 1932 that H. J. Eastman operated these steel wedges to deliberately deviate and control the borehole trajectory (Close, 1939). This achievement was made possible by the then-recent development of gyroscopic and magnetic tools that were able to measure the borehole inclination, and sometimes its azimuth, at different discrete points (Eastman, 1937). The placement and control of the orientation of the whipstocks, among others, were time consuming and thus this approach was progressively supplanted by other deflection mechanisms.

With the systematic use of stabilizers along the BHA (MacDonald and Lubinski, 1951), their relative positions can theoretically be designed to give the BHA a dropping, holding, or building tendency, *i.e.*, the system would tend to reduce, maintain, or increase its inclination (Lubinski and Woods, 1953; Woods and Lubinski, 1955). This approach mostly relied on experience; at that time, directional drilling was more an art than a science.

Before the RSS revolution, the most common way to steer the borehole was the use of

[4] The role of the stabilizers was originally to limit the deflection of the BHA, following the buckling of the drill collars (MacDonald and Lubinski, 1951). Buckling was originally thought to be the major cause of borehole deviation (Muller, 1924; Capelushnikov, 1930).

downhole motors and bent subs. The downhole motor enabled to drive the bit without rotating the drillstring. The borehole deviation was then imposed by placing a bent sub above the motor that would create a kink, up to 3°, in the BHA (Inglis, 1987; Haugen, 1998). The non-rotation of the drillstring in *sliding mode*, *i.e.*, when the borehole is steered, sometimes created friction issues, especially for large inclinations and extended-reach wells. This inconvenience, among others, led to the development of RSSs that deviate the borehole while rotating the drillstring (Haugen, 1998; Downton et al., 2000).

The first breed of RSSs was designed in the late 1980s by engineers at Eastman Christensen GmbH, paradoxically to control the verticality of the Continental Deep Drilling (KTB) borehole (Haugen, 1998). It was part of an experimental project in Southern Germany of drilling a 30,000-ft-deep well to investigate the Earth's crust. With the success of the operation (the borehole inclination is reported not to have crossed 0.3°), drilling system developers realized that actuated pads in a close-loop system could be used to control borehole trajectory.

Engineers at Agip S.p.A. and Baker Hughes Inteq then collaborated to develop the first push-the-bit RSS using the concept tested during the KTB project (Haugen, 1998). In the words of a product manager at Baker Hugues, "the rotary steerable system combines the drilling efficiency advantages of rotary assemblies with the course control associated with bent-housing motor techniques" (Haugen, 1998).

Below the RSS, at the extremity of the BHA sits the drill bit whose role is to shear or crush the rock. The two main types of bits for directional applications are the polycrystalline diamond compact (PDC) and the roller-cone bits (Fig. 1.1c and d). The first is characterized by a complex distribution of cutters made of synthetic diamonds that continuously shear and scrap the rock formation while roller cone bits have three rotating cones whose teeth crush and shear the rock. The general better resistance to wear and abrasion of PDC bits made them more and more widely used in the field: Nowadays, it is estimated that more that 90% of total footage are drilled with PDC bits. They are moreover particularly well-suited for directional operations because of their lateral-cutting abilities.

PDC bits are theoretically adapted specifically to each application. Bit manufacturers claim that each bit has a unique design depending on as many factors as the rock formation, the borehole inclination, the steering system, the predicted borehole curvature, and the geometry of

the BHA. Their configuration is consequently elaborate: the amount and positions of the cutters and blades offer many degrees of freedom to adapt the bit to each particular field situation while minimizing undesired effects such as imbalance or instability.

The blade geometry is especially important in directional drilling systems: its interaction with the wellbore plays a central role in dictating the bit relative ability to drill laterally and thus in shaping the directional tendency of the system. In the following, the nomenclature introduced by Dupriest and Sowers (2009) is used to characterize bit gauges (Fig. 1.2). The three main qualitative properties of a gauge are its length, profile, and aggressiveness. The gauge length has been shown to directly correlate to the bit propensity to induce borehole curvatures: under identical conditions, a short gauge provokes naturally a larger lateral penetrations (Menand et al., 2002). However it also leads to less dynamically stable bits (Dupriest and Sowers, 2009). In directional drilling, gauge lengths usually range between 2" and 6".

Four different bit profiles are most common (Fig. 1.2). Full-gauge profiles have the bit diameter along the blade corresponding to that of the drilling structure, *i.e.*, it coincides to the radial position of the last cutter on the bit face. In the full-taper or full-undercut geometries, the diameter along the gauge is smaller than that of the bit. When tapered, the gauge diameter is progressively reduced following a constant angle starting at the last outside cutter; when undercut, the gauge diameter is uniform. The partial-undercut configuration is similar to the full-undercut, but the profile typically contains first 1" to 2" of full gauge before the reduction in diameter. Bit manufacturers are cautious about not publishing any bit specifics, but the maximum dimensional relief in tapered or undercut gauges is of the order of $O(1^\circ)$.

The intrinsic aggressiveness of each bit profile may be improved by adding extra cutters along the gauge; these cutters are referred to as *active* and the part of the gauge on which they are located is the *active gauge*. The industry commonly refers to the lateral aggressiveness in terms of passive, active, or semi-active terms (Fig. 1.2); these notions do not generally bear, however, any specific quantifiable meaning.

The bit selection contributes to defining the directional properties of the system but the force (or kink) at the RSS is central to control the building rate of the borehole. As the transmission rate of information between the bottom-hole and the surface is still low, continuous control of RSS is virtually impossible. Hence, RSS are equipped with built-in sensors and integrated

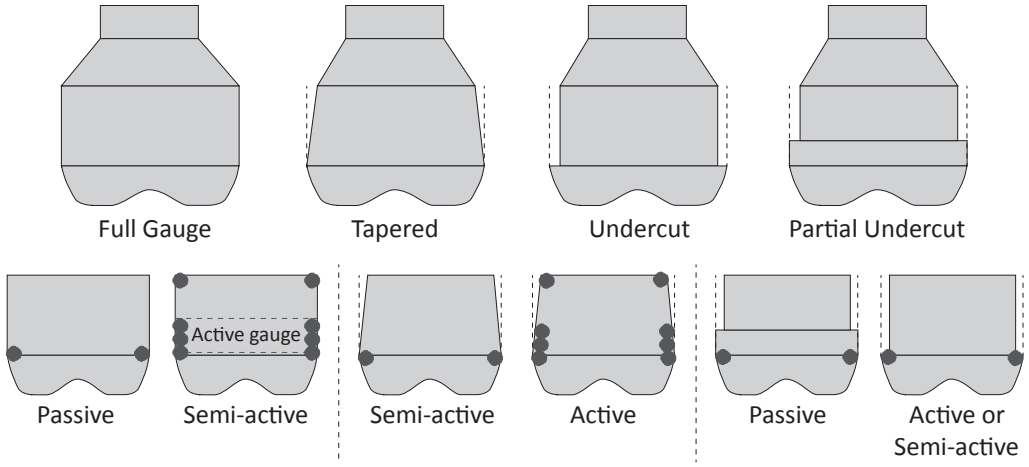

Figure 1.2: General characteristic of PDC bits: geometry and aggressiveness of the bit gauge [adapted from Dupriest and Sowers (2009)]. [Theoretically the choice of bit is dictated by the rock formation, the anticipated borehole curvature, or the geometry of the BHA. The gauge properties significantly influence the lateral-cutting ability of the PDC bit.]

control algorithms to steer the system almost independently in the desired direction.

Even though little information is available, these algorithms are thought to use simple drilling models whose imprecision can lead to significant deviations from the desired trajectory but also to excessive borehole tortuosity: data pertaining to boreholes drilled with BHAs equipped with a largely available push-the-bit RSS presented a corkscrew pattern whose characteristic wavelength almost perfectly corresponded to the distance between the bit and the RSS pads (Sugiura and Jones, 2008b; Marck et al., 2014). Therefore, borehole quality and control-algorithm efficiency are related.

Directional drilling operations should aim not only at efficiently tracking a predefined well path, but also at limiting the tortuosity of the borehole, that is, reducing the borehole oscillations around the intended trajectory. An excessively tortuous well complicates the drilling operations and compromises the proper completion of the well (MacDonald and Lubinski, 1951; Gaynor et al., 2001; Russell, 2002).

1.4 Motivations and Objectives

Although much effort has been spent, generally with success, on improving drilling rates and controlling the global trajectory, borehole quality has been generally neglected, likely because measurement tools were not adequate (Russell, 2002). Borehole spiraling has been largely identified in recent years (Bellay et al., 1996; Gaynor et al., 2001; Chen et al., 2002b; Sugiura and Jones, 2008a) but its causes are still not well commonly accepted (MacDonald and Lubinski, 1951; Pastusek and Brackin, 2003; Stuart et al., 2003; Dupriest and Sowers, 2009; Menand, 2013). It leads, however, to many technological issues, such as lower-than-expected rates of penetration, increased shocks and vibrations, or smaller drift diameters (Gaynor et al., 2001).

A two-dimensional, phenomenological model was proposed first by Pastusek and Brackin (2003): it explains the initiation of spiraling by self-excited oscillations due to the geometric feedback of the stabilizers on the drilling direction at the bit. An initial perturbation in the borehole is then progressively amplified if the system is deemed to be directionally unstable.

Research on the formulation of a model of borehole propagation has been ongoing at the University of Minnesota for several years (Detournay, 2009; Perneder et al., 2012; Perneder and Detournay, 2013a,b; Perneder, 2013). This research has established the fundamental basis for the mechanics of directional drilling and the model has been shown to be qualitatively consistent with field orders of magnitude and observations as well as capable of explaining some counter-intuitive situations observed *in situ* (Perneder, 2013).

Some two-dimensional borehole simulations with that model showed that, under certain conditions, a perturbation in the borehole trajectory could also be progressively amplified due to the geometric feedback of the stabilizers (Perneder, 2013). This growing perturbation exhibited, moreover, the characteristic of borehole rippling (the two-dimensional equivalent of spiraling), as expressed by Pastusek and Brackin (2003): the oscillations had a regular wavelength related to the distance between the bit and the first stabilizer. It is consequently thought that spiraling is the expression of some limit cycle[5] undergone by the BHA that affects the borehole geometry.

Despite key parameters being identified – the weight on bit, the bit lateral drillability, or

[5] A limit cycle is mathematically defined as a closed trajectory in the phase space of a nonlinear dynamic system. In other words, it is a repetitive, periodic pattern in terms of the system state variables.

the geometry of the BHA (Pastusek and Brackin, 2003; Downton, 2007; Perneder, 2013), the existing studies are far from being complete; no parametric analysis has been conducted and little quantitative information is available. All the published models for spiraling are also limited to a planar representation of the borehole. Extending the analysis to the third dimension would not only enable to capture actual spirals but also to study the influence of the bit walk on the directional stability of the system.

Similarly, all the current models are linear. As so, they are only able to provide information on the directional stability, but not on the limit cycle. Key information such as the amplitude of the oscillations is missing.

The objectives of the current research are thus threefold. First, it focuses on evaluating the conditions that lead to borehole spiraling by performing a systematic parametric analysis of the directional stability of drilling systems. This analysis is extended to the third dimension to capture the influence of the bit walk. The existing model of borehole propagation will also be extended to include new elements that may impact the directional stability. The influence of the constrained rotation of the stabilizers as well as that of the lateral stiffness of the RSS pads are studied by attributing them with a linear spring in tilt or deflection, respectively.

Second, the characteristics of the spiral are captured by introducing some nonlinearity into the model. Experimental data have highlighted that the bit tilt, the relative orientation of the drill bit on that of the borehole, reaches a saturation, $O(1^\circ)$, when the lateral force at the bit is larger than a given threshold (Pastusek et al., 2005; Ernst et al., 2007). As oscillations in the borehole trajectory also betray fluctuations in the tilt, imposing a saturation naturally limits the spiral amplitude. These results can then be compared to the clearance between the drill collars and the borehole, which provides a technological upper limit to the amplitude of the oscillations (MacDonald and Lubinski, 1951).

The last objective is to test and validate the model with field data pertaining to spiraled boreholes. Applications are also highlighted and general recommendations are presented in terms of BHA design and bit selection.

1.5 Organization

Chapter 2 first provides an account of the state of the literature about models of borehole propagation and spiraling. Chapter 3 then introduces the building blocks of the global model of propagation and the main assumptions on which they are formulated. This model is constructed for a BHA equipped with a push-the-bit RSS and a PDC bit in a homogeneous and isotropic rock formation. The concepts of bit/rock interaction law, kinematic relationships, and BHA model are presented and two sets of expressions for the force and the moment at the bit are derived.

Chapter 4 focuses on a reduced two-dimensional model corresponding to a planar trajectory. It starts with a derivation of the delay differential equation (DDE) defining the evolution of the borehole inclination. Properties of DDEs are presented and the influence of some parameters of the system is discussed: the rigidity in tilt of the stabilizer, the lateral stiffness of the RSS pads, and the angular steering resistance of the bit. The phenomenological nature of spiraling and the planar limit cycle are introduced and commented.

Keeping only the most relevant parameters, the analysis is extended to the third-dimension in Chapter 5. Focus is put on the influence of the bit walk and the description of the limit cycle.

Chapter 6 describes the validation and applications of the model. Field data from spiraled boreholes are compared with the model predictions and commented. Finally Chapter 7 summarizes the main findings of this research and proposes some leads for further work.

Chapter 2

Literature Review

Drilling is characterized by a wide range of scales, both in time and length: from millimeters for the depth of cut to kilometers for the borehole length, and from seconds for the period of revolution of the bit to weeks for the completion of the borehole. Different phenomena occur at different scales and it is the challenge to the modeler to pose the correct assumptions, in order to capture the relevant phenomena at a given scale.

The most relevant works about models of borehole propagation and about bit/rock interaction and BHA modeling have been exhaustively presented by Perneder (2013). This section summarizes this contribution, which is followed by an introduction to borehole tortuosity and in particular spiraling.

2.1 Modeling of Directional Drilling

The Pioneers

The first model for directional drilling, and certainly the most influential in the industry for years, is due to Lubinski and Woods (1953). This work, followed by that of Murphey and Cheatham (1966), is analytical and mostly qualitative: the drill bit is assumed to be *isotropic*, *i.e.*, in an isotropic and homogeneous rock formation, the bit drills in the direction direction of the force acting on it. Directional behavior was viewed as an expression of rock anisotropy and

inhomogeneity, or consequent to the deflection/buckling of the BHA.

By combining a simple bit/rock interaction law and a BHA model, both publications developed two-dimensional *equilibrium solutions*, corresponding to straight (Lubinski and Woods, 1953) or circular (Murphey and Cheatham, 1966) boreholes. The equilibrium solutions are assumed to be the (quasi-)stationary trajectories to which drilling systems converge. They did not compute, however, expressions for the borehole propagation.

Bit/Rock Interaction Law

The assumption of coaxiality between the force and the drilling direction at the bit was later relaxed, based on the observation that drill bits usually have a stronger tendency to drill along their axis of symmetry than laterally (Bradley, 1975; Millheim and Warren, 1978; Callas, 1981).

The concept of bit/rock interaction law was first introduced in the (unpublished) work of Cheatham and Ho (1981); but Ho (1987; 1989; 1995; 1997) further improved the initial model and presented a most influential work. (He never attempted, however, to solve the equation of propagation by combining its bit/rock interaction law with a model for the BHA.) The bit/rock interaction law was presented as a series of linear relationships between the components, at the bit, of the force and moment and the drilling and turning rate vectors, respectively. Separate contributions came from the rock anisotropy and the bit *anisotropy*, *i.e.*, the measure of the relative difficulty to impose a lateral penetration to the bit respective to an axial one.

Bit/rock interaction laws published in the literature generally distinguished themselves by two main characteristics, which are still matters of debate: the presence of a bending moment at the bit and the nature of the kinematic quantities. The no-moment condition (which relates to the component orthogonal to the bit axis, as the *axial* component, the torque, does not vanish) is usually justified by the borehole overgauge at the bit (Voinov and Reutov, 1991). Only a few contributions consider a bending moment (Voinov and Reutov, 1991; Simon, 1996; Maouche, 1999) or incorporate it into the interface laws (Chen and Geradin, 1993; Ho, 1995; Neubert, 1997; Menand, 2001; Perneder and Detournay, 2013b; Perneder, 2013). The kinematic variables are either defined as drilling rates, which have dimensions of a velocity (Cheatham and Ho, 1981; Ho, 1995) or as penetrations per revolution (Teale, 1965; Detournay and Defourny, 1992; Menand, 2001; Palmov and Vetyukov, 2002; Detournay et al., 2008; Franca, 2010; Perneder

et al., 2012).

Bit/rock interaction laws are derived numerically or experimentally. Numerical approaches presume a single-cutter/rock interaction law, whose influence for each single cutter, generally under kinematically controlled conditions, is computed and then coalesced to obtain the interface law for the entire bit (Chen and Geradin, 1993). Experimental setups usually impose an axial velocity (and sometimes an angular one) to the bit and either a lateral force or velocity from which the general bit/rock interaction law is extracted (Millheim and Warren, 1978; Brown et al., 1981; Clark and Walker, 1985; Pastusek et al., 1992; Norris et al., 1998; Ernst et al., 2007).

The influence of rock interfaces is the focus of some publications. Deviations in the borehole trajectory have been reproduced experimentally (Bradley, 1974; Horibe et al., 1979; Brown et al., 1981; Boualleg et al., 2006). It stresses the complex local perturbation caused by the interface. Models have been advanced to explain this deviation, either qualitatively (Rollins, 1959; Sultanov and Shandalov, 1961; Knapp, 1961, 1965; Murphey and Cheatham, 1966; Bradley, 1974) or quantitatively (Lubinski and Woods, 1953; McLamore, 1971; Pariseau, 1971; Bradley, 1974; Smith and Cheatham, 1977; Boualleg et al., 2006). These models all justify, however, the local borehole deviation by parasitic forces and/or moments that arise from the transition from one rock formation to the other.

Finally some other investigations are concerned with the influence of the rock anisotropy on the borehole trajectory (Lubinski and Woods, 1953; Bradley, 1975; Brown et al., 1981; Voinov and Reutov, 1991; Simon, 1996; Boualleg et al., 2006) or with the evolution of bit wear while drilling (Cheatham and Loeb, 1985; Faÿ, 1993; Waughman et al., 2002; Rashidi et al., 2008).

Modeling of the BHA

In the late 1970s and 1980s, much effort focused on the representation of the drillstring, thought to be central to the general directional behavior of the system. The influence of the bit/rock interaction law on the borehole propagation was overlooked: The directional tendency of the borehole was assumed to be only related to the lateral force at the bit (Millheim, 1977; Millheim et al., 1978; Millheim, 1979; Birades and Fenoul, 1986, 1988). Progressively the relative orientation of the bit on that of the borehole has been deemed relevant and incorporated into the

modeling (Callas and Callas, 1980; Brett et al., 1986; Williamson and Lubinski, 1986; Pastusek et al., 2005; Menand et al., 2012; Perneder, 2013).

With the advent of numerical methods, the characterization of the BHA was based on finite elements or finite differences (Fischer, 1974; Millheim, 1977; Millheim and Warren, 1978; Callas and Callas, 1980; Amara, 1985; Birades and Fenoul, 1986; Brett et al., 1986; Rafie et al., 1986; Birades and Fenoul, 1988; Chen and Wu, 2008). Some others still proposed analytical formulations (Lubinski and Woods, 1953; Murphey and Cheatham, 1966; Bai, 1986; Chandra, 1986; Ho, 1986; Miska et al., 1988; Aadnoy and Huusgaard, 2002). Birades and Fenoul (1986) suggest that BHA dynamics do not have a strong influence of the borehole trajectory if averaged over several revolutions.

Model of Borehole Propagation

Almost systematically, the problem of borehole propagation is addressed using numerical tools (Callas, 1981; Millheim, 1982; Brett et al., 1986; Rafie, 1988; Maouche, 1999; Boualleg et al., 2006; Studer et al., 2007). The coupling between the BHA and the bit/rock interaction law is not considered, however: the drillstring model is used to compute the forces acting on the bit, from which the drilling direction is estimated using the bit/rock interaction. Moreover, underlying assumptions and models are not always made readily available.

Only a handful of contributions have derived analytical equations of borehole propagation (Neubert and Heisig, 1996; Neubert, 1997; Downton, 2007; Detournay, 2009; Downton and Ignova, 2011; Detournay and Perneder, 2011; Perneder and Detournay, 2013a; Perneder, 2013). These models aim at developing control strategies for the borehole trajectory through the RSS or to understanding some phenomenological issues in directional drilling.

2.2 Borehole Spiraling

Tortuosity has components at different scales. At the larger scale, it is related to the planned borehole trajectory and the corrections around the desired path, with curvatures intentionally imposed to steer the borehole toward the desired target. Fluctuations at an intermediate scale, $O(30 - 100$ ft), have also been observed (Gaynor et al., 2002; Stockhausen and Lesso Jr, 2003;

Menand, 2013). These are sometimes related to downhole motors or turbines, whose steering capacities are turn on and off, to stay as close as possible to the desired trajectory (Weijermans et al., 2001; Samuel and Liu, 2009; Menand, 2013). Early observations of borehole spiraling are related to horizontal drilling, where *rippling* was measured as the measurement equipment was laying on the low side of the horizontal section and only measured the oscillations in one direction (Nieto et al., 1995; Ogawa and Minh, 1997; Russell, 2002). Finally, what has been referred to as spiraling, *i.e.*, regular oscillations in the borehole geometry at the length scale of the foot, has been detected. In recent studies, even higher frequencies have been observed, of the order of $O(1")$, that may be related to the contact pattern between the bit gauge and the borehole (Sugiura, 2009).

Identification of tortuosity is intertwined with the progressive sophistication of borehole surveys. The first "one-shot" measurement devices indicated that borehole were not systematically vertical, owing to the nature of the subsurface with its anisotropy, faults, or interfaces (Lubinski and Woods, 1953; Inglis, 1987; Boualleg et al., 2006; Marck and Detournay, 2014b). Despite this realization, definitions for such concepts as crookedness, straightness, or verticality were not commonly accepted (MacDonald and Lubinski, 1951). Somehow this confusion has perdured; there is still no consensual definition of borehole tortuosity (Bang et al., 2015).

Nonetheless with the development of directional drilling, the notion of crookedness needed to be revisited to account for the increasing complexity in borehole profiles. To control the adequacy between the planned and actual trajectories, measurements of the borehole orientation were usually taken every 100 ft[1]. These discrete measurements provided a first definition for tortuosity: the difference between the *planned* and the *macro-scale* tortuosities. They are computed as the sums of all the planned or measured *increment of curvatures* along the well (only differences in inclination and azimuth between measurement points are accounted for) divided by the borehole length (Gaynor et al., 2001). These indicators, as sensitive as they are on the accuracy of the data (Bang et al., 2015), entered in borehole-quality classifications or drilling-performance benchmarks (Oag and Williams, 2000; Williams et al., 2001; Mason and Chen, 2005, 2006).

[1] It is from this systematic survey sampling that borehole curvatures are still measured in degree/100 ft.

As spatial sampling rates in measurements significantly improved, it was realized that the largest source of tortuosity takes place at a length scale related to the distance between the bit and the first stabilizer (Gaynor et al., 2001; Stuart et al., 2003; Samuel et al., 2005; Sugiura and Jones, 2008b). Now that borehole inclination and azimuth can virtually be measured continuously along the borehole (Lesso Jr et al., 2001; Stockhausen and Lesso Jr, 2003) and that cross sections can be reconstructed from caliper logs (Maeso and Tribe, 2001; Pastusek and Brackin, 2003; Sugiura and Jones, 2008a,b; Sugiura, 2009), local micro-tortuosity can be depicted with high precision: It was observed that boreholes exhibit regular oscillating patterns (Stuart et al., 2003; Sugiura and Jones, 2008a,b). Because of its shape, similar to a corkscrew or helix, this type of micro-tortuosity has been referred to, maybe misleadingly, as borehole spiraling (Fig. 2.1).

Spiraling can only be inferred from advanced wireline survey techniques and measurement-while-drilling caliper tools (Gaynor et al., 2001; Chen et al., 2002a). It has, however, been widely documented and presented as the primary form of borehole (micro-)tortuosity (Gaynor et al., 2001). Some authors even believe that spiraling happens to some degree in virtually all wellbore that are drilled by conventional methods[2] (Gaynor et al., 2001; Chen et al., 2002b). The regularity of the pitch, usually ranging between 2 and 10 ft (Gaynor et al., 2001; Sugiura and Jones, 2008a) and related to the distance between the bit and the first piece of equipment is contact with the wellbore, *e.g.*, a stabilizer or the RSS pads (Bellay et al., 1996; Stuart et al., 2003; Sugiura and Jones, 2008b), has perplexed some observers about its possible causes, especially as it was observed that spiraling seemed independent of ROP and RPM (Stuart et al., 2003). This suggests its independence of downhole dynamics as well.

Borehole tortuosity at all scales leads to some technological issues (Banks et al., 1992; Guild et al., 1995; Stuart et al., 2003; Menand, 2013). Similarly spiraling affects negatively many aspects of drilling; the common issues associated to spiraling are (Gaynor et al., 2001; Chen et al., 2002a): (a) lower-than-expected rates of penetration, (b) reduction of bit life, (c) decreased reliability of the measurement/logging-while-drilling tools, (d) difficulty to clean the hole, (e) increased wear of the stabilizers and pipes (Matthews and Dunn, 1993), (f) increased torque and

[2] These conventional methods are listed as short-gauge bits on rotary, motor, or rotary steerable assemblies.

drag, (g) issues in posing the casing, (h) poor cementing conditions, and (i) lower performances for push-the-bit RSSs (Sugiura and Jones, 2008b).

The reality of the influence of spiraling on borehole completion has been accepted by the industry. Micro-tortuosity is now included in many indices aiming at classifying the quality and difficulty to drill boreholes (Gaynor et al., 2001, 2002; Brands and Lowdon, 2012; Bang et al., 2015). The influence of spiraling is also more systematically included empirically in torque and drag models (Gaynor et al., 2002; Stuart et al., 2003; Samuel et al., 2005; Samuel and Liu, 2009).

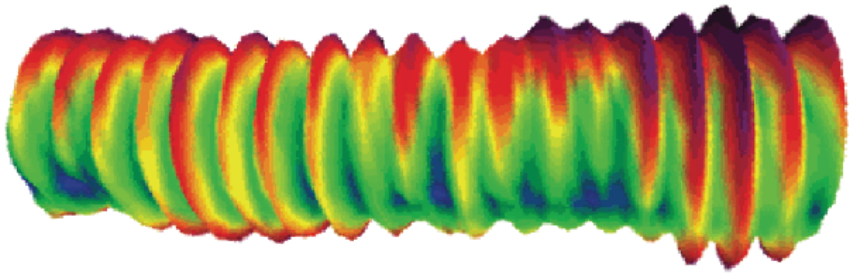

Figure 2.1: Borehole spiraling reconstructed from field measurements. [The plot is not to scale as the lateral component is usually stretched. A clear and regular pattern is observed in which the pitch of the spiral directly correlates to the distance between the bit and the first element of the BHA in contact with the borehole, either the first stabilizer or the pads of the RSS. This pattern leads to many technological issues due to the fluctuations in the borehole axis and the reduced effective cross section.]

Once more, Arthur Lubinski is co-author of the first two papers referring to spiraled holes. The first one focuses in general on the lack of a clear definition to describe *crooked* holes (MacDonald and Lubinski, 1951); he noted that a "hole following a tight spiral" would not be seen on discrete inclination measurements but would still lead to "serious key-seating difficulties or drill-pipe wear". In a second paper (Woods and Lubinski, 1954), maybe the most important formula pertaining to spiraling is presented. Later known as the "crooked-hole country formula" (Gaynor et al., 2001), it relates the amplitude of the spiral to the gauge between the drill collars and the borehole: the maximum amplitude of the spiral is in fact half the overgauge. Field measurements have shown, however, that the amplitude of the spiral does not always correspond to this technological upper bound (Bellay et al., 1996; Sugiura and Jones, 2008b): there is likely another limiting phenomenon. In the present research, it is advanced that the spiral amplitude is directly related to the saturation of the bit tilt, as observed experimentally (Pastusek et al.,

2005; Ernst et al., 2007).

Empirical approaches based on field observations have been proposed to mitigate spiraling. The use of drill bits with longer gauge naturally limits the bit propensity to drill laterally and to initiate the spiral (Gaynor et al., 2001; Chen et al., 2002a; Al-Suwaidi et al., 2003; Sugiura and Jones, 2008b; Dupriest and Sowers, 2009). The geometry of the gauge has also been shown to influence the quality of the borehole (Dupriest and Sowers, 2009): in a recent study tapered and undercut gauges seem to present a larger tendency to induce spiraled holes (Sugiura and Jones, 2008b). Finally point-the-bit systems are less likely to spiral than push-the-bit ones as the deviation of the borehole is induced by a kink of the BHA and relies less on the lateral-cutting properties of the bit. It can thus work with longer-gauge bits without altering the steering potential of the system (Stroud et al., 2004).

To date, only a handful of papers have focused on analyzing borehole oscillations analytically, yet for planar trajectories. The self-perpetuating nature of the spiral was discussed first by Pastusek and Brackin (2003), who described how the geometry of the BHA could lead to a growing oscillating pattern in the borehole trajectory. Downton (2007) demonstrated that a rigid BHA — *i.e.*, a BHA with a theoretically infinite stiffness — having three point contacts with the borehole is always directionally unstable, *i.e.*, tends to produce spiraled holes, except for a few discrete configurations. Downton further showed that the system could be made directionally stable with the addition of a flexible element in the BHA. Finally, Detournay and Perneder (2011) and Perneder (2013) proved, with an analytical model of planar borehole propagation, that a deformable BHA is directionally stable provided that the active weight on bit (the WOB reduced by the axial force transmitted by wear flats) is sufficiently large.

Chapter 3

Components of the Model

The directional tendency of the drilling system hinges on the interaction between two objects: a geometrical one, the evolving borehole, and a mechanical one, the BHA, which is constrained to deform within the wellbore. From the deflection of the BHA, the force and moment at the bit are computed. From this force and moment, the bit kinematics are determined, in relation to its rock-cutting properties. From the bit motion, the local borehole geometry is extracted and the computation of the force at the bit updated. Consequently, the model is formulated from considerations involving three components (Detournay, 2009; Perneder, 2013; Perneder and Detournay, 2013b): (a) a bit/rock interaction law that describes the relation between the force and moment applied on the bit and its penetration into the rock; (b) kinematic relationships that relate the bit motion to the local borehole geometry; and (c) a model for the BHA that computes the force and the moment acting on the bit from the deflection of the BHA, subjected not only to its own external loading, but also to constraints arising from its interaction with the wellbore (Fig. 3.1).

The model is formulated at the length scale of the BHA, $O(10\text{ m})$. Modeling the drilling system up to a few stabilizers behind the bit is justified by the fact that the lateral force and moment at the bit are influenced predominantly by the BHA components and contact points with the borehole closest to the bit (Perneder, 2013). Indeed the interaction of the rest of the drillstring with the borehole mainly impact the transmission of the axial force and the

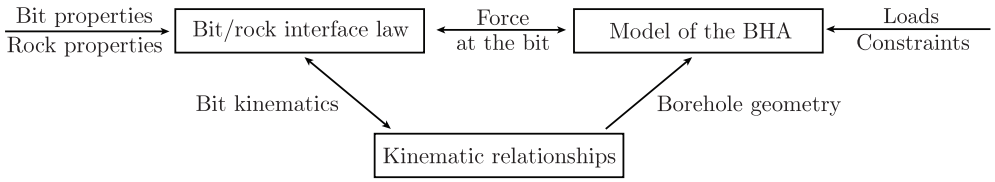

Figure 3.1: Three coupled components of the model of borehole propagation: a bit/rock interaction law, kinematic relationships, and a model for the BHA.

torque. The influence of the drillstring is thus accounted for here through a force and a moment imposed at the upper boundary of the BHA. They are theoretically obtained from so-called torque-and-drag models (Ho, 1988; Aarrestad and Blikra, 1994; Aadnoy and Andersen, 1998; Menand et al., 2006; Denoël and Detournay, 2011; Huynen et al., 2014), the main objective of which is to quantify the transmission of the loads from the rig to the bit (or in this case, to the last modeled stabilizer). To do so, they focus on identifying the evolution and nature of the contacts between the drillstring and the wellbore, from which the variation of force and moment along the drillstring is computed. The drillstring is usually modeled as a rod or *elastica*, as large displacements need to be considered.

The resulting axial force is assumed to be known with sufficient accuracy and to be small enough not to cause buckling of the drill collars while the influence of the torque is neglected, following the assumed rate-independence of the bit/rock interaction law. The lower boundary condition of the model is given by the bit/rock interaction law, as the drill bit is collapsed onto a point at the lower extremity of the BHA; the bit dimensions, $O(10\text{ cm})$, are indeed negligible at the scale of the model. The derivation of the interaction law requires, however, to account for the geometry and properties of the bit.

The model of borehole propagation is then formulated at an *intermediate* length scale, where the phenomena occurring at the other ones – the interaction of the drillstring with the borehole and the cutting process at the bit – are lumped into boundary conditions.

3.1 General Assumptions

The borehole propagation model is constructed by considering the coupling between three components. Its formulation also relies on the following general assumptions:

- The directional tendency is still captured even if the drilling process is averaged over several rotations of the drilling structure. This is a consequence not only of the time scale separation between dynamic processes and the global directional evolution, but also of the length scale separation between the (axial) penetration per revolution of the bit and the resolution of the model. Indeed, downhole dynamics have frequencies related to or smaller than the bit revolution, $O(10 \sim 100 \text{ rpm})$ (Richard et al., 2007; Germay et al., 2009), while the borehole directional tendency is defined over hundreds of them. Similarly, the resolution of the model, $O(10 \text{ cm})$ as the bit is collapsed onto a point, is significantly larger than the penetration per revolution, $O(1 - 10 \text{ mm})$. The instantaneous resultants of the force and moment at the bit are then irrelevant when studying the propagation of a borehole; only values averaged over several revolutions are relevant when formulating a directional drilling model.

- Downhole dynamics do not influence the global directional evolution of the borehole, *i.e.*, it is assumed that the resultants of the dynamic fluctuations of the force and the moment at the bit are zero on average. Furthermore, any borehole enlargements, such as those caused by drilling-fluid or downhole dynamics—*e.g.*, bit/BHA whirl—are presently not considered. (It may be conceived, however, that nonzero components, if known, could be lumped into parameters of the model such as additional components to the force and moment at the bit, or even borehole over-gauging if included later in the model.)

- The directional stability of the drilling system and the establishment of a regime of self-excited oscillations are rate-independent for the typical range of rotation speeds encountered in the field— *i.e.*, they do not depend on the angular velocity of the bit. This is a consequence of the averaging process and the assumed independence of the bit/rock interface law with respect to the bit angular velocity: the reaction force on the bit primarily depends on the volume of rock shaved from the formation, not on the rate at which it

is performed (Detournay et al., 2008; Franca, 2010). In particular, Franca (2010) shows that for a constant depth of cut, the torque on bit is independent of the angular velocity. Hence, the borehole length is the appropriate variable to track the evolution of the system — not time spent drilling. It also means that the model is quasi-static.

3.2 Geometry

Due to its slenderness[1], the borehole can be seen globally as a one-dimensional object that is described by its axis, a three-dimensional curve in Cartesian reference system ($\boldsymbol{e}_x$,$\boldsymbol{e}_y$,$\boldsymbol{e}_z$), with $\boldsymbol{e}_z$ pointing in the direction of gravity (Fig. 3.2). This curve is defined by vector $\boldsymbol{R}(S)$ of curvilinear coordinate S along the borehole, with $S = 0$ at the rig and $S = L$ at the bit. Parameter L thus indicates the current length of the borehole. For a smooth trajectory, the tangent to the borehole

$$\boldsymbol{I}_1(S) = \frac{\mathrm{d}\boldsymbol{R}}{\mathrm{d}S} \tag{3.1}$$

uniquely defines its inclination $\Theta(S) \in [0, \pi]$ and azimuth $\Phi(S) \in [0, 2\pi)$ (Fig. 3.2a). The inclination is measured with respect to $\boldsymbol{e}_z$, *i.e.*, a vertical borehole has zero inclination, and the azimuth clockwise respective to $\boldsymbol{e}_x$ from the projection of $\boldsymbol{I}_1$ in horizontal plane ($\boldsymbol{e}_x$,$\boldsymbol{e}_y$). (The azimuth is undetermined for $\Theta = 0$.) The local borehole reference system ($\boldsymbol{I}_1$,$\boldsymbol{I}_2$,$\boldsymbol{I}_3$) is defined with $\boldsymbol{I}_2$ in the same vertical plane as $\boldsymbol{I}_1$, and $\boldsymbol{I}_3 = \boldsymbol{I}_1 \times \boldsymbol{I}_2$. In ($\boldsymbol{e}_x$,$\boldsymbol{e}_y$,$\boldsymbol{e}_z$), coordinates of $\boldsymbol{I}_1$, $\boldsymbol{I}_2$, and $\boldsymbol{I}_3$ read

$$\boldsymbol{I}_1 = (\sin\Theta\cos\Phi; \sin\Theta\sin\Phi; \cos\Theta), \tag{3.2}$$

$$\boldsymbol{I}_2 = (\cos\Theta\cos\Phi; \cos\Theta\sin\Phi; -\sin\Theta), \tag{3.3}$$

$$\boldsymbol{I}_3 = (-\sin\Phi; \cos\Phi; 0). \tag{3.4}$$

Similarly, a local reference system ($\boldsymbol{i}_1$,$\boldsymbol{i}_2$,$\boldsymbol{i}_3$) attached to the point of reference of the bit is introduced. The point of reference is the arbitrarily chosen point along the bit axis at which the bit/rock interaction law is computed. (For practical purposes, this point can be chosen to

[1] A *deep* borehole has a length of the order of $O(10^3$ m) while its diameter is related to that of the drill bit, $O(10^{-1}$ m); this leads of a slenderness of the order of $O(10^4)$, equivalent to that of a (long) human hair or a guitar string. In that sense, the borehole can be qualified as having a dimension of $1 + \epsilon$ where ϵ is a small number defined as the inverse of the slenderness [This concept has been formerly introduced by Detournay].

be at the *center* of the cutting structure.) It also corresponds to the lower extremity of the BHA in the model, where the boundary conditions are imposed, once the bit is collapsed onto a point. The trajectory of the point of reference defines then the borehole axis. The local reference system is defined in such a way that $\boldsymbol{i}_1$ is on the bit axis of symmetry and pointing ahead of the bit, $\boldsymbol{i}_2$ is in the same vertical plane as $\boldsymbol{i}_1$, and $\boldsymbol{i}_3 = \boldsymbol{i}_1 \times \boldsymbol{i}_2$. Vector $\boldsymbol{i}_1$ defines bit inclination θ and azimuth ϕ (Fig. 3.2b). Substituting θ and ϕ for Θ and Φ in (3.2)-(3.4) expresses system $(\boldsymbol{i}_1,\boldsymbol{i}_2,\boldsymbol{i}_3)$ in reference frame $(\boldsymbol{e}_x,\boldsymbol{e}_y,\boldsymbol{e}_z)$.

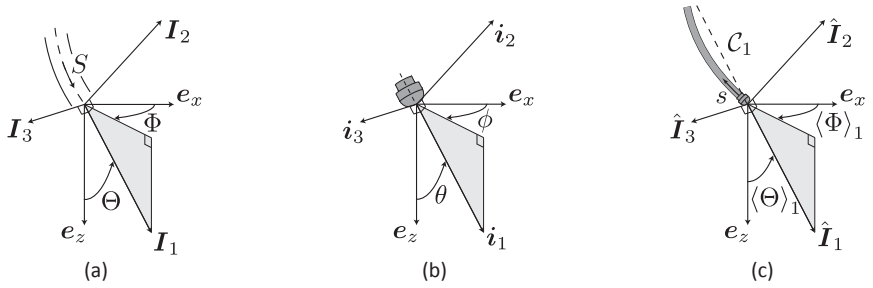

Figure 3.2: Definition of the systems of reference attached (a) to the borehole, (b) to the bit, and (c) to the first section of the BHA. Related nomenclature for the inclinations and azimuths in Cartesian system $(\boldsymbol{e}_x,\boldsymbol{e}_y,\boldsymbol{e}_z)$.

At the scale of the borehole, the centerline of the BHA can be seen as a small perturbation to the borehole axis owing to the small clearance between the BHA and the borehole, $O(1\text{ cm})$, respective to the length scale of the problem. The relative orientation of reference systems $(\boldsymbol{I}_1,\boldsymbol{I}_2,\boldsymbol{I}_3)$ and $(\boldsymbol{i}_1,\boldsymbol{i}_2,\boldsymbol{i}_3)$ at the bit is thus small and is quantified by the so-called bit tilt, the angle between $\boldsymbol{i}_1$ and $\boldsymbol{I}_1$. The magnitude and *orientation* of the tilt provide the kinematic information required at the scale of the bit to describe the local borehole geometry: Combined with the bit profile, the tilt is also a measure of borehole overgauge, *i.e.*, a way to qualify, in combination with downhole dynamics, the borehole cross section. Any zero-tilt trajectory, for example a theoretically straight vertical borehole, would have a nominal diameter corresponding to that of the bit once the influence of downhole dynamics is neglected. But as soon as $\boldsymbol{i}_1$ is not aligned with $\boldsymbol{I}_1$, the tilt creates a slight overgauge, approximately proportional to the tilt and the length of the bit gauge (Detournay, 2009; Perneder, 2013).

Finally, a third reference system $(\hat{\boldsymbol{I}}_1,\hat{\boldsymbol{I}}_2,\hat{\boldsymbol{I}}_3)$ is defined respective to the BHA, with $\hat{\boldsymbol{I}}_1$ aligned

with chord $\mathcal{C}_1$, which is delimited by the point of reference of the bit and the position of the first stabilizer. The position of the latter in ($\boldsymbol{e}_x$,$\boldsymbol{e}_y$,$\boldsymbol{e}_z$) is given by $\boldsymbol{r}(s_1, L)$, where s_i is the position of the i^{th} stabilizer behind the bit — taken respective to its center — measured along curvilinear s of the BHA, with $s = 0$ at the bit and evolving opposite to S. As axial deformations of the BHA, $O(10^{-4})$, are negligible and the first stabilizer is assumed, on average, to be centered within the borehole, position $\boldsymbol{r}(s_1, L)$ can be replaced advantageously by $\boldsymbol{R}(S_1)$, where S_1 is the position of the first stabilizer measured along S, *i.e.*, $s_1 \simeq L - S_1$. Vector $\hat{\boldsymbol{I}}_2$ is in the same vertical plane as $\hat{\boldsymbol{I}}_1$, and $\hat{\boldsymbol{I}}_3 = \hat{\boldsymbol{I}}_1 \times \hat{\boldsymbol{I}}_2$ (Fig. 3.2c). Inclination and azimuth of chord $\mathcal{C}_1$ are given respectively by $\langle\Theta\rangle_1$ and $\langle\Phi\rangle_1$.

Reference system ($\boldsymbol{I}_1$,$\boldsymbol{I}_2$,$\boldsymbol{I}_3$) tracks the borehole geometry. The bit/rock interaction law is described respective to ($\boldsymbol{i}_1$,$\boldsymbol{i}_2$,$\boldsymbol{i}_3$), and the force and moment acting on the BHA are computed in basis ($\hat{\boldsymbol{I}}_1$,$\hat{\boldsymbol{I}}_2$,$\hat{\boldsymbol{I}}_3$). The difference between these reference frames is usually small, as their relative orientation is defined by angles of about the same magnitude as the tilt— *i.e.*, of the order of $O(0.1 - 1^\circ)$. Accounting for this relative orientation unnecessarily complicates the equations of propagation. This distinction then is neglected when balancing the expressions for the force and moment at the bit, expressed within the BHA and bit/rock interaction models. Nevertheless, the tilt remains explicitly in the interface law. For similar reasons, it is also assumed that $\sin\Theta \simeq \sin\theta \simeq \sin\langle\Theta\rangle_1$ when projecting azimuths in the inclined planes defined by the inclinations of the bit, borehole, or chord $\mathcal{C}_1$, respectively.

3.3 Bit/Rock Interaction Law

The bit/rock interaction law describes the relation between the force and moment acting on the bit and its kinematics (Ho, 1987; Perneder et al., 2012). As the force and moment are understood as being averaged over at least one revolution of the drilling structure, the related kinematic quantities define the motion of the bit/rock interface over one revolution of the bit as well: they are referred to as penetrations per revolution and characterize the translation and the change of orientation of the bit/rock interface over one bit revolution[2].

[2] The bit/rock interaction law described here is consequently ill-suited to handle processes occurring on a time scale smaller than that of the bit revolution. Downhole dynamics cannot be studied then using this *averaged* bit/rock interaction law.

In the context of the present work, the bit/rock interaction law pertains to PDC bits drilling in isotropic and homogeneous formations. The general theoretical framework for deriving it has already been described in depth elsewhere (Perneder et al., 2012). This section summarizes thus the key notions and assumptions leading to the determination of the general linear bit/rock interaction law used in the global model of propagation.

3.3.1 Bit Kinematics

The bit kinematics are defined by its instantaneous velocity $\boldsymbol{v}$ and spin $\boldsymbol{\omega}$, the latter defined as being orthogonal to the bit axis (Fig. 3.3a). The rotation of the bit around $\boldsymbol{i}_1$ is characterized by angular velocity $\boldsymbol{\Omega}$, which does not influence, however, the motion of the bit/rock interface. Denoting Ω the magnitude of $\boldsymbol{\Omega}$, *i.e.*, $\boldsymbol{\Omega} = \Omega \boldsymbol{i}_1$, penetration vector $\boldsymbol{d}$ and angular penetration vector $\boldsymbol{\varphi}$ are given by[3]

$$\boldsymbol{d} = \frac{2\pi \boldsymbol{v}}{\Omega}, \quad \text{and} \quad \boldsymbol{\varphi} = \frac{2\pi \boldsymbol{\omega}}{\Omega}. \tag{3.5}$$

In reference system ($\boldsymbol{i}_1$,$\boldsymbol{i}_2$,$\boldsymbol{i}_3$), these vectors decompose into axial penetration $\boldsymbol{d}_1$, lateral penetrations $\boldsymbol{d}_2$ and $\boldsymbol{d}_3$, and angular penetrations $\boldsymbol{\varphi}_2$ and $\boldsymbol{\varphi}_3$ when projected on the system axes (Fig. 3.3b). Penetration $\boldsymbol{d}$ defines the drilling direction at the bit, *i.e.*, it defines tangent $\boldsymbol{I}_1$ to the borehole axis: $\boldsymbol{d} = d\boldsymbol{I}_1$ where $d = \sqrt{d_1^2 + d_2^2 + d_3^2}$ is the norm of $\boldsymbol{d}$. Angular penetration $\boldsymbol{\varphi}$ characterizes the instantaneous change of orientation of the bit. Even though $\boldsymbol{d}$ and $\boldsymbol{\varphi}$ are still understood as *velocities*, they measure change *per revolution* of the bit.

The drill bit is also subjected to force $\boldsymbol{F}$, moment $\boldsymbol{M}$, and torque $\boldsymbol{C}$ ($\boldsymbol{C}$ is perpendicular to $\boldsymbol{M}$), resulting from the reaction of the drilling process onto the bit. When decomposed in ($\boldsymbol{i}_1$,$\boldsymbol{i}_2$,$\boldsymbol{i}_3$), force $\boldsymbol{F}$ has one axial and two lateral components, respectively denominated F_1, F_2, and F_3 (Fig. 3.3b). Because of the convention adopted for $\boldsymbol{i}_1$, $F_1 = -W$, where W denotes the weight on bit. Similarly, the moment is defined by its components M_2 and M_3 along axes $\boldsymbol{i}_2$ and $\boldsymbol{i}_3$. (Reaction torque $C = -T$ where T is the torque on bit, does not affect the bit trajectory.)

[3] Penetration vector $\boldsymbol{d}$ is not coaxial with resultant for $\boldsymbol{F}$ because of the bit rotation (this phenomenon is called the walk). However angle ϖ between $\boldsymbol{d}$ and $\boldsymbol{F}$ is assumed to be independent of the angular velocity for the range of velocities relevant to drilling applications. Therefore, penetration vector $\boldsymbol{d}$ and angular penetration vector $\boldsymbol{\varphi}$ are themselves dependent on $\boldsymbol{\Omega}$, but presumably not on its magnitude.

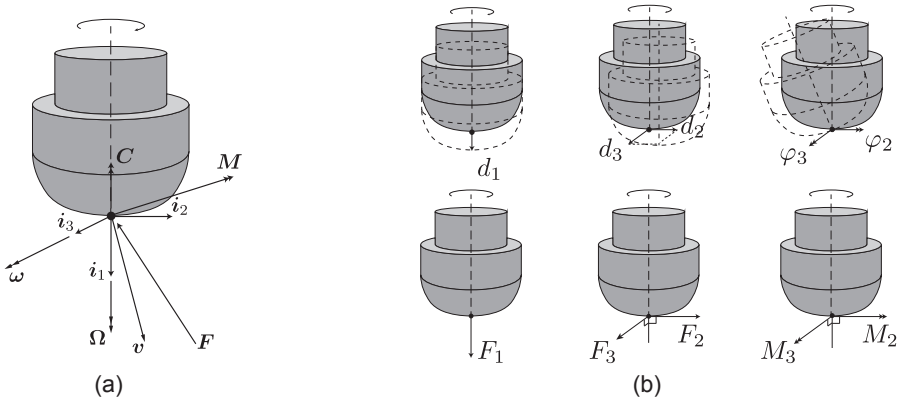

Figure 3.3: (a) Kinematics of the drill bit. (b) Projections of the force and moment at the bit, and the related penetrations per revolution in reference system ($\boldsymbol{i}_1$,$\boldsymbol{i}_2$,$\boldsymbol{i}_3$) attached to the bit.

The bit/rock interface law describes the relationship

$$\boldsymbol{\mathcal{F}} = \mathcal{L}(\boldsymbol{\mathcal{P}}), \tag{3.6}$$

where $\boldsymbol{\mathcal{F}} = (F_1, F_2, F_3, M_2, M_3)$ is the vector of the generalized forces, $\boldsymbol{\mathcal{P}} = (d_1, d_2, d_3, \varphi_2, \varphi_3)$ is the vector of the generalized penetrations, and $\mathcal{L}(\cdot)$ is a tensorial operator, which depends both on bit and rock properties and on the interaction pattern between the bit gauge and the wellbore. Theoretically, this operator is derived by integrating and averaging the local forces on each cutter of the bit under kinematically controlled conditions. Alternatively, laboratory experiments can provide such laws for any drill bit.

3.3.2 Single-Cutter/Rock Bilinear Law

The bit/rock interaction law is here constructed assuming a bilinear single-cutter/rock interaction law that captures the main features of the interaction between a single bit cutter and the rock formation (Detournay and Defourny, 1992). This general law has been abundantly validated by experimental observations from *scratch tests* (Detournay et al., 2008).

An isolated cutter is submitted to two sets of forces due to the existence of two distinct surfaces interacting with the rock: the cutting face and the wearflat, the latter being subparallel to cutter velocity $\boldsymbol{V}$ (Fig. 3.4a). As suggested by experiments, two distinct ductile regimes can be identified for depths of cuts relevant for drilling applications, *i.e.*, ranging between 0.1 and

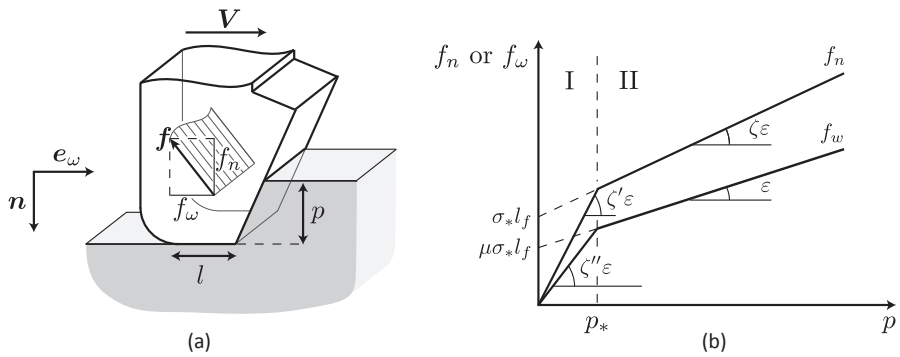

Figure 3.4: (a) Two contact surfaces between the cutter and the rock: the cutting face and the wearflat [adapted from Perneder (2013)]. (b) Bilinear single-cutter/rock interface law due to the saturation of the contact forces for a critical depth of cut p_*.

2 mm per revolution[4] (Detournay and Defourny, 1992; Detournay et al., 2008). In Regime I at small depths of cut p, both the cutting forces at the cutting face and the contact forces along the wearflat are proportional to p. However beyond critical depth of cut p_*, the contact forces saturate and only the cutting forces keep increasing with p (Fig. 3.4b). The regimes are thus contact- and cutting-dominated, respectively.

The cutter is assumed to be large enough respective to the depth of cut for the resultant force to be proportional to its width; the normal and tangent components of force on the cutter (for a unit cutter width) are given by

$$f_n = \zeta' \iota p, \quad f_w = \zeta'' \iota p, \quad p < p^* \quad \text{(Regime I)},$$

$$f_n = \sigma_* l + \zeta \iota p, \quad f_w = \upsilon \sigma_* l + \iota p, \quad p > p^* \quad \text{(Regime II)},$$

where ι is the intrinsic specific energy of the rock — *i.e.*, the amount of energy necessary to drill a unit volume of rock without any frictional contribution[5], σ_* is the maximum contact stress at the cutter wearflat, l is the nominal length of the wearflat, υ is the coefficient of friction at

[4] For larger depths of cut, there exists a third, brittle regime called *chipping* where the cutting process is characterized by the formation of rock fragments called chips, by reference to the name given to waste from turning operations.

[5] This energy (usually expressed in J/cm^3 or MPa) refers to the energy required to drill a unit volume of rock when only a *pure* cutting process is involved. In laboratory testing at atmospheric pressure, this parameter has been shown to correlate to the unconfined compressive strength (UCS) of the rock (Richard et al., 2012). However downhole, it also depends on the mud pressure (Zijsling, 1987; Detournay and Atkinson, 2000) but the influence of the inclination of the cutter is weak for the typical range of rake angles on PDC bits (Coudyzer and Richard, 2005).

the wearflat/rock interface, and ζ, ζ' and ζ'' are coefficients that define the single-cutter/rock bilinear law and mainly depend on the relative inclination of the wearflat and of the cutting face on the cutter velocity, V [6](Detournay et al., 2008; Zhou and Detournay, 2014). This law hardly depends on the velocity of the cutter (Detournay et al., 2008; Franca, 2010), which justifies the rate-independence of the model.

3.3.3 General Construction of the Bit/Rock Interface Law

The passage from the single-cutter/rock interaction law to the general bit/rock interaction one consists in averaging and integrating the distributed forces on each bit cutter under given kinematically controlled conditions. Because of the complex cutter distribution on PDC bits, the concept of *equivalent blade* is introduced (Perneder et al., 2012): the cutter distribution is lumped into a unique blade along the bit profile whose properties (which do not have to be uniform along the blade) are in such a way that, when all the local forces along the blade are integrated and averaged over one revolution, the resultant generalized forces are the same as those that would have been computed by coalescing the influence of each individual cutter. As the equivalent blade can also be seen as a continuous cutter, the transition from the single-cutter/rock to the bit/rock interface law is conceptually trivial.

The force density along the equivalent blade is computed from the local penetration distribution, obtained from penetration vector $\boldsymbol{d}$ and angular penetration vector $\boldsymbol{\varphi}$. The local forces are then integrated along the blade, averaged over one revolution, and lumped onto a force and a moment at the point of reference of the bit to obtain the bit/rock interaction law for the imposed kinematic.

By assuming that the bit gauge interacts with the rock in Regime I and the cutting structure in Regime II, the bit/rock interaction law takes the following linear form, which captures the

[6] Parameter ζ is $O(1)$ and ζ' and ζ'' are $O(10)$ (Detournay et al., 2008). Parameter ζ, ζ', ζ'', and υ are not independent theoretically; they are related by relation $\upsilon\zeta' = \zeta'' - 1 + \upsilon\zeta$ (Fig. 3.4b).

main directional features of PDC bits

$$\begin{Bmatrix} F_1 \\ F_2 \\ F_3 \\ M_2 \\ M_3 \end{Bmatrix} = - \begin{Bmatrix} G_1 \\ 0 \\ 0 \\ 0 \\ 0 \end{Bmatrix} - \begin{bmatrix} H_1 & 0 & 0 & 0 & 0 \\ 0 & H_2 & H_3 & 0 & 0 \\ 0 & -H_3 & H_2 & 0 & 0 \\ 0 & 0 & 0 & H_4 & H_5 \\ 0 & 0 & 0 & -H_5 & H_4 \end{bmatrix} \begin{Bmatrix} d_1 \\ d_2 \\ d_3 \\ \varphi_2 \\ \varphi_3 \end{Bmatrix}. \tag{3.7}$$

Terms G_1 and H_i depend on the bit geometry, on the equivalent blade properties, on the rock strength, and on the parameters of the single-cutter/rock interaction law (Perneder et al., 2012). As they relate (averaged) force and moment to penetrations per revolution, terms H_i can be interpreted as damping coefficients.

According to (3.7), the axial force at the bit is uncoupled from the lateral force and the moment. There is coupling, however, between F_2 and F_3 through off-diagonal term H_3 and between M_2 and M_3 through H_5. (See Appendix A for the evaluation of the coefficients of the interface law for an idealized cylindrical bit.) Axial penetration d_1 is proportional to active weight W_a, defined as

$$W_a = -F_1 - G_1 = W - G_1. \tag{3.8}$$

Active weight W_a is the weight on bit reduced by $G_1 \geq 0$, the axial resultant of the contact forces at the cutters wearflats. Parameter G_1 represents thus the part of the weight on bit that is mobilized in contact forces and does not directly participate in the drilling process; W_a is the effective part of the weight on bit actually used to drill the rock. Saturation resultant force G_1 is mainly related to the state of wear of the bit (theoretically to the nominal length of the wearflats) and the rock strength. For an ideal sharp bit, $G_1 = 0$ and the strength of the rock does not directly influence the borehole geometry. (It still influences the depth of cut, the rate of penetration, and downhole dynamics.) Downhole pressure also indirectly influences G_1, as it modifies the apparent rock strength. The fundamental distinction between the weight on bit and the active weight is not generally recognized in the Industry.

3.4 Kinematic Relationships

The penetration variables are related kinematically to the local borehole geometry. A first set of relations pertains to the bit attitude relative to the local borehole orientation, measured by the relative orientation of tangent $\boldsymbol{I}_1$ to the borehole axis to that of the bit axis of symmetry $\boldsymbol{i}_1$.

Penetration vector $\boldsymbol{d}$, also tangent to the borehole, has components (d_1, d_2, d_3) in reference frame ($\boldsymbol{i}_1$,$\boldsymbol{i}_2$,$\boldsymbol{i}_3$) (Fig. 3.3b). In that frame, the tilt is defined by two small angles in terms of the penetrations according to

$$\psi_2 \simeq -\frac{d_2}{d_1}, \quad \psi_3 \simeq -\frac{d_3}{d_1}, \tag{3.9}$$

where the small-angle approximation for a tangent has been used owing to $d_2 \ll d_1$ and $d_3 \ll d_1$ under normal drilling conditions. These angles correspond to the relative inclinations of the projections of $\boldsymbol{d}$ in planes ($\boldsymbol{i}_1$,$\boldsymbol{i}_2$) and ($\boldsymbol{i}_1$,$\boldsymbol{i}_3$), respectively (Fig. 3.5). They are measured from $\boldsymbol{i}_1$ and around $-\boldsymbol{i}_3$ and $\boldsymbol{i}_2$, respectively: *Positive* lateral penetrations thus correspond to *negative* tilts but tend to increase both the borehole inclination and azimuth.

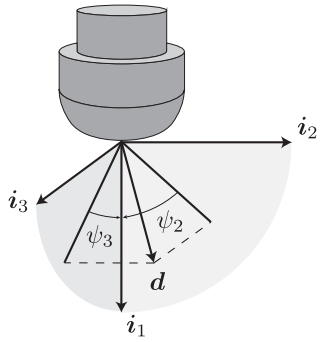

Figure 3.5: Definition of tilt angles ψ_2 and ψ_3 by projecting penetration vector $\boldsymbol{d}$ onto planes ($\boldsymbol{i}_1$,$\boldsymbol{i}_2$) and ($\boldsymbol{i}_1$,$\boldsymbol{i}_3$) attached to the bit. [Due to the sign convention, both angles are negative on this figure.]

In Cartesian system ($\boldsymbol{e}_x$,$\boldsymbol{e}_y$,$\boldsymbol{e}_z$), $\boldsymbol{i}_1$ and $\boldsymbol{I}_1$ are fully described in terms of their inclinations, θ and Θ, and azimuths, ϕ and Φ, according to (3.2). Systems ($\boldsymbol{e}_x$,$\boldsymbol{e}_y$,$\boldsymbol{e}_z$) and ($\boldsymbol{i}_1$,$\boldsymbol{i}_2$,$\boldsymbol{i}_3$) are then related by rotation matrix R

$$\left\{ \begin{array}{c} \boldsymbol{i}_1 \\ \boldsymbol{i}_2 \\ \boldsymbol{i}_3 \end{array} \right\} = R \left\{ \begin{array}{c} \boldsymbol{e}_x \\ \boldsymbol{e}_y \\ \boldsymbol{e}_z \end{array} \right\}, \tag{3.10}$$

with

$$R = \begin{bmatrix} \sin\theta\cos\phi & \sin\theta\sin\phi & \cos\theta \\ \cos\theta\cos\phi & \cos\theta\sin\phi & -\sin\theta \\ -\sin\theta & \cos\phi & 0 \end{bmatrix}. \tag{3.11}$$

In ($\boldsymbol{i}_1$,$\boldsymbol{i}_2$,$\boldsymbol{i}_3$), vector $\boldsymbol{I}_1$ has thus coordinates

$$\boldsymbol{I}_1 = \begin{Bmatrix} \cos\theta\cos\Theta + \cos(\phi-\Phi)\sin\theta\sin\Theta \\ \cos\theta\sin\Theta\cos(\phi-\Phi) - \sin\theta\cos\Theta \\ -\sin\Theta\sin(\phi-\Phi) \end{Bmatrix}. \tag{3.12}$$

Substituting components (3.12) of $\boldsymbol{I}_1$ in (3.9) and using the facts that $|\theta-\Theta| \ll 1$ and $|\phi-\Phi| \ll 1$, the projection of the tilt can be expressed at first order as a function of the bit and borehole inclinations and azimuths as

$$\psi_2 \simeq \theta - \Theta, \quad \psi_3 \simeq (\phi-\Phi)\sin\Theta. \tag{3.13}$$

Angle ψ_2 then measures the difference of inclination between $\boldsymbol{i}_1$ and $\boldsymbol{I}_1$, while ψ_3 can be seen as a proxy for the difference of azimuth.

A second set of kinematic relationships describes how the angular penetration alters the bit orientation. Angular penetrations per revolution φ_2 and φ_3 are related to the change of orientation of $\boldsymbol{i}_1$ around $\boldsymbol{i}_2$ and $\boldsymbol{i}_3$, respectively — *i.e.*, they measure how the orientation of the bit/rock interface varies with borehole length L. Mathematically, in local planes ($\boldsymbol{i}_1$,$\boldsymbol{i}_2$) and ($\boldsymbol{i}_1$,$\boldsymbol{i}_3$) attached to the bit,

$$\frac{\varphi_2}{d_1} = -\sin\theta\frac{\mathrm{d}\phi}{\mathrm{d}L}, \quad \frac{\varphi_3}{d_1} = \frac{\mathrm{d}\theta}{\mathrm{d}L}, \tag{3.14}$$

where the approximation $d \simeq d_1$ has been used, still due to $d_2 \ll d_1$ and $d_3 \ll d_1$.

Correspondence between expressions (3.9) and (3.13), as well as relations (3.14), enables to use the general bit/rock interaction law, defined in terms of the bit penetrations per revolution, in conjunction with the local borehole geometry to provide a first set of expressions for the force and moment at the bit.

3.5 Model for the Bottom-hole Assembly

The last building-block of the model is a representation of the BHA, from which a second set of expressions for the force and moment at the bit is derived. Because the borehole radius of curvature is large compared to ℓ_1, the BHA is conveniently approximated by an Euler-Bernoulli beam[7]. The force and moment at the bit are thus obtained according to this linear model as functions of the loads acting on the BHA. These generalized loads are of two kinds: (a) the external loads that directly operate on the BHA, and (b) the constraints imposed by the borehole geometry that limit its deflection.

3.5.1 Loading of the BHA

The undeformed BHA is assumed to be oriented initially along chord $\mathcal{C}_1$, delimited by the bit and the first stabilizer. Components F_1, F_2, F_3, M_2 and M_3 of the force and moment at the bit thus are expressed with respect to basis $(\hat{\boldsymbol{I}}_1,\hat{\boldsymbol{I}}_2,\hat{\boldsymbol{I}}_3)$. The BHA is equipped with n stabilizers, which delimit n sections of length ℓ_i, $i = 1, ..., n$ and n chords $\mathcal{C}_i$ with inclination $\langle\Theta\rangle_i$ and azimuth $\langle\Phi\rangle_i$ (Fig. 3.6).

Within the framework of the Euler-Bernoulli beam model, the axial equilibrium of the beam uncouples from the transversal one. Similarly, the transversal deflections of the BHA in planes $(\hat{\boldsymbol{I}}_1,\hat{\boldsymbol{I}}_2)$ and $(\hat{\boldsymbol{I}}_1,\hat{\boldsymbol{I}}_3)$ are independent and bear the same general expression, *i.e.*, the influence of a generalized load in $(\hat{\boldsymbol{I}}_1,\hat{\boldsymbol{I}}_2)$ has an identical influence as that of a similar load in $(\hat{\boldsymbol{I}}_1,\hat{\boldsymbol{I}}_3)$. These generalized loads are: (a) the relative orientation of the bit respective to $\mathcal{C}_1$, (b) the RSS force, (c) the geometrical constraints imposed by the stabilizers that need to conform to the borehole, (d) the moment they transmit, (e) the influence of gravity, and (f) the force and moment at the last stabilizer coming from the drillstring *torque and drag*.

Relative Orientation of the Bit The bit orientation, given by θ and ϕ, does not correspond in general to that of the first section of the BHA, defined by $\langle\Theta\rangle_1$ and $\langle\Phi\rangle_1$. (However, due to

[7] Drillers refer to borehole curvatures as dogleg severities, measured in degree/100 ft. Dogleg severities of 5°/100 ft are not uncommon, which correspond to a radius of curvature of about 350 m. Perneder (2013) accurately lists the conditions under which the BHA can be safely approximated by an Euler-Bernoulli beam; most of them are trivially verified under the assumption of small deformations.

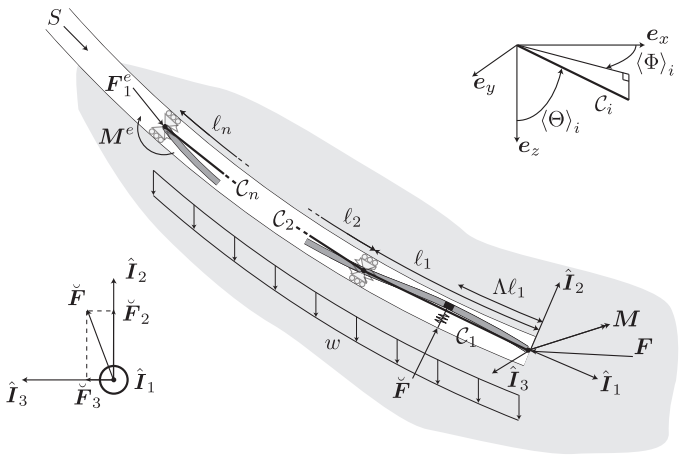

Figure 3.6: Model for the BHA. [The BHA is approximated by an Euler-Bernoulli beam; the components of the lateral force and moment at the bit can be expressed as linear combinations of the generalized loads applied on the the BHA, *i.e.*, the external loads and the constraints imposed by the borehole geometry on its deflection. Adapted from Perneder (2013).]

the large stiffness of the latter, they differ at most by an angle of the order of the tilt.) The BHA deflection needs thus to accommodate for the *prescribed* orientation of the bit. In plane $(\hat{\boldsymbol{I}}_1,\hat{\boldsymbol{I}}_2)$, the relative inclination of the bit reads $\theta - \langle\Theta\rangle_1$ while in $(\hat{\boldsymbol{I}}_1,\hat{\boldsymbol{I}}_3)$, the difference is given by $(\phi - \langle\Phi\rangle_i)\sin\langle\Theta\rangle_1$; the sine comes from the projection of the azimuth in $(\hat{\boldsymbol{I}}_1,\hat{\boldsymbol{I}}_3)$.

The explicit presence of the bit orientation in the BHA model enables to connect it to the bit/rock interaction law (and the kinematic relationships) and to extract equations for the borehole propagation.

RSS Force The pads of the push-the-bit RSS are located at a distance $\Lambda\ell_1$ behind the bit, $\Lambda \in]0,1)$, and apply on average a force $\breve{\boldsymbol{F}}$ orthogonal to $\hat{\boldsymbol{I}}_1$, which has components $\breve{F}_2$ and $\breve{F}_3$ along $\hat{\boldsymbol{I}}_2$ and $\hat{\boldsymbol{I}}_3$, respectively (Fig. 3.6).

Rotary steerable systems influence the borehole propagation, but can also trigger spiraled holes: In field data related to BHAs equipped with a common class of push-the-bit RSS, the pitch of the spirals corresponds to the distance between the bit and the pads (Sugiura and Jones, 2008b; Marck et al., 2014). This influence is not well understood (Dupriest and Sowers, 2009); but despite the scarcity of technical details about internal mechanisms and control algorithms

of RSSs, it is evident that significant differences exist in their actuation principles (Barr et al., 1995). Indeed, different systems impose different lateral constraints on the deflection of the BHA at the level of their pads, depending on how they adapt to and interact with the wellbore. In the literature, some models and descriptions represent push-the-bit RSSs as an imposed eccentricity (Neubert and Heisig, 1996; Downton, 2007; Sugiura and Jones, 2008b), while others lump the RSS into a known external force (Barr et al., 1995; Dupriest and Sowers, 2009; Perneder, 2013; Perneder and Detournay, 2013b).

The simple approach used here bridges these two extreme cases: the lateral constraint imposed by the RSS pads is modeled as a pre-stressed elastic spring, resulting in a variation of the resultant RSS force with the relative deflection of the BHA in the borehole at the level of the pads. The attribution of a lateral stiffness to the pads then is consistent with their characterization in the literature for two limiting cases: a zero stiffness corresponds to an imposed force, and an infinite one to an imposed eccentricity. A push-the-bit RSS with pads that strongly constrain the deflection of the BHA behaves thus as a pseudo-stabilizer with a known eccentricity. In contrast, pads that adapt smoothly to any perturbation in the borehole trajectory can be viewed as simply applying a controlled lateral force on the BHA.

With the RSS modeled as a prestressed spring, current force $\breve{\boldsymbol{F}}_t$ at the level of the pads is given by

$$\breve{\boldsymbol{F}}_t = \breve{\boldsymbol{F}} - K(\boldsymbol{y} - \boldsymbol{y}_r), \tag{3.15}$$

where $\breve{\boldsymbol{F}}$ is the initially-set RSS force that corresponds to initial relative deflection $\boldsymbol{y}_r$[8]; $\boldsymbol{y}$ is the current relative deflection of the BHA axis on that of the borehole (defined in such a way that a larger *positive* $\breve{\boldsymbol{F}}$ tends to reduce $\boldsymbol{y}$), and K is the stiffness of the equivalent spring. The total force at the RSS thus has two components: one that is set, and another that reacts to local perturbations in the borehole geometry. The latter component is proportional to a stiffness K, a quantity that is assumed to embody the actuation mechanism as well as the control algorithm

[8] Relative initial deflection $\boldsymbol{y}_r$ also depends on the other generalized loads: it is by definition the relative deflection of the BHA at the level of the RSS pads right after the prescribed force is imposed. Reference deflection $\boldsymbol{y}_r$ does not influence the directional stability of the system if it can be assumed to be constant or slowly varying. It is, however, an important parameter when propagating the borehole, because it can be related to the time or distance that the pads take to adapt to the wellbore. The evolution of $\boldsymbol{y}_r$ can be in principle related to RSS control algorithms; a more accurate representation of its evolution may open the way to designing more efficient control schemes. The fact that current servo-controllers are not always effective in mitigating borehole oscillations is corroborated by field data (Sugiura and Jones, 2008b; Marck et al., 2014).

of the pads. Little information is known about the magnitude of rigidity K; however, it enables the transition between two extreme cases: an imposed eccentricity or an imposed force.

Constraints Imposed by the Stabilizers The deflection of the BHA is constrained by the position of the stabilizers, which need to conform to the borehole trajectory. It is assumed that the stabilizers (with the bit) are the only contact points between the BHA and the borehole, and that, on average, they are centered on the borehole axis. (The influence of the stabilizer undergauge on the directional stability is then not considered.) Their positions along the BHA are computed respective to the point of reference of the bit.

The conformity of the stabilizer positions is enforced through the averaged orientations of the BHA sections. The position of the i^{th} stabilizer behind the bit is given by $L - S_i$ or s_i when measured along curvilinear coordinates S or s of the borehole or of the BHA, respectively. Due to the BHA negligible axial compressibility and its small relative deflection, $L - S_i \simeq s_i$. Therefore, the isoperimetric constraints that impose the relative positions of the stabilizers can be expressed equivalently in terms of the BHA or borehole inclinations and azimuths, *i.e.*,

$$\langle\theta\rangle_i = \frac{1}{\ell_i}\int_{s_{i-1}}^{s_i} \theta(s)\,\mathrm{d}s \simeq \frac{1}{\ell_i}\int_{S_i}^{S_{i-1}} \Theta(S)\,\mathrm{d}S = \langle\Theta\rangle_i\,, \tag{3.16}$$

$$\langle\phi\rangle_i = \frac{1}{\ell_i}\int_{s_{i-1}}^{s_i} \phi(s)\,\mathrm{d}s \simeq \frac{1}{\ell_i}\int_{S_i}^{S_{i-1}} \Phi(S)\,\mathrm{d}S = \langle\Phi\rangle_i\,. \tag{3.17}$$

The stabilizers are also assumed to transmit a moment $[\![\boldsymbol{M}_i]\!] = \boldsymbol{M}(S_i^+) - \boldsymbol{M}(S_i^-)$ between the wellbore and the BHA that is proportional to their tilts

$$[\![M_{2,i}]\!] = -T(\phi_i - \Phi_i)\sin\langle\Theta\rangle_1\,, \qquad [\![M_{3,i}]\!] = T(\theta_i - \Theta_i), \tag{3.18}$$

where T is the stiffness of the equivalent elastic hinge, and θ_i, Θ_i, ϕ_i, and Φ_i are the BHA and borehole inclination and azimuth at the i^{th} stabilizer.

Gravity Loading Gravity loading is accounted for via (buoyant) weight per unit length w of the BHA, applied in vertical plane ($\hat{\boldsymbol{I}}_1$,$\hat{\boldsymbol{I}}_2$). Weight w is assumed to be projected uniformly along each section according to inclination $\langle\Theta\rangle_i$.

Moment at the Last Stabilizer As the model is formulated at the length scale of the BHA, the complex interaction between the drillstring and the borehole has been reduced to an axial force $\boldsymbol{F}_1^e$ and a moment $\boldsymbol{M}^e$ applied at the last (modeled) stabilizer[9].

From the uncoupling of the evolution of the axial force and the assumption that the axial friction force induced at the stabilizers is negligible (following the rotation of the BHA), the weight on bit reads

$$W = F_1^e + \sum_{i=1}^{n} \bar{w}_i \ell_i \cos \langle \Theta \rangle_i \,, \tag{3.19}$$

where weight $\bar{w}$ is the averaged weight per unit length of section i.

The moment at the last stabilizer influences the force and moment at the bit. However, this influence rapidly decreases with the number n of stabilizers as each intermediate stabilizer between the bit and the applied moment reduces its impact; from the third or fourth stabilizer, this moment can be in general safely neglected relative to the force and moment induced by the other generalized loads along the first few sections of the BHA (Perneder, 2013).

3.5.2 Lateral Force and Moment at the Bit

The BHA can be further divided into j segments ($j \geq n$) of uniform mechanical properties, numerated from the bit to the last stabilizer. These segments are delimited either by a change of drill collar geometry[10]or by particular equipments, such as stabilizers or RSS pads, that induce a discontinuity in the bending moment or the shear force. Along segment j of bending stiffness EI_j and linear weight w_j along section i, the evolution of the BHA inclination and azimuth is given by $\theta_j(s)$ and $\phi_j(s)$. To each segment, the fundamental equation of the Euler-Bernoulli beam theory applies: The bending moment is proportional to the curvature, the constant of proportionality being the bending stiffness of the segment. This relation reads

$$M_{2,k}(s) = EI_k \phi_k(s)' \sin \langle \Theta \rangle_1 \quad \text{or} \quad M_{3,k}(s) = -EI_k \theta_k(s)', \quad k = 1, ..., j, \; s \in [s_{k-1}, s_k], \tag{3.20}$$

[9] The possible presence of a lateral force is assumed to be directly absorbed by the stabilizer. The torque has been shown not to influence the drilling direction at the bit, following the assumptions of rate-independence of the bit/rock interaction law.

[10] This approach enables to account for changes in collar diameters. However, beam theory only successfully applies to elements with one characteristic dimension being an order of magnitude larger than the other two. Short elements thus should not be modeled within this framework. In the following, the smallest elements that have been explicitly represented are the stabilizers, even though they do not unquestionably pertain to the class of *beam elements*.

where s_k denotes the end of segment k along curvilinear coordinate s. The shear force and the BHA orientation verify

$$F_{2,k}(s) = -EI_k\theta_k(s)'' \quad \text{and} \quad F_{3,k}(s) = -EI_k\phi_k(s)'' \sin\langle\Theta\rangle_1 , \tag{3.21}$$

$$0 = EI_k\phi_k(s)''' \sin\langle\Theta\rangle_1 \quad \text{and} \quad w_k \sin\langle\Theta\rangle_i = EI_k\theta_k(s)'''. \tag{3.22}$$

By direct integration, the inclination and azimuth along each segment then have the following cubic expressions

$$EI_k\theta_k(s) = \frac{w_k \sin\langle\Theta\rangle_i}{6} s^3 + A_{2,k}s^2 + A_{1,k}s + A_{0,k}, \tag{3.23}$$

$$EI_k\phi_k(s)\sin\langle\Theta\rangle_1 = B_{2,k}s^2 + B_{1,k}s + B_{0,k}. \tag{3.24}$$

The beam problem consists in solving for constants $A_{i,k}$ and $B_{i,k}$ in (3.23) and (3.24) for each segment by applying the corresponding boundary conditions (Perneder, 2013). The components of the lateral force and moment at the bit are then given by

$$F_2 = F_{2,1}(0) = -2A_{2,1}, \quad F_3 = F_{3,1}(0) = -2B_{2,1}, \tag{3.25}$$

$$M_2 = M_{2,1}(0) = B_{1,1}, \quad M_3 = M_{3,1}(0) = -A_{1,1}. \tag{3.26}$$

In view of the linear nature of the Euler-Bernoulli beam theory, the lateral force and moment at the bit can ultimately be expressed as a linear combination of the external loads and constraints applied on the BHA.

$$\begin{aligned} F_2 = {} & \frac{3EI}{\ell_1^2}\mathcal{F}_b\left(\theta - \langle\Theta\rangle_1\right) + \sum_{i=1}^{n}\mathcal{F}_{w,i}w\ell_1\sin\langle\Theta\rangle_i + \mathcal{F}_r\breve{F}_2 + \frac{3EI}{\ell_1^2}\sum_{i=1}^{n-1}\mathcal{F}_{k,i}\left(\langle\Theta\rangle_i - \langle\Theta\rangle_{i+1}\right) \\ & + \frac{3EI}{\ell_1^2}\mathcal{F}_s\left(\langle\Theta\rangle_0 - \langle\Theta\rangle_1 - \frac{y_{r,2}}{\Lambda\ell_1}\right) + \frac{3EI}{\ell_1^2}\sum_{i=1}^{n}\mathcal{F}_{c,i}\left(\Theta_i - \langle\Theta\rangle_i\right) + \mathcal{F}_m\frac{M_3^e}{\ell_1}, \end{aligned} \tag{3.27}$$

$$\begin{aligned} F_3 = {} & \frac{3EI}{\ell_1^2}\mathcal{F}_b\left(\phi - \langle\Phi\rangle_1\right)\sin\langle\Theta\rangle_1 + \mathcal{F}_r\breve{F}_3 + \frac{3EI}{\ell_1^2}\sum_{i=1}^{n-1}\mathcal{F}_{k,i}\left(\langle\Phi\rangle_i - \langle\Phi\rangle_{i+1}\right)\sin\langle\Theta\rangle_1 \\ & + \frac{3EI}{\ell_1^2}\mathcal{F}_s\left(\left(\langle\Phi\rangle_0 - \langle\Phi\rangle_1\right)\sin\langle\Theta\rangle_1 - \frac{y_{r,3}}{\Lambda}\right) + \frac{3EI}{\ell_1^2}\sum_{i=1}^{n}\mathcal{F}_{c,i}\left(\Phi_i - \langle\Phi\rangle_i\right)\sin\langle\Theta\rangle_1 - \mathcal{F}_m\frac{M_2^e}{\ell_1}, \end{aligned} \tag{3.28}$$

$$M_2 = -\frac{3EI}{\ell_1}\mathcal{M}_b\left(\phi - \langle\Phi\rangle_1\right)\sin\langle\Theta\rangle_1 - \mathcal{M}_r\ell_1\breve{F}_3 - \frac{3EI}{\ell_1}\sum_{i=1}^{n-1}\mathcal{M}_{k,i}\left(\langle\Phi\rangle_i - \langle\Phi\rangle_{i+1}\right)\sin\langle\Theta\rangle_1$$
$$- \frac{3EI}{\ell_1}\mathcal{M}_s\left(\left(\langle\Phi\rangle_0 - \langle\Phi\rangle_1\right)\sin\langle\Theta\rangle_1 - \frac{y_{r,3}}{\Lambda}\right) - \frac{3EI}{\ell_1}\sum_{i=1}^{n}\mathcal{M}_{c,i}\left(\Phi_i - \langle\Phi\rangle_i\right)\sin\langle\Theta\rangle_1 + \mathcal{M}_m M_2^e, \tag{3.29}$$

$$M_3 = \frac{3EI}{\ell_1^2}\mathcal{M}_b\left(\theta - \langle\Theta\rangle_1\right) + \sum_{i=1}^{n}\mathcal{M}_{w,i}w\ell_1^2\sin\langle\Theta\rangle_i + \mathcal{M}_r\ell_1\breve{F}_2 + \frac{3EI}{\ell_1}\sum_{i=1}^{n-1}\mathcal{M}_{k,i}\left(\langle\Theta\rangle_i - \langle\Theta\rangle_{i+1}\right)$$
$$+ \frac{3EI}{\ell_1^2}\mathcal{M}_s\left(\langle\Theta\rangle_0 - \langle\Theta\rangle_1 - \frac{y_{r,2}}{\Lambda}\right) + \frac{3EI}{\ell_1}\sum_{i=1}^{n}\mathcal{M}_{c,i}\left(\Theta_i - \langle\Theta\rangle_i\right) + \mathcal{M}_m M_3^e, \tag{3.30}$$

where $\langle\Theta\rangle_0$ and $\langle\Phi\rangle_0$ are the borehole averaged inclination and azimuth between the bit and the RSS pads.

Coefficients of influence $\mathcal{F}_i$ and $\mathcal{M}_i$, which quantify the influence of a (generalized) load on the force or moment at the bit, only depend on the BHA configuration and on the stiffnesses K and T defining the RSS pads and the stabilizers, respectively. If the BHA can be approximated as a pipe of uniform cross section, its geometry is defined completely by the relative positions of the stabilizers and of the RSS pads behind the bit (Appendix B). As long as linearity of the underlying model holds, which implies restrictions to the nature of the contacts between the BHA and the borehole, as well as to the borehole curvature (geometric linearity), the magnitude of these coefficients could be computed, for example, by the use of a finite-element discretization of the BHA. The model description and the formulation of the propagation equations would remain completely similar. The term proportional to w only affects F_2 and M_3 as gravity acts in vertical plane ($\hat{\boldsymbol{I}}_1$,$\hat{\boldsymbol{I}}_2$).

3.6 Scaling

The model is expressed in dimensionless form, from which the relevant parameters can be extracted. Nondimensionalization of the equations requires identifying first the relevant length and force scales. As the model is formulated at the scale of the BHA, the characteristic length is chosen to be the distance ℓ_1 between the bit and the first stabilizer. The reference force is

defined as

$$F_* = \frac{3EI}{\ell_1^2}, \tag{3.31}$$

where EI is the nominal bending stiffness of the drill collars. This characteristic force represents the lateral reaction force at the bit for a BHA reduced to the interval between the bit and the first stabilizer when a rotation of one radian is imposed at the bit. The scaled lateral force at the bit is then expected to be of order $O(10^{-2}F_*)$ or less, because of the small deflection of the BHA. In the following, a tilde above a force or a moment means that it is a scaled quantity, *e.g.*, $\tilde{F}_2$ refers to the scaled magnitude of component F_2.

For future developments, it is convenient to introduce scaled active weight Π:

$$\Pi = \frac{W_a}{F_*}. \tag{3.32}$$

Using relation (3.32), scaled components of the lateral reaction force $\tilde{F}_2$ and $\tilde{F}_3$ read

$$\left\{ \begin{array}{c} \tilde{F}_2 \\ \tilde{F}_3 \end{array} \right\} = \eta\Pi \left[\begin{array}{cc} \cos\varpi & \sin\varpi \\ -\sin\varpi & \cos\varpi \end{array} \right] \left\{ \begin{array}{c} \psi_2 \\ \psi_3 \end{array} \right\}, \tag{3.33}$$

where $\xi = L/\ell_1$ is the scaled current length of the borehole and bit lateral steering resistance η and bit walk ϖ are given by

$$\eta = \frac{\sqrt{H_2^2 + H_3^2}}{H_1}, \quad \text{and} \quad \varpi = \arctan\frac{H_3}{H_2}.$$

The coefficients of the bit/rock interaction law relate thus to the macro-properties of the bit. Lateral steering resistance η defines how difficult it is to impose a lateral penetration to the bit respective to an axial one[11]. This parameter mainly depends on the length, the geometry (full-gauged, undercut, tapered), and the aggressiveness (passive, semi-active, active) of the bit gauge (Dupriest and Sowers, 2009), but theoretically, not on the downhole rock strength. (All coefficients are expected to be proportional to the strength.) Laboratory experiments have shown that the lateral steering resistance for PDC bits usually varies between about 3 and 100 for bits with a short active or with a long passive gauge, respectively (Menand et al., 2002).

[11] Lateral steering resistance η can be easily related to some other measures of the bit relative tendency to drill laterally such as the bit lateral drillability or its anisotropy index, as sometimes referred to in the literature (see, *e.g.*, Ho 1987; Menand et al. 2002).

Walk ϖ represents the angle between the lateral penetration and the lateral force on the bit. If $\varpi = 0°$, the lateral force and penetration are coaxial; otherwise, the bit is said to have a right ($\varpi > 0°$) or left ($\varpi < 0°$) walk tendency, depending on the relative orientation of the lateral penetration vector $\boldsymbol{d}_l = d_2\boldsymbol{i}_2 + d_3\boldsymbol{i}_3$ on that of the lateral force when looking in the direction of $\boldsymbol{i}_1$ (Fig. 3.7). For PDC bits, walk angles of $-10°$ are not uncommon (Menand et al., 2002) but depend on the downhole field conditions, when, for instance, the rock is not isotropic or homogeneous, or when the borehole is overgauged (Chen et al., 2008).

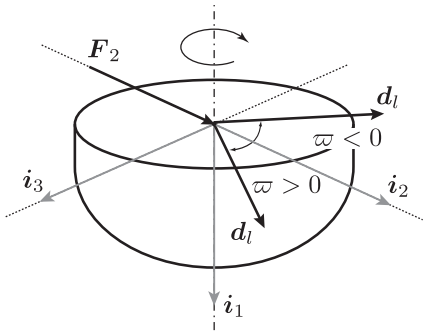

Figure 3.7: Definition of the bit walk [adapted from Menand et al. (2002)].

Scaling of the bit/rock interaction law for the moment gives

$$\left\{ \begin{array}{c} \tilde{M}_2 \\ \tilde{M}_3 \end{array} \right\} = -\chi\Pi \left[\begin{array}{cc} -\cos\varsigma & \sin\varsigma \\ \sin\varsigma & \cos\varsigma \end{array} \right] \left\{ \begin{array}{c} \sin\theta \frac{\mathrm{d}\phi}{\mathrm{d}\xi} \\ \frac{\mathrm{d}\theta}{\mathrm{d}S} \end{array} \right\}, \tag{3.34}$$

where angular steering resistance χ and bit flip ς are expressed as

$$\chi = \frac{\sqrt{H_4^2 + H_5^2}}{\ell_1^2 H_1} \quad \text{and} \quad \varsigma = \arctan\frac{H_5}{H_4}.$$

Angular steering resistance χ measures the relative difficulty of imposing an angular penetration to the bit. This small number, of order $O(10^{-2} - 10^{-1})$, also depends on the position of the first contact between the borehole and the BHA behind the bit. Bits with a long passive gauge and a close near-bit stabilizer are characterized by a larger angular steering resistance. The bit flip is defined by analogy with the bit walk; it expresses that the change of bit orientation is not contained in the same plane as moment $\tilde{\boldsymbol{M}} = \tilde{M}_2\boldsymbol{i}_2 + \tilde{M}_3\boldsymbol{i}_3$.

The general behavior of the bit then can be defined by four parameters: η, χ, ϖ and ς, which depend mostly on the bit design (cutter distributions, nature of the gauge, cutter design, etc.),

except for angular steering resistance χ, which also depends on ℓ_1. The two numbers η and χ are measures of bit steerability, and the two angles ϖ and ς define the coupling between the lateral force and moment at the bit, and the lateral and angular penetrations, respectively. In practice, reasonable estimates for these parameters can be obtained by systematic bit testing or by the use of numerical codes designed to compute the bit behavior.

Finally, scaling of equations (3.27)-(3.30) pertaining to the BHA model read

$$\begin{aligned}\tilde{F}_2 &= \mathcal{F}_b\left(\theta - \langle\Theta\rangle_1\right) + \sum_{i=1}^{n}\mathcal{F}_{w,i}\Upsilon\sin\langle\Theta\rangle_i + \mathcal{F}_r\Gamma_2 + \sum_{i=1}^{n-1}\mathcal{F}_{k,i}\left(\langle\Theta\rangle_i - \langle\Theta\rangle_{i+1}\right)\\ &\quad + \mathcal{F}_s\left(\langle\Theta\rangle_0 - \langle\Theta\rangle_1 - \frac{\Delta_{r,2}}{\Lambda}\right) + \sum_{i=1}^{n}\mathcal{F}_{c,i}\left(\Theta_i - \langle\Theta\rangle_i\right) + \mathcal{F}_m\tilde{M}_3^e, \qquad (3.35)\\ \tilde{F}_3 &= \mathcal{F}_b\left(\phi - \langle\Phi\rangle_1\right)\sin\langle\Theta\rangle_1 + \mathcal{F}_r\Gamma_3 + \sum_{i=1}^{n-1}\mathcal{F}_{k,i}\left(\langle\Phi\rangle_i - \langle\Phi\rangle_{i+1}\right)\sin\langle\Theta\rangle_1\\ &\quad + \mathcal{F}_s\left(\left(\langle\Phi\rangle_0 - \langle\Phi\rangle_1\right)\sin\langle\Theta\rangle_1 - \frac{\Delta_{r,3}}{\Lambda}\right) + \sum_{i=1}^{n}\mathcal{F}_{c,i}\left(\Phi_i - \langle\Phi\rangle_i\right)\sin\langle\Theta\rangle_1 - \mathcal{F}_m\tilde{M}_2^e, \qquad (3.36)\\ \tilde{M}_2 &= -\mathcal{M}_b\left(\phi - \langle\Phi\rangle_1\right)\sin\langle\Theta\rangle_1 - \mathcal{M}_r\Gamma_3 - \sum_{i=1}^{n-1}\mathcal{M}_{k,i}\left(\langle\Phi\rangle_i - \langle\Phi\rangle_{i+1}\right)\sin\langle\Theta\rangle_1\\ &\quad - \mathcal{M}_s\left(\left(\langle\Phi\rangle_0 - \langle\Phi\rangle_1\right)\sin\langle\Theta\rangle_1 - \frac{\Delta_{r,3}}{\Lambda}\right) - \sum_{i=1}^{n}\mathcal{M}_{c,i}\left(\Phi_i - \langle\Phi\rangle_i\right)\sin\langle\Theta\rangle_1 + \mathcal{M}_m\tilde{M}_2^e, \qquad (3.37)\\ \tilde{M}_3 &= \mathcal{M}_b\left(\theta - \langle\Theta\rangle_1\right) + \sum_{i=1}^{n}\mathcal{M}_{w,i}\Upsilon\sin\langle\Theta\rangle_i + \mathcal{M}_r\Gamma_2 + \sum_{i=1}^{n-1}\mathcal{M}_{k,i}\left(\langle\Theta\rangle_i - \langle\Theta\rangle_{i+1}\right)\\ &\quad + \mathcal{M}_s\left(\langle\Theta\rangle_0 - \langle\Theta\rangle_1 - \frac{\Delta_{r,2}}{\Lambda}\right) + \sum_{i=1}^{n}\mathcal{M}_{c,i}\left(\Theta_i - \langle\Theta\rangle_i\right) + \mathcal{M}_m\tilde{M}_3^e, \qquad (3.38)\end{aligned}$$

where Γ_2 and Γ_3 are the scaled components of the RSS force, and $\Delta_{r,2}$ and $\Delta_{r,3}$ are the components of the scaled position of reference of the RSS. The coefficients of influence are only function of the BHA geometry and scaled rigidities $\mu = \ell_1 K/F_*$ and $\tau = T/\ell_1 F_*$ of the RSS pads and of the stabilizers, respectively.

3.7 General Expressions

By balancing expressions (3.33)-(3.34) and (3.35)-(3.38), two coupled functional delay differential equations (DDE) are obtained for the evolution of the borehole inclination and azimuth. Their

explicit expressions are not relevant here, but their general form can be expressed as

$$\Theta'(\xi) = F_\Theta(\Theta, \Phi, \Theta_i, \Phi_i, \langle\Theta\rangle_i, \langle\Phi\rangle_i, \mathbf{\Gamma}, \mathbf{\Gamma}', \Upsilon), \tag{3.39}$$

$$\Phi'(\xi) = F_\Phi(\Theta, \Phi, \Theta_i, \Phi_i, \langle\Theta\rangle_i, \langle\Phi\rangle_i, \Gamma, \Gamma', \Upsilon). \tag{3.40}$$

In these equations, delays ξ_i (through inclinations Θ_i and azimuths Φ_i), averaged inclinations $\langle\Theta\rangle_i$, and averaged azimuths $\langle\Phi\rangle_i$ capture the feedback of the borehole trajectory on the curvature at the bit. (The positions of the stabilizers behind the bit are denominated $\xi_i = \sum_{j=1}^{i} \lambda_j$, where $\lambda_j = \ell_j/\ell_1$ is the relative positions of stabilizer j behind stabilizer $j-1$. Parameter $\lambda_1 = 1$ denotes the position of the first stabilizer behind the bit.) The drilling direction does not only depend on the external loads applied onto the BHA, but also on the constraints that the borehole impose on its deflection.

Linear delay differential equations have some properties that differ from linear ordinary differential equations (ODE) (see further details at the beginning of the next section). One of them is that the solution of even the simplest first-order DDEs can sustain an oscillatory behavior without external loading. The existence of these solutions directly correlate to the observation of borehole spiraling in the field: Its intrinsic nature hinges on the establishment of self-excited oscillations with a period related to the distance between the bit and the first contact between the BHA and the borehole (Pastusek and Brackin, 2003; Sugiura and Jones, 2008b; Marck and Detournay, 2014a, 2015a,b).

Because of their analytical form, equations (3.39) and (3.40) can be readily studied in order to evaluate their propensity to induce self-sustained fluctuations in the borehole inclination and azimuth under given field conditions, *i.e.*, their tendency to produce spiraled holes. The property of a given drilling system to generate a spiraled hole or not is referred to as its directional tendency: A directionally unstable system tends to progressively amplify any local perturbation in the borehole trajectory until a limit cycle, the spiral, is reached.

Equations (3.39) and (3.40) also have different applications (Perneder and Detournay, 2013a,b). One of them is the derivation of the directional tendency of the system. This stationary or quasi-stationary solution depends on factors such as the borehole inclination (for the influence of gravity), the steering cycles (for the averaged value and direction of the RSS force), the active weight, and bit properties (Perneder and Detournay, 2013a). The attribute of being

quasi-stationary alludes to the slowly varying borehole inclination, the effect of which on the directional tendency is felt at a length scale at least one order of magnitude larger than that at which borehole spiraling develops.

The notions of directional stability and directional tendency are thus two distinct concepts. The directional tendency is the smooth convergence toward long-range, (quasi-)stationary solutions, while stability directional pertains to whether a perturbation around these long-term solutions is amplified or reduced progressively along the borehole due to the local geometric feedback at the level of the stabilizers.

Chapter 4

Two-dimensional Model

4.1 General Properties of Delay Differential Equations

Delay differential equations (DDEs) find applications in a growing number of scientific fields; they model systems with feedback, for which the rate of change of some state variables depends on their history (Hale, 1977; Stepan, 1989; Michiels and Niculescu, 2007). Common examples pertain to population or fluid dynamics, economics, or transportation (Erneux, 2009). Control strategies incorporating the time for acquiring or transmitting information are based on DDEs.

DDEs differ from ordinary differential equations (ODEs) in the nature of their initial conditions, in their ability to commonly exhibit oscillatory behaviors, and in the form of their characteristic equations (Stepan, 1989; Erneux, 2009). DDEs are commonly divided in two classes. In *neutral* DDEs, the rate of change of some state variables is function of past rates, *i.e.*, the state-space representation includes *delayed* state derivatives. *Retarded* DDEs are independent of the history of the rates of change, *i.e.*, the system evolution is only function of its current and past configuration. Theorems for the existence and uniqueness of solutions have been derived (Hale, 1977). Retarded DDEs with constant coefficients have a continuous dependence on initial conditions, parameters, and delays; neutral DDEs do not share this property (Hale, 1977), which requires caution when investigating them.

Initial Conditions Contrary to ODEs where only the initial magnitudes of the state variables are needed to fully describe the system, DDEs further require their history over an interval as long as largest delay τ_{max}; DDEs are thus infinitely dimensional problems (Stepan, 1989; Erneux, 2009). In most cases, continuity of the derivative is not enforced, that is, the initial conditions do not satisfy necessarily the actual DDE.

Another particularity is that discontinuities are propagated. They require thus a particular care in numerical methods (Shampine and Thompson, 2001; Shampine, 2005; Bellen and Zennaro, 2013). For retarded DDEs, a discontinuity propagates into discontinuities of lower order, *i.e.*, for an initial condition continuous on $[-\tau_{max}, 0)$, the solution is continuously differentiable on $]0, \tau_{max})$, twice continuously differentiable on $]\tau_{max}, 2\tau_{max})$, and so on (Michiels and Niculescu, 2007). Neutral DDEs have no *smoothing* effect; they maintain the order of a discontinuity as it is propagated. The amplitude of the discontinuity, however, is progressively amplified or reduced depending on the feedback gain.

Oscillatory Behavior Even the simplest linear DDEs have the particularity of producing, under certain conditions, large-time oscillations without any external excitation (Erneux, 2009). These oscillating solutions are defined by their wavelength and exponential growth or decay; linear DDEs admit long-term solutions of the form

$$x(t) = Ce^{\alpha t}, \quad \alpha, C \in \mathbb{C}, \tag{4.1}$$

where α is a characteristic root of the system.

Characteristic Equation In general, the stability analysis of DDEs relies on a linearized version of the evolution equations from which a characteristic equation is derived (Hale, 1977). This characteristic equation is obtained by substituting general solution (4.1) in the linearized problem. Unlike the polynomial characteristic equations of ODEs, those of DDEs are transcendental. There are thus an infinity of characteristic roots, which are usually computed numerically (Michiels and Niculescu, 2007; Erneux, 2009). Different methods exist to extract these roots (Tweten et al., 2012), such as the semi-discretization (Insperger and Stepan, 2002) or the spectral element (Wu and Michiels, 2012) methods. The latter has been used in the context of this research using a Matlab package developed at the University of Leuven (Wu and Michiels, 2012).

As for ODEs, the system stability is related to the real part of the rightmost characteristic root, *i.e.*, the characteristic root with the largest real part. If all the roots have a negative real part, the system is stable. However, if at least one root has a positive real part, the system is unstable, because the general solution to the equation has at least one component that grows exponentially.

The class of the DDE affects the stability of the high-frequency roots. For retarded system, all roots with a large imaginary part are stable (Insperger and Stepan, 2002; Michiels and Niculescu, 2007). For neutral equations, there is a finite asymptote for the real part of these roots, possibly positive depending on the system parameters.

4.2 Equations of Borehole Propagation

4.2.1 Global Equation of Borehole Propagation

In this chapter, the borehole trajectory is assumed to be constrained to a vertical plane, *i.e.*, its azimuth is constant. The bit walk is thus zero and no exterior load is imposed to deviate the well from the vertical plane (or the out-of-plane loading exactly compensate for the influence of the walk). This simplification is motivated by the fact that the influence of some system parameters in two dimensions is qualitatively similar to the more general three-dimensional problem.

Only one equation in terms of the borehole inclination is required to fully described the borehole trajectory. This equation is obtained by equating expressions (3.35) and (3.38) with the relevant relations in (3.33) and (3.34). Using kinematic relationships (3.13) and (3.14) and setting $\varpi = 0°$, $\Gamma_3 = 0$, and $\tilde{M}_2^e = 0$, the resulting DDE in terms of borehole inclination Θ reads

$$\begin{aligned}\varepsilon\Theta'(\xi) \;=\; & \mathcal{A}\Theta(\xi) + \sum_{i=1}^{n} \mathcal{B}_i\Theta(\xi-\xi_i) + \sum_{i=1}^{n} \mathcal{C}_i \left\langle\Theta\right\rangle_i + \mathcal{B}_0\Theta(\xi-\Lambda) + \mathcal{C}_0\left(\left\langle\Theta\right\rangle_0 - \frac{\Delta_r}{\Lambda}\right) \\ & + \sum_{i=1}^{n} \mathcal{D}_i\Upsilon \sin\left\langle\Theta\right\rangle_i + \sum_{i=1}^{n} \mathcal{E}_i\Upsilon \cos\left\langle\Theta\right\rangle_i \left(\Theta(\xi-\xi_{i-1}) - \Theta(\xi-\xi_i)\right) \\ & + \mathcal{F}\Gamma + \mathcal{G}\tilde{M}^e + \sum_{i=0}^{n} \mathcal{H}_i\Theta'(\xi-\xi_i), \end{aligned} \tag{4.2}$$

where delay $\xi_0 = 0$ corresponds to the bit position, $\Gamma = \Gamma_2$, and $\tilde{M}^e = \tilde{M_3}^e$. The right-hand side of equation (4.2) can be divided into three contributions: (a) the geometrical terms that

only pertain to the borehole trajectory (terms related to coefficients $\mathcal{A}$, $\mathcal{B}$, $\mathcal{C}$, and $\mathcal{H}$), (b) the influence of gravity that introduces some non-linearity into the equation of propagation[1] (terms in $\mathcal{D}$ and $\mathcal{E}$), and (c) the terms related to the *exterior* loads (proportional to $\mathcal{F}$ and $\mathcal{G}$).

Equation (4.2) relies on the assumption that the active weight, the force at the RSS, and the moment at the last stabilizer are prescribed as piecewise constant functions of ξ. Their derivatives respective to ξ are thus trivially zero everywhere except at points where their magnitudes are allowed to jump. Equation (4.2) is only valid between these singular points with the corresponding loading parameters. Accounting for continuously varying loads is possible, but would in general add three terms in equation (4.2) proportional to the derivatives of Π, Γ, and $\tilde{M}^e$, respectively. The term in Γ' is central to control strategies centered on the magnitude of the RSS force and its variation (see, for example, van de Wouw et al. (2015) and Kremers et al. (2015), who developed control algorithms based on this model).

Parameters $\mathcal{A}$ to $\mathcal{H}$ are functions of the coefficients of influence coming from the BHA model but also on dimensionless groups $\varepsilon = \chi/\eta$ and $\eta\Pi$ (Appendix C). The former is a measure of the relative difficulty to impose an angular penetration to the bit with respect to a lateral one. It is expected to be $O(10^{-2})$ or less considering that $\chi = O(10^{-1})$ and $\eta = O(10)$.

Propagation equation (4.2) is a DDE, *i.e.*, the rate of change of borehole inclination Θ does not only depend on the external loads and on the current inclination, but also on its past history. The delays, corresponding to the positions of the stabilizers, capture the geometric feedback of the borehole geometry on the force and moment at the bit: Borehole inclination Θ along the entire BHA influences thus the drilling direction through secular terms $\Theta(\xi - \xi_i)$, $\langle\Theta\rangle_i$, and $\Theta'(\xi - \xi_i)$.

In the following initial conditions correspond to a straight borehole, *i.e.*, it is defined by initial constant inclination Θ_0 (and azimuth Φ_0 in 3D). This initial geometry generally does not solve the propagation equation. Consequently at $\xi = 0$, there is a discontinuity in the borehole trajectory, in general a jump both in inclination and curvature[2]. This initial discontinuity

[1] The introduced nonlinearity is not strong, however: scaled weight Υ is a small parameter, $O(10^{-3})$, whose influence on the borehole trajectory is only felt over length scales at least one order of magnitude larger than that of the model (Perneder, 2013).

[2] In the following of the dissertation, $\xi = 0$ does not not correspond to the position of the rig but is conveniently redefined as the beginning of the simulation.

has three components: one due to the *sudden* application of the buoyant weight, one to the initial RSS force, and one to the exterior moment. During the simulation, changes in active weight or in any load parameter also generate discontinuities. Rock interfaces, defined as a sudden change in rock properties, have shown to induce complex and local perturbations in the borehole geometry (Boualleg et al., 2006; Marck and Detournay, 2014b). At the resolution of the model, these are modeled as a shift in the bit position, or equivalently a jump in the averaged inclination of the first section. Layer interfaces then produce a discontinuity of a higher order than sudden variations in the loads (Marck and Detournay, 2014b). Finally each stabilizer crossing a discontinuity propagates it at the bit. (Discontinuities lower than a jump in the curvature do not need to be tracked.)

The magnitude and order of discontinuities are obtained analytically by ensuring the compatibility between the lateral force at the bit and the resulting tilt after the initiating event. These expressions are derived within the framework of generalized functions and can be found in Appendix D.

4.2.2 Perturbed Equation of Propagation

The (quasi-)stationary solutions of the system have already been derived (Perneder and Detournay, 2013a,b; Perneder, 2013). However, the onset of borehole spiraling is of a different nature: it is concerned with whether a perturbation in the borehole trajectory is progressively amplified or dampened along the borehole due to the geometric feedback embedded in the system. As spirals are observed around and along stationary solutions, they can be seen as perturbations to these solutions. Equation (4.2) is thus advantageously regarded as the superposition of two components: quasi-stationary solution $\Theta_s(\xi)$ due to the quasi-constant loads on the BHA and the dynamics of the perturbation $\delta\Theta(\xi)$. Inserting this decomposition into (4.2) leads to the following equation governing the perturbation

$$\varepsilon\delta\Theta'(\xi) = \mathcal{A}\delta\Theta(\xi) + \sum_{i=1}^{n} \mathcal{B}_i\delta\Theta(\xi-\xi_i) + \mathcal{B}_0\delta\Theta(\xi-\Lambda) + \sum_{i=1}^{n} \mathcal{C}_i \left\langle\delta\Theta\right\rangle_i + \mathcal{C}_0 \left\langle\delta\Theta\right\rangle_0 + \sum_{i=1}^{n} \mathcal{H}_i\delta\Theta'(\xi-\xi_i). \tag{4.3}$$

The terms related to the constant RSS force and exterior moment naturally disappear as they only influence the quasi-stationary solution (if sufficiently smooth) and those associated with gravity are neglected, as their influence can be shown to be negligible on the onset of spiraling. Indeed, the component of the weight that is not accounted for in the quasi-stationary solution does not significantly influence the perturbed dynamics, owing to $\mathcal{D}\Upsilon \ll \mathcal{C}_1$ and $\mathcal{E}\Upsilon$ being a second-order term in (4.3). The evolution of the perturbation is thus, at first order, purely geometric: right-hand side of (4.3) is related only to the borehole trajectory. Equation (4.3) then propagates the perturbation around quasi-stationary solution $\Theta_s(\xi)$.

The nature of the perturbed equation (4.3) depends on stiffness in tilt τ of the stabilizers, with implications on its stability properties. It is of a neutral type if $\tau > 0$, but becomes retarded one if $\tau = 0$. If $\varepsilon = 0$, equation (4.3) becomes technically a delay algebraic equation.

Borehole spiraling occurs when the equations of propagation are directionally unstable. Any local perturbation in the bit trajectory then is amplified progressively by the interaction of the stabilizers with the borehole, until a limit cycle is reached. The initial perturbation can be induced by the crossing of layer interfaces, dynamic vibrations, or sudden significant changes in WOB or RSS force. The crossing of interfaces has been identified in the field as a trigger for spiraling (Dupriest and Sowers, 2009). These may result rapidly in large oscillations in the borehole trajectory when the transition is from a softer to a harder rock, as it generates perturbations in the borehole geometry and reduces the active weight by increasing G_1. The perturbations induced by a change of WOB or RSS force are an order of continuity lower, leading to a longer transient before significant oscillations develop.

4.3 Directional Stability

4.3.1 General Considerations

The current analysis relies on the observation that there exists a critical value of dimensionless group $\eta\Pi$, called $\eta\Pi|_s$, a function of ε, μ, τ and the BHA configuration, so that the system is stable for $\eta\Pi > \eta\Pi|_s$. For a planar borehole and a BHA with uniform mechanical properties, $\eta\Pi|_s = f(\lambda_i, \mu, \tau, \varepsilon)$. This critical value corresponds to a Hopf bifurcation of equilibrium —

i.e., when the rightmost pair of complex-conjugate roots crosses the imaginary axis. (In general the system has a real root close to zero. This root is disregarded here as it does not induce oscillations in the borehole trajectory.)

The directional stability of any particular drilling system is assessed by comparing $\eta\Pi$, encapsulating the current field conditions, with $\eta\Pi|_s$. Given a BHA configuration, the bit and the downhole WOB can be selected to mitigate or prevent borehole spiraling by enforcing that the system operates within spiral-free conditions. Dimensionless group $\eta\Pi$, representative of the drilling conditions, reads

$$\eta\Pi = \eta\frac{(W - G_1)\ell_1^2}{3EI}. \tag{4.4}$$

It represents the ratio between two stiffnesses, that of the bit/rock interaction law and that of the BHA. This group embeds downhole WOB W, axial resultant of contact forces G_1 (a measure of the bit wear and the rock strength), lateral steering resistance η, and BHA properties EI and ℓ_1. Consequently, computing $\eta\Pi|_s$ for a BHA configuration provides a guideline — not only for selecting an appropriate bit, but also for assessing the field conditions that are unlikely to induce spiraled holes. The BHA configuration can help make a system intrinsically more stable (*i.e.*, a system having a smaller $\eta\Pi|_s$), but it is ultimately the field conditions that define the directional stability: virtually any system can become directionally unstable with varying downhole conditions. For instance, a system directionally stable initially may become unstable with increasing bit wear, higher rock strength, or reduced downhole WOB, all of which reduce active weight W_a.

The importance of dimensionless group $\eta\Pi$ is directly related to the fundamental mechanism of borehole spiraling. For a given lateral force at the bit, a smaller $\eta\Pi$ induces a larger bit tilt, that is, a locally larger side-cutting action. Fluctuations in the lateral force at the bit, when the RSS pads or the stabilizers interact with a perturbation in the borehole, influence the bit tilt in a way inversely proportional to $\eta\Pi$. They can result in an amplified perturbation in the borehole trajectory if $\eta\Pi$ becomes smaller than a threshold, corresponding to critical value $\eta\Pi|_s$.

Analysis of directional stability is undergone here for *simple* BHAs, equipped with one or two stabilizers and possibly a push-the-bit RSS. (Validation of the model with field data is concerned with more realistic configurations. The qualitative features of the analysis are similar.) The

following sections aim at studying the influence of small parameter ε and stiffnesses τ and μ, on the system directional stability. The BHA is assumed to have uniform mechanical properties. The relative position of the RSS pads is denoted by Λ and that of the second stabilizer by λ_2 (Fig. 4.1).

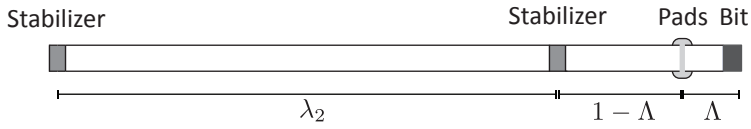

Figure 4.1: Typical two-stabilizer BHA with a push-the-bit RSS. The pads are located at distance Λ behind the bit and the relative position of the second stabilizer is given by λ_2.

4.3.2 Influence of ε and τ

One-Stabilizer BHA

The first system under study is a BHA equipped with only one stabilizer and no RSS. The perturbed propagation equation reads

$$\varepsilon\Theta'(\xi) = \mathcal{A}\Theta(\xi) + \mathcal{B}_1\Theta(\xi-1) + \mathcal{C}_1\left\langle\Theta\right\rangle_1 + \mathcal{H}_1\Theta'(\xi-1), \tag{4.5}$$

or in terms of the coefficients of influence

$$\begin{aligned}\varepsilon\Theta'(\xi) = {} & \frac{(\mathcal{F}_b+\mathcal{F}_s)\varepsilon - \mathcal{M}_b}{\eta\Pi}\Theta(\xi) + \frac{\mathcal{F}_b\mathcal{M}_s - \mathcal{F}_s\mathcal{M}_b - (\mathcal{F}_b+\mathcal{F}_s)\eta\Pi\varepsilon - \eta\Pi\mathcal{M}_s}{(\eta\Pi)^2}\Theta(\xi-1) \\ & + \frac{\mathcal{F}_s\mathcal{M}_b - \mathcal{F}_b\mathcal{M}_s + \eta\Pi(\mathcal{M}_b+\mathcal{M}_s)}{(\eta\Pi)^2}\left\langle\Theta\right\rangle_1 - \frac{\varepsilon\mathcal{F}_s}{\eta\Pi}\Theta'(\xi-1),\end{aligned} \tag{4.6}$$

where symbol δ denoting the perturbed solution has been dropped for simplicity. By substituting general solution (4.1) into (4.5), the characteristic equation yields

$$\mathcal{A} - \varepsilon\alpha + \frac{\mathcal{C}_1}{\alpha} + (\mathcal{B}_1 + \alpha\mathcal{H}_1 - \frac{\mathcal{C}_1}{\alpha})e^{-\alpha} = 0, \tag{4.7}$$

which needs to be solved for $\alpha \in \mathbb{C}$.

For this simple system critical value $\eta\Pi\big|_s$ depends only on τ and ε. If the stabilizer does not offer any resistance to a change of inclination ($\tau = 0$), it is free to tilt and does not influence the drilling direction at the bit. The system is thus always directionally stable irrespective of

the BHA stiffness, the bit lateral steering resistance, and the weight on bit, *i.e.*, $\eta\Pi|_s = 0$. As soon as some constraint is imposed on the tilt ($\tau > 0$), critical value $\eta\Pi|_s > 0$ and the spiraling tendency depends on downhole field conditions. If $\varepsilon = 0$, the bifurcation limit $\eta\Pi|_s$ is given by

$$\eta\Pi|_s = \frac{\mathcal{F}_b\mathcal{M}_s - \mathcal{F}_s\mathcal{M}_b}{\mathcal{M}_b + \mathcal{M}_s} = \frac{2\tau}{2 + 3\tau}. \tag{4.8}$$

However if $\varepsilon > 0$, bifurcation occurs at

$$\eta\Pi|_s = -\mathcal{F}_s = \frac{6\tau}{4 + 3\tau}. \tag{4.9}$$

Both expressions (4.8) and (4.9) are directly deduced from characteristic equation (4.7) by looking at the limit of a characteristic root with an *infinite* imaginary part crossing the imaginary axis (Fig. 4.2a). When $\varepsilon = 0$, the system is thus intrinsically more stable. As the bit is free to tilt and adapts instantaneously to changes in the BHA loading, a discontinuity in the borehole inclination (corresponding to $\Im(\alpha) = \infty$) induces both a jump in the bit and borehole inclinations when sensed by a stabilizer. When $\varepsilon > 0$, the same discontinuity only translates in a – larger – jump in the borehole inclination. (It theoretically requires an infinite moment at the bit to create a jump in θ.) The geometric gain of the system is then more critical for $\varepsilon > 0$ than for $\varepsilon = 0$.

The discontinuity in critical value $\eta\Pi|_s$ at $\varepsilon = 0$ can actually be tracked to the presence of terms proportional to ε in the propagation equation, which influence the position of the characteristic roots with a large imaginary part. If $\varepsilon = 0$ all the characteristic roots simultaneously cross the imaginary axis at bifurcation limit (4.8), with the crossings located at $2k\pi i$, $k \in \mathbb{Z}$. On the other hand, if $\varepsilon > 0$ the bifurcation limit is given by (4.9), which now corresponds to the crossing of the imaginary axis by the (infinitely) high-frequency roots (Fig. 4.2a and b). The behavior of the low-frequency roots, in particular those with $\Im(\alpha) \simeq \pm 2\pi$, is barely affected by ε as long as $\varepsilon\Im(\alpha) \ll 1$. The crossing of the imaginary axis by these roots takes place when $\eta\Pi$ is about equal to bifurcation limit (4.8) corresponding to $\varepsilon = 0$.

The high-frequency modes that are unstable at small ε are actually irrelevant, as they are an artifact of collapsing the bit onto a point in the formulation of the model. In fact, borehole propagation equation (4.2) can only be used to analyze features of the borehole trajectory at spatial resolutions that are not smaller than the dimensions of the bit. By introducing a cut-off

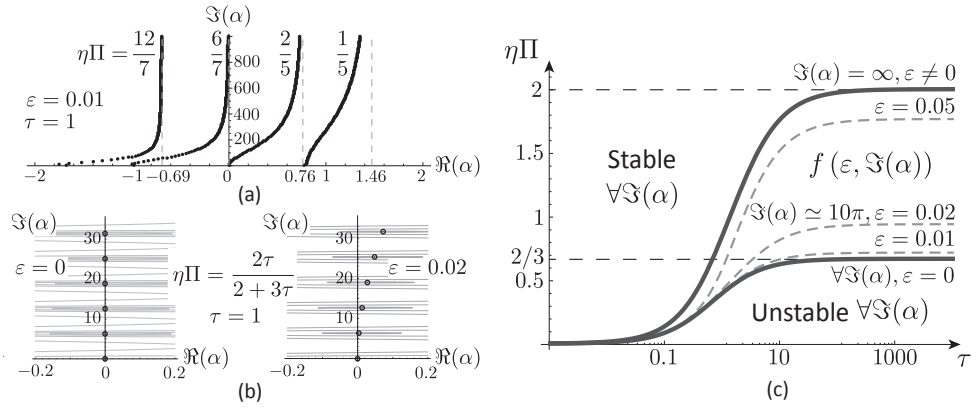

Figure 4.2: (a) Positions of the characteristic roots for particular values of $\eta\Pi$, $\varepsilon = 0.01$, and $\tau = 1$. [When $\eta\Pi < \frac{2\tau}{2+3\tau}$, all the roots have a positive real part; when $\eta\Pi \simeq \frac{2\tau}{2+3\tau}$, the roots with $\Im(\alpha) \simeq 2\pi$ becomes stable (as $\varepsilon\Im(\alpha) \ll 1$); only when $\eta\Pi = \frac{6\tau}{4+3\tau}$ do the high-frequency roots become stable; and when $\eta\Pi > \frac{6\tau}{4+3\tau}$ all the roots have a negative real part.] (b) Low-frequency characteristic roots for $\tau = 1$ and $\eta\Pi = \frac{2\tau}{2+3\tau}$. [On the left, $\varepsilon = 0$ and all the roots simultaneously cross the imaginary axis. On the right, $\varepsilon = 0.02$ but only significantly influences the roots with a larger imaginary part.] (c) Stability in the $\tau - \eta\Pi$ space, which can be divided in three regions depending on whether all frequencies are stable or unstable, or when the low frequencies are stable and the high ones unstable. The dashed lines represent the bifurcation of stability with an arbitrary cutting frequency of about $5\xi^{-1}$ for different values of ε. Its influence on $\eta\Pi|_s$ increases with τ and $\Im(\alpha)$ but is negligible as long as $\varepsilon\Im(\alpha) \ll 1$.

frequency, related to the bit dimensions, bifurcation value $\eta\Pi|_s$ evolves monotonically with ε between the two asymptotes given by (4.8) and (4.9) (Fig. 4.2c).

Two-Stabilizer BHA

With the addition of a second stabilizer, bifurcation limit $\eta\Pi|_s$ needs to be computed numerically. The constraint brought by the extra stabilizer causes $\eta\Pi|_s$ to be always positive, irrespective of the values of ε and τ. Thus there is always a range of $\eta\Pi$ for which the drilling system is directionally unstable.

Unconstrained Stabilizers ($\tau = 0$) The stability diagram in the $\lambda_2 - \eta\Pi$ plane is presented on Figure 4.3a. For some positions of the second stabilizer, different stability transitions occur for different $\eta\Pi$: different marginally stable solutions, characterized by different $\eta\Pi$ and wavelengths are possible. In these cases, $\eta\Pi|_s$ is defined as the largest bifurcation value so that the system is

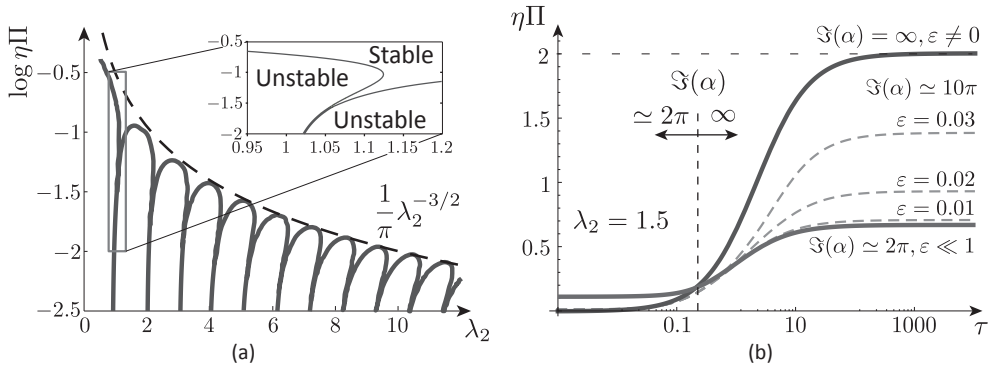

Figure 4.3: (a) Variation of the bifurcation of stability with λ_2 for a two-stabilizer BHA with $\varepsilon = 0$. [For some λ_2, different Hopf bifurcations are possible for different $\eta\Pi$. Parameter $\eta\Pi|_s$ is defined as the largest critical value of the bifurcation parameter. The dashed line represents the asymptotic behavior for large λ_2 of the envelope to $\eta\Pi|_s$.] (b) If the stabilizers are not free to tilt ($\tau > 0$), the stability of the system is assessed by comparing the real part of the low- and high-frequency characteristic roots. [For small τ, the stability is dictated by the low-frequency roots while for large τ, $\eta\Pi|_s$ is obtained from the roots with a large imaginary part. A cut-off frequency can be chosen, the influence of ε may not be negligible if its magnitude is sufficiently large.]

always stable for $\eta\Pi > \eta\Pi|_s$. The large-λ_2 asymptotic envelope to $\eta\Pi|_s(\lambda_2)$ can be determined analytically

$$\eta\Pi|_s \overset{\lambda_2 \gg 1}{\sim} \frac{1}{\pi}\lambda_2^{-3/2}. \tag{4.10}$$

This result is obtained by asymptotic development around $\Im(\alpha) = 2\pi$ for $\lambda_2 \to \infty$ of the nonlinear equation in terms of $\eta\Pi$, λ_2, and $\Im(\alpha)$ that solves for purely imaginary roots. The solutions of this equation correspond then to complex-conjugate roots crossing the imaginary axis. Asymptote (4.10), which is represented by a dashed line in Fig. 4.3a, is practically valid for $\lambda_2 \geq 4$. However if the second stabilizer is sufficiently far away from the first one, additional contacts between the BHA and the borehole are likely. Since these contacts also influence the system stability (Marck et al., 2014), this asymptote is of limited applicability.

When the two stabilizers are close to each other ($\lambda_2 \to 0$), the system behaves as if it had only one clamped stabilizer and $\eta\Pi|_s$ progressively tends to 2/3 or 2 depending on whether $\varepsilon = 0$ or not; the limit for $\tau \to \infty$ for the one-stabilizer case is recovered, with the previous considerations about the model spatial resolution still pertinent.

For an infinitely rigid BHA ($\eta\Pi = 0$), the system is always unstable except when λ_2 is an

integer (Downton, 2007). The bit trajectory for a rigid BHA is kinematically determined and only straight or sinusoidal boreholes (with a period in $1/k$, with $k \in \mathbb{N}$) are admissible; in such cases the system is marginally stable. These particular solutions explain the branches of stability starting at $\lambda_2 \in \mathbb{N}$ and $\eta\Pi = 0$ in the stability diagram (Fig. 4.3a).

Constrained Stabilizers ($\tau \neq 0$) Directional stability of a drilling system with a tilt constraint on the stabilizers requires to compare the positions of the low- and high-frequency roots.

The position of the vertical asymptote to the high-frequency roots can be computed analytically. If $\varepsilon = 0$, an upper bound for the stability of the asymptote (exact for $\lambda_2 \notin \mathbb{N}$) is given by

$$\eta\Pi|_{\Im(\alpha)\to\infty} = \frac{\mathcal{F}_b\mathcal{M}_{s,1} - \mathcal{F}_{s,1}\mathcal{M}_b}{\mathcal{M}_b + \mathcal{M}_{s,1}} = \frac{2\lambda_2\tau(3\lambda_2\tau + 4)}{\lambda_2(\tau(\lambda_2(9\tau + 6) + 20) + 8) + 8}. \tag{4.11}$$

If $\varepsilon > 0$, this upper bound occurs at

$$\eta\Pi|_{\Im(\alpha)\to\infty} = -\mathcal{F}_{s,1} = \frac{6\lambda_2\tau(3\lambda_2\tau + 4)}{3\lambda_2^2\tau(3\tau + 4) + 8\lambda_2(3\tau + 2) + 12}. \tag{4.12}$$

The one-stabilizer case is trivially recovered by taking the limit $\lambda_2 \to \infty$. (If $\lambda_2 \in \mathbb{N}$, it positively affects the stability of the high-frequency roots. This simultaneity is, however, an artifact of the model.)

The bifurcation value for the low-frequency roots does not depend on ε as long as it remains small enough. Therefore the stability of any system relies on comparing the real part of the high frequency roots (or any cutting frequency that may be chosen) with the particular value of $\eta\Pi$ obtained for the crossing of the complex-conjugate roots with an imaginary part around 2π.

When $\varepsilon = 0$, the stability is always determined by the position of the roots with $\Im(\alpha) \simeq \pm 2\pi$. However when $\varepsilon > 0$, the frequency of the rightmost roots depends on the magnitude of stiffness τ. For small τ, the induced oscillations are usually directly related to the distance between the bit and the first stabilizer: $\Im(\alpha_{rm}) \simeq \pm 2\pi$ corresponds to a pitch of about 1, the scaled distance between the bit and the first stabilizer. For large τ, the bifurcation of stability is dictated by the high-frequency roots and the stability diagram presents similar features as the one computed for a BHA with a single stabilizer (Fig. 4.3b).

This observation is an a posteriori indication that the stiffness of the stabilizers can generally be considered as small, since field observations indicate that the pitch of the spiral is related

to the position of the first contact point behind the bit. More generally, the relevance of the high-frequency content is doubtful on three counts. First, the amplitude of the oscillations is generally inversely proportional to their frequency, so that high frequencies may not induce notable borehole oscillations. Second, no significant high-frequency content relative to the BHA was measured in a spectral analysis of spiraled boreholes (Sugiura and Jones, 2008b). Third, the model of borehole propagation is not formulated to capture features with a resolution smaller than the bit dimension. Parameter τ is thus henceforth neglected.

4.3.3 Influence of μ

Consider now a BHA equipped with two stabilizers and a push-the-bit RSS. The RSS pads are modeled by a prestressed spring of scaled stiffness μ. The perturbed equation of propagation reads

$$\varepsilon\Theta'(\xi) = \mathcal{A}\Theta(\xi) + \sum_{i=1}^{2} \mathcal{B}_i\Theta(\xi - \xi_i) + \mathcal{B}_0\Theta(\xi - \Lambda) + \sum_{i=0}^{2} \mathcal{C}_i \left\langle\Theta\right\rangle_i , \tag{4.13}$$

where $\left\langle\Theta\right\rangle_0$ is the averaged borehole inclination between the bit and the RSS pads. Figure 4.4a illustrates the directional stability of the system and the pitch of the resulting ripple as a function of $\eta\Pi$ and μ for $\Lambda = 0.25$ and $\lambda_2 = 3$. The superimposed curve represents bifurcation of stability $\eta\Pi|_s$ as a function of μ.

For low values of μ, the intrinsic stability of the system improves first: The magnitude of $\eta\Pi|_s$ progressively decreases (here, up to $\mu_1^* \simeq 0.15$). The pads dampen the influence of the stabilizers on the bit drilling direction whereas their own influence remains small. However, when the stiffness becomes larger than a certain threshold μ_2^* (here, approximately equal to 1.7), the pads drive the stability of the system. Their impact on drilling direction $\boldsymbol{d}$ surpasses that of any stabilizer. From that point on, the value of $\eta\Pi|_s$ increases significantly with μ; the pads constrain the BHA deflection more and more and progressively act as an extra stabilizer close to the bit.

Two opposite effects take then place simultaneously: An increase of stiffness μ augments the influence of the RSS pads on the drilling direction at the bit, but also reduces that of the first stabilizer. When $\mu = 0$, the value of $\eta\Pi|_s$ corresponds to that of a two-stabilizer BHA, on which the RSS simply imposes a prescribed force. When $\mu \to \infty$, it imposes a kinematic constraint

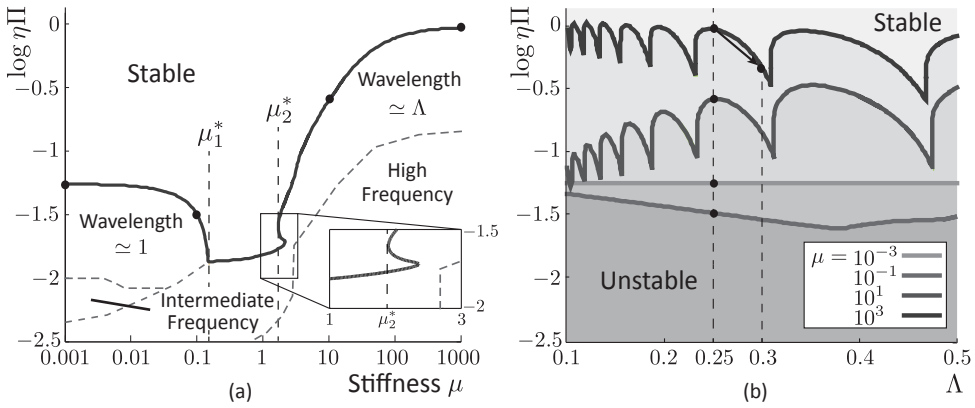

Figure 4.4: (a) Stability and pitch of a two-stabilizer BHA equipped with a push-the-bit RSS as a function of scaled lateral stiffness of the pads μ, and dimensionless parameter $\eta\Pi$. [The parameters are $\Lambda = 0.25$ and $\lambda_2 = 3$. Close to μ_2^*, $\eta\Pi|_s$ is not defined uniquely. In general, the variation of $\eta\Pi|_s$ between μ_1^* and μ_2^* exhibits a rich behavior, strongly dependent on Λ. The frequencies indicate the dominant mode in terms of stability.] (b) Variation of $\eta\Pi|_s$ with Λ for different discrete values of μ. [The shape of the curve for large μ originates from the general influence of relative position of the second stabilizer, in a BHA without RSS, on $\eta\Pi|_s$.]

on the BHA deflection and behaves as if the system had an extra stabilizer close to the bit, becoming, therefore, significantly more directionally unstable.

When the system is unstable, the pitch of the induced spiral (or ripple) generally corresponds to the element of the BHA, either the pads or the first stabilizer, which amplifies most a perturbation. In Figure 4.4a, the pitch is close to unity for small values of μ (representing the distance between the bit and the first stabilizer). When the rigidity increases, there is a sudden transition so that the pitch becomes approximately 0.25 (*i.e.*, the distance between the bit and the pads of the RSS): The self-excited oscillations are dominantly maintained by the influence of the pads and the pitch of the spiraled hole, then, is related directly to their position along the BHA.

Field observations confirmed this change of pitch (Pastusek and Brackin, 2003; Sugiura and Jones, 2008b; Marck et al., 2014) that is also observed in numerical simulations using (4.13): Two simulations were conducted, assuming the pads to have either a low or a large lateral stiffness (Fig. 4.5). When different bifurcations of stability coexist, $\eta\Pi|_s$ is again defined as the largest of them. This nontrivial variation of $\eta\Pi|_s$ is related to the non-smooth motion of the rightmost characteristic root in the complex plane with $\eta\Pi$.

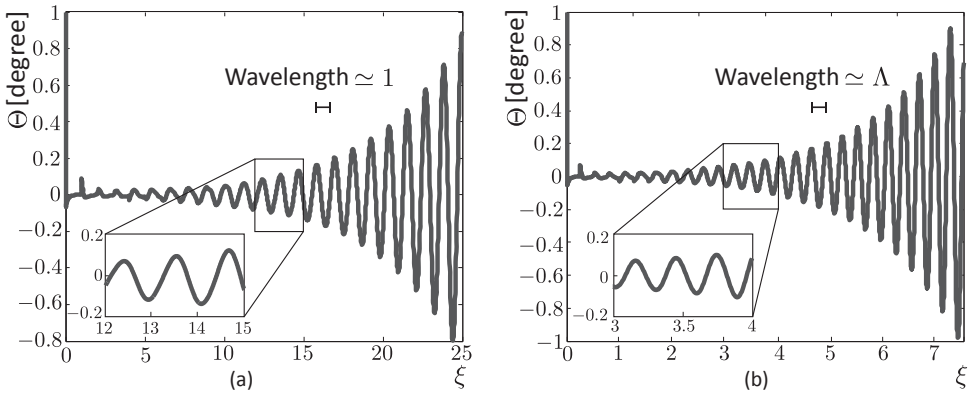

Figure 4.5: Simulations of two-stabilizer BHAs equipped with a push-the-bit RSS characterized by a lateral stiffness that is (a) small ($\mu = 10^{-3}$) and (b) large ($\mu = 10^{3}$). Parameters are $\lambda_2 = 3$ and $\Lambda = 0.25$. [Oscillations were triggered by imposing a local kink in the borehole inclination, a proxy for a sudden change in the RSS force or the weight on bit. The pitch of the induced oscillations corresponds to the bit-first stabilizer distance at small μ, but is related to the position of the pads at large μ. Parameter $\eta\Pi$ has been chosen as making the system directionally unstable without exciting higher frequency modes. The imposed $\eta\Pi$ is significantly smaller in the first case, a direct consequence of the better intrinsic directional stability of the system at small μ.]

Position of the pads Λ becomes a key parameter for large μ; with the pads acting more and more as an extra stabilizer, their positions have a significant effect on $\eta\Pi|_s$. For example, for $\mu = 1000$, $\eta\Pi|_s$ is halved for Λ increasing from 0.25 to 0.3 (Fig. 4.4b). The variation of $\eta\Pi|_s$ at large μ is reminiscent of that on Figure 4.3a for a two-stabilizer BHA. If the shape of these curves is confirmed by field observations, one could use this model to optimize BHA designs by identifying the positions of the RSS pads and the stabilizers in a way such that the irregular shape of the stability diagram can be accounted for fully.

In the intermediate range of stiffness μ, the region of stability in the $\mu - \eta\Pi$ plane exhibits a rich behavior. Within this range, both the RSS pads and the first stabilizer have a similar influence on the drilling direction at the bit, with their combined action possibly exciting higher-frequency modes that are strongly related to position of the pads Λ. Figure 4.6 testifies to this complex behavior, as shown for $\Lambda = 0.3$ and $\Lambda = 0.4$, respectively.

The fact that some high frequencies become dominant does not mean that lower frequencies, especially those related to the pads and the first stabilizer, are stable. The previous observations about the relevance of high frequencies are still valid.

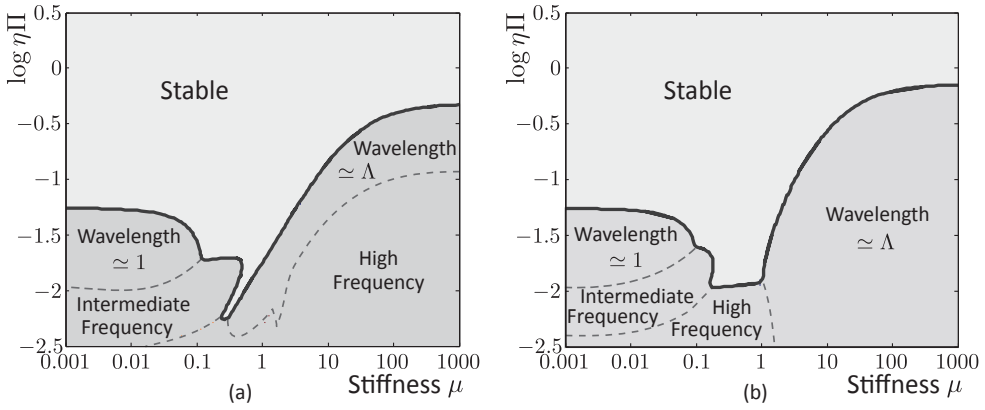

Figure 4.6: Strong dependence of the directional stability on Λ for intermediate μ for $\lambda_2 = 3$: (a) $\Lambda = 0.3$ and (b) $\Lambda = 0.4$. [For intermediate values of the stiffness, the pads and the first stabilizer exert a similar influence on the drilling direction at the bit. Their combined effect leads to a rich behavior and high-frequency modes may be excited.]

4.4 Borehole Rippling

4.4.1 Influence of ε

Small parameter ε does not have a significant influence on the directional stability of the system. The question is then whether it can be safely neglected when propagating the borehole. Because it multiplies the higher-order derivative in (4.2), parameter ε controls the short-range behavior of the propagation equation, *i.e.*, it introduces an *internal* boundary layer in the solution following any discontinuity in the borehole inclination. If $\varepsilon = 0$, the moment at the bit vanishes and the bit adapts instantaneously its orientation to any change in the load pattern. On the contrary if $\varepsilon \neq 0$, it theoretically requires an *infinite* moment at the bit to impose a sudden change in its orientation.

Figure 4.7 illustrates the short-range influence of ε on the borehole and bit inclinations. The borehole and BHA are initially vertical, *i.e.*, $\Theta_0 = \theta_0 = 0$ over $[-\sum_{i=1}^{n} \lambda_i, 0]$, and at $\xi = 0^+$, a constant RSS force is imposed. Independently of the value of ε, the jump in the RSS force induces a kink in the borehole inclination; its magnitude is however different whether $\varepsilon = 0$ or not (Appendix D). Bit inclination θ does not sustain any jump as long as $\varepsilon > 0$. (However, rate of change $\theta'(\xi)$ of the bit inclination jumps at $\xi = 0^+$.) Both inclinations exhibit a boundary

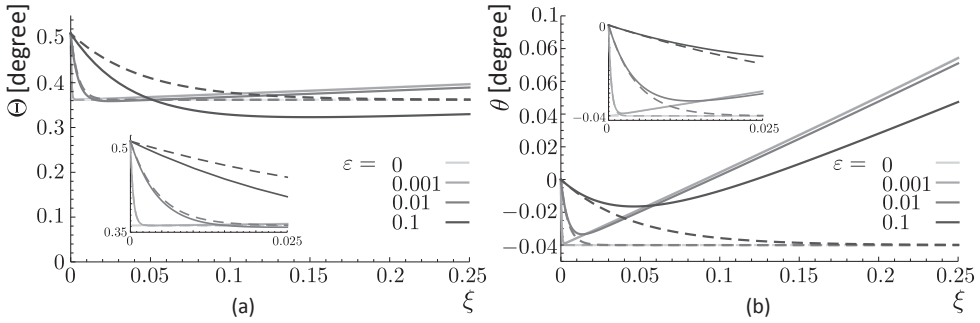

Figure 4.7: Short-range influence of small parameter ε for a three-stabilizer BHA in (a) the borehole and (b) the bit inclinations. The numerical solutions are in solid lines and the inner solutions in dashed ones. [The borehole and BHA are initially vertical; a constant RSS force is imposed at $\xi = 0$. A boundary layer is observed whose characteristic length is related to ε; when it vanishes, the boundary layer collapsed in a jump in θ and Θ. Parameters are $\lambda_2 = 1.5$, $\lambda_3 = 5$, $\Lambda = 0.25$, $\Gamma = 5 \times 10^{-3}$, $\eta\Pi = 0.5$, $\Upsilon = 6.3 \times 10^{-3}$, and $\mu = \tau = \tilde{M}^e = 0$.]

layer whose characteristic length is proportional to $\varepsilon \neq 0$ and in the limit case when it vanishes, the boundary layers collapse into discontinuities.

At the scale of the boundary layer, the external loading as well as the average orientations of the BHA sections can be seen as constant at first order. Indeed averaged inclinations are evaluated over a windows that is shifted at most by an increment $\delta\xi = O(\varepsilon)$, so that their variations are also of $O(\varepsilon)$. Loading parameters and history of the borehole inclination are also assumed to be smooth over the boundary layer. Introducing stretched coordinate

$$\zeta = \frac{\xi}{\varepsilon\eta\Pi}, \tag{4.14}$$

bit inclination $\hat{\theta}(\zeta)$ satisfies

$$\begin{aligned} -\hat{\theta}'(\zeta) = \mathcal{M}_b \left(\hat{\theta}(\zeta) - \langle\Theta\rangle_1 \right) + \sum_{i=1}^{n} \mathcal{M}_{w,i} \Upsilon \sin \langle\Theta\rangle_i + \mathcal{M}_r \Gamma + \sum_{i=1}^{n-1} \mathcal{M}_{k,i} \left(\langle\Theta\rangle_i - \langle\Theta\rangle_{i+1} \right) \\ + \mathcal{M}_s \left(\langle\Theta\rangle_0 - \langle\Theta\rangle_1 - \frac{\Delta_r}{\Lambda} \right) + \sum_{i=1}^{n} \mathcal{M}_{c,i} \left(\Theta_i - \langle\Theta\rangle_i \right) + \mathcal{M}_m \tilde{M}^e. \end{aligned} \tag{4.15}$$

This equation can be solved readily to yield

$$\hat{\theta}(\zeta) = (e^{-\mathcal{M}_b\zeta} - 1)\left[- \langle\Theta\rangle_1 + \sum_{i=1}^{n} \frac{\mathcal{M}_{w,i}}{\mathcal{M}_b}\Upsilon \sin\langle\Theta\rangle_i + \frac{\mathcal{M}_r}{\mathcal{M}_b}\Gamma + \sum_{i=1}^{n-1} \frac{\mathcal{M}_{k,i}}{\mathcal{M}_b}\left(\langle\Theta\rangle_i - \langle\Theta\rangle_{i+1}\right) \right.$$
$$\left. + \frac{\mathcal{M}_s}{\mathcal{M}_b}\left(\langle\Theta\rangle_0 - \langle\Theta\rangle_1 - \frac{\Delta_r}{\Lambda}\right) + \sum_{i=1}^{n} \frac{\mathcal{M}_{c,i}}{\mathcal{M}_b}\left(\Theta_i - \langle\Theta\rangle_i\right) + \frac{\mathcal{M}_m}{\mathcal{M}_b}\tilde{M}^e \right] + \Theta_0 e^{-\mathcal{M}_b\zeta}, \qquad (4.16)$$

where initial condition $\theta(0) = \Theta_0$ corresponds to an initially straight borehole of inclination Θ_0. Expression (4.16) confirms that the thickness of the boundary layer is of the order of $O(\varepsilon\eta\Pi/\mathcal{M}_b) = O(\varepsilon\eta\Pi) \leq O(\varepsilon)$ as $\mathcal{M}_b = O(1)$ and $\eta\Pi = O(10^{-1} - 1)$ or less. Inner solution (4.16) is plotted in Figure 4.7; departure from the actual solution is due to the average inclinations, which cannot be considered as constant outside the boundary layer.

As the drilling model has a resolution related to the bit dimensions, the boundary layer is likely not to be relevant. It is only the case for a bit with a long gauge and a close stabilizer. The boundary layer should thus rather be collapsed onto a jump in both θ and Θ at the scale of the model. Beyond its strong influence close to discontinuities, parameter ε has been shown to weakly influence the intermediate- and long-range responses of the system (Perneder, 2013). It will henceforth be set to zero for the rest of this chapter. It is inferred consequently that the bit is free to tilt and adapts instantaneously to any change in the loading pattern[3].

4.4.2 Geometric Approach to Rippling

With $\varepsilon = 0$ and $\tau = 0$, equation of propagation (4.2) reduces to

$$\mathcal{A}\Theta(\xi) = \mathcal{C}_i\langle\Theta\rangle_i + \mathcal{C}_0\left(\langle\Theta\rangle_0 - \frac{\Delta_r}{\Lambda}\right) + \mathcal{D}_i\Upsilon\sin\langle\Theta\rangle_i + \mathcal{F}\Gamma + \mathcal{G}\tilde{M}^e. \qquad (4.17)$$

Equation (4.17) is a functional delay algebraic equation, as is its perturbed form

$$\delta\Theta(\xi) = \sum_{i=0}^{n} \frac{\mathcal{C}_i}{\mathcal{A}}\langle\delta\Theta\rangle_i. \qquad (4.18)$$

The directional stability then only depends on the averaged *perturbed* inclinations of the BHA sections (and that related to the RSS), *i.e.*, it only depends on the position of the stabilizers relative to the bit, as enforced by isoperimetric constraints (3.16). Equation (4.18) can readily

[3] When deriving the general bit/rock interaction law, the contact pattern between the bit and the borehole was assumed not to vary too much. This assumption may be in jeopardy at the scale of any discontinuity.

be used to study the mechanism behind borehole rippling, starting from the geometry of the perturbation, by imposing a perturbed borehole trajectory of the form

$$\gamma(\xi) = A \sin\left(\frac{2\pi\xi}{\tilde{\ell}}\right), \tag{4.19}$$

where γ measures the relative position of the borehole axis around the (quasi)stationary trajectory, A is the amplitude of the perturbation (as the system is linear, this magnitude does not influence the results of this section), and $\tilde{\ell}$ is the wavelength of the oscillations. The bit is assumed to follow this sinusoidal path as do the stabilizers. The relative deflection of stabilizer i around the stationary solution relative to the bit is then given by

$$\triangle\gamma_i(\xi) = A \sin\left(\frac{2\pi(\xi - \xi_i)}{\tilde{\ell}}\right) - \gamma(\xi), \tag{4.20}$$

from which the perturbed deflection of the BHA and the lateral force at the bit can be computed by solving the related beam problem. The bit inclination is obtained by ensuring that the moment at the bit vanishes ($\varepsilon = 0$). The imposed sinusoidal trajectory is a physically acceptable solution only if at each point, drilling direction $\boldsymbol{d}$ at the bit is tangent to the prescribed borehole axis. This condition is satisfied only for some discrete combinations of dimensionless group $\eta\Pi$ and wavelength $\tilde{\ell}$. These acceptable solutions correspond to pairs of complex-conjugate roots crossing the imaginary axis; strictly speaking such modes characterize marginally stable cases. By focusing on solutions where $\tilde{\ell} \simeq 1$, critical $\eta\Pi$ and the corresponding wavelength are recovered, *i.e.*, $\eta\Pi = \eta\Pi|_s$ and $\Im(\alpha) = 2\pi/\tilde{\ell}$.

This approach is illustrated here for a three-stabilizer BHA with no RSS. The BHA is characterized by $\lambda_2 = 1.5$ and $\lambda_3 = 5$. The relative position of the second stabilizer has been chosen as to tentatively maximize the BHA deflection. Directional stability is defined by $\eta\Pi|_s \simeq 0.122$ and $\tilde{\ell} \simeq 1.14$.

The first observation is that the fluctuations in the borehole trajectory actual betray oscillations of the bit tilt, because the orientation of the bit axis remains almost constant (Fig. 4.8a). The fact that the tilt drives the spiraling mechanism justifies further the central role of dimensionless group $\eta\Pi$ in evaluating the directional stability of the system. This fluctuation of the tilt results from to the relative positions of the stabilizers, which, as they follow the regular

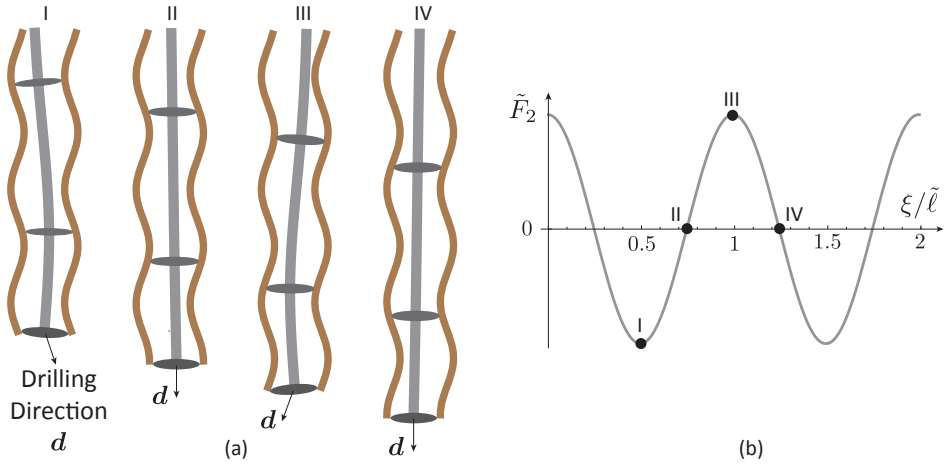

Figure 4.8: (a) Borehole rippling mechanism and (b) evolution of the lateral force at the bit. [Being constrained by the borehole, the relative position of the stabilizers induce an oscillating lateral force at the bit, affecting the drilling direction in such a way that it is tangent to the prescribed trajectory. The lateral force is defined as the reaction force from the rock on the bit, what explains its sign.]

rippled trajectory, induce a similarly fluctuating lateral force at the bit (Fig. 4.8b). Measurement devices recording either the inclination of the BHA or the bit then are likely to undervalue the actual micro-tortuosity of the borehole as well as its amplitude.

From a physically acceptable configuration, unilaterally modifying $\eta\Pi$ (while keeping $\tilde{\ell}$ constant) breaks the coaxiality between the tangent to the borehole and the drilling direction at the bit. A small value of $\eta\Pi$ (*i.e.*, smaller than $\eta\Pi|_s$) leads to larger tilts and progressively growing oscillations; inversely a larger $\eta\Pi$ would dampen the oscillations (Fig. 4.9a). These situations are however non-physical as no regular oscillating pattern can be maintained out of the combinations of $\eta\Pi$ and $\tilde{\ell}$ corresponding to purely imaginary characteristic roots. (The dynamics of the perturbation could be assumed to have an exponential growth or decay and virtually track all the critical characteristic roots.) Modifying wavelength $\tilde{\ell}$ without adapting $\eta\Pi$ similarly leads to unrealistic situations.

Positions of the stabilizers along the BHA affect the magnitude of the lateral force at the bit. Different positions of the stabilizers lead thus to different acceptable combinations of $\tilde{\ell}$ and $\eta\Pi$. Ripples defined with a period close to one present, however, a qualitative similar pattern (Fig. 4.9b). The deflection of the BHA and the lateral force at the bit are fully described

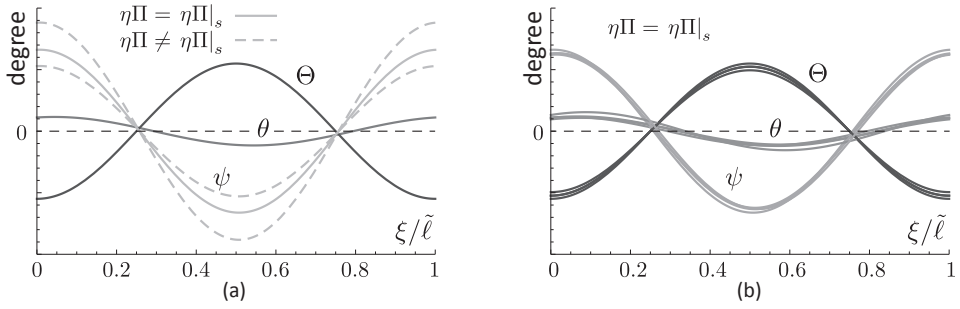

Figure 4.9: (a) Tilt, borehole and bit inclinations for the studied BHA over one period of oscillation [For $\eta\Pi = \eta\Pi|_s$, the drilling direction is coaxial to the drilling direction, *i.e.*, $\psi = \theta - \Theta$. Larger $\eta\Pi$ reduces the tilt and smaller ones augments it. Variations in the bit inclinations are smaller than these of the borehole inclination and θ and Θ are almost in opposition of phase. Varying $\eta\Pi$ without adapting $\tilde{\ell}$ leads to unrealistic situations as no oscillating pattern can be maintained.] (b) Tilt, borehole and bit inclinations for $\lambda_2 = 1.5, 2, 3,$ and 4.5 and $\lambda_3 = 5$ over one period of oscillation for $\eta\Pi = \eta\Pi|_s$. [Irrespective of the BHA configuration, the oscillation pattern, when scaled over the period, remains similar. For growing λ_2, wavelengths are 1.14, 1.27, 1.2, and 1.2 and critical value $\eta\Pi|_s$ are 0.12, 0.11, 0.07, and 0.03, respectively.]

by the positions of the stabilizers. (Unscaled lateral force F_2 is, however proportional to EI.) Consequently, stabilizer positions that tend to induce a larger BHA deflection when interacting with the prescribed borehole trajectory require a larger $\eta\Pi$ to prevent the tilt from being too large. Different solutions are possible for a same BHA geometry, corresponding to different periods and tilts, as well as corresponding BHA compliances.

4.4.3 Definition of the Limit Cycle

The previous linear stability analysis has provided information about the conditions under which a drilling system is prone to spiral. It is not able, however, to provide any information about the geometry and properties of the limit cycle: simulations for directionally unstable systems produce an exponentially growing oscillation of the borehole trajectory. Therefore a relevant nonlinearity is introduced to capture the limit cycle: a saturation of the bit tilt. This saturation has been observed experimentally (Pastusek et al., 2005; Ernst et al., 2007). Its origin is easily grasped for some bit geometries: for tapered or undercut bits, there exists a critical tilt for which most of bit gauge theoretically starts interacting with the wellbore, suddenly limiting its lateral aggressiveness. The saturation value is of the order of $O(1^\circ)$ but seems to depend on the

rock formation for full-gauge bits (Ernst et al., 2007). The influence of the stiffness of the RSS pads is here neglected but leads conceptually to similar results.

Propagation Equation with Saturation of the Tilt

Once the tilt has saturated, the lateral force at the bit does not affect the propagation of the borehole anymore (as long as its magnitude $\left|\tilde{F}_2\right|$ is larger than critical value $\tilde{F}_{2,c} = \eta\Pi\psi_c$). In order to derive the equation of propagation, expression (3.35) is then substituted by the kinematic condition

$$\psi = \psi_c, \tag{4.21}$$

or equivalently

$$\theta = \psi_c + \Theta, \tag{4.22}$$

where ψ_c is the saturation value of the tilt.

The saturation of the bit tilt does not influence the lateral force and moment at the bit when computed from the BHA perspective. Consequently, the bit inclination always verifies

$$\theta(\xi) = \sum_{i=1}^{n} \mathcal{C}_{\theta,i} \left\langle \Theta \right\rangle_i + \sum_{i=1}^{n} \mathcal{D}_{\theta,i} \Upsilon \sin \left\langle \Theta \right\rangle_i + \mathcal{F}_\theta \Gamma + \mathcal{G}_\theta \tilde{M}^e. \tag{4.23}$$

which is deduced by setting to zero expression (3.38) for the moment at the bit. Coefficients $\mathcal{C}_{\theta,i}$, $\mathcal{D}_{\theta,i}$, and $\mathcal{F}_\theta$ only depend on the coefficients of influence (Appendix C). By substituting (4.23) into (3.35), a similar general expression for the lateral force at the bit is obtained

$$\tilde{F}_2(\xi) = \sum_{i=1}^{n} \mathcal{C}_{F_2,i} \left\langle \Theta \right\rangle_i + \sum_{i=1}^{n} \mathcal{D}_{F_2,i} \Upsilon \sin \left\langle \Theta \right\rangle_i + \mathcal{F}_{F_2} \Gamma + \mathcal{G}_{F_2} \tilde{M}^e. \tag{4.24}$$

The equation of propagation is given by equation (4.17) when the tilt has not saturated, and by combining equations (4.22) and (4.23), when it has. All together, the general expression for the borehole inclination is given by

$$\Theta(\xi) = \sum_{i=1}^{n} \mathcal{C}_{\Theta,i} \left\langle \Theta \right\rangle_i + \sum_{i=1}^{n} \mathcal{D}_{\Theta,i} \Upsilon \sin \left\langle \Theta \right\rangle_i + \mathcal{F}_\Theta \Gamma + \mathcal{G}_\Theta \tilde{M}^e + \mathcal{S}\psi_c, \tag{4.25}$$

where $\mathcal{S}$ is zero when the bit has not saturated and one otherwise. The coefficients of the equation of propagation depend on dimensionless group $\eta\Pi$ and on the state of the system, that is, whether the tilt has saturated or not. If the tilt has saturated, they are only a function of

the coefficients of influence, not of $\eta\Pi$. Deriving (4.25) once with respect to scaled curvilinear coordinate ξ yields

$$\Theta'(\xi) = \mathcal{A}_\Theta \Theta(\xi) + \sum_{i=1}^{n} \mathcal{B}_{\Theta,i} \Theta(\xi - \xi_1) + \sum_{i=1}^{n} \mathcal{E}_{\Theta,i} \Upsilon \cos\langle\Theta\rangle_i \left(\Theta(\xi - \xi_{i-1}) - \Theta(\xi - \xi_i)\right). \quad (4.26)$$

Theoretically there is an extra term $\mathcal{S}'\psi_c$ in the right-hand side of (4.26), but is not represented as the propagation algorithm is assumed to rely on a event-detection algorithm that ensures a consistent state transition of the system. Equation (4.26) is a DDE where the different terms measure the evolution of the BHA loading (the constraints imposed on its deflection by the stabilizers, its weight, and the RSS force). The entire influence of the loading is now embedded in discontinuities in the borehole geometry and only their evolution is captured by (4.26). This particularity makes equation (4.26) peculiarly sensitive to numerical errors and approximations.

Limit Cycle for the Perturbation

The limit cycle for the inclinations of the bit and the borehole is presented in Figure 4.10 for a BHA with three stabilizers located at distances 1, 3.5, and 6 behind the bit. Dimensionless group $\eta\Pi$ is equal to 5×10^{-2} as to make the system directionally unstable ($\eta\Pi|_s = 6.46 \times 10^{-2}$).

Following the geometric feedback embedded in the borehole geometry, the tilt oscillates between prescribed saturation values $\pm\psi_c$. Because of the absence of external loads on the BHA, *i.e.*, $\Gamma = \Upsilon = \tilde{M}^e = 0$, the resulting limit cycle is symmetric in terms of shape and amplitude. The amplitude of the oscillations in the borehole inclination is about equal to the saturation value of the tilt (Fig. 4.10a). (It is a bit smaller because of the opposition of phase between θ and Θ.) The borehole trajectory does not correspond to a sinusoidal path: the succession of fast transitions between pseudo-plateaus in the inclination induces a trajectory closer to a triangular wave (Fig. 4.10b).

By approximating the oscillations in the borehole by a square signal of period $\tilde{\ell}$ and extrema of $\pm\psi_c$, an upper bound for the amplitude of the ripple is given by

$$A_{max} \simeq \frac{\tilde{\ell}\psi_c}{4}. \quad (4.27)$$

High frequencies thus create smaller oscillations. For the studied BHA, wavelength is $\tilde{\ell} \simeq 1.09$, which leads to upper bounds of about 2.4×10^{-3}, 4.8×10^{-3}, and 9.6×10^{-3} for $\psi_c = 0.5°$,

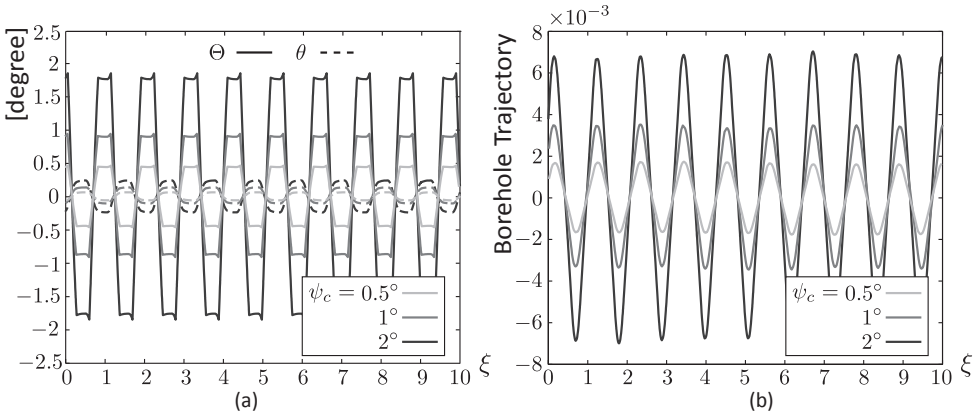

Figure 4.10: Limit cycle for different saturation values of the tilt ($\psi_c = 0.5°$, $1°$, $2°$). No external load is applied on the BHA ($\Gamma = \Upsilon = \tilde{M}^e = 0$). Other parameters for the simulation are $\lambda_2 = \lambda_3 = 2.5$ and $\eta\Pi = 0.05$. [The amplitude of the oscillations are proportional to ψ_c. Wavelength depends on the system geometry and $\eta\Pi$. The limit cycle is symmetric; it is generally not the case when part of the tilt is mobilized by the (quasi-)stationary loads on the BHA.]

$1°$ and $2°$, respectively. (Taking $\tilde{\ell} \in [1 - 1.2]$ generally provides a fair estimate of the upper bound.) A lower bound is obtained by assuming a sinusoidal shape for the oscillations;

$$A_{min} \simeq \frac{\tilde{\ell}\psi_c}{2\pi}, \tag{4.28}$$

providing amplitudes of 1.5×10^{-3}, 3×10^{-3}, and 6.1×10^{-3}, respectively. This lower bound is of limited application, however, as part of the tilt is generally mobilized by the (quasi-)stationary loads on the BHA in directional applications.

These approximations are to be compared with the *crooked-hole* formula, which defines the technological limit for the amplitude of the oscillations as half the overgauge between the drill collars and the wellbore (Woods and Lubinski, 1954; Gaynor et al., 2001). For small values of the saturation, the tilt drives the amplitude of the oscillations while it is limited by contacts between the drill collars and the wellbore for large saturation values. For tapered and undercut bits, it is likely that the saturation naturally limits the amplitude of the oscillations. This observation may explain field happenstances where the spiral amplitude was reported to be smaller than that predicted by the crooked-hole formula (Bellay et al., 1996; Sugiura and Jones, 2008b). Estimation of the ripple amplitude is central to estimate drift diameters and torque and drag.

Quasi-stationary Solutions

Assume a BHA submitted to constant RSS force Γ, exterior moment $\tilde{M}^e$, and active weight Π. The *unperturbed*, quasi-stationary component of the weight and the geometric feedback only evolves slowly along the borehole; they can be seen as quasi-constant over the *long* range, *i.e.*, over a distance longer than the BHA. This quasi-invariance leads to borehole trajectories defined by slowly varying curvatures (Perneder, 2013). They represent quasi-rigid body motions of the BHA characterized by quasi-stationary penetrations variables.

Without loss of generality, the weight of the BHA is assumed to be applied along inclination $\langle\Theta\rangle$ of the BHA. (Quasi-stationarity refers thus to the slow evolution of $\langle\Theta\rangle$ along the borehole.) Its influence on the lateral force and moment at the bit is then given by $\mathcal{F}_w\Upsilon\sin\langle\Theta\rangle$ and $\mathcal{M}_w\Upsilon\sin\langle\Theta\rangle$ where $\mathcal{F}_w=\sum\mathcal{F}_{w,i}$ and $\mathcal{M}_w=\sum\mathcal{M}_{w,i}$.

Two parameters are sufficient to completely define the long-range solution: curvature κ_s and tilt ψ_s (Perneder, 2013). The quasi-stationary borehole trajectory then reads

$$\Theta(\xi)=\Theta_0+\kappa_s\xi, \tag{4.29}$$

$$\theta(\xi)=\Theta_0+\kappa_s\xi+\psi_s. \tag{4.30}$$

By substituting (4.29) and (4.30) into the equations for the lateral force and moment at the bit, the system can be solved for κ_s and ψ_s. Depending whether the tilt is assumed to have saturated or not, expressions for κ_s differ but together provide an upper bound for the borehole curvature.

The Bit Tilt Does not Saturate Independently of the directional stability of the system, quasi-stationary curvature κ_s and tilt ψ_s are given by

$$\kappa_s=\frac{(\mathcal{F}_b-\eta\Pi)(\mathcal{M}_m\tilde{M}^e+\Gamma\mathcal{M}_r)-\mathcal{F}_m\mathcal{M}_b\tilde{M}^e-\Gamma\mathcal{F}_r\mathcal{M}_b-\Upsilon\sin\langle\Theta\rangle\left(\mathcal{M}_w(\eta\Pi-\mathcal{F}_b)+\mathcal{F}_w\mathcal{M}_b\right)}{\mathcal{M}_\kappa(\eta\Pi-\mathcal{F}_b)+\mathcal{F}_\kappa\mathcal{M}_b}, \tag{4.31}$$

$$\psi_s=\frac{-\mathcal{F}_\kappa(\mathcal{M}_m\tilde{M}^e+\mathcal{M}_r\Gamma)+\mathcal{M}_\kappa(\mathcal{F}_m\tilde{M}^e+\mathcal{F}_r\Gamma)+\tilde{\Upsilon}\sin\langle\Theta\rangle\left(\mathcal{F}_w\mathcal{M}_\kappa-\mathcal{F}_\kappa\mathcal{M}_w\right)}{\mathcal{M}_\kappa(\eta\Pi-\mathcal{F}_b)+\mathcal{F}_\kappa\mathcal{M}_b}, \tag{4.32}$$

where coefficients

$$\mathcal{F}_\kappa=\frac{1}{2}\left[\mathcal{F}_b+\sum_{i=1}^{n-1}\mathcal{F}_{k,i}(\lambda_i+\lambda_{i+1})\right], \tag{4.33}$$

$$\mathcal{M}_\kappa = \frac{1}{2}\left[\mathcal{M}_b + \sum_{i=1}^{n-1}\mathcal{M}_{k,i}(\lambda_i + \lambda_{i+1})\right], \tag{4.34}$$

encapsulate the influence of curvature κ_s on the lateral force and moment at the bit (Perneder, 2013). If $\eta\Pi$ is smaller than critical value $\eta\Pi|_\Gamma = (\mathcal{F}_b\mathcal{M}_r - \mathcal{F}_r\mathcal{M}_b)/\mathcal{M}_r$ – which is likely – RSS force Γ tend to increase borehole curvature κ_s. Otherwise, it leads to the counter-intuitive fact of a growing Γ reducing κ_s. In the case when $\eta\Pi = \eta\Pi|_\Gamma$, the RSS force has theoretically no influence on the borehole trajectory (Perneder, 2013). These results are valid as long as the tilt does not saturate (Fig. 4.11).

When the system is directionally unstable but that the quasi-stationary lateral force is not large enough to force a permanent saturation of the tilt, fluctuations in the inclination progressively growth until a limit cycle is reached. The partial mobilization of the tilt by the quasi-stationary loading breaks the symmetry of the limit cycle and leads to quasi-constant curvatures slightly lower than (4.31) as a portion of the lateral force is ineffectual when the tilt saturates. Curvature (4.31) corresponds thus to an upper bound. Directionally stable systems are not affected by the tilt saturation and virtually perform at upper bound (4.31).

The Tilt Is Permanently Saturated When the combined influence of Γ, $\tilde{M}^e$, and $\Upsilon\sin\langle\Theta\rangle$ on the lateral force at the bit is so that $\left|\tilde{F}_2\right| > \tilde{F}_{2,c} = \eta\Pi\psi_c$, stationary tilt ψ_s is trivially $\pm\psi_c$ depending on the sign of $\tilde{F}_2$. Expression for κ_s then is given by

$$\kappa_s = \frac{\mp\mathcal{M}_b\psi_c - \mathcal{M}_m\tilde{M}^e - \mathcal{M}_r\Gamma - \mathcal{M}_w\Upsilon\sin\langle\Theta\rangle}{\mathcal{M}_\kappa}. \tag{4.35}$$

As the tilt saturates, the response of the system is independent of $\eta\Pi$. The notion of directional stability also becomes irrelevant. Stationary curvature (4.35) is valid as soon as $\left|\tilde{F}_2\right| > \tilde{F}_{2,c}$; for a vertical borehole ($\langle\Theta\rangle = 0$) and no moment at the last stabilizer, this condition is verified for $\Gamma > \Gamma_*$ where Γ_* is given by

$$\Gamma_* = \frac{\mathcal{M}_\kappa(\eta\Pi - \mathcal{F}_b) + \mathcal{F}_\kappa\mathcal{M}_b}{\mathcal{F}_r\mathcal{M}_\kappa - \mathcal{F}_\kappa\mathcal{M}_r}\psi_c. \tag{4.36}$$

It corresponds to the magnitude of the RSS force for which tilt ψ_s theoretically saturates.

As $\mathcal{M}_r > 0$ and $\mathcal{M}_\kappa > 0$, an increase in RSS force Γ reduces curvature κ_s: once the tilt fully saturates, increasing Γ leads to reduced steering abilities (Fig. 4.11). Increasing saturation

value ψ_c leads to larger curvatures. Orders of magnitude for the RSS force are so that complete saturation is achievable for small ψ_c only. Evaluating saturation ψ_c is thus central to assess the drilling performance of any drilling system.

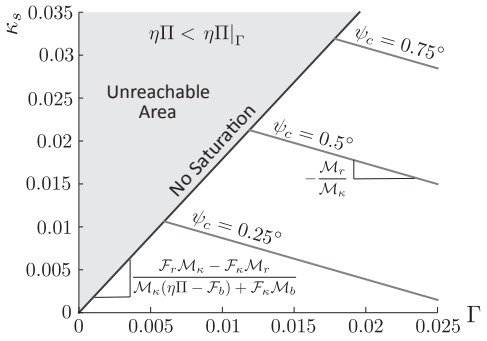

Figure 4.11: Upper bound for curvature κ_s. [The values correspond to a 3-stabilizer BHA with $\lambda_2 = \lambda_3 = 2.5$, $\Lambda = 0.29$ and $\eta\Pi = 0.05$. The plot focuses on building systems with $\eta\Pi < \eta\Pi|_\Gamma$.]

Borehole Simulation

Typical results of simulations are presented on Figure 4.12 for a three-stabilizer BHA ($\lambda_2 = \lambda_3 = 2.5$) and $\Gamma = 0.001$ initiated at $\xi = 0$. The borehole is initially vertical; the observed drift is due to the influence of the RSS force. (Here, weight Υ was set to zero so that the quasi-stationary solution is described by a constant curvature.) Tilt saturation $\psi_c = 0.5°$ and dimensionless group $\eta\Pi$ is equal to 5×10^{-2}.

A limit cycle rapidly settles. Rippling is seen as a consequence of tilt fluctuations; oscillations in the bit inclination are one order of magnitude smaller than those in that of the borehole (Fig. 4.12a, b, e, and f). As prescribed, the tilt saturates when the lateral force $\left|\tilde{F}_2\right|$ at the bit crosses threshold $\tilde{F}_{2,c} = \eta\Pi\psi_c$ (Fig. 4.12c and d). The superposition of the quasi-stationary solution and the ripple is observed on Fig. 4.12a. Finally, the borehole trajectory is shown in phase plane around the stationary solution (Fig. 4.12e). Local curvature is limited following saturation of the tilt (Fig. 4.12b); when the tilt saturates, evolution of the borehole inclination is prescribed by that of the bit, which is constrained by the stiffness of the BHA.

The constant loading of the BHA mobilizes part of the tilt according to (4.32); this breaks

the symmetry of the limit cycle around the stationary solution. If the combined influence of the RSS force, the weight, and the exterior moment on the lateral force at the bit is in such a way that the tilt is constantly saturated, no oscillations in the borehole are possible. For the system under consideration ($\Upsilon = \tilde{M}^e = 0$), permanent saturation of the tilt occurs if RSS force $\Gamma > \Gamma_* \gtrsim 0.012$ (Fig. 4.13). For $\Gamma = 0.01$, the tilt already saturates during most of the run, which affects the shape and amplitude of the limit cycle (Fig. 4.13 b and e).

Saturation of the tilt could thus explain as to why occurrences of spiraling were reported to depend on the borehole inclination and the amplitude of the RSS force. Beyond critical force Γ_*, the directional features of the BHA are limited: Figure 4.13 illustrates the influence of the RSS on both the possibility to exhibit large borehole oscillations and the directional capacity of the system. The order of magnitude for the RSS is representative of actual capabilities of RSSs. The results of this section argue for a more systematic study of the tilt saturation, especially for tapered and undercut bits, as it may lead to better borehole quality while meeting directional requirements.

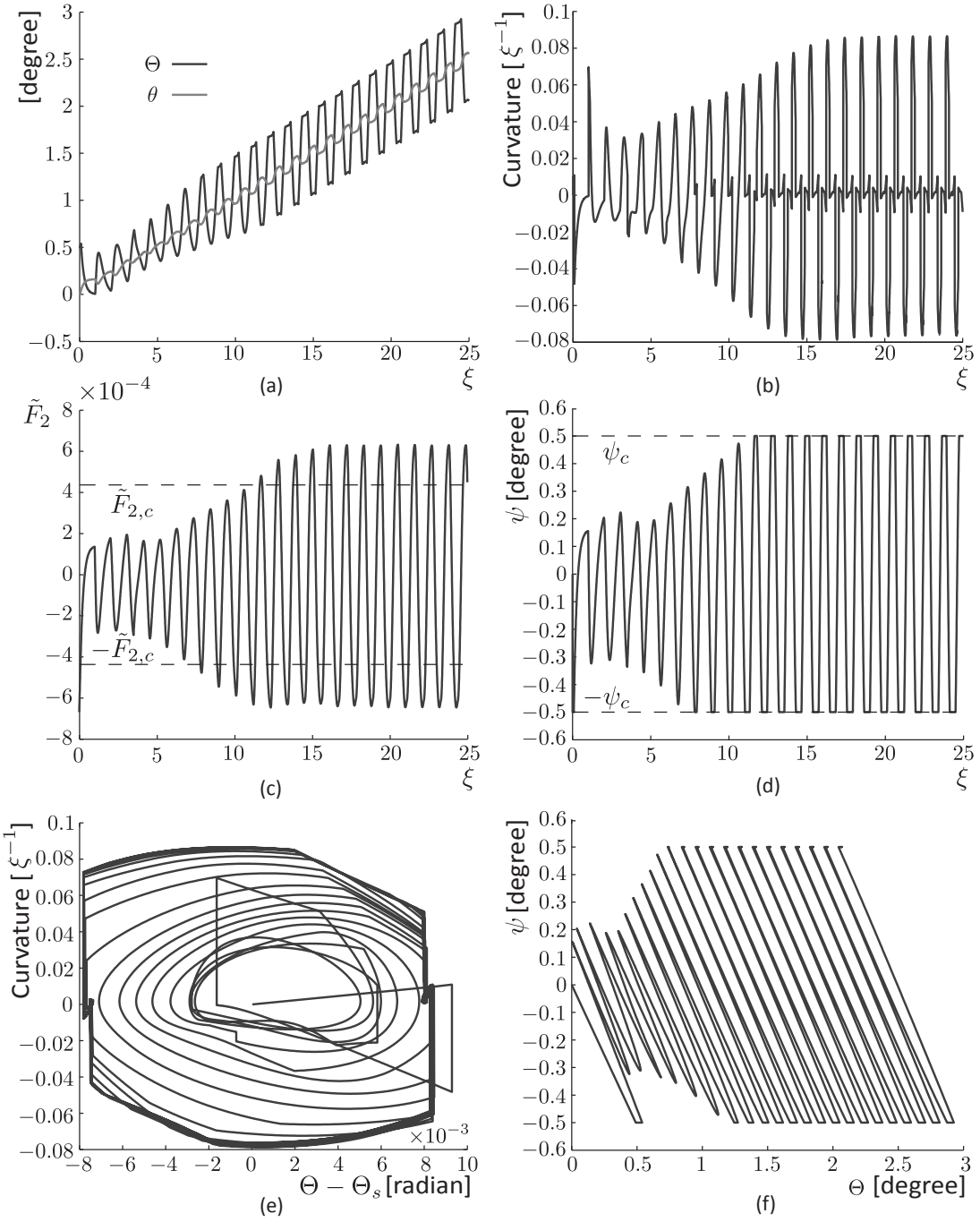

Figure 4.12: Typical results of borehole simulation. (a) Bit and borehole inclinations, (b) borehole curvature, (c) lateral force at the bit, (d) bit tilt, (e) limit cycle in phase plane, and (f) trajectory in plane $\Theta - \psi$. The BHA has three stabilizers located 1, 3.5, and 6 behind the bit. The other parameters of the simulations are $\Lambda = 0.29$, $\Gamma = 0.001$, $\Upsilon = 0$, $\eta\Pi = 0.05$, and $\psi_c = 0.5°$.

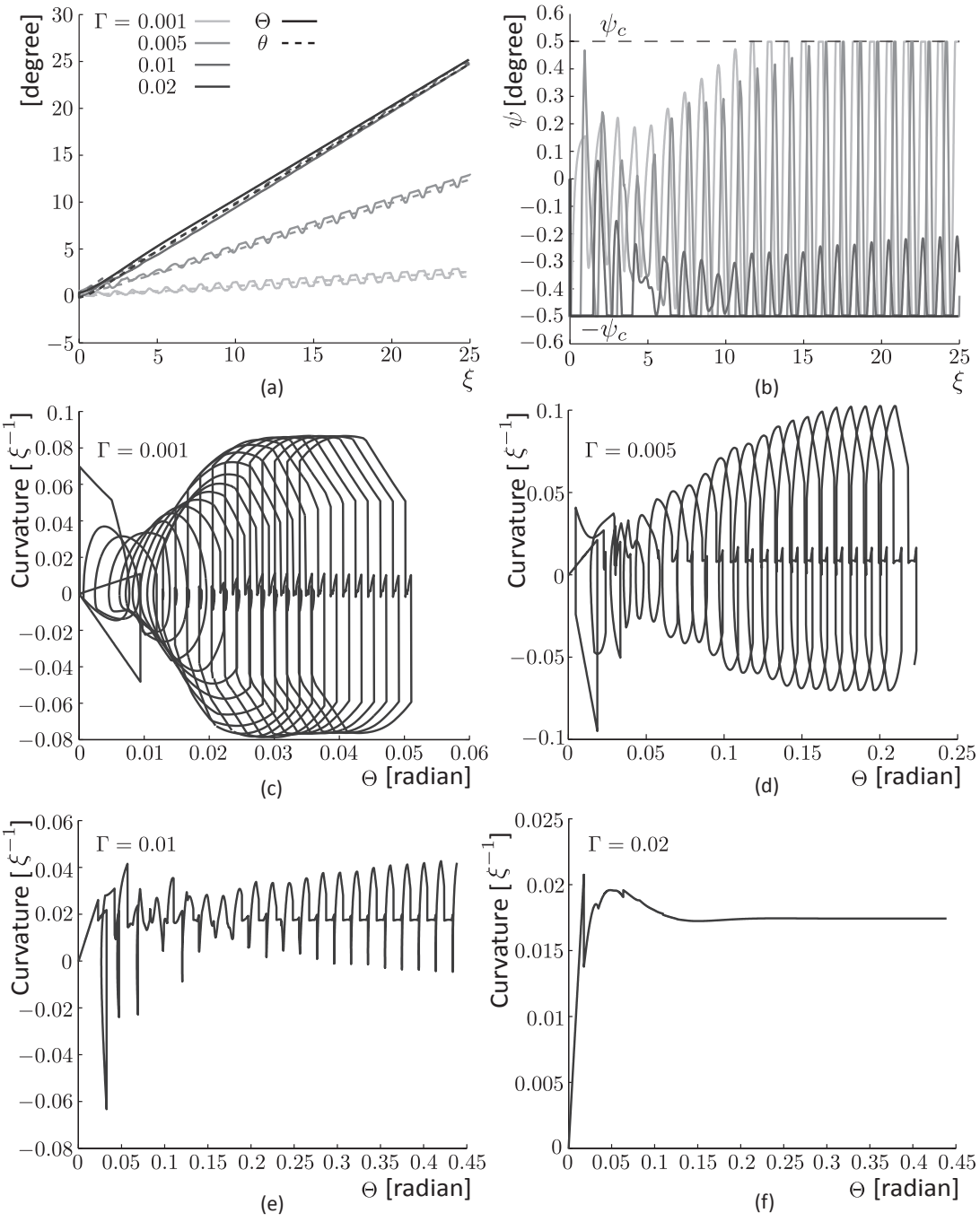

Figure 4.13: Influence of the RSS force on the limit cycle and the achievable curvature. [As the quasi-stationary lateral force increases, it mobilizes a greater part of the tilt. If this force is so large that the tilt constantly saturates, it suppresses any possibility of borehole oscillations. It also leads, however, to a reduction in the achievable curvature.]

Chapter 5

Three-dimensional Model

5.1 Equations of Borehole Propagation

Viewed as a three-dimensional curve, a borehole can be described by its inclination and azimuth, as functions of the arc-length coordinate. Two equations of propagation are thus needed. It is assumed here that the stabilizers are free to tilt ($\tau = 0$), that the RSS pads do not sense perturbations in the borehole ($\mu = 0$), and that the moment at the last stabilizer vanishes ($\tilde{\boldsymbol{M}}^e = 0$). The drill bit is first assumed not be free to tilt ($\varepsilon > 0$). The equations of propagation are obtained by equating expressions (3.35)-(3.38) and (3.33)-(3.34) for the components of the lateral force and the moment at the bit, and using kinematics relationships (3.14):

$$\eta\Pi\left[\cos\varpi(\theta-\Theta)+\sin\varpi\sin\Theta(\phi-\Phi)\right]=$$
$$\mathcal{F}_b\left(\theta-\langle\Theta\rangle_1\right)+\sum_{i=1}^{n}\mathcal{F}_{w,i}\Upsilon\sin\langle\Theta\rangle_i+\mathcal{F}_r\Gamma_2+\sum_{i=1}^{n-1}\mathcal{F}_{k,i}\left(\langle\Theta\rangle_i-\langle\Theta\rangle_{i+1}\right), \tag{5.1}$$

$$\eta\Pi\left[-\sin\varpi(\theta-\Theta)+\cos\varpi\sin\Theta(\phi-\Phi)\right]=$$
$$\mathcal{F}_b\left(\phi-\langle\Phi\rangle_1\right)\sin\langle\Theta\rangle_1+\mathcal{F}_r\Gamma_3+\sum_{i=1}^{n-1}\mathcal{F}_{k,i}\left(\langle\Phi\rangle_i-\langle\Phi\rangle_{i+1}\right)\sin\langle\Theta\rangle_1, \tag{5.2}$$

$$-\varepsilon\eta\Pi\left[-\theta'\cos\varsigma+\phi'\sin\varsigma\sin\theta\right]=$$

$$-\mathcal{M}_b\left(\phi-\langle\Phi\rangle_1\right)\sin\langle\Theta\rangle_1-\mathcal{M}_r\Gamma_3-\sum_{i=1}^{n-1}\mathcal{M}_{k,i}\left(\langle\Phi\rangle_i-\langle\Phi\rangle_{i+1}\right)\sin\langle\Theta\rangle_1\,, \tag{5.3}$$

$$-\varepsilon\eta\Pi\left[\theta'\sin\varsigma+\phi'\cos\varsigma\sin\theta\right]=$$

$$\mathcal{M}_b\left(\theta-\langle\Theta\rangle_1\right)+\sum_{i=1}^{n}\mathcal{M}_{w,i}\Upsilon\sin\langle\Theta\rangle_i+\mathcal{M}_r\Gamma_2+\sum_{i=1}^{n-1}\mathcal{M}_{k,i}\left(\langle\Theta\rangle_i-\langle\Theta\rangle_{i+1}\right). \tag{5.4}$$

Expressions (5.1) and (5.2) for the lateral force enable to express the bit inclination θ and azimuth ϕ as a function of the loading of the BHA. These are then derived once respective to coordinate ξ and substituted in equations (5.3) and (5.4) for the moment to obtain equations solely in terms of the borehole inclination Θ and azimuth Φ. These can be reduced to expressions of the form

$$\Theta'(\xi)=F_\Theta(\Theta,\Phi,\Theta_i,\Phi_i,\langle\Theta\rangle_i,\langle\Phi\rangle_i,\mathbf{\Gamma},\Upsilon), \tag{5.5}$$

$$\Phi'(\xi)=F_\Phi(\Theta,\Phi,\Theta_i,\Phi_i,\langle\Theta\rangle_i,\langle\Phi\rangle_i,\mathbf{\Gamma},\Upsilon). \tag{5.6}$$

Equations (5.5) and (5.6) are coupled and have nonlinear terms coming from the projection of the azimuth on plane ($\hat{\boldsymbol{I}}_1$, $\hat{\boldsymbol{I}}_3$) to derive the force and moment at the bit.

5.2 Shape of the Perturbation

In order to study the propensity of a perturbation in the borehole trajectory to grow or decay, *i.e.*, to analyze the directional stability of the drilling system, equations of propagation (5.5) and (5.6) can be rewritten advantageously in terms of pseudo-azimuth Δ, which describes the orientation of the projection of the azimuth, respective to that of $\boldsymbol{e}_x$ in plane ($\boldsymbol{I}_1$,$\boldsymbol{I}_3$). Introducing pseudo-azimuth $\Delta\simeq\Phi\sin\Theta$ simplifies the equation of propagation as the nonlinear dependence of the azimuth on the inclination drops. (It is assumed implicitly that $\sin\theta\simeq\sin\langle\Theta\rangle_1\simeq\sin\Theta$.) Pseudo-azimuth Δ plays in plane ($\boldsymbol{I}_1$,$\boldsymbol{I}_3$) the role that inclination Θ plays in ($\boldsymbol{I}_1$,$\boldsymbol{e}_z$), in measuring the relative orientation of the borehole.

The equations of borehole propagation can then be redefined; DDEs for the evolution of the inclination and pseudo-azimuth have similar features and can be written as follows:

$$\begin{aligned}\varepsilon\Xi'(\xi) &= \mathcal{A}_{\Xi\Theta}\Theta(\xi) + \sum_{i=1}^{n}\mathcal{B}_{\Xi\Theta,i}\Theta(\xi-\xi_i) + \sum_{i=1}^{n}\mathcal{C}_{\Xi\Theta,i}\left\langle\Theta\right\rangle_i + \sum_{i=1}^{n}\mathcal{D}_{\Xi\Theta,i}\Upsilon\sin\left\langle\Theta\right\rangle_i \\ &+ \sum_{i=1}^{n}\mathcal{E}_{\Xi\Theta,i}\Upsilon\cos\left\langle\Theta\right\rangle_i\left(\Theta(\xi-\xi_{i-1}) - \Theta(\xi-\xi_i)\right) + \mathcal{F}_{\Xi\Theta}\Gamma_2 \\ &+ \mathcal{A}_{\Xi\Delta}\Delta(\xi) + \sum_{i=1}^{n}\mathcal{B}_{\Xi\Delta,i}\Delta(\xi-\xi_i) + \sum_{i=1}^{n}\mathcal{C}_{\Xi\Delta,i}\left\langle\Delta\right\rangle_i + \mathcal{F}_{\Xi\Delta}\Gamma_3, \end{aligned} \tag{5.7}$$

with $\Xi = \Theta$ or Δ. Because of symmetry in the bit/rock interaction law and in the expressions from the BHA model, coefficients of (5.7) satisfy the relations[1]

$$\mathcal{I}_{\Theta\Theta} = \mathcal{I}_{\Delta\Delta},\ \mathcal{I}_{\Theta\Delta} = -\mathcal{I}_{\Delta\Theta},\ \mathcal{I} = \mathcal{A},\mathcal{B},\mathcal{C},\mathcal{F},\mathcal{G}. \tag{5.8}$$

These coefficients only depend on the coefficients of influence in (3.35)-(3.38), on dimensionless groups $\eta\Pi$ and ε, and on the bit walk and flip (Appendix C). In particular, when ϖ and ς are zero, there are no cross-terms in the bit/rock interface law (3.7) and propagation equations (5.7) uncouple; each of them reduces to the equation governing the planar propagation of a borehole.

While simplifying the expressions for the DDEs, propagation equations (5.7) are valid only as long as the borehole inclination does sustain too large a curvature. In that case, the geometric influence of the borehole trajectory on $\left\langle\Delta\right\rangle_i$ can be neglected, *i.e.*,

$$\left\langle\Delta\right\rangle_i = \frac{\sin\left\langle\Theta\right\rangle_1}{\ell_i}\int_{\xi_i}^{\xi_{i-1}}\frac{\Delta(\zeta)}{\sin\Theta(\zeta)}\,\mathrm{d}\zeta \simeq \frac{1}{\ell_i}\int_{\xi_i}^{\xi_{i-1}}\Delta(\zeta)\,\mathrm{d}\zeta. \tag{5.9}$$

The directional stability of the borehole is not affected by this approach because it is similar to a linearization of the equation of propagation at any point along the borehole trajectory (Marck and Detournay, 2015b). Moreover significant changes of inclination only appear on a length scale larger than that at which spiraling develops. This formulation also facilitates the systematic characterization of spiral properties as Θ and Δ have similar behaviors in their respective planes. Finally, it has the advantage of removing the indetermination of the azimuth for vertical borehole, as suggested by Monsieurs (2015).

A borehole trajectory can be seen again as the superposition of two solutions: the quasi-stationary trajectory $\Theta_s(\xi)$ and $\Delta_s(\xi)$ due to the quasi-constant loads on the BHA, and the

[1] When the exterior moment at the last stabilizer is considered, this equality is not respected because of the sign convention used for that moment. It can be easily circumvented, however.

dynamics of perturbations $\delta\Theta(\xi)$ and $\delta\Delta(\xi)$. Inserting this decomposition in (5.7) leads to the following equations governing the perturbation of the borehole around the quasi-stationary trajectory

$$\begin{aligned}\varepsilon\delta\Xi(\xi) &= \mathcal{A}_{\Xi\Theta}\delta\Theta(\xi)+\sum_{i=1}^{n}\mathcal{B}_{\Xi\Theta,i}\delta\Theta(\xi-\xi_i)+\sum_{i=1}^{n}\mathcal{C}_{\Xi\Theta,i}\left\langle\delta\Theta\right\rangle_i \\ &+ \mathcal{A}_{\Xi\Delta}\delta\Delta(\xi)+\sum_{i=1}^{n}\mathcal{B}_{\Xi\Delta,i}\delta\Delta(\xi-\xi_i)+\sum_{i=1}^{n}\mathcal{C}_{\Xi\Delta,i}\left\langle\delta\Delta\right\rangle_i . \end{aligned} \tag{5.10}$$

The evolution of the perturbation is still, at first order, purely geometric. Equation (5.10) describes the dynamics of the perturbation around the quasi-stationary solution (Θ_s,Δ_s) and can be analyzed readily for stability, in view of its analytical form. Stability of system (5.10) is assessed by determining whether perturbations grow or decay exponentially. Due to the independence of (5.10) on the orientation of reference frame ($\tilde{\boldsymbol{I}}_1$,$\tilde{\boldsymbol{I}}_2$,$\tilde{\boldsymbol{I}}_3$) attached to the quasi-stationary solution, perturbations of the form

$$\delta\Theta(\xi)=e^{\alpha\xi},\quad \delta\Delta(\xi)=e^{\alpha\xi+i\phi},\quad \alpha\in\mathbb{C},\phi\in\mathbb{R}, \tag{5.11}$$

are considered, which represent perturbations in the form of oscillations for $\delta\Theta(\xi)$ and $\delta\Delta(\xi)$ that have the same spatial wavelength and similar exponential growth in amplitude, but possibly a different phase. The stability of the system is determined by computing characteristic roots α, solutions of the transcendental characteristic equations of the problem:

$$\begin{aligned}&\left(\mathcal{A}_{\Theta\Theta}-\epsilon\alpha+\sum_{k=1}^{n}\mathcal{B}_{\Theta\Theta,k}e^{-\alpha\xi_k}+\mathcal{C}_{\Theta\Theta,1}\frac{1-e^{-\alpha}}{\alpha}+\sum_{k=2}^{n}\mathcal{C}_{\Theta\Theta,k}\frac{e^{-\alpha\xi_{k-1}}-e^{-\alpha\xi_k}}{\alpha}\right)\\ &+e^{i\phi}\left(\mathcal{A}_{\Theta\Delta}-\epsilon\alpha+\sum_{k=1}^{n}\mathcal{B}_{\Theta\Delta,k}e^{-\alpha\xi_k}+\mathcal{C}_{\Theta\Delta,1}\frac{1-e^{-\alpha}}{\alpha}+\sum_{k=2}^{n}\mathcal{C}_{\Theta\Delta,k}\frac{e^{-\alpha\xi_{k-1}}-e^{-\alpha\xi_k}}{\alpha}\right)=0,\end{aligned} \tag{5.12}$$

$$\begin{aligned}&\left(\mathcal{A}_{\Delta\Theta}-\epsilon\alpha+\sum_{k=1}^{n}\mathcal{B}_{\Delta\Theta,k}e^{-\alpha\xi_k}+\mathcal{C}_{\Delta\Theta,1}\frac{1-e^{-\alpha}}{\alpha}+\sum_{k=2}^{n}\mathcal{C}_{\Delta\Theta,k}\frac{e^{-\alpha\xi_{k-1}}-e^{-\alpha\xi_k}}{\alpha}\right)\\ &+e^{i\phi}\left(\mathcal{A}_{\Delta\Delta}-\epsilon\alpha+\sum_{k=1}^{n}\mathcal{B}_{\Delta\Delta,k}e^{-\alpha\xi_k}+\mathcal{C}_{\Delta\Delta,1}\frac{1-e^{-\alpha}}{\alpha}+\sum_{k=2}^{n}\mathcal{C}_{\Delta\Delta,k}\frac{e^{-\alpha\xi_{k-1}}-e^{-\alpha\xi_k}}{\alpha}\right)=0,\end{aligned} \tag{5.13}$$

By substituting (5.8) in (5.12)-(5.13), phase ϕ satisfies $e^{2i\phi} = -1$, meaning that

$$\phi = \pm\frac{\pi}{2}.$$

This phase corresponds to the development of a spiral or, more precisely, a helix. Indeed, the general parameterization of the propagating perturbation in orthogonal system ($\tilde{\boldsymbol{I}}_1$,$\tilde{\boldsymbol{I}}_2$,$\tilde{\boldsymbol{I}}_3$) around the (quasi-)stationary solution reads

$$\delta\Theta(\xi) \sim e^{\Re(\alpha)\xi}\sin\Im(\alpha)\xi, \quad \delta\Delta(\xi) \sim \pm e^{\Re(\alpha)\xi}\cos\Im(\alpha)\xi, \tag{5.14}$$

where $\Re(\alpha)$ and $\Im(\alpha)$ denote the real and imaginary parts of characteristic root α, respectively. The actual borehole trajectory is obtained by integration of the inclination and pseudo-azimuth. In principle, the sign of the phase is determined by the walk tendency of the bit. The uniqueness of the phase means that, as soon as there exists some coupling between $\delta\Theta(\xi)$ and $\delta\Delta(\xi)$, all perturbations are combinations of helices, which grow or shrink exponentially depending on the associated characteristic root. At bifurcation, the real part of the rightmost characteristic roots is zero, $\Re(\alpha_{rm}) = 0$, and the radius of the spiral, after some transient, remains theoretically constant (Fig. 5.1a); otherwise, the radius has exponential growth/decay, typifying the directional stability of the system. It corresponds to a conic helix — *i.e.*, a spiral on a conic surface (Fig. 5.1b). In the limit case when $\varpi = 0°$, the phase is undefined, and the inclination and pseudo-azimuth oscillate independently; rippling, in general, is recovered.

For unstable systems, a growing spiral means that all quantities pertaining to the perturbed solution similarly exhibit an exponential growth, in a referential rotating along with the helix: the magnitude of the perturbed bit tilt, the amplitude of the spiral, or the relative position of the stabilizers respective to the bit, all grow exponentially at a rate given by $\Re(\alpha)$. At bifurcation, the BHA has a stationary (perturbed) deflection, which rotates with the spiral. Amplitudes of the force and moment at the bit are then also stationary as is the bit tilt so that stationarity of the perturbation is maintained naturally.

5.3 Directional Stability - Influence of ϖ

Qualitatively correct tendencies for $\eta\Pi|_s$ are obtained when limiting the BHA description to two stabilizers; relative position λ_2 is the dominant BHA-parameter controlling $\eta\Pi|_s$. Analysis

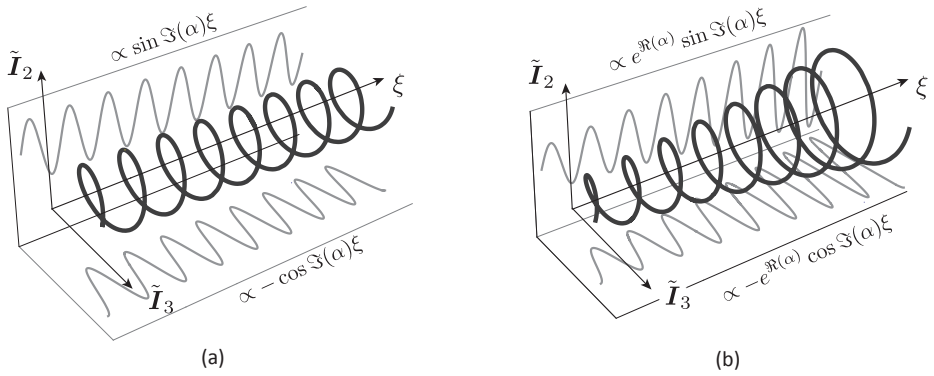

Figure 5.1: Mathematical description of a helix, representing the dynamics of the perturbed solution. (a) Parametric definition of a circular helix in a Cartesian system, corresponding to a marginally stale characteristic root ($\Re(\alpha) = 0$); (b) conic helix, as an example of an unstable trajectory ($\Re(\alpha) > 0$).

of equations (5.10) is conducted here by considering a simple BHA with uniform mechanical properties and two stabilizers located at 1 and $1 + \lambda_2$ above the bit.

As for the two-dimensional case, the directional stability of the system generally improves as dimensionless group $\eta\Pi$ increases (Fig. 5.2a). This variation is not monotonic, however; for some combinations of λ_2 and ϖ, different Hopf bifurcations may coexist (Fig. 5.2b). Nevertheless, the intermediate zones of stability between two bifurcation values are generally small, so that considering $\eta\Pi|_s$ as the largest of the bifurcation values is convenient in practice.

Figure 5.3 illustrates two simulations of a borehole trajectory conducted with identical BHAs but different $\eta\Pi$. The plots show the evolutions of borehole inclination Θ and azimuth $\Phi = \Delta \csc \Theta$, following an imposed perturbation in the borehole inclination (5° over a scaled distance of 0.04).

The pitch of the spiral is approximately equal to the distance between the bit and the first stabilizer. Thus, the model is able not only to capture the geometrical feedback imposed by the stabilizers, but also to reproduce the emergence of spirals as observed in the field. (When $\eta\Pi$ is small, other modes with higher frequencies also may be unstable. Their relevance is not ascertained, however.)

Walk ϖ and relative position λ_2 of the second stabilizer have a strong impact on $\eta\Pi|_s$. In general, the directional stability of the system is improved by moving the second stabilizer away

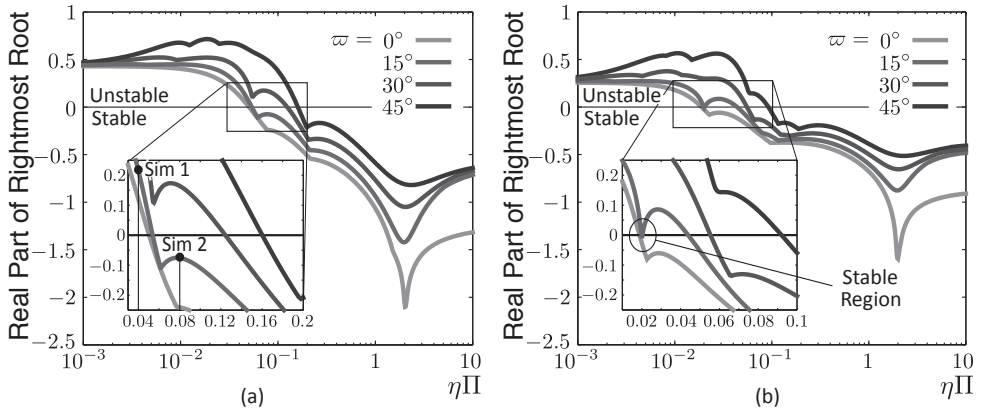

Figure 5.2: (a) Evolution of $\Re(\alpha_{rm})$ with dimensionless group $\eta\Pi$ and $\lambda_2 = 2.5$ for different bit walk ϖ. The markers symbolize systems used for the upcoming simulations. (b) Similar plot for $\lambda_2 = 4.5$. [Intermediate zones or stability are sometimes observed but usually remain small. Walk ϖ tends to make a system directionally more unstable.]

from the first one (Fig. 5.4). However, the risk of extraneous contacts between the BHA and the borehole simultaneously increases, with potential adverse influence on the directional stability. The general tendency is unequivocal: the bit walk makes the drilling system intrinsically less stable and consequently more prone to spiral.

An abrupt decrease of $\eta\Pi|_s$ around $\lambda_2 \simeq 2.5$ offers a first indication on where to locate the second stabilizer on the BHA to improve the intrinsic directional stability of the system significantly (Fig. 5.4b). Figure 5.4 also suggests the non-monotonic influence of the walk on $\eta\Pi|_s$ with λ_2, indicated by the varying distance between the curves for $\varpi = 0°$ and $\varpi = 15°$. In fact as long as the bit walk remains smaller than threshold $\varpi_*(\lambda_2)$, it hardly affects the critical value $\eta\Pi|_s$. The two-dimensional model is then sufficient to predict directional stability if $\varpi < \varpi_*$. Beyond this threshold, $\eta\Pi|_s$ exhibits a large increase (Fig. 5.5).

Critical walk ϖ_* strongly depends on λ_2. For instance, for $\lambda_2 = 2.5$, $\eta\Pi|_s$ only increases by 8% up to a walk of 20° ($\eta\Pi|_s = 5.46 \times 10^{-2}$ instead of 5.04×10^{-2} for $\varpi = 0°$), but then jumps to 12.4×10^{-2} for $\varpi = 30°$— more than a two-fold increase (Fig. 5.5). In terms of field conditions, the system will maintain somewhat similar stability features up to $\varpi = \varpi_*$; a much larger downhole WOB then is required beyond that threshold in order to keep the system directionally stable. In contrast for $\lambda_2 = 2.25$, the influence of the walk is rapidly significant:

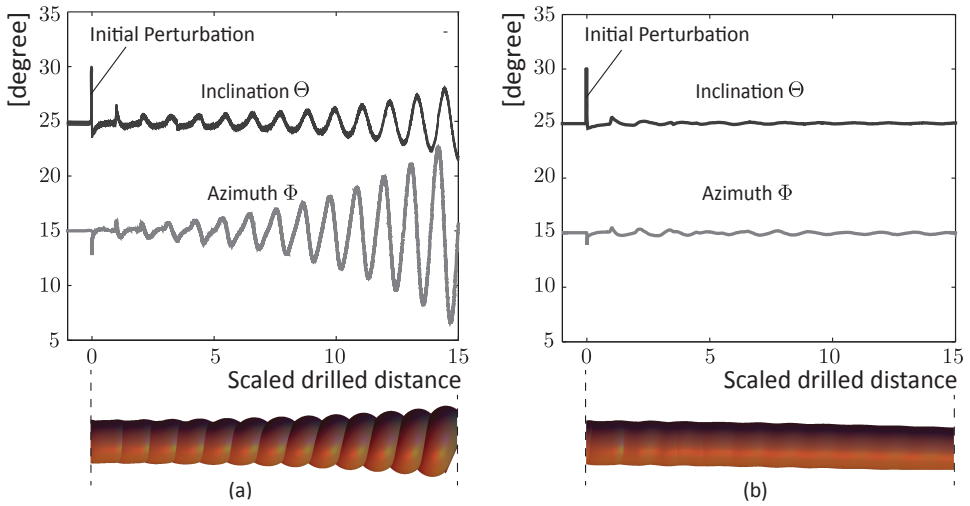

Figure 5.3: Borehole simulations with $\lambda_2 = 2.5$ and $\varpi = 15°$, leading to $\eta\Pi|_s = 5.4 \times 10^{-2}$. (a) Directionally unstable system ($\eta\Pi|_s = 4 \times 10^{-2}$); (b) directionally stable system ($\eta\Pi|_s = 8 \times 10^{-2}$). [The only difference between the simulations is the value of dimensionless group $\eta\Pi$. The same initial perturbation in the borehole trajectory is amplified progressively or dampened, depending on the directional stability of the system. The reconstructed lateral deformation of the borehole is not to scale, but presents a realistic picture. In practice, nonlinearity in the response of the system limit the amplitude of the fluctuations. The linear model is able, however, to capture the onset of spiraling.]

the critical value of the walk is around 4°. (It translates to $\eta\Pi|_s$, increasing to 6.95×10^{-2} for $\varpi = 5°$ from 3.27×10^{-2} for $\varpi = 0°$.)

The pitch of the spiral, when the system is directionally unstable, also increases with ϖ and can be up to 2 for large, rather unrealistic walks (greater than about 30°) and small λ_2. In general, this difference between the wavelength of the spiral and the distance between the bit and the first stabilizer progressively leads to larger BHA deflections close to the bit.

While some parameters of the model, such as EI or w always are known accurately, others are not. Factors influencing the bit walk downhole are not well understood (Chen et al., 2008). Determination of evolving parameter (due to bit wear and/or change of formation) requires systematic drill-off tests, and lateral steering resistance η requires laboratory testing. Nonetheless, good estimates can be obtained for $\eta\Pi|_s$ knowing the BHA geometry and a reasonable range for the bit walk. Directional stability then can be evaluated with educated guesses for η and G_1.

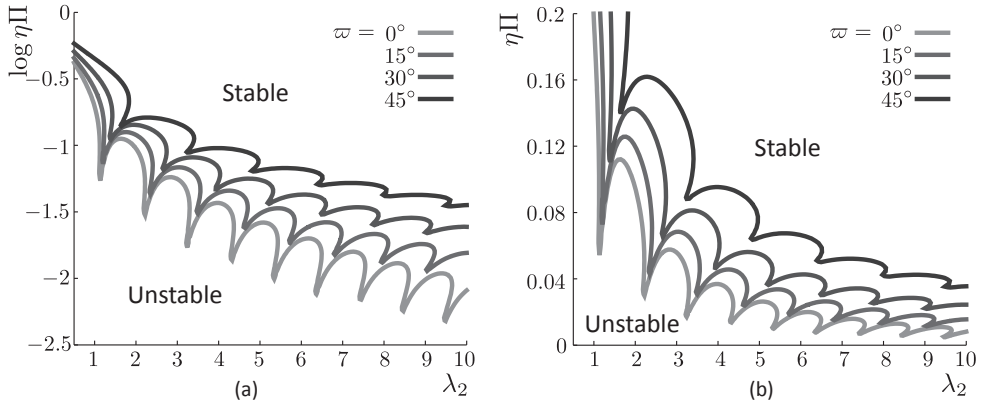

Figure 5.4: Influence of λ_2 on the directional tendency of the drilling system: (a) on a logarithmic scale and (b) on a linear scale. If the shape of this curve is confirmed is confirmed by field data, it enables identification of optimum λ_2 so that the intrinsic stability of the system is improved significantly.

5.4 Borehole Spiraling

The influence of small parameter ε mostly induces local *internal* boundary layers in the borehole trajectory, following discontinuous change in the loading of the BHA. It is therefore neglected henceforth, with the same reservations as argued in Section 4.4.1. (When ε is zero, the influence of the bit flip on the borehole propagation also naturally disappear.) With this simplification, the moment at the bit vanishes and the equations of propagation read

$$\begin{aligned}\Theta(\xi) = &\sum_{i=1}^{n} \mathcal{C}_{\Theta\Theta,i} \langle\Theta\rangle_i + \sum_{i=1}^{n} \mathcal{D}_{\Theta\Theta,i}\Upsilon \sin\langle\Theta\rangle_i + \mathcal{F}_{\Theta\Theta}\Gamma_2 \\ &+ \sum_{i=1}^{n} \mathcal{C}_{\Theta\Phi,i} \langle\Phi\rangle_i \sin\Theta + \mathcal{F}_{\Theta\Phi}\Gamma_3, \qquad (5.15)\\ \Phi(\xi)\sin\Theta = &\sum_{i=1}^{n} \mathcal{C}_{\Phi\Theta,i} \langle\Theta\rangle_i + \sum_{i=1}^{n} \mathcal{D}_{\Phi\Theta,i}\Upsilon \sin\langle\Theta\rangle_i + \mathcal{F}_{\Phi\Theta}\Gamma_2 \\ &+ \sum_{i=1}^{n} \mathcal{C}_{\Phi\Phi,i} \langle\Phi\rangle_i \sin\Theta + \mathcal{F}_{\Phi\Phi}\Gamma_3. \qquad (5.16)\end{aligned}$$

Consequently, the propagation equations for the perturbation are given by

$$\delta\Theta(\xi) = \sum_{i=i}^{n} \mathcal{C}_{\Theta\Theta,i} \langle\delta\Theta\rangle_i + \sum_{i=1}^{n} \mathcal{C}_{\Theta\Phi,i} \langle\delta\Phi\rangle_i \sin\Theta, \qquad (5.17)$$

$$\delta\Phi(\xi)\sin\Theta = \sum_{i=i}^{n} \mathcal{C}_{\Phi\Theta,i} \langle\delta\Theta\rangle_i + \sum_{i=1}^{n} \mathcal{C}_{\Phi\Phi,i} \langle\delta\Phi\rangle_i \sin\Theta. \qquad (5.18)$$

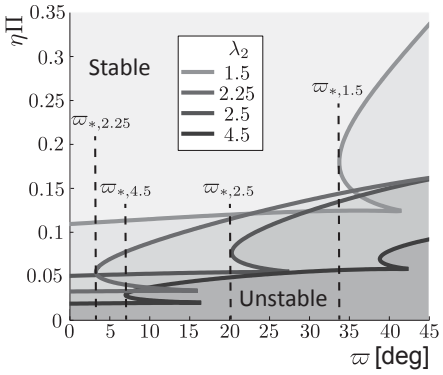

Figure 5.5: Influence of bit walk ϖ on the bifurcation value $\eta\Pi|_s$ for different positions of the second stabilizer λ_2. For each λ_2, there exists a critical value, ϖ_*, under which the influence of the walk remains small.

When expressed in terms of the pseudo-azimuth, expressions (5.17) and (5.18) drop the dependence on $\sin\Theta$; $\delta\Phi\sin\Theta$ is homologous to $\delta\Delta$. The evolution of the perturbation only depends on averaged orientations $\langle\delta\Theta\rangle_i$ and $\langle\delta\Delta\rangle_i$, *i.e.*, on the relative positions of the stabilizers in space respective to the bit.

5.4.1 Geometric Approach

The approach developed in Section 4.4.2 is extended here to the third dimension. The trajectory of the perturbation respective to frame $(\tilde{\boldsymbol{I}}_1,\tilde{\boldsymbol{I}}_2,\tilde{\boldsymbol{I}}_3)$ is given by

$$\gamma_2(\xi) = A\sin\left(\frac{2\pi\xi}{\tilde{\ell}}\right), \quad \gamma_3(\xi) = \mathrm{sgn}(\varpi)A\cos\left(\frac{2\pi\xi}{\tilde{\ell}}\right), \tag{5.19}$$

where $\gamma_2(\xi)$ and $\gamma_3(\xi)$ denote the bit position in planes $(\tilde{\boldsymbol{I}}_1,\tilde{\boldsymbol{I}}_2)$ and $(\tilde{\boldsymbol{I}}_1,\tilde{\boldsymbol{I}}_3)$, respectively. As deflections (5.19) are uncoupled, the relative position of stabilizer i respective to the bit reads

$$\triangle\gamma_{2,i}(\xi) = A\sin\left(\frac{2\pi(\xi-\xi_i)}{\tilde{\ell}}\right) - \gamma_2(\xi), \quad \triangle\gamma_{3,i}(\xi) = \mathrm{sgn}(\varpi)A\cos\left(\frac{2\pi(\xi-\xi_i)}{\tilde{\ell}}\right) - \gamma_3(\xi). \tag{5.20}$$

Like in two dimensions, the lateral force and the tilt at the bit can be computed from $\triangle\gamma_{2,i}$ and $\triangle\gamma_{3,i}$. Results are here discussed for a BHA with 2 stabilizers and $\lambda_2 = 2.5$ but can be generalized for more complex BHAs. The evolution of $\eta\Pi|_s$ with the walk is presented on Fig. 5.5; critical walk ϖ_* is about 20°.

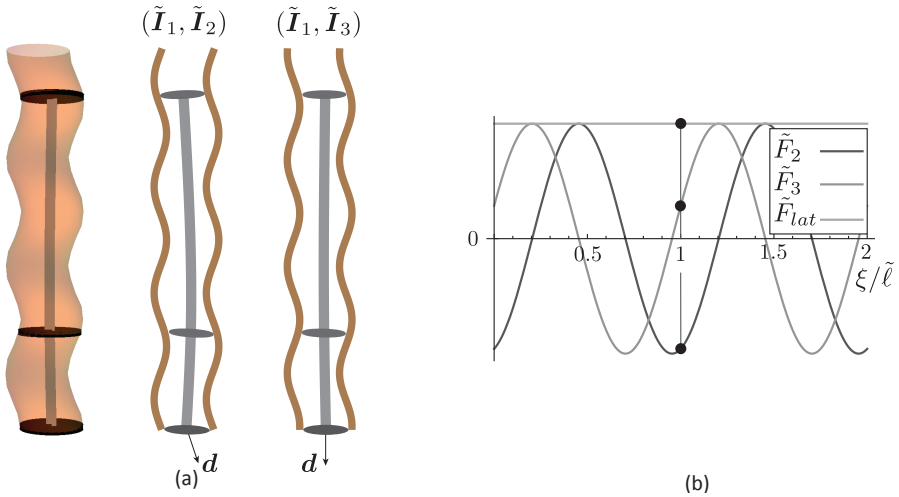

Figure 5.6: (a) Deformation of the BHA in the spiraled borehole for $\xi = k\tilde{\ell}$, $k \in \mathbb{N}$. (b) Evolution of the lateral force and its components along the helical path. [While its components oscillate, the resultant lateral force is constant, as is the bit tilt.]

Deformation of the BHA in the spiraled borehole at $\xi = k\tilde{\ell}$, $k \in \mathbb{N}$ is shown on Figure 5.6a for walk $\varpi = 15°$. It corresponds to $\eta\Pi|_s \simeq 5.4 \times 10^{-2}$ and $\tilde{\ell} \simeq 1.14$. As the bit follows the helical path, relative position of the stabilizers in plane $(\tilde{\boldsymbol{I}}_1,\tilde{\boldsymbol{I}}_2)$ and $(\tilde{\boldsymbol{I}}_1,\tilde{\boldsymbol{I}}_3)$ follow respectively sine and cosine evolutions. However, contrarily to the two-dimensional case, the resultant of lateral force at the bit does not fluctuate (Fig. 5.6b). (Its two components $\tilde{F}_2$ and $\tilde{F}_3$ do oscillate, however.) The spiral is thus maintained by the influence of the walk; the *rotating* lateral force imposes oscillating components ψ_2 and ψ_3 but the magnitude of the tilt $\psi = \sqrt{\psi_2^2 + \psi_3^2}$ remains constant and turns with the helical path of the borehole. The two-dimensional case can then be seen as the projection in plane $(\tilde{\boldsymbol{I}}_1,\tilde{\boldsymbol{I}}_2)$ of the more general three-dimensional one (Fig. 5.6a). (Once more, this geometric approach illustrates marginally stable cases. In the general case, the component of the force would increase or decrease exponentially, while keeping a rotational component in $(\tilde{\boldsymbol{I}}_1,\tilde{\boldsymbol{I}}_2,\tilde{\boldsymbol{I}}_3)$.)

Another difference compared to rippling is that other modes of deformation are possible for large values of the walk, that is, larger than critical value ϖ_*; these modes are characterized by a larger wavelength, which can reach twice the distance between the bit and the first stabilizer but strongly depend on λ_2. These modes impose in general a larger deflection of the BHA and thus a

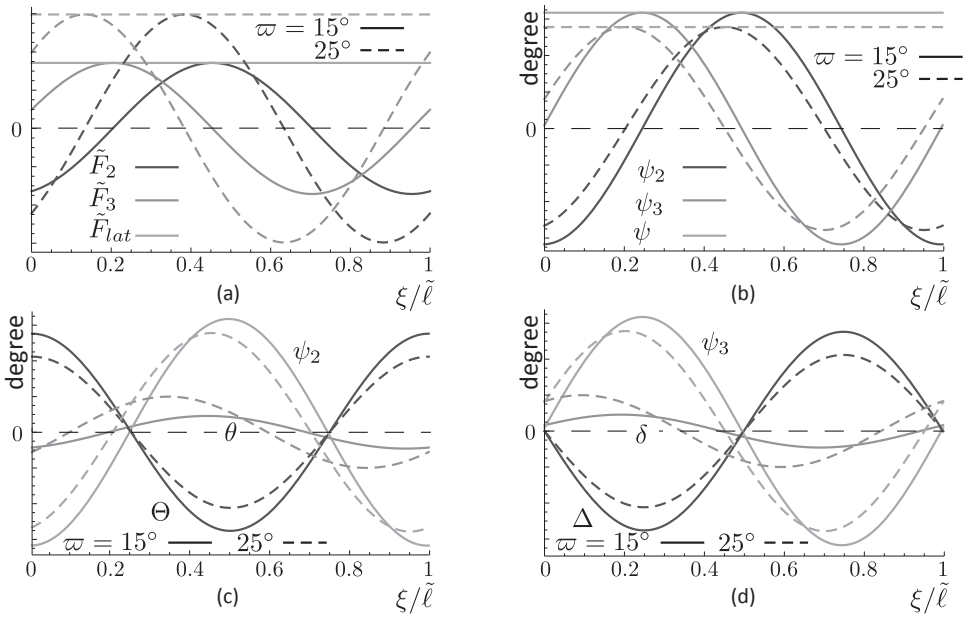

Figure 5.7: (a) Amplitude of the lateral force and its components over one period of revolution for two values of the bit walk, one below and one above the critical value. (b) Amplitude of the tilt and its components for the same configurations. (c) Comparison of the bit and borehole inclinations and the tilt in plane ($\tilde{\boldsymbol{I}}_1$,$\tilde{\boldsymbol{I}}_2$). (d) Comparison of the bit and borehole pseudo-azimuths and the tilt in plane ($\tilde{\boldsymbol{I}}_1$,$\tilde{\boldsymbol{I}}_3$).

larger lateral force at the bit. However, a larger force does not mean a significantly larger bit tilt, as these marginally stable modes are also related to larger $\eta\Pi$. (As the geometry of the borehole is imposed, so are $\theta - \psi_2$ and $\delta - \psi_3$, where δ is the pseudo-azimuth of the bit. At constant amplitude, larger wavelengths also lead to smaller Θ and Δ.) Moreover, larger deformations of the BHA increase the relative orientation of the bit and further reduce the amplitude of the tilt, as the bit and borehole orientations are almost in opposition of phase. Figure 5.7 illustrates the difference between these two modes for the studied BHA. For $\varpi = 25°$, $\eta\Pi|_s \simeq= 0.11$ and $\tilde{\ell} \simeq 1.48$. Note again the significant increases in $\eta\Pi|_s$ and in the wavelength beyond threshold ϖ_*. Such wavelengths cannot be sustained in two dimensions as the lateral force that would be induced at the bit for such configurations would remain, on average, too small at similar $\eta\Pi$ to maintain the fluctuations. The *out-of-plane* component is necessary to maintain the oscillations for larger $\eta\Pi$.

As the marginally stable path is defined by constant lateral force and tilt, analysis of amplitude A of oscillations (5.20) leading to a tilt saturation is trivial: tilt ψ is proportional to amplitude A. The coefficient of proportionality is an analytical function of $\eta\Pi$, $\tilde{\ell}$, and the geometry of the BHA. For a two-stabilizer BHA, it reads

$$A = \eta\Pi\psi_c \frac{\lambda_2(\lambda_2+1)}{\sqrt{2}\sqrt{\lambda_2^2+\lambda_2-(\lambda_2+1)\lambda_2\cos\left(\frac{2\pi}{\tilde{\ell}}\right)+\lambda_2\cos\left(\frac{2\pi(\lambda_2+1)}{\tilde{\ell}}\right)-(\lambda_2+1)\cos\left(\frac{2\pi\lambda_2}{\tilde{\ell}}\right)+1}}. \tag{5.21}$$

Relations between the amplitude of the oscillations and the critical saturation value ψ_c is illustrated for different λ_2 and walks ϖ in Figure 5.8a. It can be seen that for $\varpi > \varpi_*$, amplitudes of the oscillations can be significantly larger as: (a) the induced tilt is generally smaller (and so amplitudes can be larger before it reaches saturation) and (b) longer wavelengths leads to larger amplitudes. These modes thus not only influence the directional stability of the system, they also tend to increase the amplitude of the oscillations, which can be compared with the *crooked-hole* formula. The saturation of the tilt may explain field oscillations smaller than this technological upper bound. (For illustration purposes only, the vertical line in Figure 5.8a corresponds to a stabilizer located 9 ft behind the bit and the drill collars having a diameter 2 in. smaller than the nominal wellbore.)

Expression (5.21) can be extended to any combination of $\eta\Pi$, $\tilde{\ell}$, and λ_2 to find an upper bound to the amplitude of the spiral. It does not account for the stability of the system, however (Fig. 5.8b).

5.4.2 Definition of the Limit Cycle

Definition of the Equations of Propagation with Saturation of the Tilt

In three dimensions, two kinematic variables define the tilt once it has saturated: its amplitude ψ_c and its orientation τ_ϖ computed in plane ($\boldsymbol{I}_2$,$\boldsymbol{I}_3$) for the projection of $\boldsymbol{d}$ from $\boldsymbol{I}_2$. In terms of tilt components ψ_2 and ψ_3, angle τ_ϖ reads

$$\tau_\varpi = \arctan\frac{\psi_3}{\psi_2}, \tag{5.22}$$

so that $\psi_2 = \psi_c\cos\tau_\varpi$ and $\psi_3 = \psi_c\sin\tau_\varpi$. (As both ψ_2 and ψ_3 can be either positive or negative, the arctan function must here be understood as being defined over $[0, 2\pi)$.) Orientation of the

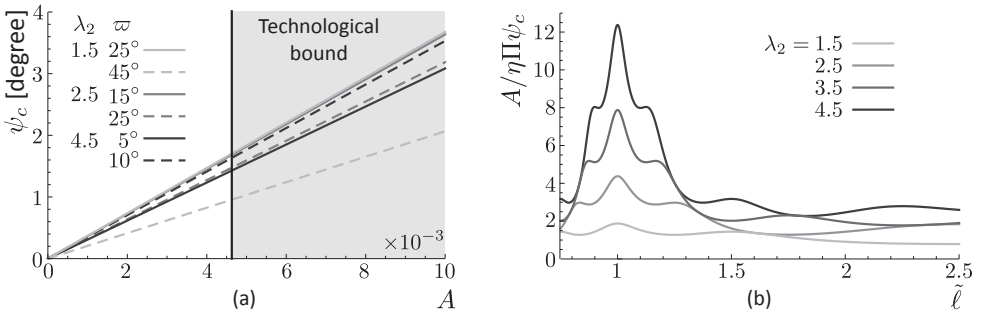

Figure 5.8: (a) Amplitude of the spiral for different λ_2 and ϖ. These can be compared to the *crooked-hole* formula. (b) Variation of equation (5.21) for different λ_2 as a function of the period of oscillations [This function increases with λ_2; but smaller $\eta\Pi$ are usually related to these values so that this curve is of limited interest without proper stability analysis.]

tilt is related to the components of the lateral force at the bit. Indeed, the orientation of the projection of $\boldsymbol{d}$ in ($\boldsymbol{I}_2$,$\boldsymbol{I}_3$) is related to that of lateral $\tilde{\boldsymbol{F}}_{lat}$ by

$$\tau_\varpi = \tau_F + \varpi, \tag{5.23}$$

with $\tau_F = \arctan F_3/F_2$. Expression (5.23) translates that the lateral penetration of the bit is not coaxial with the lateral force; their relative orientation is given by walk ϖ.

With the moment at the bit vanishing, bit inclination and azimuth always verifies

$$\theta(\xi) = \sum_{i=1}^{n} \mathcal{C}_{\theta,i} \langle\Theta\rangle_i + \sum_{i=1}^{n} \mathcal{D}_{\theta,i}\Upsilon \sin\langle\Theta\rangle_i + \mathcal{F}_\theta\Gamma_2, \tag{5.24}$$

$$\phi(\xi) = \sum_{i=1}^{n} \mathcal{C}_{\theta,i} \langle\Phi\rangle_i + \mathcal{F}_\theta \frac{\Gamma_3}{\sin\Theta}. \tag{5.25}$$

Component Γ_3 of the RSS force is *amplified* by $1/\sin\Theta$ that accounts for it being defined in plane ($\boldsymbol{I}_1$,$\boldsymbol{I}_3$) of inclination Θ. Components of the lateral force can also be expressed as

$$\tilde{F}_2(\xi) = \sum_{i=1}^{n} \mathcal{C}_{F_2,i} \langle\Theta\rangle_i + \sum_{i=1}^{n} \mathcal{D}_{F_2,i}\Upsilon \sin\langle\Theta\rangle_i + \mathcal{F}_{F_2}\Gamma_2. \tag{5.26}$$

$$\tilde{F}_3(\xi) = \sum_{i=1}^{n} \mathcal{C}_{F_2,i} \langle\Phi\rangle_i \sin\Theta + \mathcal{F}_{F_2}\Gamma_3. \tag{5.27}$$

These expressions are similar to those in the two-dimensional case and only depend on the generalized loads acting on the BHA. When the tilt has not saturated, *i.e.*, when $\tilde{\boldsymbol{F}}_{lat} < \tilde{\boldsymbol{F}}_{lat,c} = \eta\Pi\psi_c$, equations of propagation are given by (5.15) and (5.16). Once the tilt has saturated, the

amplitude of the lateral force becomes irrelevant but not its orientation τ_F, which hinges on the relative magnitude of its components. The equations of propagation are obtained from (5.3) and (5.4), with $\varepsilon = 0$, and kinematic conditions

$$\theta - \Theta = \psi_c \cos \tau_\varpi, \quad (\phi - \Phi) \sin \Theta = \psi_c \sin \tau_\varpi. \tag{5.28}$$

The equations of propagation then read

$$\Theta(\xi) = \sum_{i=1}^{n} \mathcal{C}_{\Theta,i} \langle \Theta \rangle_i + \sum_{i=1}^{n} \mathcal{D}_{\Theta,i} \Upsilon \sin \langle \Theta \rangle_i + \mathcal{F}_\Theta \Gamma_2 + \mathcal{S} \psi_c \cos \tau_\varpi, \tag{5.29}$$

$$\Phi(\xi) = \sum_{i=1}^{n} \mathcal{C}_{\Theta,i} \langle \Phi \rangle_i + \mathcal{F}_\Theta \frac{\Gamma_3}{\sin \Theta} + \mathcal{S} \psi_c \frac{\sin \tau_\varpi}{\sin \Theta}. \tag{5.30}$$

Contrarily to equations (5.15) and (5.16), expressions (5.29) (5.30) are coupled only through angle τ_ϖ and the projection of the azimuth on ($\boldsymbol{I}_1$,$\boldsymbol{I}_3$).

Limit Cycle for the Perturbation

The limit cycle of the bit and borehole oscillations is presented in Figure 5.9 for a BHA with three stabilizers located at distances 1, 3.5, and 6 behind the bit and $\varpi = -15°$. (Note that phase ϕ between the inclination and azimuthal dynamics is inverted compared to the illustrations of the last section when the walk was positive.) Dimensionless group $\eta\Pi$ is equal to 5×10^{-2} as to make the system directionally unstable.

The amplitude of the perturbations in the borehole inclination and pseudo-azimuth is about equal to the saturation value of the tilt (Fig. 4.10a and b). Contrarily to the two-dimensional case, the tilt remains permanently saturated. As angle τ_ϖ evolves linearly along the BHA, the spiral is recovered.

The limit cycle is defined by a helix; an upper bound for the amplitude is thus given by assuming a sinusoidal shape of amplitude ψ_c for the oscillations in the inclination and pseudo-azimuth (Fig. 4.10c and d)

$$A_{max} \simeq \frac{\tilde{\ell} \psi_c}{2\pi}. \tag{5.31}$$

For the studied BHA, wavelength is $\tilde{\ell} \simeq 1.12$, providing estimates of 1.56×10^{-3}, 3.1×10^{-3}, and 6.2×10^{-3}, respectively. The amplitude of the spiral is thus smaller than that of the ripple. (The difference is mainly due to the pseudo-plateau in the inclination that are observed in

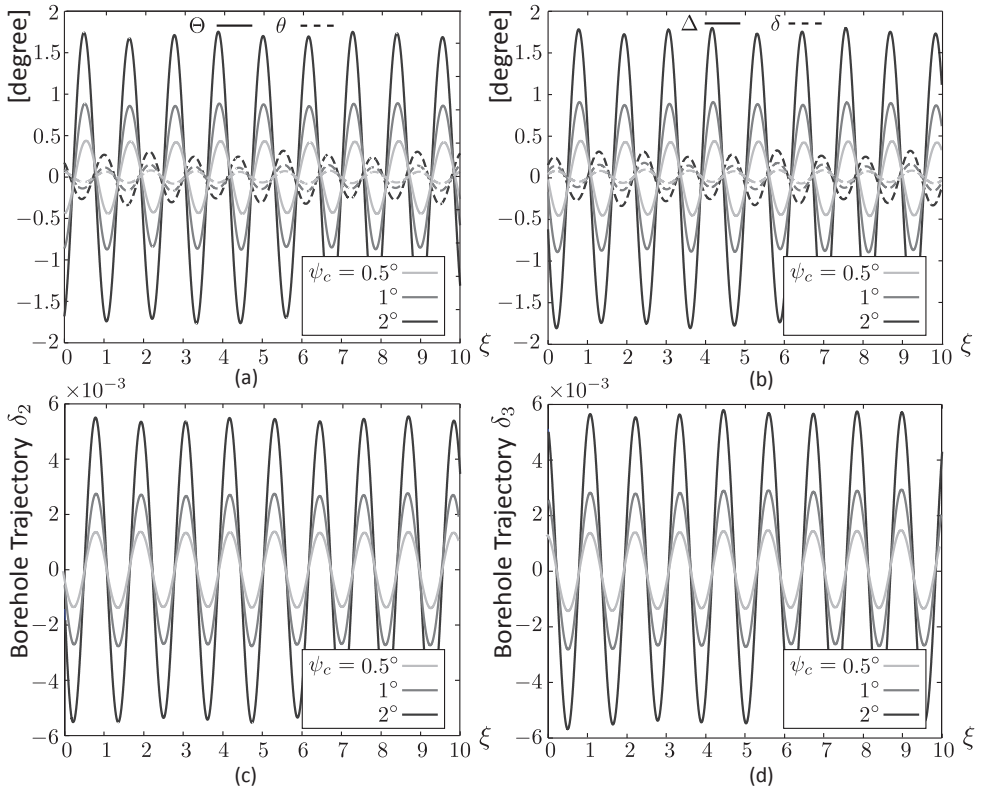

Figure 5.9: Properties of the limit cycle for the studied BHA and three different saturation values ψ_c. (a) Bit and borehole inclination; (b) bit and borehole pseudo-azimuth; (c) components of the tilts and its total magnitude; and (d) borehole trajectory.

two dimensions when the tilt saturates.) The difference between the actual amplitude of the oscillations and the saturation value of the tilt is prescribed by the bit orientation, which is in general larger for $\varpi > \varpi_*$. For large values of the walk, this estimate may then be a bit less precise.

Quasi-stationary Solutions

The (quasi-)stationary trajectories are now defined by four kinematic quantities: tilt angles ψ_{2s} and ψ_{3s} and components κ_{2s} and κ_{3s} along axes $\boldsymbol{I}_2$ and $\boldsymbol{I}_3$ of curvature vector $\boldsymbol{\kappa}_s$ (Perneder, 2013). Evolution of the bit and borehole inclinations and azimuths then reads

$$\Theta(\xi) = \Theta_0 + \kappa_{2s}\xi, \tag{5.32}$$

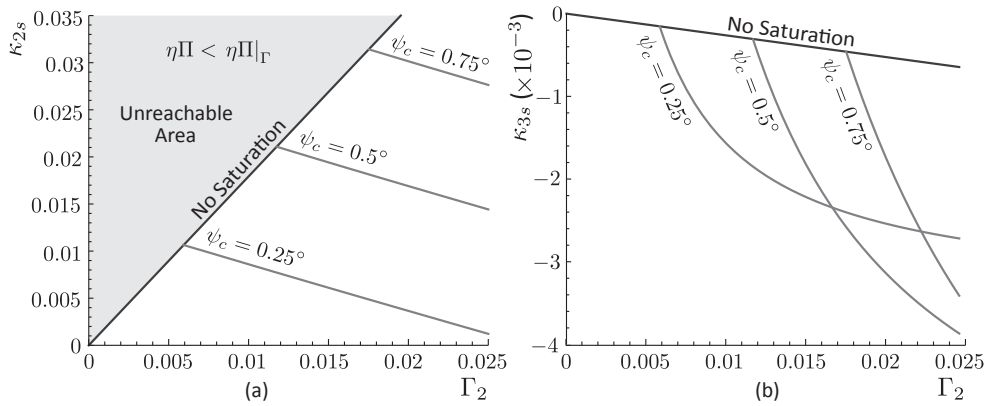

Figure 5.10: Upper bound for curvature κ_{2s} and κ_{3s} as a function of Γ_2. [The values correspond to a 3-stabilizer BHA with $\lambda_2 = \lambda_3 = 2.5$, $\Lambda = 0.29$, $\eta\Pi = 0.05$, $\Gamma_3 = 0$, and $\varpi = -15°$. The general tendency of the plot focuses on building systems with $\eta\Pi < \eta\Pi|_\Gamma$. After complete saturation of the tilt, there is a progressive reduction of κ_{2s} but a steep increases of κ_{3s}: the *walk* tendency of the system may become problematic and may need to be compensated.]

$$\begin{aligned}
\theta(\xi) &= \Theta_0 + \kappa_{2s}\xi + \psi_{2s}, \\
\Phi(\xi) &= \Phi_0 + \frac{\kappa_{3s}\xi}{\sin\langle\Theta\rangle}, \\
\phi(\xi) &= \Phi_0 + \frac{\kappa_{3s}\xi + \psi_{3s}}{\sin\langle\Theta\rangle},
\end{aligned} \tag{5.33}$$

where $\langle\Theta\rangle$ denotes the averaged inclination of the BHA. By substituting (5.32)-(5.33) into the equations for the lateral force and moment at the bit, the system can be solved for κ_s and ψ_s.

The Bit Tilt Does not Saturate In the general case when the bit does not saturate, the stationary kinematic quantities have the general form

$$\psi_{2s} = \mathcal{S}^{\psi_2}_{\Gamma_2}\Gamma_2 + \mathcal{S}^{\psi_2}_{\Gamma_3}\Gamma_3 + \mathcal{S}^{\psi_2}_{\Upsilon}\Upsilon\sin\langle\Theta\rangle\,, \tag{5.34}$$

$$\kappa_{2s} = \mathcal{S}^{\kappa_2}_{\Gamma_2}\Gamma_2 + \mathcal{S}^{\kappa_2}_{\Gamma_3}\Gamma_3 + \mathcal{S}^{\kappa_2}_{\Upsilon}\Upsilon\sin\langle\Theta\rangle\,, \tag{5.35}$$

$$\psi_{3s} = \mathcal{S}^{\psi_3}_{\Gamma_2}\Gamma_2 + \mathcal{S}^{\psi_3}_{\Gamma_3}\Gamma_3 + \mathcal{S}^{\psi_3}_{\Upsilon}\Upsilon\sin\langle\Theta\rangle\,, \tag{5.36}$$

$$\kappa_{3s} = \mathcal{S}^{\kappa_3}_{\Gamma_2}\Gamma_2 + \mathcal{S}^{\kappa_3}_{\Gamma_3}\Gamma_3 + \mathcal{S}^{\kappa_3}_{\Upsilon}\Upsilon\sin\langle\Theta\rangle\,. \tag{5.37}$$

Expressions for coefficients S can be found in Appendix C. The dependence of ψ_{2s} and κ_{2s} on Γ_3 and inversely of ψ_{3s} and κ_{3s} on Γ_2 illustrates the coupling induced by the walk on the drilling direction at the bit: Γ_2 not only tends to increase the borehole inclination, but also influences

the azimuthal behavior of the system. This out-of-plane coupling remains in general one order of magnitude lower than the in-plane influence of $\mathbf{\Gamma}$ for low to average walks, *i.e.*, $\varpi \in [-15°, 15°]$ (Fig. 5.10).

When $\varpi = 0°$, influence of Γ_2 and Υ on the azimuthal behavior and that of Γ_3 on the inclination vanish. Equations (5.34)-(5.37) then reduce to

$$\psi_{2s} = \frac{\mathcal{F}_r\mathcal{M}_\kappa - \mathcal{F}_\kappa\mathcal{M}_r}{\mathcal{M}_\kappa(\eta\Pi - \mathcal{F}_b) + \mathcal{F}_\kappa\mathcal{M}_b}\Gamma_2 + \frac{\mathcal{F}_w\mathcal{M}_\kappa - \mathcal{F}_\kappa\mathcal{M}_w}{\mathcal{M}_\kappa(\eta\Pi - \mathcal{F}_b) + \mathcal{F}_\kappa\mathcal{M}_b}\Upsilon \sin\langle\Theta\rangle\,, \tag{5.38}$$

$$\kappa_{2s} = -\frac{-\mathcal{F}_b\mathcal{M}_r + \mathcal{F}_r\mathcal{M}_b + \eta\Pi\mathcal{M}_r}{-\mathcal{F}_b\mathcal{M}_\kappa + \mathcal{F}_\kappa\mathcal{M}_b + \eta\Pi\mathcal{M}_\kappa}\Gamma_2 - \frac{-\mathcal{F}_b\mathcal{M}_w + \mathcal{F}_w\mathcal{M}_b + \eta\Pi\mathcal{M}_w}{-\mathcal{F}_b\mathcal{M}_\kappa + \mathcal{F}_\kappa\mathcal{M}_b + \eta\Pi\mathcal{M}_\kappa}\Upsilon \sin\langle\Theta\rangle\,, \tag{5.39}$$

$$\psi_{3s} = \frac{\mathcal{F}_r\mathcal{M}_\kappa - \mathcal{F}_\kappa\mathcal{M}_r}{\mathcal{M}_\kappa(\eta\Pi - \mathcal{F}_b) + \mathcal{F}_\kappa\mathcal{M}_b}\Gamma_3, \tag{5.40}$$

$$\kappa_{3s} = -\frac{-\mathcal{F}_b\mathcal{M}_r + \mathcal{F}_r\mathcal{M}_b + \eta\Pi\mathcal{M}_r}{-\mathcal{F}_b\mathcal{M}_\kappa + \mathcal{F}_\kappa\mathcal{M}_b + \eta\Pi\mathcal{M}_\kappa}\Gamma_3. \tag{5.41}$$

The two-dimensional case is recovered.

The Tilt Is Permanently Saturated When the combined influence of $\mathbf{\Gamma}$, and $\Upsilon \sin\langle\Theta\rangle$ on the lateral force at the bit is in such a way that $\left|\tilde{\boldsymbol{F}}_{lat}\right| > \tilde{\boldsymbol{F}}_{lat,c} = \eta\Pi\psi_c$, the magnitude of the tilt is given by ψ_c. The magnitude of the RSS force for when the tilt fully saturates is identical to the 2D case

$$|\mathbf{\Gamma}_*| = \frac{\mathcal{M}_\kappa(\eta\Pi - \mathcal{F}_b) + \mathcal{F}_\kappa\mathcal{M}_b}{\mathcal{F}_r\mathcal{M}_\kappa - \mathcal{F}_\kappa\mathcal{M}_r}\psi_c. \tag{5.42}$$

The (quasi-)stationary relative orientation $\tau_{\varpi s}$ of the tilt depends on the relative magnitude of Γ_2 and Γ_3 and is a solution of transcendental equation

$$\begin{aligned}\arctan\big[&(\psi_s \sin(\tau_{\varpi s})(\mathcal{F}_\kappa\mathcal{M}_b - \mathcal{F}_b\mathcal{M}_\kappa) + \Gamma_3(\mathcal{F}_\kappa\mathcal{M}_r - \mathcal{F}_r\mathcal{M}_\kappa))\\ &(\psi_s \cos\tau_{\varpi s}(\mathcal{F}_\kappa\mathcal{M}_b - \mathcal{F}_b\mathcal{M}_\kappa) + \Gamma_2\mathcal{F}_\kappa\mathcal{M}_r + \mathcal{F}_\kappa\mathcal{M}_w\Upsilon \sin\langle\Theta\rangle\\ &\qquad -\Gamma_2\mathcal{F}_r\mathcal{M}_\kappa - \mathcal{M}_w\mathcal{M}_\kappa\Upsilon \sin\langle\Theta\rangle)^{-1}\big] = \tau_{\varpi s} - \varpi,\end{aligned} \tag{5.43}$$

where the arctan function must once again be understood as being defined on $[0, 2\pi)$. Stationary components of the tilt and the curvature are then given by

$$\psi_{2s} = \psi_c \cos\tau_{\varpi s}, \tag{5.44}$$

$$\kappa_{2s} = -\frac{\mathcal{M}_b\psi_c \cos\tau_{\varpi s} + \mathcal{M}_r\Gamma_2 + \mathcal{M}_w\Upsilon \sin\langle\Theta\rangle}{\mathcal{M}_\kappa}, \tag{5.45}$$

$$\psi_{3s} = \psi_c \sin \tau_{\varpi s}, \tag{5.46}$$

$$\kappa_{3s} = -\frac{\mathcal{M}_b \psi_c \sin \tau_{\varpi s} + \mathcal{M}_r \Gamma_3}{\mathcal{M}_\kappa}. \tag{5.47}$$

Figure 5.10 illustrates the evolution of the stationary curvature with Γ_2 for a three stabilizer BHA ($\lambda_2 = \lambda_3 = 2.5$) when $\eta\Pi = 0.05$, $\Gamma_3 = 0$ and $\varpi = -15°$. An increase in Γ_2 reduces curvature κ_{s2}, like in the two-dimensional case[2], but leads to a sharp increase in the walk tendency of the system, *i.e.*, its propensity to deviate from the vertical. Increasing the RSS force beyond the point where the tilt saturates thus does not only lead to smaller building rates but also to higher out-of-plane deviations. This sudden increase in $|\kappa_{3s}|$ is explained by the fact that after saturation, an increase in Γ_2 paradoxically leads to a smaller component $\tilde{F}_2$ at the bit so that the combined influence of the walk and component $\tilde{F}_3$ steer the bit more and more out of the vertical plane. Larger ψ_c leads to larger curvatures and complete saturation is achievable in the field for small ψ_c only.

Simulation of Borehole Propagation

The results presented at the end of chapter 4 are revisited by providing the drill bit with a walk of $-15°$. To raise any indetermination, initial borehole inclination is $\Theta_0 = 20°$; the initial azimuth Φ_0 is set at $0°$. All the other parameters of the simulation remain the same (Fig. 5.11).

A limit cycle, which here almost perfectly corresponds to a spiral, rapidly settles following the directional instability of the system. (In fact the symmetry of the spiral is slightly broken as RSS force Γ_2 mobilizes a small part of the tilt.) It is superimposed to the stationary drift imposed by the RSS force (Fig. 5.11a and b). The phase of $\pi/2$ between inclination and azimuth is best observed in the evolution of the components of tilt (Fig. 5.11d), but can also be seen when comparing oscillations in the inclinations and the azimuths, as well as in the curvatures (Fig. 5.11a, b, and c). Amplitude of the oscillations in the azimuth are larger than these in the inclination; when multiplied by $\sin\Theta$ to recover pseudo-azimuth Δ, oscillations are then similar to that in the inclination.

The stationary component of the borehole curvature for the inclination is somewhat smaller

[2] Stationary curvature κ_{2s} is slightly smaller than its two-dimensional equivalent κ_s due to the influence of the walk, which reduces the effective influence of Γ_2 in the vertical plane.

that its two-dimensional equivalent. It follows from part of Γ_2 being mobilized, because of the walk, by the azimuthal behavior of the system. This influence remains marginal, however, for common magnitudes of the walk; effective component of the RSS force can be approximated by $\Gamma_2 \cos \varpi$. (It leads to a drop of about 3.5% for $\varpi = \pm 15°$.) Finally, the borehole trajectory is presented is phase plane for the borehole inclination and azimuth (Fig. 5.11e and f).

Figure 5.12 illustrates the critical influence of the lateral force and the tilt saturation on the shape of the limit cycle, on the limitation of the achievable steering capacities, and on the drift out of the vertical plane. As component Γ_2 increases, it mobilizes a growing part of the tilt and breaks the symmetry of the spiral (Fig. 5.12c, d, e, and f). For the current system, $\Gamma_{2*} \simeq 0.012$. As in the two-dimensional case, going beyond this threshold limits the achievable curvature but suppress any possibility of spiraling. Here, it also leads to a drastic increase in the walk tendency. This tendency is best seen in Figure 5.12b for $\Gamma_2 = 0.02$.

Finally for $\Gamma_2 = 0.01$, an intermediate situation between the spiral and complete saturation is observed. Initial fluctuations in the vertical plane enables the perturbation to develop in the azimuthal direction. However, because most of the tilt is mobilized by the constant loading, out-of-plane oscillations cannot develop fully, *i.e.*, tilt component ψ_3 does not reach ψ_c (Fig. 5.12e).

These results stress the intricacy of the limit cycle once a significant part of the tilt is mobilized. More field data with a systematic assessment of the system and bit properties, would then be needed to validate these observations.

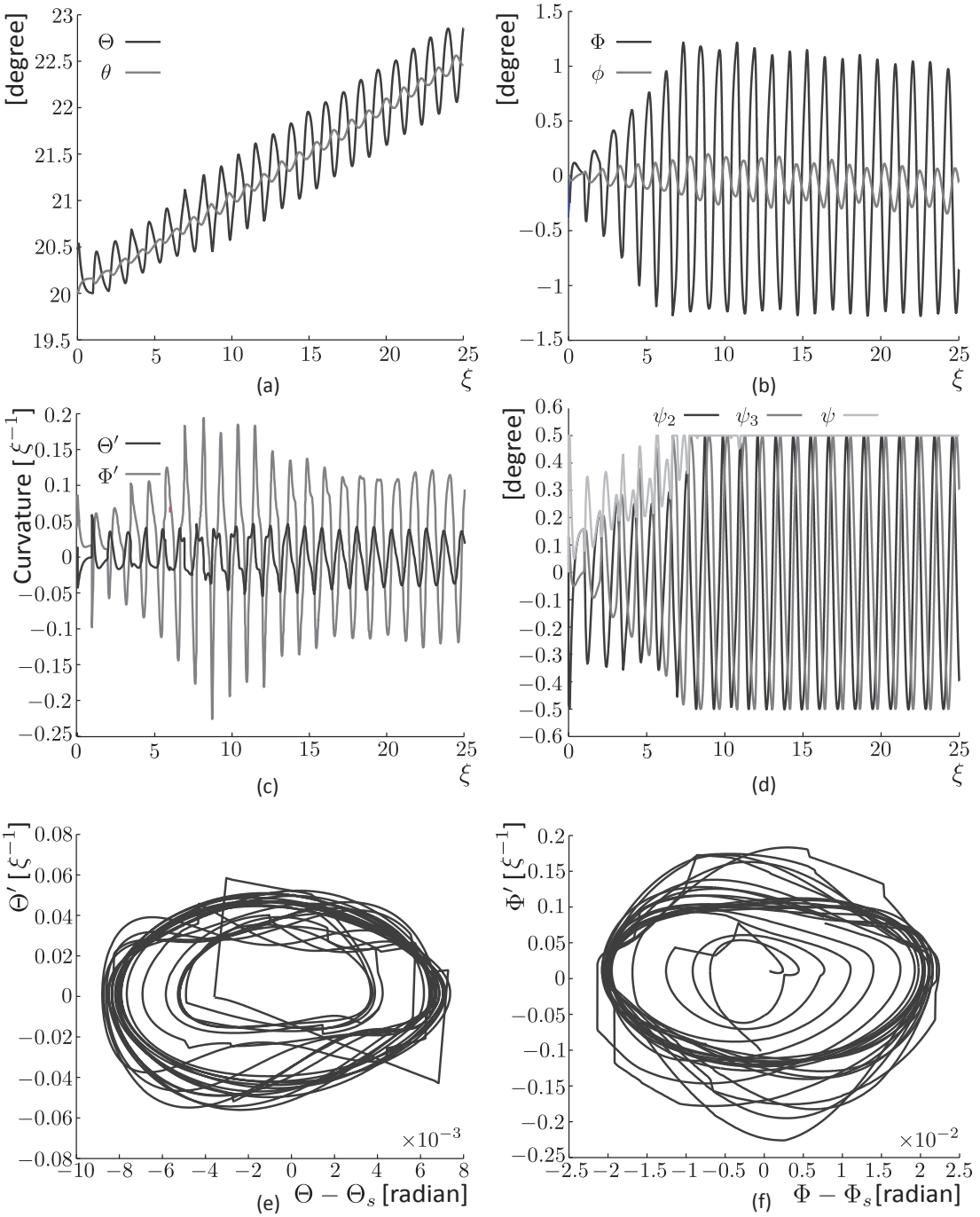

Figure 5.11: Typical results of borehole simulation. (a) Bit and borehole inclinations, (b) bit and borehole azimuths, (c) borehole curvatures, (d) bit tilt ant its components, (e) limit cycle in phase plane for the inclination, and (f) limit cycle in phase plane for the azimuth. The BHA has three stabilizers located 1, 3.5, and 6 behind the bit. The other parameters of the simulations are $\Lambda = 0.29$, $\Gamma_2 = 0.001$, $\Gamma_3 = 0$, $\Upsilon = 0$, $\eta\Pi = 0.05$, $\varpi = -15^\circ$ and $\psi_c = 0.5^\circ$.

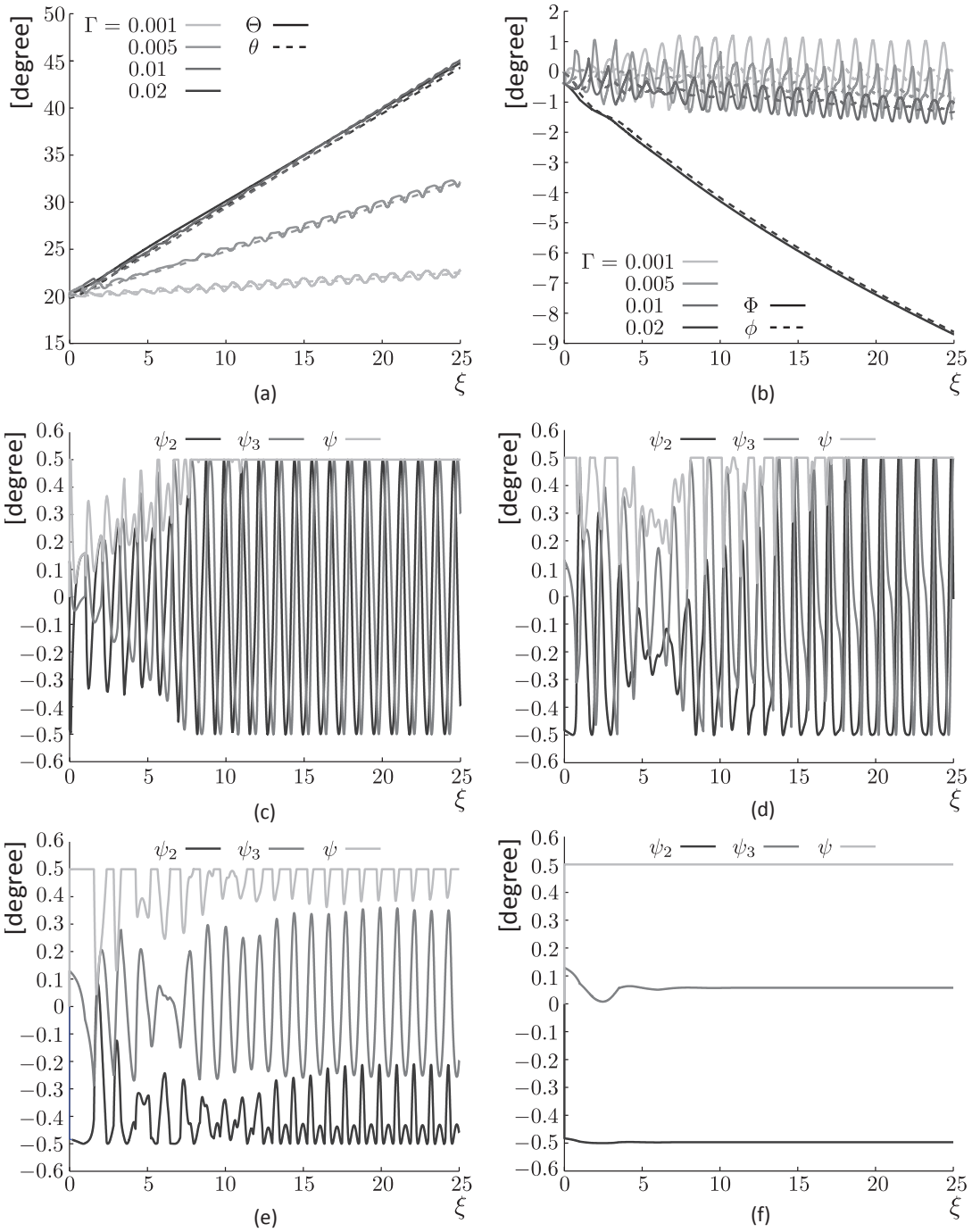

Figure 5.12: Influence of the RSS force on the limit cycle and the achievable curvature. [As the quasi-stationary lateral force increases, it mobilizes a greater part of the tilt. If this force is so large that it saturates the tilt, it suppresses any possibility of borehole oscillations. It also leads to a reduction in the achievable curvature and a higher tendency to deviate out of the vertical plane.]

Chapter 6

Validation and Applications

6.1 Methodology of the Validation

Data from several wells, most of them exhibiting micro-tortuosity, were analyzed to assess the ability of the directional stability analysis to predict the occurrence of spiraling. As shown in Tables 6.1 and 6.2, these data pertain to nine sections from four wells drilled with different steering systems and BHA configurations representing a variety of field situations. To help understand the analysis, the results are presented in terms of ηW_a and $\eta W_a|_s$; these are the dimensional counterparts of $\eta\Pi$ and $\eta\Pi|_s$. For each run, the analysis involved three steps: (a) calculation of critical value $\eta W_a|_s$ from the known properties and configuration of the BHA (and sometimes for different bit walks and RSS pads rigidities); (b) assessment of the plausible range of ηW_a from the available information on the actual field conditions (reported WOB, bit wear, and characteristics of the bit gauge); and (c) validation of the predictions, deduced from a comparison between $\eta W_a|_s$ and ηW_a and with post-run logs or other field measurements indicating the occurrence of spiraling.

Discussion of a case study is best summarized on a picture similar to Figure 6.1 in the $\eta - W_a$ plane. The bifurcation of stability is represented by a solid line. (It could be expanded to a set of lines for different walks and rigidities.) Estimates for the downhole active weight W_a and lateral steering resistance η defines a rectangular area in the $\eta - W_a$ plane, which provides a first

evaluation of the directional stability of the system, when compared with the stability limit.

When confronted with a system likely to be unstable, drilling engineers face in general three options to improve the directional stability: (a) increasing the active weight on bit, (b) selecting a bit less laterally aggressive or characterized by a smaller walk, or (c) modifying the BHA configuration, especially the positions of the stabilizers and RSS pads to reduce critical value $\eta W_a|_s$ (Fig. 6.1). These choices are always a question of compromises as other issues are related to high weight on bit (such as stick/slip), or as directional requirements need to be met.

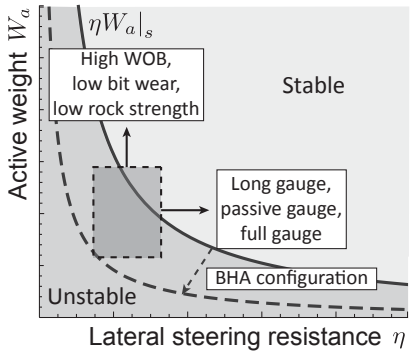

Figure 6.1: General representation of the directional stability of a drilling system in the $\eta - W_a$ plane. [From the BHA configuration and the bit walk, bifurcation value $\eta W_a|_s$ is computed. From the bit selection and the downhole field conditions, dimensionless group ηW_a is estimated. If the system is deemed directionally unstable, the operator faces three choices: increasing the weight on bit, choosing a less laterally aggressive bit, or modifying the BHA configuration as to lower $\eta W_a|_s$.]

Well	Run	Trajectory	Number of stabilizers (Distance from bit [ft])	Drive system	WOB [kips]
1	1	Tangent	5 (10, 43, 71, 111, 120)	Push-the-bit	5-10
	2	Tangent	5 (10, 44, 71, 111, 120)	Push-the-bit	10-18
2	1	Vertical	3 (3.7, 40, 75)	Rotary	25-40
	2	Vertical	3 (4, 88, 123)	Rotary	10-20
3	1	Vertical	4 (3.2, 30, 67, 103)	Rotary	12-25
	2	Build	2 (3.5, 14)	Point-the-bit	10-50
	3	Build	2 (3, 14)	Point-the-bit	15-25
4	1	Build	2 (10, 42)	Push-the-bit	10-30
	2	Build	4 (10, 42, 61.5, 67)	Push-the-bit	20-35

Table 6.1: Properties of the analyzed runs: type of trajectory, number of stabilizers and positions with respect to the bit, type of drive system, and range for the weight on bit. [To improve accessibility, units have been chosen to be those most commonly used in the field.]

Bifurcation of stability $\eta W_a|_s$ is computed from the BHA configuration, including variations of its inner and outer diameters (as well as the bit walk and the RSS pads lateral rigidity in some cases). Local variations of geometry do not significantly influence, however, critical value $\eta W_a|_s$: $\eta W_a|_s$ could actually be estimated by assuming that the stabilizers, on average 1 ft long, perfectly fit the nominal borehole diameter and that the BHA consists of pipes of uniform cross sections given by the drill collars closest to the bit. The relative positions of the stabilizers and of the RSS pads must be represented accurately, however, as they primarily influence the magnitude of $\eta W_a|_s$.

Estimation of ηW_a for each run requires assessing both lateral steering resistance η and active weight W_a. Evaluation of η is derived from the length and the aggressiveness of the bit gauges with some considerations given to their geometries and published experimental results (Menand et al., 2002; Sugiura and Jones, 2008b; Dupriest and Sowers, 2009). Evaluation of the component of the WOB mobilized in contact forces is more intricate. The downhole WOB is used as an upper bound of the active weight. In some cases, this limit is sufficient to explain the field observations. In other cases, the occurrence of spiraling could be explained only by invoking the mobilization of a non-negligible part of the WOB into contact forces. Contact force G_1, thought to have caused spiraling, is then assessed and related, when the information is available, to the dull grading of the bit, *i.e.*, to the qualitative evaluation of the wear usually performed after each run[1]. All the back-analyzes are subordinated on the assumption that the downhole WOB inferred from the surface measurements was entirely transmitted to the bit.

The collected data are not complete: no quantitative property pertaining to drill bit responses was available. No information about lateral steering resistance η, or bit walk ϖ was communicated. While *educated* guesses for η can be inferred from the gauge characteristics, estimations for walk ϖ or pads stiffness K are not straightforward. The main objective of this validation is thus to test whether the phenomena observed in the field could be explained based

[1] Here only the first three slots of the IADC dull grading are of practical interest. The first two give, on a qualitative scale ranging from 0 to 8, a measure of the wear of the inner and outer cutting structures, respectively. The inner structure is defined as being approximately along the first two thirds of the bit radius. The third field refer to the dull characteristics (here, WT is for worn cutters and CT for chipped cutters). It should be noted, however, that on this qualitative scale, even states of wear rated 1 or 2 may lead to significant drops in active weight. Indeed, experimental investigations in sandstone suggest that these drops may reach a few kips for a moderately blunt $6^{1/2}$-in. PDC bit (Detournay et al., 2008).

Well	Run	Bit type	Diam. [in.]	Gauge length [in.] and geometry	OD [in.]	ID [in.]	$F_* \times 10^2$ [kips]
1	1	PDC	$10^{5/8}$	2; semi-active; full gauge	$7^{3/4}$	$2^{1/4}$	12
	2	PDC	$10^{5/8}$	4; passive; undercut	$7^{3/4}$	$2^{1/4}$	11
2	1	Roller Cone	$8^{1/2}$	-	$6^{1/2}$	$2^{1/4}$	40
	2	PDC	$8^{1/2}$	3; passive; undercut	$6^{1/2}$	$2^{1/4}$	35
3	1	PDC	$8^{3/8}$	4; passive; tapered	$6^{5/16}$	$2^{1/4}$	49
	2	PDC	$8^{3/8}$	4; passive; undercut	$5^{7/8}$	$2^{1/4}$	29
	3	PDC	$8^{3/8}$	2; semi active; full gauge	$5^{7/8}$	$2^{1/4}$	40
4	1	PDC	$8^{1/2}$	2.5; semi active; full gauge	7	1.54	7
	2	PDC	$8^{1/2}$	2.5; passive; undercut	7	1.54	7

Table 6.2: Properties of the analyzed runs: bit type and diameter; size, aggressiveness, and geometry of the bit gauge; outer and inner diameters for the BHA; and resulting characteristic force.

on the model and on a consistent set of quantitative estimates for its parameters. The analysis is mostly based on predictions from the two-dimensional version of the model. When predictions are extended to the influence of the walk or the pad stiffness, they involve a larger part of speculation.

6.2 Field Data

6.2.1 Well 1

Run 1

The analysis focuses on a 1,750-ft tangent section with a constant inclination of 49° maintained with a push-the-bit RSS. The RSS force is applied through three pads, which do not rotate with the drillstring. In view of their design, they are here treated as an additional stabilizer close to the bit, a $10^{5/8}$-in. PDC bit with a 2-in. semi-active full gauge.

From the BHA configuration and the mechanical properties of its various segments (Fig. 6.2a), bifurcation value $\eta W_a|_s$ is computed to be 983 kips if the bit has a neutral walk tendency (Fig. 6.2d). Because of the small gauge length, the lateral steering resistance is estimated to be relatively low (*i.e.*, $\eta \simeq 5-10$). As the WOB varies between approximately 5 and 10 kips (Table 6.1), group ηW_a is estimated to range between 20 and 100 kips, assuming a possible slight wear

of the cutters ($G_1 \leq 1$ kips). As the upper bound of ηW_a is smaller than $\eta W_a|_s$, the system is considered directionally unstable for all reasonable combinations of W_a and η, irrespective of ϖ (Fig. 6.2b and c). (Critical value $\eta W_a|_s$ raises to 1096 kips for $\varpi = -15°$; this walk is still below the critical threshold for which a significant increase of the critical value has been identified.)

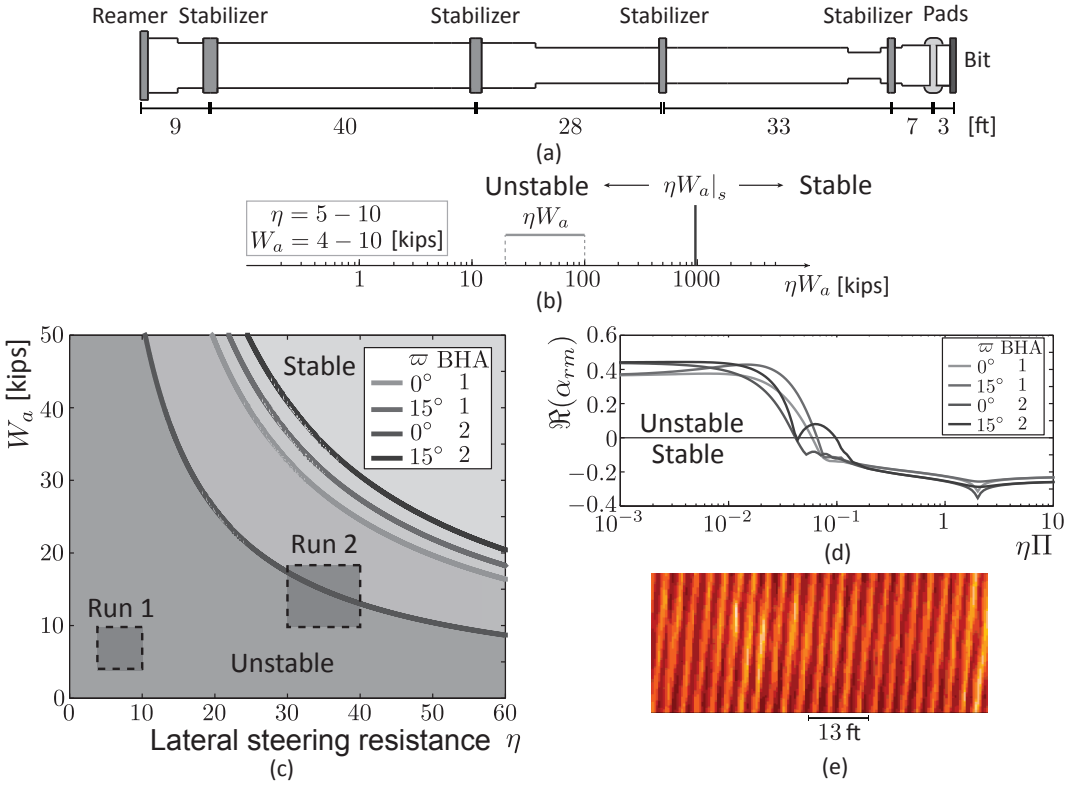

Figure 6.2: Summary for well 1. (a) BHA configuration; (b) Stability properties along the ηW_a line; (c) Assessment of the directional stability in the $\eta - W_a$ plane; (d) Directional stability as a function of $\eta\Pi$; and (e) Borehole spiraling for run 1 detected by an azimuthal density log.

Post-run analysis of the LWD azimuthal short-space density log showed a clear spiral with a regular pitch of approximately 2.6 ft over most of the run (Fig. 6.2e). This pitch corresponds to the distance between the bit and the pads of the RSS, which is also the first contact point between the BHA and the borehole. The observed pitch justifies the assumption of treating the

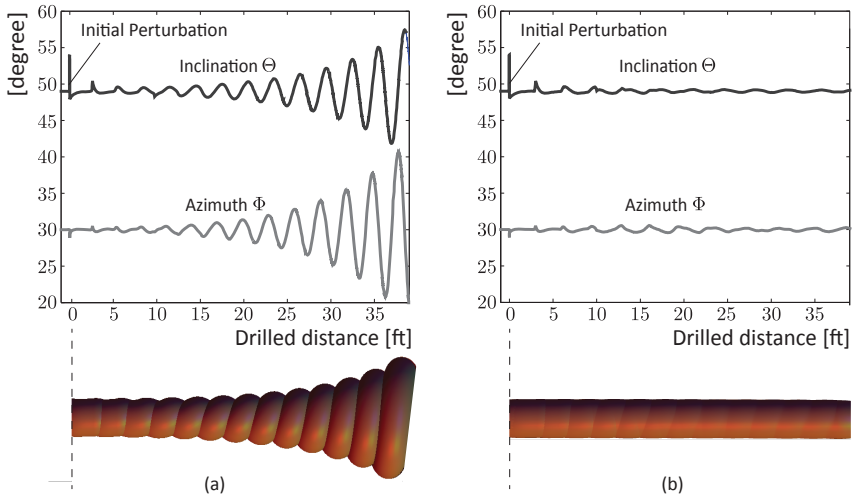

Figure 6.3: Simulations for well 1 by use of the model on the basis of field data. (a) First unstable run for $\eta W_a = 665$ kips. This value, higher that what was imposed in the field, shows than in comparison with the next run, a higher ηW_a does not necessarily mean a more-stable system if BHA configurations differ. (b) Run drilled with a less laterally aggressive bit and a higher downhole WOB for $\eta W_a = 600$ kips. The lateral deformation of the borehole is not to scale.

RSS pads as having a large rigidity[2].

Results of simulations based on the 3D borehole propagation model can be found in Figure 6.3a. An initial perturbation in the borehole trajectory (5° over 0.1 ft) was imposed to trigger the oscillations. The model is able not only to reproduce the spiraled run, but also to capture a pitch close to 3 ft. The difference between the pitch observed in the field and the simulation may be related to the lateral rigidity of the pads (assumed here to be infinite) and the imposed value of ηW_a, which both tend to increase it.

Run 2

The subsequent run was drilled using a PDC bit with a 4-in. undercut passive gauge, whereas the BHA configuration remained approximately the same. The bifurcation parameter decreases, however, to 521 kips mainly because of the longer bit shank. (The shank—a pipe-like short section above the bit—is now approximately 0.4 ft larger and affects λ_2, the scaled relative

[2] Technically, a stiffness sufficient to significantly induce oscillations related to the pads would have been enough. Few information is available, however, about this stiffness.

position of the second stabilizer.) With an estimated lateral steering resistance between 30 and 40 to account for the new bit and a downhole WOB of 10–18 kips, the system is likely to be more stable, even though the uncertainty on the key parameters does not enable an unambiguous prediction (Fig. 6.2b and c). No spiraling was reported in the post-run analysis; the directional stability was improved by a different bit selection and a higher WOB.

The critical walk for this configuration is about 8°; any value significantly above this threshold would made the model predict a directionally unstable system. For example, a walk of $-15°$ makes $\eta W_a|_s$ jump to 1225 kips (Fig. 6.2d). As no information on the walk is available, this suggests either that the walk was, indeed, sufficiently small as to not influence $\eta W_a|_s$ greatly, that lateral resistance η is underestimated, that the assumption of considering the RSS as an extra stabilizer is, in this case, too strong, or a combination of these. This field case also concretely illustrates the possibly large influence of the walk for specific ranges of the position of the second stabilizer. (Here, $\lambda_2 = 2.32$ is in the region of the stability diagram where the influence of the walk is largest.)

A simulation, with the same initial perturbation as before, a walk of $-5°$, and $\eta W_a = 600$ kips ($\eta W_a|_s = 526$ kips) shows that, after a short transient response, the borehole resumes an almost straight trajectory (Fig. 6.3b).

6.2.2 Well 2

Two consecutive vertical rotary-assembly runs are analyzed. These two runs had different bit types and BHA configurations, as shown in Tables 1 and 2.

Run 1

This run is 500 ft long and was drilled with a BHA equipped with three stabilizers located 3.7, 40, and 75 ft behind the bit (Fig. 6.4a). The corresponding bifurcation value $\eta W_a|_s$ is calculated to be 64 kips. The bit is an $8^{1/2}$-in. roller cone[3]; its lateral steering resistance is estimated to be of order $O(1)$, because the existence of a gap between its gauge and the wellbore allowed the bit to tilt with little lateral restriction. With the applied WOB range (Table 6.1), the system

[3] To be accurate, it was an IADC 6-4-7 roller-cone bit, in the jargon of field engineers. This information is not relevant in this context.

is expected to be unstable (Fig. 6.4b). Post-run analysis of the caliper log showed oscillations with a wavelength related to the distance between the bit and the first stabilizer (Fig. 6.4c). The effect of wear and walk of the roller-cone bit (8-8-WT dull grade) is neglected because the system is already predicted to be unstable without accounting for their influence on the active weight.

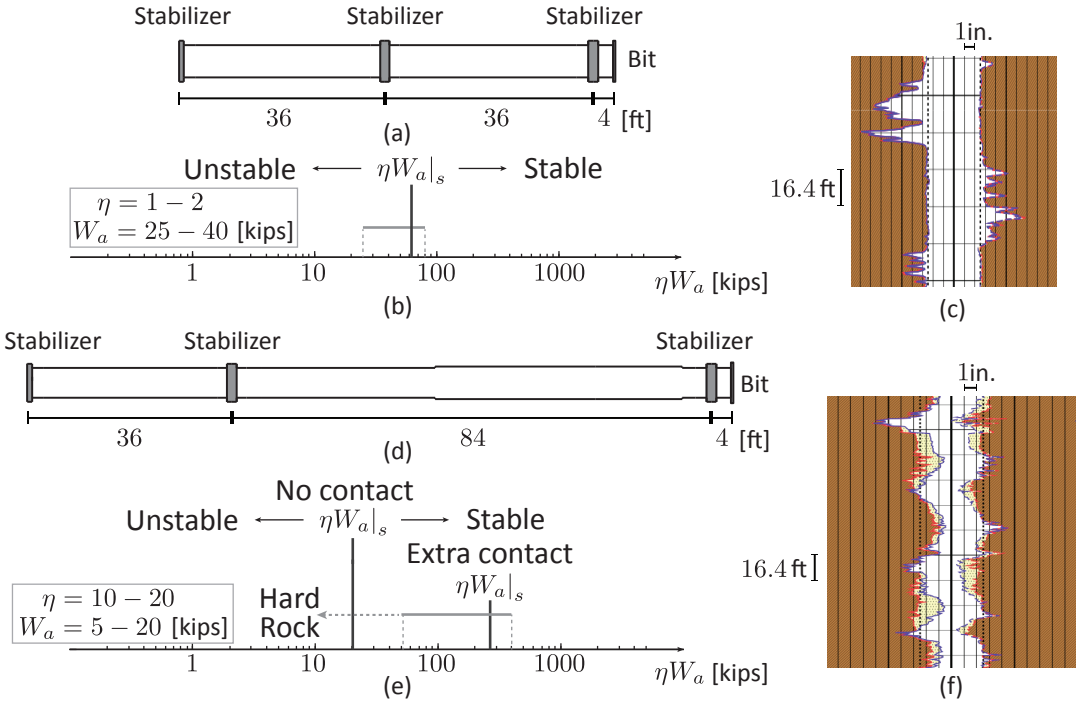

Figure 6.4: Summary for well 2. (a) BHA configuration for the first run; (b) Stability properties along the ηW_a line for the first run; (c) Caliper log where mild spiraling is observed; (d) BHA configuration for the second run; (e) Stability properties along the ηW_a line for the second run; and (f) Caliper log where two types of spiraling appear.

Run 2

The second vertical section was 900 ft in length. The stabilizers were located 4, 88, and 123 ft behind the bit (Fig. 6.4d), which was an $8^{1/2}$-in. PDC bit with a 3-in. passive undercut gauge. The stability analysis was conducted on the basis of an active weight ranging between 5 and 20 kips ($G_1 \leq 5$ kips) and a bit lateral steering resistance between 10 and 20. The repositioning of the second stabilizer and the larger lateral steering resistance improve the directional stability

of the system. This is reflected in a low value of $\eta W_a|_s$, now equal to 20 kips. With ηW_a in the range [50–400], the system is first predicted to be stable (Fig. 6.4e).

Post-run analysis of the caliper log indicated small- and large-pitch spiraling of the borehole, especially in the lower part of the run (Fig. 6.4f). The wavelength of the small-pitch spiral was related to the distance between the bit and the first stabilizer, whereas the large-pitch spiral had a varying wavelength, starting at 15 ft but progressively increasing up to 42 ft. The spiraling also was influenced by rock hardness; further in the run, an increase in rock compressive strength correlated with an increase in spiraling severity.

The difference between the model prediction and the observed field data may be explained by an additional contact point between the BHA and the borehole. The existence of this contact is caused by the interference from the spiral generated during the previous run and the increased distance between the first and second stabilizer for the current BHA. When computing the deflection of the BHA within the borehole, a contact point appears relatively close to the bit during most of the run (even though its actual position fluctuates as the borehole propagates). By imposing an extra contact point, approximated as an additional stabilizer 15 ft behind the bit, $\eta W_a|_s$ increases to 264 kips; under this assumption, the model predicts the system to be unstable (Fig. 6.4e).

This highlights an aspect of the complex nature of BHA design: A BHA initially expected to be more stable can become unstable because of the creation of additional contact points. When the bit was pulled out of the hole, it was graded 1-1-WT; part of the WOB was transmitted at the cutter wear flats. In rocks with a higher compressive strength, this wear-flat-transmitted portion of the WOB increases, the active weight decreases, and the system becomes more unstable.

6.2.3 Well 3

Three successive runs over a distance of 2,300 ft were examined. They encompass a variety of borehole conditions: smooth segments, small-pitch spiraling, and the combination of small- and large-pitch spirals. For the modeling, each of the runs was subdivided further into smaller sections because of local WOB variations.

Run 1

A vertical run of 700 ft was drilled with a packed rotary assembly with four stabilizers (Fig. 6.5a). A $8^{3/8}$-in. PDC bit was used with a 4-in. tapered passive gauge; η is estimated to be approximately 10–15. Because $\eta W_a|_s = 75$ kips, the model predicts the system to be stable given the applied WOB of 12–25 kips.

Post-run analysis of the caliper log indicated that the run can be roughly separated into three sections, which are differentiated either by the applied WOB or by the borehole pattern (Fig. 6.5c). Again, an extra contact is expected 13–16 ft behind the bit, increasing the value of $\eta W_a|_s$ to 218–298 kips. In the first section, the system is expected to be unstable with the additional contact point, with the WOB ranging between 12 and 17 kips (Fig. 6.5b). Further in the run, the WOB was increased (20–25 kips). Although this leads to the expectation of a more stable BHA, the nature of the borehole perturbations could not be clearly identified even though the borehole seemed smoother (Fig. 6.5c); no conclusion is drawn. In the third section, a spiraling pattern was again identified. The sudden instability of the system may be explained by the increasing wear of the cutters on the bit (graded 2-2-WT). If the active weight was reduced, even by a few kips, it causes the system to switch toward the unstable side of the bifurcation of stability (Fig. 6.5b). It is active weight W_a and not the applied WOB that drives the directional stability of the system.

Run 2

In this run, the inclination built from 0° to 37° over 1,400 ft through a point-the-bit RSS. The BHA was equipped with two stabilizers at 3.5 and 14 ft behind the bit (Fig. 6.5d). The bifurcation value for this configuration is 218 kips. The bit was an $8^{3/8}$-in. PDC bit with a 4-in. undercut passive gauge that was reported as less aggressive laterally than the bit from the preceding run.

This run is also characterized by a succession of sections with different WOB and spiraling patterns (Fig. 6.5f). The WOB, ranging between 10 and 50 kips, increases during the run. With a lateral steering resistance of 10–20, ηW_a is estimated between 100 and 300 kips for the first section, 300 and 700 kips for the second, and 350 and 1,000 kips for the last. Hence, the system

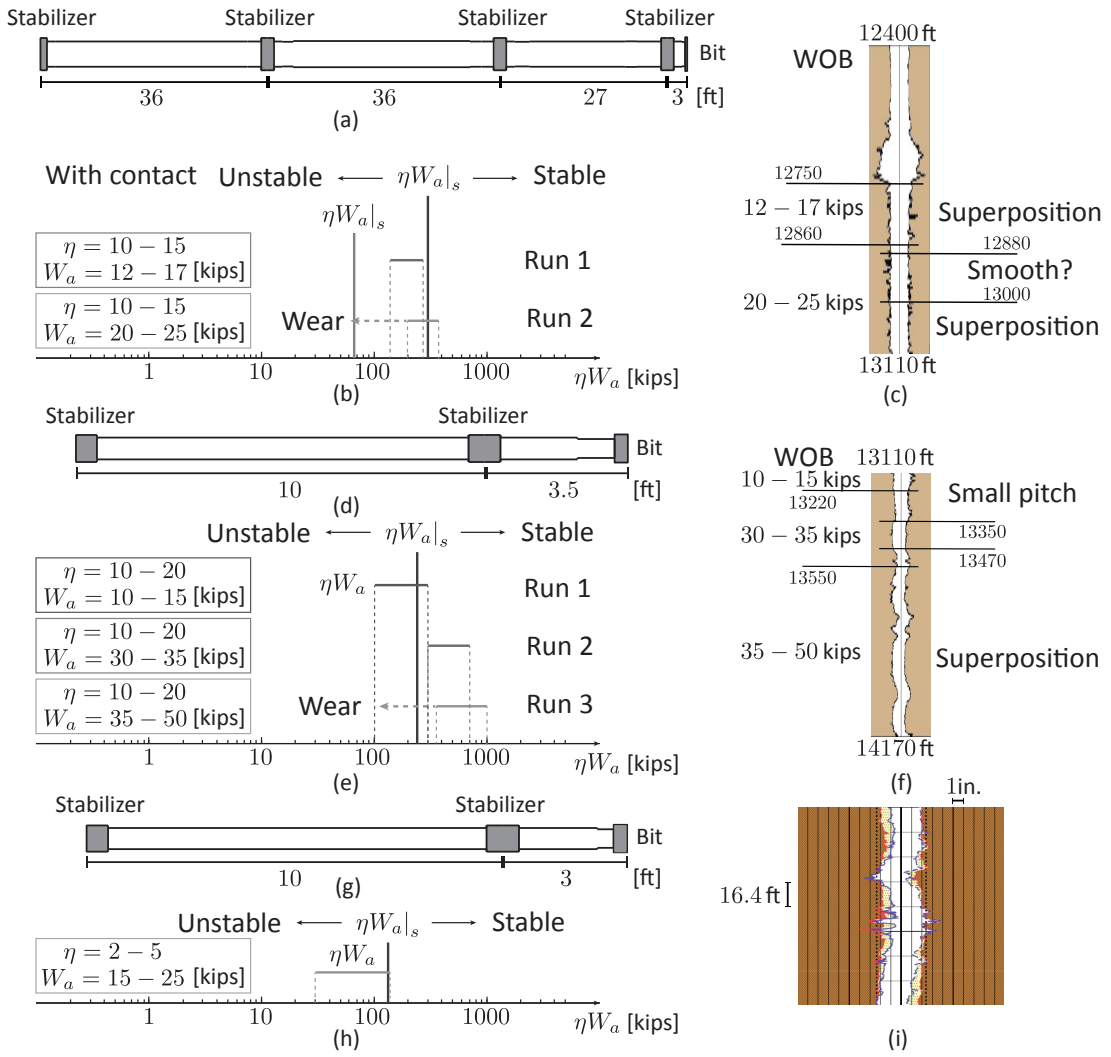

Figure 6.5: Summary for well 3. (a) BHA configuration for the first run; (b) Stability properties along the ηW_a line for the first run; (c) General evolution of the WOB and spiraling over the first run; (d) BHA configuration for the second run; (e) Stability properties along the ηW_a line for the second run; (f) Ranges of WOB and evolution of spiraling; (g) BHA configuration for the third run; (h) Stability properties along the ηW_a line for the third run; (i) Caliper log where spiraling is identified.

is likely to be at first unstable because of low WOB (Fig. 6.5e). However, with the increase of WOB, in the later sections the system is expected to be stable. Post-run analysis of the caliper log showed that the borehole exhibited at first small-pitch spiraling with a pitch of approximately 3.5 ft, then became smooth and eventually spiraled again (Fig. 6.5f). The appearance of spiraling in the last section, despite the model predicting stability with the increased WOB, might again be explained by the wear of the cutters. More than half the WOB would have to be transmitted, however, in contact forces (G_1 should be larger than 15 kips). The damage to the bit (1-2-WT) may justify this drop of active weight. (A large walk may also justify more unstable systems. It could also explain the discrepancy for η between this run and the second of Well 1. Without more information, the current analysis focuses on the lateral steering resistance and active weight.)

Run 3

This run was a 650-ft building section with a point-the-bit RSS. The BHA configuration was similar to that of the second run (Fig. 6.5g), with a slight change to the position of the first stabilizer (3 ft behind the bit vs. 3.5 ft in the previous run), leading to $\eta W_a|_s = 119$ kips. With a WOB between 15 and 25 kips, a low η would explain the instability. (A walk above the critical threshold would also work but no information is available.) The PDC bit, with a 2-in. semi-active gauge, would justify a lateral steering resistance between 2 and 5; ηW_a is then estimated in the range 30–125 kips and the system can be classified as unstable (Fig. 6.5h). The post-run analysis showed that a combination of large- and small-pitch spiraling occurred (Fig. 6.5i). In particular, the most severe spiraling coincides with a local drop of WOB. Also, the dull grade of the bit post-run was 0-1-WT, certainly leading to no significant contact forces (G_1 is likely to be small).

6.2.4 Well 4

Run 1

This run was a 500-ft building section from 11° to 30° inclination through a push-the-bit RSS, achieving an average dogleg severity of approximately 4.4°/100 ft. It was drilled using an $8^{1/2}$-in. PDC bit with a 2.5-in. semi-active full gauge, resulting in an estimate of the lateral steering

resistance of 10–20. On the basis of the BHA configuration and modeling first the RSS as an extra stabilizer (Fig. 6.6a), the stability limit $\eta W_a|_s$ is computed to be 649 kips.

The WOB applied in the field ranged between 10 and 32 kips; hence, the system was predicted to be unstable, independently of possible bit wear (Fig. 6.6b). Post-run analysis of the caliper log confirmed that a spiral developed throughout the entire run. The spiraling could be identified by the fluctuations of the near-bit inclination (of approximately 0.25°) and the bending moment with a wavelength of approximately 3 ft (Fig. 6.6c), which is related to the distance between the bit and the pads of the RSS. Even when the assumption of an infinite pad stiffness is relaxed, the system is still likely to be directionally unstable: For rigid RSS pads (*i.e.*, $\mu \in 50 - 1000$), $\eta W_a|_s$ varies between 434 and 627 kips (Fig. 6.6d).

While keeping the same BHA configuration, the application of a larger WOB or the selection of a drill bit with a larger lateral steering resistance could have made the system less unstable (or more stable). These considerations may not, however, meet other requirements. For instance, an increased WOB would augment the occurrence of stick/slip (apparently, a concern when drilling that section), and a larger η would limit the achievable dogleg severity of the system. A more extreme approach would have been to change the push-the-bit RSS for a softer system that would be less sensitive to perturbations in the borehole geometry. If the pads had a scaled stiffness ranging between 0.001 and 5, $\eta W_a|_s$ would vary between 19 and 105 kips, leading to a directionally stable system (Fig. 6.6d).

Run 2

The new BHA had two additional stabilizers at 61.5 and 67 ft behind the bit (Fig. 6.7a); overall, $\eta W_a|_s$ varies only slightly, to 674 kips. (The difference is explained by a difference of diameter — and so bending stiffness — for the BHA and a different value of λ_2 because of slight differences in the design of the bit and the RSS.) The bit has a less-aggressive side-cutting structure compared with that in Run 1, but the same gauge length of 2.5 in. It was characterized, therefore, by a larger lateral steering resistance η estimated to be between 20 and 30.

The model predicts then stability for the larger values of the active weight and instability for the lower ones (Fig. 6.7b). This prediction is consistent with the post-run analysis, which showed no spiraling in the first and third sections of this run, where the WOB is large enough.

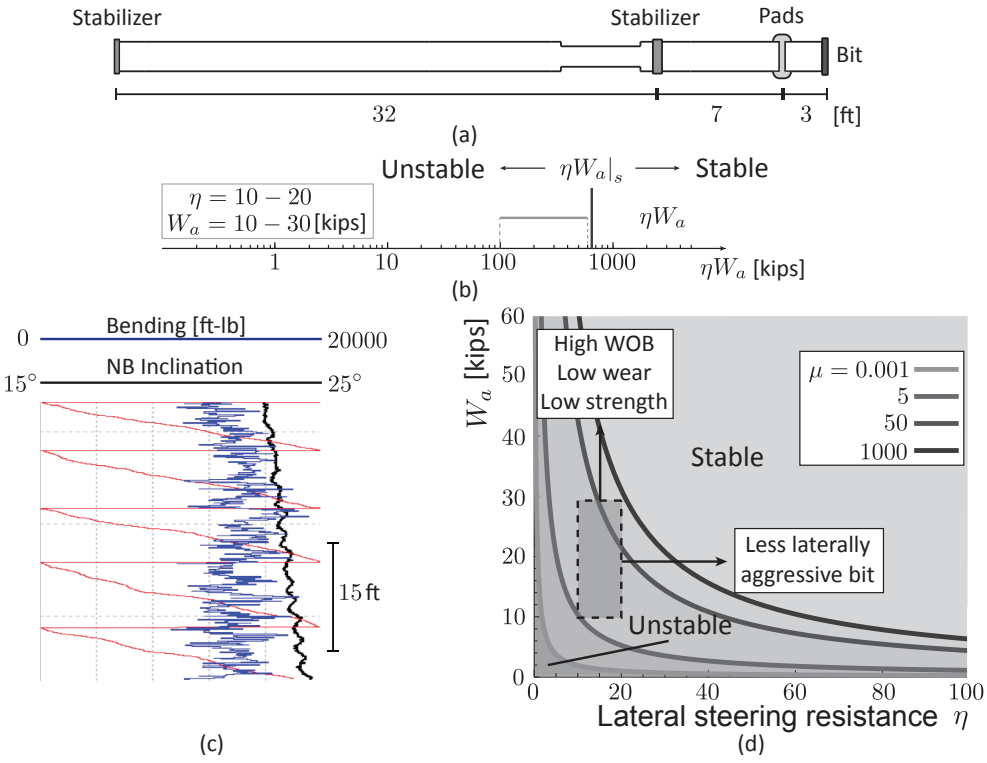

Figure 6.6: Summary for Well 4 Run 1. (a) BHA configuration; (b) Stability properties along the ηW_a line; (c) Field measurements from which spiraling was inferred (the black curve refers to the near-bit inclination; the blue one to the bending moment); and (d) Directional stability as a function of μ.

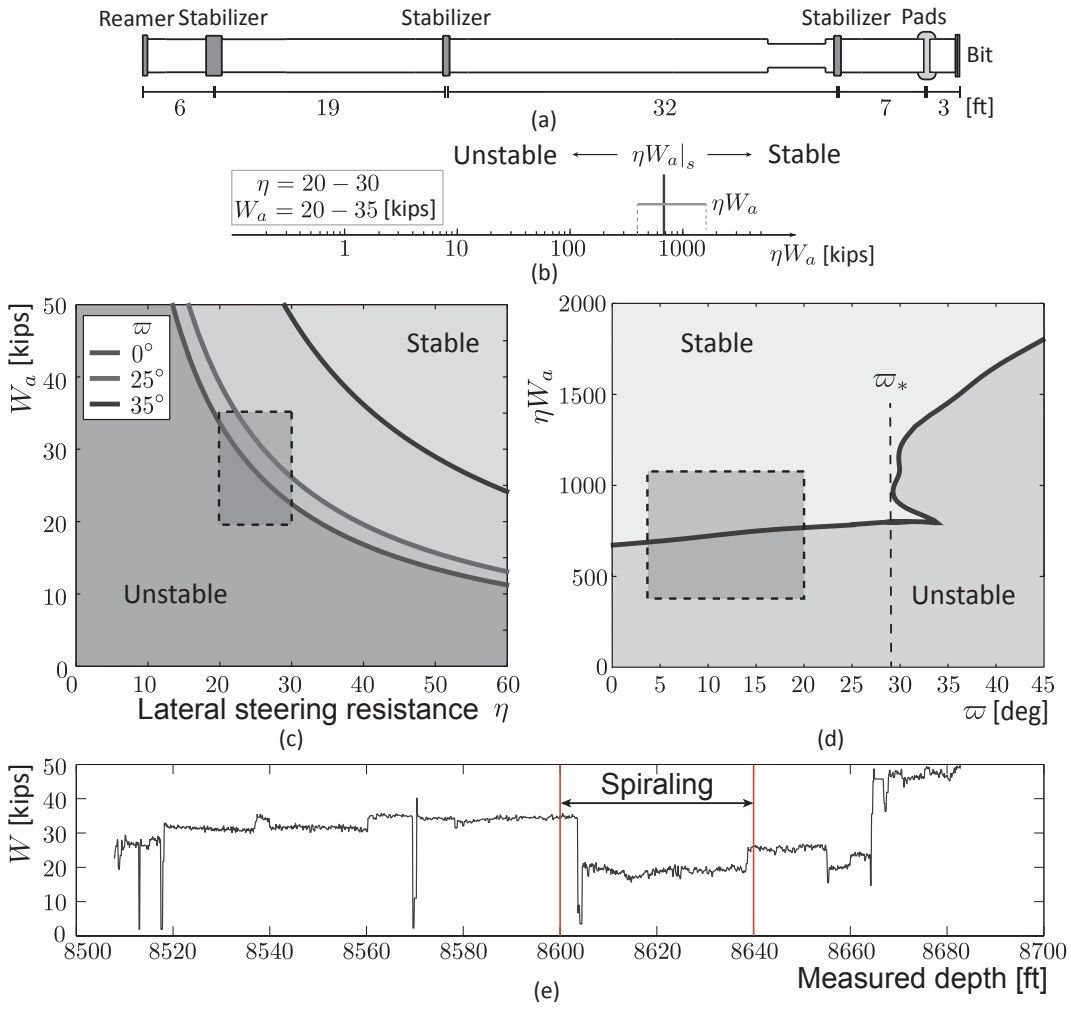

Figure 6.7: Summary for well 4 run 2. (a) BHA configuration; (b) Stability properties along the ηW_a line; (c) Assessment of the directional stability in the $\eta - W_a$ plane for different walks; (d) Directional stability as a function of ϖ; and (e) Evolution of the downhole WOB with the measured depth [Occurrence of spiraling correlates with a drop in downhole WOB.].

However, a spiral was identified from bending-moment data for the middle section, where the WOB was approximately 20 kips (Fig. 6.7e). The wear of the bit at the end of the run (1-2-CT) may also have influenced the active weight. The fact that the identification of spiraling almost perfectly corresponds to the drop in WOB is, however, consistent with the qualitative predictions of the model[4].

Figure 6.7c and d shows the variation of ηW_a with walk ϖ for this particular BHA; the critical walk is about 29°. As ϖ_* is larger than plausible field values of ϖ, the influence of the walk is deemed negligible from a directional stability point of view and the two-dimensional analysis is sufficient to assess the directional stability of the system. This BHA exemplifies a walk-robust design.

6.3 Application of the Model

This investigation and comparison between field observations and theoretical predictions suggest that, despite the uncertainty regarding the model parameters, the occurrence of spiral holes can indeed be predicted from a linear-stability analysis of the borehole-propagation equations. Thus, the theoretical model can be used to provide guidance for BHA designs, to compare different BHA configurations, or to define the WOB range recommended to avoid inducing spiraling.

6.3.1 Optimization of the BHA

The model indicates that optimizing the distance between the stabilizers and the bit improves the directional stability of the system. This reasoning, correct when considering only the spiraling tendency, could be misleading, however, because it does not consider other phenomena that influence borehole quality or directional requirements. For instance, bit whirl may be mitigated by using a well-stabilized BHA, when drilling a large-diameter hole with a PDC bit in a hard-rock application. Furthermore, the relative positions of the stabilizers may be in such a way that extra contacts between the borehole and the BHA impair significantly the system stability. Finally, increasing WOB helps stabilize the BHA and reduces the borehole-spiraling tendency.

[4] Between approximately 8,655 and 8,660 ft, there is also a drop in WOB, but no spiraling was reported in the post-well report; the short distance of this drop in WOB may explain this lack of information.

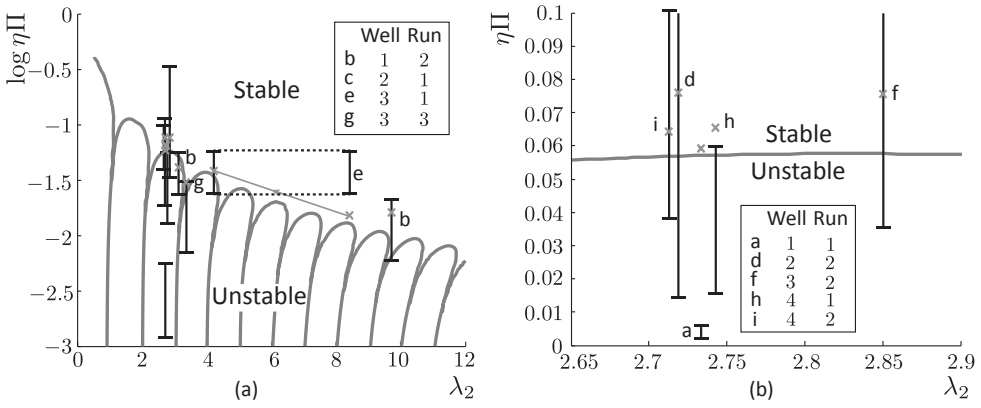

Figure 6.8: (a) Variation of stability limit $\eta\Pi|_s$ with parameter λ_2. The crosses represent the values of $\eta\Pi|_s$ for the analyzed BHAs. The crosses for the first and fourth wells are adapted to account for the RSS pads being modeled as a stabilizer close to the bit; the subscript c indicates extra contacts. The range illustrates the estimated variation of $\eta\Pi$. (b) Details for $\lambda_2 \in [2.65 - 2.9]$.

However, it may also induce additional contact points, affect the directional-drilling objectives negatively, or also cause downhole dynamics problems, such as stick/slip, that may damage the bit and other BHA components.

Despite these limitations, the model may provide guidelines. From a design perspective, the relative position of the first two stabilizers is sufficient to provide a good approximation of the bifurcation value $\eta\Pi|_s$, because local variations in the BHA geometry do not significantly influence $\eta\Pi|_s$. Despite the larger number of stabilizers and the local variations in diameters, the computed values of $\eta\Pi|_s$ for the studied cases are relatively close to the values computed for the idealized two-stabilizer BHA (Fig. 6.8). (This justifies *a posteriori* the study of the directional stability of idealized BHAs with only two stabilizers.) The complex variation of $\eta\Pi|_s$ with relative position of the second stabilizer λ_2 may lead to significant change in $\eta\Pi|_s$ for slight modification of the BHA configuration. In Well 3, for example, $\eta W_a|_s$ decreases from 218 kips in the second run to 119 kips in the third run; the only difference between the BHAs comes from the shorter bit element in the third run that increases the value of λ_2 and moves the system to a sweet spot of the stability curve (marker "g" in Fig. 6.8a). If further field data confirm the shape of this curve, the positions of the first two stabilizers could then be tuned to improve the directional stability of the drilling system. (It is also worth mentioning that stabilizers are

modeled here as point contacts along the BHA. In practice, their actual shapes and interaction with the wellbore may smoothen the bifurcation-of-stability curve.) Positions of the stabilizers can also be adapted to design walk-robust BHAs, as was coincidentally the case for the second run in well 4.

6.3.2 Choice and Design of Push-the-bit RSSs

The selection of the push-the-bit RSS may also significantly impact the system directional stability, as shown here for an actual, but simple, BHA. The analyzed BHA is equipped with two stabilizers 10 and 40 ft behind the bit and with a push-the-bit RSS with pads located 2.5 ft behind the bit so that $\Lambda = 0.25$. The bit has an 8.5-in. diameter, and the BHA is assumed to have uniform outer and inner radii of 7 and 2.25 in., respectively. The stabilizers are 1-ft long and have an outer diameter of 8.5 in. Parameter ε is assumed to be zero or small enough not to influence the stability of the system. This geometry leads to a characteristic stiffness $K_* = F_*/\ell_1 \simeq 1080$ kN/m, which needs to be compared to rigidities of the order of $O(100$ MN/m) for soft to medium rock formation used when modeling lateral penetration of point stabilizers.

	$\mu = 10^{-3}$	$\mu = 10^{-1}$	$\mu = 10^{1}$	$\mu = 10^{3}$
$\eta\Pi\big\vert_s (\times 10^{-2})$	5.8	3.5	26.7	102
$\eta W_a\big\vert_s$ [kips]	41	24.5	188	720
$\min(W_a)\big\vert_{\eta=5}$ [kips]	8.2	4.9	37.6	144
$\min(W_a)\big\vert_{\eta=20}$ [kips]	2	1.2	9.4	36
$\min(W_a)\big\vert_{\eta=50}$ [kips]	0.8	0.5	3.8	14.4

Table 6.3: Critical Value of $\eta\Pi$ and minimum active weight for different values of μ. The active weight is not the actual weight on bit (WOB); it also accounts for the wear of the bit and the rock strength (*i.e.*, $W_a < W$).

Table 6.3 summarizes critical values $\eta\Pi\big\vert_s$ and corresponding $\eta W_a\big\vert_s$ for different values of scaled stiffness μ. It also transcribes the minimum acceptable active weight to be imposed downhole to avoid spiraling for three different types of bit: a bit with a short active gauge (represented by an assumed lateral steering resistance η equal to 5), one with a longer passive gauge ($\eta = 50$), and an intermediate one ($\eta = 20$).

When $\mu = 10^{-3}$, the value of $\eta W_a\big\vert_s$ is approximately 41 kips ($\eta\Pi\big\vert_s \simeq 5.8 \times 10^{-2}$). This

value increases to 720 kips ($\eta\Pi|_s \simeq 1$) for $\mu = 10^3$. To put this number in perspective, the former system, with a bit characterized by $\eta = 20$, will be stable theoretically for an active weight greater than 2 kips, which is achieved easily; for the latter one, this critical active weight increases to 36 kips, and the system is more likely to induce spiraled boreholes. Parameter $\eta\Pi|_s$ first decreases for low values of μ then increases again after a threshold is crossed. Figure 6.9 illustrates the regions of stability as a function of field parameters η and W_a for different rigidities of the pads.

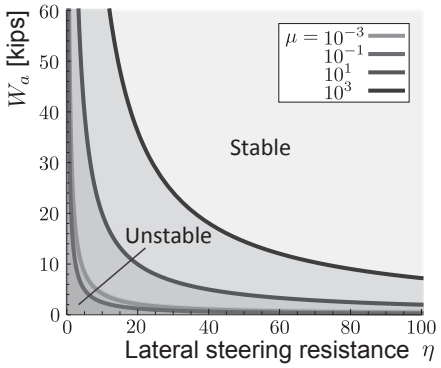

Figure 6.9: Directional stability for different stiffnesses μ of the RSS pads. Parameters are $\Lambda = 0.25$, $\lambda_2 = 3$, $OD = 7$" and $ID = 2.25$"; the stabilizers are one foot long and have an outer diameter of 8.5". [An increasing stiffness first makes the system intrinsically more stable, but then dramatically increases its tendency to induce spiraled boreholes.]

In general having a system with a low lateral rigidity is significantly better than a large one. Producers of RSSs are protective of sharing any data that would tarnish the reputation of their systems or the advanced efficiency of their control algorithms. It is recognized, however, that all available push-the-bit RSSs are not equal in terms of spiraling and field data have confirmed the tendency of some systems to induce spiraled holes, as was the case for wells 1 and 4 in the previous analysis. Figure 6.9 not only stresses that, for a given bit, the impact of the RSS can be significant; it also shows that, for a given BHA, the bit selection similarly plays a crucial role regarding spiraling tendency. Drill bits with a large lateral steering resistance tend, indeed, to reduce the likelihood of borehole spiraling. These bits may fail, however, to meet other requirements, such as achievable dogleg severity.

6.3.3 Comparison of BHA Stability with Drilling-Parameter Recommendations

The model can also be used to assess the stability of a BHA by computing the evolution of the real part of the rightmost roots with respect to the dimensionless group $\eta\Pi$, all the other parameters being fixed. With these curves, drilling engineers can estimate, at the design stage, which BHA from a set of different configurations is intrinsically the most stable and what the critical drilling-parameter limit is to avoid spiraled holes.

As an illustration, the position of the right-most characteristic roots is plotted for an idealized two-stabilizer rotary BHA derived from the BHA used in the second run of Well 3 ($\mu = \tau = \tilde{M}^e = 0$, $\varpi = 0°$). The relative position of the second stabilizer then is varied between three discrete values (Fig. 6.10).

Bifurcation values $\eta\Pi|_s$ are 3.73×10^{-2} for $\lambda_2 = 2.3$, 5.76×10^{-2} for $\lambda_2 = 2.85$, and 2.5×10^{-2} for $\lambda_2 = 3.4$. By placing the second stabilizer farther from the bit, such that λ_2 increases from 2.85 to 3.4, the bifurcation value decreases by more than double. Moreover, the relative stability of each system can be compared for a given $\eta\Pi$ by looking at the rightmost roots. For this example, the combination of a bit with a short semi-aggressive gauge (low η) and low WOB results in the least-unstable BHA being that with $\lambda_2 = 3.4$ (*e.g.*, $\eta\Pi \leq 4 \times 10^{-2}$). Similarly, it is better to place the second stabilizer slightly closer to the bit— $\lambda_2 = 2.3$—when the bit is less aggressive laterally or higher WOB is required (*i.e.*, when $\eta\Pi > 0.1$). The geometry used in the run with the second stabilizer located such that $\lambda_2 = 2.85$ is only the optimum design from a stability perspective when $4 \times 10^{-2} \leq \eta\Pi \leq 5 \times 10^{-2}$).

The previous exercise can be inverted: Knowing the BHA configuration, what is the critical minimum active weight to ensure stability? By looking at Fig. 6.10b it can be seen that, for a BHA with $\lambda_2 = 2.85$, stability is achieved for $\eta\Pi > 5.76 \times 10^{-2}$. From the geometric properties of the actual BHA, this corresponds to $\eta W_a \simeq 167.5$ kips. In other words, if a bit with an *intermediate* lateral aggressiveness is chosen (for example, $\eta = 20$), the active weight must be at least 8.4 kips for the BHA to be stable.

From the analytical expression of the characteristic equation, a sweet spot appears close to $\eta\Pi = 2$. For that particular value, the influence of the second BHA section on the force and

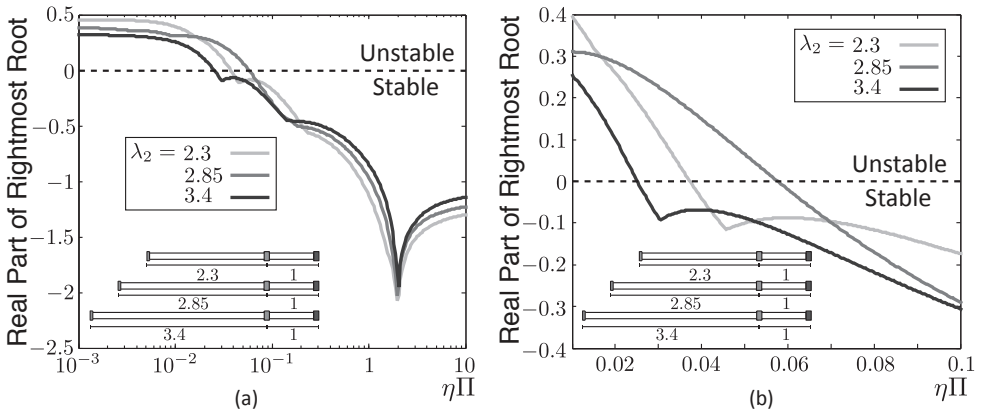

Figure 6.10: (a) Comparison of three idealized BHAs with two stabilizers. (b) Details close to the bifurcation of stability.

moment at the bit vanishes, consequently leading to an ideal one-stabilizer BHA. This value is only achievable, however, in the cases of large η and large active weights.

Similar analyzes can obviously be extended to any parameters of the model, as has been shown throughout Chapters 4 and 5 and some field cases. In general, if the shape of the stability curves can be validated, significant gain could be obtained by located the system close to *sweet spots*. Despite the fact that trends were obtained that may be systematically incorporated into general recommendations, lack of actual information about some parameters of the model, notably the stiffness of the RSS pads, limits here the reach of a more comprehensive analysis of actual BHAs. Systematic comparison of typical drilling systems, supported by supplementary field observations and refined description of drill bits, could nonetheless lead to possibly notable improved drilling performances.

Chapter 7

Conclusions

7.1 Contributions

This research has led to a comprehensive analysis of borehole spiraling. It has provided a systematic parametric study of the main parameters impacting the occurrence of spiraled holes as well as a conceptual phenomenological description of its mechanism.

This work expands on a model of borehole propagation previously developed at the University of Minnesota; however, new parameters relevant for the occurrence of spiraling have been included and their influence studied. While a stiffness in rotation at the stabilizers is likely not to have a significant impact, a lateral rigidity at the RSS pads is deemed particularly important in explaining some field observations.

The notion of directional stability has been introduced, *i.e.*, the propensity of a drilling system to induce spiraled holes. A directionally unstable system generates spiraling of the borehole, as any perturbation in the borehole trajectory, caused by an exterior agent such as a rock-formation interface, is progressively amplified, due to the geometric feedback embedded in the borehole trajectory, until a limit cycle is reached. The growing oscillations have been shown to be a combination of helices as soon as the bit walk is not trivially zero.

The parametric stability analysis hinges on the fact that there exists a critical value of the key dimensionless group of the model, $\eta\Pi$, at which a Hopf bifurcation occurs. This crucial

group defines the proportionality between the lateral force at the bit and the tilt; if its value is smaller than a critical one, the gain of the system progressively amplifies at the bit any perturbation sensed by the stabilizers. Comparing this dimensionless group, which embeds the downhole field conditions, to its critical value, which mainly depends on the BHA configuration and the bit walk, enables thus to directly assess the directional stability of the system. A sharp bit with a long passive gauge drilling at high weight on bit in a soft rock formation reduces the risk of spiraling. These general recommendations are in good agreement with common field practice. The current models also present quantitative trends in order to refine BHA designs and bit selections.

This analysis has highlighted the negative role played by the bit walk, as it tends to make systems significantly more directionally unstable. It has also shown that all push-the-bit RSS are not equal in their tendency to limit borehole spiraling. Not only field data clearly relates the occurrence of the spiral to the RSS, the modeling of the pads as a preconstrained spring illustrates how pads constraining the BHA deflection too much lead to intrinsically less directionally stable systems. Such systems are characterized by producing spirals having a pitch related to the distance between the bit and the RSS pads.

The amplitude of the spiral has been studied by adding a saturation of the bit tilt into the model. This nonlinearity explains why field measurements sometimes indicate fluctuation in the borehole orientation significantly smaller than the technological upper bound related to the overgauge of the borehole respective to the drill collars. It reinforces the idea that using tapered or undercut PDC bits may offer, under certain conditions, a compromise between steering capabilities and borehole quality. For straight boreholes, long passive full-gauge PDC bits are recommended.

Numerical codes have also been written to study the stability of any BHA and simulate borehole propagations. These tools were used to validate the model on field data pertaining to actual spiraled boreholes, despite the unavailability of crucial pieces of information. The predictions and trends of the model were substantiated and would motivate a systematic implementation in the field.

This research has thus direct practical applications in terms of understanding sources for spiraling, and acting on them by adapting the BHA geometry or the bit selection. This work

provides a set of guidelines to suppress or mitigate occurrences of borehole spiraling as part of an optimization process. Characterization of the limit cycle also enables to incorporate it better into torque and drag models or estimate the drift diameter of the borehole. These further improve borehole designs and completion times.

7.2 Future Work

Some elements were overlooked that may influence the system stability. These elements are: (a) steering systems such as point-the-bit RSS or downhole turbines, (b) rock anisotropy, (c) borehole overgauge, and (d) control algorithms.

Even though field data included point-the-bit systems, they have not yet been modeled completely. As point-the-bit RSSs are able to work with longer-gauge bits, the systematic study of the resulting equations may highlight some inherent advantages for that system in terms of steerability and borehole quality. Similarly isotropic and homogeneous rocks are the exception rather than the rule. The global influence of rock anisotropy on the directional tendency is relevant both is terms of prediction and post-calculation.

Other nonlinearities may have a significant impact on the directional stability. First, stabilizers never perfectly fit the wellbore; there is always some overgauge due to both the actual stabilizer diameter – usually slightly smaller than that of the bit – and phenomena such as downhole dynamics. The stabilizers may not be centered on average in the borehole, or even not be in contact. This influences the constraints imposed on the BHA deflection and thus the drilling direction at the bit. The potential impact on directional stability of adjustable-diameter stabilizers may be a fascinating topic for future research. Similarly, it was assumed that the stabilizers and the bit are the only contact points between the BHA and the wellbore; this is not always the case, especially if the distance between the first and second stabilizer is large. Accounting for extraneous contacts that constrain even more the BHA may have a significant influence on both the linear stability analysis and the limit cycle. Finally, direct implementation of control algorithms at the RSS would enable to test their efficiency in terms not only of directional tendency but also of borehole quality.

Another crucial challenge is concerned with the identification of the model parameters, especially the active weight, the bit lateral steering resistance, and the walk. While the latter two may already be known with sufficient accuracy by bit manufacturers, their systematic quantification would help many aspects of field prediction. The identification of the evolution of the active weight is even more critical as it also relates to efficient drilling and optimization of the rate of penetration. This concept of active weight is not yet commonly recognized by the Industry despite its possibly significant impact on drilling performances.

While some of the model parameters may be obtained from laboratory testing or from specifically designed numerical codes, a field campaign would unravel the full potential of the model. Systematic evaluation of the active weight with drill-off tests and full knowledge of the bit characteristics would open possibilities in terms of drilling efficiency, prediction, and post-calculation. This field campaign, however, could be considered only within a partnership with the Industry.

Finally, the current model can in principle be used to design robust model-based controllers for RSSs. Beyond steering the borehole in the desired direction, what they already accomplish, such controllers should also aim at limiting borehole tortuosity and spiraling.

Bibliography

Aadnoy, B. S. and Andersen, K. (1998). Friction analysis for long-reach wells. In *IADC/SPE Drilling Conference*, number IADC/SPE 39391, pages 819–834, Dallas, Texas, USA.

Aadnoy, B. S. and Huusgaard, P. P. (2002). Analytical models for design of wellpath and BHA. In *IADC/SPE Asia Pacific Drilling Technology*, number IADC/SPE 77220, Jakarta, Indonesia.

Aarrestad, T. V. and Blikra, H. (1994). Torque and drag: Key factors in extended-reach drilling. In *IADC/SPE Drilling Conference*, number IADC/SPE 27491, pages 547–552, Dallas, Texas, USA.

Al-Suwaidi, A., Allen, F., Taylor, R., Hussein, K., and Russell, R. (2003). Experience with rotary steerable systems in onshore Abu Dhabi fields. In *SPE/IADC Middle East Drilling Technology Conference and Exhibition*, number SPE 85291, Abu Dhabi, UAE.

Amara, M. H. (1985). Use of drillstring models and data bases for the scientific control of vertical and directional hole paths. In *SPE/IADC Drilling Conference*, number SPE/IADC 13495, New Orleans, Louisiana, USA.

Bai, J. (1986). An exact solution for bottomhole assembly analysis. In *37th Annual Technical Meeting of the Petroleum Society of CIM*, Calgary, Alberta, Canada.

Bang, J., Jegbefume, O., Ledroz, A., and Thompson, J. (2015). Wellbore tortuosity analysed by a novel method may help to improve drilling, completion, and production operations. In *SPE/IADC Drilling Conference and Exhibition*, number SPE 173103, London, England, UK.

Banks, S., Hogg, T., and Thorogood, J. (1992). Increasing extended-reach capabilities through wellbore profile optimisation. In *SPE/IADC Drilling Conference*, number SPE 23850, New Orleans, Louisiana, USA.

Barr, J., Clegg, J., and Russell, M. (1995). Steerable rotary drilling with an experimental system. In *SPE/IADC Drilling Conference*, number SPE 29382, Amsterdam, Netherlands.

Bellay, G., Al-Waheed, H., and Audah, T. (1996). Cyclic borehole effects in deviated wells. In *Abu Dhabi International Petroleum Exhibition and Conference*, number SPE 36288, Abu Dhabi, UAE.

Bellen, A. and Zennaro, M. (2013). *Numerical methods for delay differential equations*. Oxford University Press.

Birades, M. and Fenoul, R. (1986). ORPHEE 2D: A microcomputer program for prediction of bottomhole assembly trajectory. In *Symposium on Petroleum Industry Application of Microcomputers of the Society of Petroleum Engineers*, number SPE 15285, pages 31–38, Silver Creek, Colorado, USA.

Birades, M. and Fenoul, R. (1988). A microcomputer program for prediction of bottomhole assembly trajectory. *SPE Drilling Engineering*, 3(2):167–172.

Boualleg, R., Sellami, H., Menand, S., and Simon, C. (2006). Effect of formations anisotropy on directional tendencies of drilling systems. In *IADC/SPE Drilling Conference*, number SPE 98865, Miami, Florida, USA.

BP (2015). Bp Energy Outlook 2035.

Bradley, W. B. (1974). Deviation forces from the penetration failure of anisotropic rock. *J. Engng Ind., Trans. Am. Soc. mech. Engrs Ser B*, 95:1093–1101.

Bradley, W. B. (1975). Factors affecting the control of borehole angle in straight and directional wells. *Journal of Petroleum Technology*, 27(6):679–688.

Brands, S. and Lowdon, R. (2012). Scaled tortuosity index: Quantification of borehole undulations in terms of hole curvature, clearance and pipe stiffness. In *IADC/SPE Drilling Conference and Exhibition*, number SPE 151274, San Diego, California, USA.

Brantly, J. E. (1971). *History of Oil Well Drilling*. Book Division, Gulf Publishing Company.

Brett, J. F., Gray, J. A., Bell, R. K., and Dunbar, M. E. (1986). A method of modeling the directional behavior of bottomhole assemblies including those with bent subs and downhole motors. In *IADC/SPE Drilling Conference*, number IADC/SPE 14767, pages 365–376, Dallas, Texas, USA.

Brown, E. T., Green, S. J., and Sinha, K. P. (1981). The influence of rock anisotropy on hole deviation in rotary drilling–a review. *International Journal of Rock Mechanics and Mining Sciences*, 18(5):387–401.

Callas, N. P. (1981). Predicting borehole trajectories. *Oil & Gas Journal*, 79(34):129–133.

Callas, N. P. and Callas, R. L. (1980). Stabilizer placement–3. boundary value problem is solved. *Oil & Gas Journal*, 78(50):62–66.

Capelushnikov, M. (1930). Why holes go crooked in drilling. *World Petroleum*, pages 191–194.

Chandra, U. (1986). Basic concepts in static BHA analysis for directional drilling. In *SPE Annual Technical Conference and Exhibition*, number SPE 15467, New Orleans, Louisiana, USA.

Cheatham, C. A. and Loeb, D. A. (1985). Effects of field wear on PDC bit performance. In *SPE/IADC Drilling Conference*, number SPE/IADC 13464, pages 359–364, New Orleans, Louisiana, USA.

Cheatham, Jr., J. B. and Ho, C. Y. (1981). A theoretical model for directional drilling tendency of a drill bit in anisotropic rock. Technical report, Rice University, Houston, Texas.

Chen, D. C., Gaynor, T., and Comeaux, B. (2002a). Hole quality: why it matters. In *SPE International Petroleum Conference and Exhibition in Mexico*, number SPE 74403, Villahermosa, Mexico.

Chen, D. C., Gaynor, T., Comeaux, B., and Glass, K. (2002b). Hole quality: Gateway to efficient drilling. In *Offshore Technology Conference*, number OTC 14277, Houston, Texas, USA.

Chen, D. C.-K. and Wu, M. (2008). State-of-the-art BHA program produces unprecedented results. In *International Petroleum Technology Conference*, Kuala Lumpur, Malaysia.

Chen, S., Collins, G. J., Thomas, M. B., et al. (2008). Reexamination of PDC-bit walk in directional and horizontal wells. In *IADC/SPE Drilling Conference*, number SPE 112641, Orlando, Florida, USA.

Chen, S. L. and Geradin, M. (1993). Three dimensional modelling of PDC bit/formation interaction. Technical report, University of Liège.

Clark, D. A. and Walker, B. H. (1985). Comparison of laboratory and field data for a PDC bit. In *SPE/IADC Drilling Conference*, number SPE/IADC 13459, pages 323–330, New Orleans, Louisiana, USA.

Cleveland, C., Hogan, C. M., and Saundry, P. (2010). Deepwater horizon oil spill. *The Encyclopedia of Earth*.

Close, U. (1939). More oil from crooked wells. *Scientific American*, 161(2):84–87.

Coudyzer, C. and Richard, T. (2005). Influence of the back and side rake angles in rock cutting. In *AADE 2005 National Technical Conference and Exhibition*, pages 5–7, Houston, Texas, USA.

Denoël, V. and Detournay, E. (2011). Eulerian formulation of constrained elastica. *International Journal of Solids and Structures*, 48(3-4):625–636.

Detournay, E. (2009). Mathematical model of the near-bit region of an advancing drilling system. In *First International Colloquium on Non-Linear Dynamics of Deep Drilling Systems*, pages 99–105, Liege, Belgium.

Detournay, E. and Atkinson, C. (2000). Influence of pore pressure on the drilling response in low-permeability shear-dilatant rocks. *International Journal of Rock Mechanics and Mining Sciences*, 37(7):1091–1101.

Detournay, E. and Defourny, P. (1992). A phenomenological model for the drilling action of drag bits. *International Journal of Rock Mechanics and Mining Sciences and Geomechanics Abstracts*, 29(1):13–23.

Detournay, E. and Perneder, L. (2011). Dynamical model of a propagating borehole. In *Proceedings of the 7th EUROMECH Nonlinear Oscillations Conference (ENOC)*, Rome, Italy.

Detournay, E., Richard, T., and Shepherd, M. (2008). Drilling response of drag bits: Theory and experiment. *International Journal of Rock Mechanics and Mining Sciences*, 45(8):1347–1360.

Downton, G. C. (2007). Directional drilling system response and stability. In *16th IEEE International Conference on Control Applications*, pages 1543–1550, Singapore.

Downton, G. C., Hendricks, A., Klausen, T. S., and Pafitis, D. (2000). New directions in rotary steerable drilling. *Oilfield Review*, 12(1):18–29.

Downton, G. C. and Ignova, M. (2011). Stability and response of closed loop directional drilling system using linear delay differential equations. In *IEEE International Conference on Control Applications*.

Dupriest, F. and Sowers, S. (2009). Maintaining steerability while extending gauge length to manage whirl. In *SPE/IADC Drilling Conference and Exhibition*, number SPE 119625, Amsterdam, The Netherlands.

Eastman, H. J. (1937). The art of oil well surveying and controlled directional drilling. In *2nd World Petroleum Congress*, pages 933–942, Paris, France.

EIA (2014). International energy outlook 2014. Technical report, U.S. Energy Information Administration.

EIA (2015). Short-term energy and winter fuels outlook (STEO). Technical report, U.S. Energy Information Administration.

Erneux, T. (2009). *Applied Delay Differential Equations*. Springer Verlag.

Ernst, S., Pastusek, P., and Lutes, P. (2007). Effects of RPM and ROP on PDC bit steerability. In *SPE/IADC Drilling Conference*, number SPE/IADC 105594, Amsterdam, The Netherlands.

Faÿ, H. (1993). Practical evaluation of rock-bit wear while drilling. *SPE drilling & completion*, 8(2):99–104.

Fischer, F. J. (1974). Analysis of drillstring in curved boreholes. In *49th Annual Fall Meeting of the Society of Petroleum Engineers of AIME*, number SPE 5071, Houston, Texas, USA.

Franca, L. F. P. (2010). Drilling action of roller-cone bits: Modeling and experimental validation. *ASME Journal of Energy Resources Technology*, 132(4):043101.

Gaynor, T., Hamer, D., Chen, D. C., and Stuart, D. (2002). Quantifying tortuosities by friction factors in torque and drag model. In *SPE Annual Technical Conference and Exhibition*, number SPE 77617, San Antonio, Texas, USA.

Gaynor, T. M., Chen, D. C., Stuart, D., and Comeaux, B. (2001). Tortuosity versus micro-tortuosity-why little things mean a lot. In *SPE/IADC drilling conference*, number SPE 67818, Amsterdam, The Netherlands.

Germay, C., van de Wouw, N., Nijmeijer, H., and Sepulchre, R. (2009). Nonlinear drillstring dynamics analysis. *SIAM Journal on Applied Dynamical Systems*, 8(2):527–553.

Guild, G., Wallace, I., and Wassenborg, M. (1995). Hole cleaning program for extended reach wells. In *SPE/IADC Drilling Conference*, number SPE 29381, Amsterdam, The Netherlands.

Hale, J. K. (1977). *Theory of Functional Differential Equations*. Applied Mathematical Sciences (vol. 3). Springer Verlag, New York.

Haugen, J. (1998). Rotary steerable system replaces slide mode for directional drilling applications. *Oceanographic Literature Review*, 8(45):1471.

Ho, H.-S. (1986). General formulation of drillstring under large deformation and its use in BHA analysis. In *SPE Annual Technical Conference and Exhibition*, number SPE 15562, New Orleans, Louisiana, USA.

Ho, H.-S. (1987). Prediction of drilling trajectory in directional wells via a new rock-bit interaction model. In *SPE Annual Technology Conference and Exhibition*, number SPE 16658, pages 83–95, Dallas, Texas, USA.

Ho, H.-S. (1988). An improved modeling program for computing the torque and drag in directional and deep wells. In *SPE Annual Technical Conference and Exhibition*, number SPE 18047, pages 407–418, Houston, Texas, USA.

Ho, H.-S. (1989). *U.S. Patent No. 4,804,051.* Washington, DC: U.S. Patent and Trademark Office.

Ho, H.-S. (1995). *U.S. Patent No. 5,456,141.* Washington, DC: U.S. Patent and Trademark Office.

Ho, H.-S. (1997). *U.S. Patent No. 5,608,162.* Washington, DC: U.S. Patent and Trademark Office.

Horibe, T., Ushida, M., Okumura, K., and Sung, Y. T. (1979). Study on deviation of borehole in deep boring. Technical report.

Hughes, J. D. (1935). Value of oil-well surveying and applications of controlled directional drilling. *Drilling and Production Practice*.

Huynen, A., Detournay, E., and Denoël, V. (2014). Eulerian formulation of the torque and drag problem. In *Third International Colloquium on Nonlinear Dynamics and Control of Deep Drilling Systems*, Minneapolis, Minnesota, USA.

Inglis, T. A. (1987). *Directional Drilling*. Petroleum Engineering and Development Studies (vol. 2). Graham & Trotman.

Insperger, T. and Stepan, G. (2002). Semi-discretization method for delayed systems. *International Journal for numerical methods in engineering*, 55(5):503–518.

Kaplan, R. D. (2011). *Monsoon: the Indian Ocean and the future of American power*. Random House Incorporated.

Knapp, S. R. (1961). Are we missing the cheapest solution to our crooked hole problem? *Oil Gas J.*, 59(103-108).

Knapp, S. R. (1965). New bit concept helps control hole deviation. *Wld Oil*, 160:113–116.

Kopey, B. (2007). Development of drilling technics from ancient ages to modern times. In *12th IFToMM World Congress*, Besançon, France.

Kozlovsky, Y. A. (1984). The world's deepest well. *Scientific American*, 251(6):98–104.

Kremers, N., Detournay, E., and van de Wouw, N. (2015). Model-based robust control of directional drilling systems. *IEEE Transactions on Control Systems Technology*.

Lahee, F. H. (1929). Problem of crooked holes. *Bulletin of the American Association of Petroleum Geologists*, 13(9):1095–1162.

Lesso Jr, W. G., Rezmer-Cooper, I. M., and Chau, M. (2001). Continuous direction and inclination measurements revolutionize real-time directional drilling decision-making. In *SPE/IADC drilling conference*, number SPE 67752, Amsterdam, The Netherlands.

Lubinski, A. and Woods, H. B. (1953). Factors affecting the angle of inclination and dog-legging in rotary bore holes. In *Mid-Continent District*, pages 222–250, Tulsa, Oklahoma, USA.

MacDonald, G. C. and Lubinski, A. (1951). Straight-hole drilling in crooked-hole country. In *Spring Meeting of the Mid-Continent District, Division of Production*, Amarillo, Texas, USA.

Maeso, C. and Tribe, I. (2001). Hole shape from ultrasonic calipers and density while drilling-a tool for drillers. In *SPE Annual Technical Conference and Exhibition*, number SPE 71395, New Orleans, Louisiana, USA.

Maouche, Z. (1999). *Contribution à l'Amélioration de la Prédiction en Inclinaison des Systèmes de Forage Rotary Couplage Garniture-Outil de Forage*. PhD thesis, Ecole Nationale Supérieure des Mines de Paris, Paris, France.

Marck, J. and Detournay, E. (2014a). Estimation of the spiraling tendency of drilling systems. In *Third International Colloquium on Nonlinear Dynamics and Control of Deep Drilling Systems*, Minneapolis, USA.

Marck, J. and Detournay, E. (2014b). Perturbation to borehole trajectory across a rock interface. In *48th US Rock Mechanics/Geomechanics Symposium*, Minneapolis, USA.

Marck, J. and Detournay, E. (2015a). Influence of rotary-steerable-system design on borehole spiraling. *SPE Journal*, In print.

Marck, J. and Detournay, E. (2015b). Spiraled boreholes: An expression of 3D directional instability of drilling systems. In *SPE/IADC Drilling Conference and Exhibition*, number SPE/IADC 173156, London, UK.

Marck, J., Detournay, E., Kuesters, A., and Wingate, J. (2014). Analysis of spiraled-borehole data by use of a novel directional-drilling model. *SPE Drilling & Completion*, 29(03):267–278.

Mason, C. J. and Chen, D. C. (2005). The perfect wellbore! In *SPE Annual Technical Conference and Exhibition*, number SPE 95279, Dallas, Texas, USA.

Mason, C. J. and Chen, D. C. (2006). The wellbore quality scorecard (WQS). In *IADC/SPE Drilling Conference*, number SPE 98893, Miami, Florida, USA.

Matthews, C. and Dunn, L. (1993). Drilling and production practices to mitigate sucker rod/tubing wear-related failures in directional wells. *SPE Production & Facilities*, 8(04):251–259.

McLamore, R. T. (1971). The role of rock strength anisotropy in natural hole deviation. *J. Petrol. Technol.*, 23:1313–1321.

Menand, S. (2001). *Analyse et Validation d'un Modèle de Comportement Directionnel des Outils de Forage Monoblocs PDC*. PhD thesis, Ecole Nationale Supérieure des Mines de Paris.

Menand, S. (2013). Borehole tortuosity effect on maximum horizontal drilling length based on advanced buckling modeling. In *AADE Technical Conference and Exhibition*, Oklahoma City, Oklahoma, USA.

Menand, S., Sellami, H., Simon, C., Besson, A., and Silva, N. d. (2002). How the bit profile and gages affect the well trajectory. In *IADC/SPE Drilling Conference*, number SPE 74459, Dallas, Texas, USA.

Menand, S., Sellami, H., Tijani, M., Stab, O., and Simon, C. (2006). Advancements in 3D drillstring mechanics: From the bit to the topdrive. In *IADC/SPE Drilling Conference*, number IADC/SPE 98965, Miami, Florida, USA.

Menand, S., Simon, C., Gaombalet, J., Macresy, L., Gerbaud, L., Ben Hamida, M., Amghar, Y., Denoix, H., Cuiller, B., and Sinardet, H. (2012). PDC bit steerability modeling and testing for push-the-bit and point-the-bit RSS. In *IADC/SPE Drilling Conference and Exhibition*, San Diego, California, USA.

Michiels, W. and Niculescu, S.-I. (2007). *Stability and Stabilization of Time-Delay Systems: An Eigenvalue-Based Approach*. Advances in Design and Control. Society for Industrial and Applied Mathematics.

Millheim, K. K. (1977). The effect of hole curvature on the trajectory of a borehole. In *SPE Annual Fall Technical Conference and Exhibition*, number SPE 6779, Denver, Colorado, USA.

Millheim, K. K. (1979). Behavior of multiple-stabilizer bottom-hole assemblies. *Oil and Gas Journal*, 77(1):59–64.

Millheim, K. K. (1982). Computer simulation of the directional drilling process. In *International Petroleum Exhibition and Technical Symposium*, number SPE 9990, pages 483–496, Beijing, China.

Millheim, K. K., Jordan, S., and Ritter, C. J. (1978). Bottom-hole assembly analysis using finite-element method. *Journal of Petroleum Technology*, 30(SPE 6057):265–274.

Millheim, K. K. and Warren, T. M. (1978). Side cutting characteristics of rock bits and stabilizers while drilling. In *SPE Annual Fall Technical Conference and Exhibition*, number SPE 7518, Houston, Texas, USA.

Miska, S., Luo, F., and Chaharlang, S. (1988). A new approach to the analysis of bottom hole assembly performance. In *Eleventh Annual Energy-Source Technology Conference and Exhibit*, pages 211–220, New Orleans, Louisiana, USA.

Monsieurs, F. (2015). Model-based decoupled control of a 3D directional drilling system. Master's thesis, Eindhoven University of Technology.

Moon, F. C. (2007). *The machines of Leonardo Da Vinci and Franz Reuleaux: Kinematics of Machines from the Renaissance to the 20th Century*. Springer Verlag.

Moor, W. D. (1977). Ingenuity sparks drilling history. *Oil and Gas Journal*, 75(35):159–177.

Muller, F. G. D. (1924). Much trouble caused by crooked holes. *The Oil Weekly*.

Murphey, C. E. and Cheatham, Jr., J. B. (1966). Hole deviation and drill string behavior. *Society of Petroleum Engineers Journal*, 6(1):44–54.

Neubert, M. (1997). *Richtungsregelung beim Tiefbohren*. PhD thesis, Institut für Technische Mechanik, Technische Universität Braunschweig, Germany.

Neubert, M. and Heisig, G. (1996). Mathematical description of the directional drilling process and simulation of directional control algorithm. *Zeitschrift für angewandte Mathematik und Mechanik*, 76:361–362.

Nieto, J., Schmitt, D., and Keys, R. (1995). Removal of borehole induced noise from well logs. In *SPWLA 36th Annual Logging Symposium*, number SPWLA-1995-III, Paris, France.

Norris, J. A., Dykstra, M. W., Beuershausen, C. C., Fincher, R. W., and Ohanian, M. P. (1998). Development and successful application of unique steerable PDC bits. In *IADC/SPE Drilling Conference*, number IADC/SPE 39308, pages 153–166, Dallas, Texas, USA.

Oag, A. W. and Williams, M. (2000). The directional difficulty index-a new approach to performance benchmarking. In *IADC/SPE Drilling Conference*, number SPE 59196, New Orleans, Louisiana, USA.

Ogawa, N. and Minh, C. C. (1997). Log interpretation problems and their partial solutions in horizontal wells drilled offshore-neutral zone-between kuwait and saudi arabia. In *Middle East Oil Show and Conference*, number SPE 37775, Bahrain.

Palmov, V. A. and Vetyukov, Y. M. (2002). Model for the bit-rock interaction analysis. In *Fifth International Workshop on Nondestructive Testing and Computer Simulations in Science and Engineering*, volume 4627, pages 243–248.

Pariseau, W. G. (1971). Wedge indentation of anisotropic geologic media. In *Dynamic Rock Mechanics, Proc. 12th U.S. Symp. on Rock Mechanics*, pages 529–546, New York, USA.

Pastusek, P. and Brackin, V. (2003). A model for borehole oscillations. In *SPE Annual Technical Conference and Exhibition*, number SPE 84448, Denver, Colorado, USA.

Pastusek, P., Brackin, V., and Lutes, P. (2005). A fundamental model for prediction of hole curvature and build rates with steerable bottomhole assemblies. In *SPE Annual Technical Conference and Exhibition*, number SPE 95546, Dallas, Texas, USA.

Pastusek, P. E., Cooley, C. H., Sinor, L. A., and Anderson, M. (1992). Directional and stability characteristics of anti-whirl bits with non-axisymmetric loading. In *SPE Annual Technical Conference and Exhibition*, number SPE 24614, Washington, DC, USA.

Perneder, L. (2013). *A Three-dimensional Mathematical Model of Directional Drilling*. PhD thesis, University of Minnesota.

Perneder, L. and Detournay, E. (2013a). Equilibrium inclinations of straight boreholes. *SPE Journal*, 18(3):395–405.

Perneder, L. and Detournay, E. (2013b). Steady-state solutions of a propagating borehole. *International Journal of Solids and Structures*, 50(9):1226–1240.

Perneder, L., Detournay, E., and Downton, G. (2012). Bit-rock interface laws in directional drilling. *International Journal of Rock Mechanics and Mining Sciences*, 51:81–90.

Rafie, S. (1988). Mechanistic approach in designing BHA's and forecasting wellbore position. In *IADC/SPE Drilling Conference*, number IADC/SPE 17196, pages 161–170, Dallas, Texas, USA.

Rafie, S., Ho, H.-S., and Chandra, U. (1986). Applications of a BHA analysis program in directional drilling. In *IADC/SPE Drilling Conference*, number IADC/SPE 14765, pages 345–354, Dallas, Texas, USA.

Rashidi, B., Hareland, G., and Nygaard, R. (2008). Real-time drill bit wear prediction by combining rock energy and drilling real-time drill bit wear prediction by combining rock

energy and drilling strength concepts. In *Abu Dhabi International Petroleum Exhibition and Conference*, number SPE 117109, Abu Dhabi, UAE.

Richard, T., Dagrain, F., Poyol, E., and Detournay, E. (2012). Rock strength determination from scratch tests. *Engineering Geology*, 147:91–100.

Richard, T., Germay, C., and Detournay, E. (2007). A simplified model to explore the root cause of stick-slip vibrations in drilling systems with drag bits. *Journal of Sound and Vibration*, 305(3):432–456.

Rollins, H. M. (1959). Are 3 ° and 5 ° straight holes worth their cost? *Oil Gas J.*, 57:163–171.

Russell, R. (2002). Improving borehole quality and drilling efficiency with a new suite of drilling tools. In *Abu Dhabi International Petroleum Exhibition and Conference*, number SPE 78497, Abu Dhabi, UAE.

Samuel, G. R., Bharucha, K., and Luo, Y. (2005). Tortuosity factors for highly tortuous wells: A practical approach. In *SPE/IADC Drilling Conference*, number SPE 92565, Amsterdam, The Netherlands.

Samuel, R. and Liu, X. (2009). Wellbore tortuosity, torsion, drilling indices, and energy: What do they have to do with well path design? In *SPE Annual Technical Conference and Exhibition*, number SPE 124710, pages 4–7, New Orleans, Louisiana, USA.

Shampine, L. (2005). Solving ODEs and DDEs with residual control. *Applied Numerical Mathematics*, 52(1):113–127.

Shampine, L. F. and Thompson, S. (2001). Solving DDEs in matlab. *Applied Numerical Mathematics*, 37(4):441–458.

Simon, C. (1996). *Modélisation du Comportement Directionnel des Outils de Forage Monoblocs en Formations Anisotropes*. PhD thesis, Ecole Nationale Supérieure des Mines de Paris, Paris, France.

Smith, M. B. and Cheatham, J. B. (1977). Deviation forces arising from single bit tooth indentation of an anisotropic porous media. *J. Pressure Vessel Technol., Trans. Am. Soc. mech. Engrs, Ser. J*, 99:362–366.

Stepan, G. (1989). *Retarded Dynamical Systems: Stability and Characteristic Functions*. Longman Scientific & Technical.

Stockhausen, E. and Lesso Jr, W. (2003). Continuous direction and inclination measurements lead to an improvement in wellbore positioning. In *SPE/IADC Drilling Conference*, number SPE 79917, Amsterdam, The Netherlands.

Stroud, D., Peach, S., and Johnston, I. (2004). Optimization of rotary steerable system bottomhole assemblies minimizes wellbore tortuosity and increases directional drilling efficiency. In *SPE Annual Technical Conference and Exhibition*, number SPE 90396, Houston, Texas, USA.

Stuart, D., Hamer, C., Henderson, C., Gaynor, T., and Chen, D.-K. (2003). New drilling technology reduces torque and drag by drilling a smooth and straight wellbore. In *SPE/IADC Drilling Conference*, number SPE 79919, Amsterdam, The Netherlands.

Studer, R., Simon, C., Genevois, J.-M., and Menand, S. (2007). Learning curve benefits resulting from the use of a unique BHA directional behaviour drilling performances post-analysis. In *SPE Annual Technical Conference and Exhibition*, number SPE 110432, Anaheim, California, USA.

Sugiura, J. (2009). Improving rotary-steerable borehole quality using innovative imaging techniques. In *Offshore Technology Conference*, number OTC-19991-MS, Houston, Texas, USA.

Sugiura, J. and Jones, S. (2008a). Integrated approach to rotary-steerable drilling optimization using concurrent real-time measurement of near-bit borehole caliper and near-bit vibration. In *Intelligent Energy Conference and Exhibition*, number SPE 112163, Amsterdam, The Netherlands.

Sugiura, J. and Jones, S. (2008b). The use of the industry's first 3-D mechanical caliper image

while drilling leads to optimized rotary-steerable assemblies in push-and point-the-bit configurations. In *SPE Annual Technical Conference and Exhibition*, number SPE 115395, Denver, Colorado, USA.

Sultanov, B. and Shandalov, G. (1961). Effects of geological conditions on well deviation. *Izv. vyssh. ucheb. Zaved. geol. razved.*, 3:106.

Teale, R. (1965). The concept of specific energy in rock drilling. *International Journal of Rock Mechanics and Mining Science & Geomechanics Abstracts*, 2(1):57–73.

Tweten, D. J., Lipp, G. M., Khasawneh, F. A., and Mann, B. P. (2012). On the comparison of semi-analytical methods for the stability analysis of delay differential equations. *Journal of Sound and Vibration*, 331(17):4057–4071.

van de Wouw, N., Kremers, N., and Detournay, E. (2015). Output-feedback inclination control of directional drilling systems. *IFAC-PapersOnLine*, 48(6):260–265.

Voinov, O. V. and Reutov, V. A. (1991). Drill bit operation in an anisotropic rock. *Soviet Mining Science*, 27(2):138–146.

Waughman, R. J., Kenner, J. V., and Moore, R. A. (2002). Real-time specific energy monitoring reveals drilling inefficiency and enhances the understanding of when to pull worn PDC bits. In *IADC/SPE Drilling Conference*, number IADC/SPE 74520, Dallas, Texas, USA.

Weaver, D. K. (1946). Practical aspects of directional drilling. In *Twenty-sixth Annual Meeting*, Chicago, Illinois, USA.

Weijermans, P., Ruszka, J., Jamshidian, H., and Matheson, M. (2001). Drilling with rotary steerable system reduces wellbore tortuosity. In *SPE/IADC drilling conference*, number SPE 67715, Amsterdam, The Netherlands.

Williams, C., Mason, J. S., and Spaar, J. (2001). Operational efficiency on eight-well sidetrack program saves $ 7.3 million vs historical offsets in mp 299/144 gom. In *SPE/IADC drilling conference*, number SPE 67826, Amsterdam, The Netherlands.

Williamson, J. S. and Lubinski, A. (1986). Predicting bottomhole assembly performance. In *IADC/SPE Drilling Conference*, number SPE 14764, pages 337–341, Dallas, Texas, USA.

Woods, H. and Lubinski, A. (1954). How to determine best hole and drill-collar size. *The Oil and Gas Journal*, 7.

Woods, H. B. and Lubinski, A. (1955). Use of stabilizers in controlling hole deviation. In *Spring Meeting of the Mid-Continent District, Division of Production*, Amarillo, Texas, USA.

Wu, Z. and Michiels, W. (2012). Reliably computing all characteristic roots of delay differential equations in a given right half plane using a spectral method. *Journal of Computational and Applied Mathematics*, (236):2499–2514.

Yergin, D. (2011). *The prize: The epic quest for oil, money & power*. Simon and Schuster.

Zhou, Y. and Detournay, E. (2014). Analysis of the contact forces on a blunt pdc. In *48th US Rock Mechanics/Geomechanics Symposium*, Minneapolis, Minnesota, USA.

Zijsling, D. H. (1987). Single cutter testing - a key for PDC bit development. In *Offshore Europe*, number SPE 16529, Aberdeen, UK.

Appendix A

Bit/Rock Interaction Law for a Cylindrical Bit

The construction of the bit/rock interaction law used in this paper relies on a bilinear single-cutter/rock interaction law (Detournay and Defourny, 1992) abundantly validated by experiments with single cutters, called scratch tests (Richard et al., 2012), and with PDC bits (Detournay et al., 2008). This law relates the force acting on a single cutter to the depth of cut. Two ductile regimes can be identified: the first when both the contact and cutting forces (along the wearflat and the cutting face, respectively) are proportional to depth of cut p; and the second where the contact forces have saturated and only the cutting forces increase with p. The resultant force is assumed to be proportional to the cutter width. The normal and tangent components of force on the cutter (for a unit cutter width) are given by (Fig. 3.4):

$$f_n = \zeta' \iota p, \quad f_w = \zeta'' \iota p, \quad p < p^* \quad \text{(Regime I)},$$

$$f_n = \sigma_* l + \zeta \iota p, \quad f_w = \upsilon \sigma_* l + \iota p, \quad p > p^* \quad \text{(Regime II)},$$

where ι is the intrinsic specific energy of the rock, σ_* is the maximum contact stress at the cutter wearflat, l is the length of the wearflat, υ is the coefficient of friction at the wearflat, and ζ, ζ' and ζ'' are coefficients that define the single cutter/rock bilinear law and mainly depend on the relative inclination of the wearflat and of the cutting face on the cutter velocity, V (Zhou and

Detournay, 2014).

The passage from the single-cutter/rock interaction to the general bit/rock interaction law follows the steps introduced by Perneder et al. (2012). Because of the complex cutter distribution around PDC bits, it is unpractical to derive a single interaction for each bit, at least in the context of this research. However, the average response of any PDC bit can be captured, in principle, by four numbers: its lateral steering resistance η, its angular steering resistance χ, its walk ϖ, and its flip ς.

The general bit/rock interaction law is presented here for the case of an ideal cylindrical PDC bit of radius a and height $2b$. The bit face is assumed to drill in Regime II and the gauge to interact with the rock in Regime I. The force (and especially the moment) acting on a bit must be computed with respect to an arbitrary point of reference along the bit axis. Technically distances along the BHA are measured with respect to the point of reference. For practical purposes, these distances can be taken from the center of the cutting structure.

In the case of a cylindrical bit whose reference point is chosen to be at the center of the bit face, the general bit/rock interaction law is given by Perneder et al. (2012). However, if this point is translated to be in such a way that the averaged moment with respect to that point is cancelled when the entire gauge interacts uniformly with the rock, the bit/rock interaction law reduces to

$$\begin{Bmatrix} F_1 \\ F_2 \\ F_3 \\ M_2 \\ M_3 \end{Bmatrix} = -\begin{Bmatrix} \sigma_* a l \\ 0 \\ 0 \\ 0 \\ 0 \end{Bmatrix} - \iota \begin{bmatrix} a\zeta & 0 & 0 & 0 & 0 \\ 0 & \frac{1}{2}b\zeta' & -\frac{1}{2}b\zeta'' & -\frac{1}{4}a^2 & 0 \\ 0 & \frac{1}{2}b\zeta'' & \frac{1}{2}b\zeta' & 0 & -\frac{1}{4}a^2 \\ 0 & 0 & 0 & \frac{1}{6}a^3\zeta - \frac{5}{9}b^3\zeta' & \frac{5}{9}b^3\zeta'' \\ 0 & 0 & 0 & -\frac{5}{9}b^3\zeta'' & \frac{1}{6}a^3\zeta - \frac{5}{9}b^3\zeta' \end{bmatrix} \begin{Bmatrix} d_1 \\ d_2 \\ d_3 \\ \varphi_2 \\ \varphi_3 \end{Bmatrix} \tag{A.1}$$

The general bit/rock interaction law (3.7) assumed in this research neglects only two possible relevant terms, which relate the lateral force to the angular penetration of the bit. These terms arise, however, from the interaction of the bit face with the rock and, consequently, cannot be estimated accurately without further investigation.

For illustration purposes only, the properties of this ideal cylindrical bit can be obtained:

$$\eta = \frac{1}{2}\frac{b\sqrt{\zeta'^2 + \zeta''^2}}{a\zeta}, \quad \ell_1^2\chi = \frac{5}{9}\frac{b^3\sqrt{\left(\frac{3a^3\zeta}{10b^3} - \zeta'\right)^2 + \zeta''^2}}{a\zeta}, \tag{A.2}$$

$$\varpi = -\arctan\left(\frac{\zeta''}{\zeta'}\right), \quad \varsigma = \arctan\left(\frac{\frac{5}{9}b^3\zeta''}{\frac{1}{6}a^3\zeta - \frac{5}{9}b^3\zeta'}\right). \tag{A.3}$$

In the particular case where the effects of the bit face not related to the axial penetration are neglected, $\varpi = \varsigma$. Also, $\varepsilon = \chi/\eta = O(b^2/\ell_1^2)$ is usually a small parameter, except in the case of a bit with a particularly long gauge and a first stabilizer close to the bit. All the parameters also are independent of the intrinsic specific energy, ι. It should be noted, however, that these parameters generally depend on the downhole field conditions, when, for instance, the rock is not isotropic or homogeneous, when the borehole is overgauged (Chen et al., 2008), or when the interaction pattern between the bit and the rock varies (Perneder et al., 2012). In practice, a fair estimation of these parameters can be obtained by systematic bit testing or by numerical simulations designed to compute the behavior of the bit while accounting for the cutter distribution (Chen et al., 2008).

The notion of lateral steering resistance and walk, both connected to the lateral force, are well-established parameters defining the bit behavior. These are extended naturally here for the moment at the bit via the angular steering resistance and the flip.

Appendix B

Coefficients of Influence

The coefficients of influence are obtained by solving the beam problem for the BHA. When the BHA can be approximated by a pipe of uniform mechanical properties, analytical expressions for the coefficients of influence can be computed. (In theory, analytical coefficients can also be computed for BHAs defined as a succession of pipes of uniform properties. They depend then also on numbers defining how properties vary along the BHA; however, expressions rapidly become complicated.) In general, these coefficients could be estimated by numerical methods, by a finite-element modeling for example. As along as linearity between the generalized forces on the BHA and the force and moment at the bit can be assumed, the general form of the equations of propagation remains the same. In this Appendix, the coefficients for BHAs of uniform properties with one or two stabilizers are explicitly given.

One-Stabilizer BHA

General Expressions

$$\mathcal{F}_b = \frac{\Lambda(\Lambda-1)^2\mu(\Lambda(2-3\Lambda\tau)+3\tau+4)+6\tau+4}{(\Lambda-1)^2\Lambda^3\mu(3(\Lambda-1)\tau+\Lambda-4)-3\tau-4},$$

$$\mathcal{F}_w = \frac{(\Lambda-1)^2\Lambda^2\mu\left(3\Lambda\left(2\Lambda^2+\Lambda-4\right)\tau+2\Lambda((\Lambda-1)\Lambda-9)+3(\tau+2)\right)-4(3\tau+5)}{8\left((\Lambda-1)^2\Lambda^3\mu(3(\Lambda-1)\tau+\Lambda-4)-3\tau-4\right)},$$

$$\mathcal{F}_r = \frac{\Lambda^2(\Lambda(6\tau+2)-9\tau-6)+3\tau+4}{(\Lambda-1)^2\Lambda^3\mu(3(\Lambda-1)\tau+\Lambda-4)-3\tau-4},$$

$$\mathcal{F}_c = \frac{3\tau\left(\Lambda^2(\Lambda-1)^3\mu+2\right)}{(\Lambda-1)^2\Lambda^3\mu(3(\Lambda-1)\tau+\Lambda-4)-3\tau-4},$$
$$\mathcal{F}_s = \frac{3\tau\left(\Lambda^2(\Lambda-1)^3\mu+2\right)}{(\Lambda-1)^2\Lambda^3\mu(3(\Lambda-1)\tau+\Lambda-4)-3\tau-4},$$
$$\mathcal{F}_m = \frac{-3\Lambda^2(\Lambda-1)^3\mu-6}{(\Lambda-1)^2\Lambda^3\mu(3(\Lambda-1)\tau+\Lambda-4)-3\tau-4},$$
$$\mathcal{M}_b = \frac{(\Lambda-1)^2\Lambda^2\mu((\Lambda-1)(\Lambda+3)\tau-4)-4(\tau+1)}{(\Lambda-1)^2\Lambda^3\mu(3(\Lambda-1)\tau+\Lambda-4)-3\tau-4},$$
$$\mathcal{M}_w = \frac{2(\tau+2)-(\Lambda-1)^2\Lambda^3\mu(\Lambda(\Lambda(3\tau+2)-4\tau-6)+\tau+2)}{8\left((\Lambda-1)^2\Lambda^3\mu(3(\Lambda-1)\tau+\Lambda-4)-3\tau-4\right)},$$
$$\mathcal{M}_r = -\frac{(\Lambda-1)\Lambda(\Lambda(3\tau+2)-3\tau-4)}{(\Lambda-1)^2\Lambda^3\mu(3(\Lambda-1)\tau+\Lambda-4)-3\tau-4},$$
$$\mathcal{M}_c = \frac{\tau\left(-(\Lambda-1)^3\Lambda^3\mu-2\right)}{(\Lambda-1)^2\Lambda^3\mu(3(\Lambda-1)\tau+\Lambda-4)-3\tau-4},$$
$$\mathcal{M}_s = \frac{(\Lambda-1)\Lambda^2\mu(\Lambda(3\tau+2)-3\tau-4)}{(\Lambda-1)^2\Lambda^3\mu(3(\Lambda-1)\tau+\Lambda-4)-3\tau-4},$$
$$\mathcal{M}_m = \frac{(\Lambda-1)^3\Lambda^3\mu+2}{(\Lambda-1)^2\Lambda^3\mu(3(\Lambda-1)\tau+\Lambda-4)-3\tau-4}.$$

Special Case $\tau = 0$ and $\mu = 0$

$$\mathcal{F}_b = -1,$$
$$\mathcal{F}_w = \frac{5}{8},$$
$$\mathcal{F}_r = -\frac{1}{2}\left((\Lambda-3)\Lambda^2+2\right),$$
$$\mathcal{F}_m = \frac{3}{2},$$
$$\mathcal{M}_b = 1,$$
$$\mathcal{M}_w = -\frac{1}{8},$$
$$\mathcal{M}_r = \frac{1}{2}(\Lambda-2)(\Lambda-1)\Lambda,$$
$$\mathcal{M}_m = -\frac{1}{2}.$$

Two-Stabilizer BHA

General Expressions

$$\mathcal{F}_b = \left(-8\lambda_2\left((\Lambda-1)^2\mu\left(3\Lambda\left(\Lambda^2-1\right)\tau-\Lambda(\Lambda+2)\right)-6\tau-2\right)\right.$$

$$
\begin{aligned}
&+3\lambda_2^2\tau\left(\Lambda(\Lambda-1)^2\mu(\Lambda(2-3\Lambda\tau)+3\tau+4)+6\tau+4\right)-12\Lambda(\Lambda+1)(\Lambda-1)^3\mu+24\big)/D\\
\mathcal{F}_{w,1} &= \big(3\lambda_2^2\tau\left((\Lambda-1)^2\Lambda^2\mu\left(3\Lambda\left(2\Lambda^2+\Lambda-4\right)\tau+2\Lambda((\Lambda-1)\Lambda-9)+3(\tau+2)\right)-4(3\tau+5)\right)\\
&+8\lambda_2\left((\Lambda-1)^2\Lambda^2\mu\left(\Lambda\left(3\left(2\Lambda^2+\Lambda-4\right)\tau+\Lambda^2-\Lambda-9\right)+3(\tau+1)\right)-2(6\tau+5)\right),\\
&+12\Lambda^2(\Lambda(2\Lambda+3)-1)(\Lambda-1)^3\mu-48\big)/8D,\\
\mathcal{F}_{w,2} &= \left(3\lambda_2^3(\lambda_2\tau+2)\left(\Lambda^2(\Lambda-1)^3\mu+2\right)\right)/4D,\\
\mathcal{F}_r &= \big((\Lambda-1)\left(3\lambda_2^2\tau(\Lambda(\Lambda(6\tau+2)-3\tau-4)-3\tau-4)\right.\\
&+8\lambda_2(\Lambda(6\Lambda\tau+\Lambda-3\tau-2)-3\tau-2)+12(\Lambda-1)(2\Lambda+1))\big)/D,\\
\mathcal{F}_{k,1} &= -\left(6(3\lambda_2\tau+2)\left(\Lambda^2(\Lambda-1)^3\mu+2\right)\right)/D,\\
\mathcal{F}_{c,1} &= \left(3\lambda_2\tau(3\lambda_2\tau+4)\left(\Lambda^2(\Lambda-1)^3\mu+2\right)\right)/D,\\
\mathcal{F}_{c,2} &= -\left(6\lambda_2\tau\left(\Lambda^2(\Lambda-1)^3\mu+2\right)\right)/D,\\
\mathcal{F}_s &= \big((\Lambda-1)\Lambda\mu\left(3\lambda_2^2\tau(\Lambda(-2\Lambda(3\tau+1)+3\tau+4)+3\tau+4)\right.\\
&-8\lambda_2(\Lambda(6\Lambda\tau+\Lambda-3\tau-2)-3\tau-2)+12\left(-2\Lambda^2+\Lambda+1\right)\big)\big)/D,\\
\mathcal{F}_m &= \left(6\lambda_2\left(\Lambda^2(\Lambda-1)^3\mu+2\right)\right)/D,\\
\mathcal{M}_b &= \big(3\lambda_2^2\tau\left((\Lambda-1)^2\Lambda^2\mu((\Lambda-1)(\Lambda+3)\tau-4)-4(\tau+1)\right)\\
&+8\lambda_2\left((\Lambda-1)^2\Lambda^2\mu((\Lambda-1)(\Lambda+3)\tau-2)-4\tau-2\right)+4\Lambda^2(\Lambda+3)(\Lambda-1)^3\mu-16\big)/D,\\
\mathcal{M}_{w,1} &= \big(-3\lambda_2^2\tau\left((\Lambda-1)^2\Lambda^3\mu(\Lambda(\Lambda(3\tau+2)-4\tau-6)+\tau+2)-2(\tau+2)\right)\\
&-8\lambda_2\left((\Lambda-1)^2\Lambda^3\mu(\Lambda(3\Lambda\tau+\Lambda-4\tau-3)+\tau+1)-2(\tau+1)\right)-4(\Lambda-1)^3(3\Lambda-1)\Lambda^3\mu+8\big)/8D,\\
\mathcal{M}_{w,2} &= -\left(\lambda_2^3(\lambda_2\tau+2)\left((\Lambda-1)^3\Lambda^3\mu+2\right)\right)/4D,\\
\mathcal{M}_r &= (\Lambda-1)\Lambda\left(3\lambda_2^2\tau(-\Lambda(3\tau+2)+3\tau+4)-8\lambda_2(3(\Lambda-1)\tau+\Lambda-2)-12(\Lambda-1)\right)/D,\\
\mathcal{M}_{k,1} &= \left(2(3\lambda_2\tau+2)\left((\Lambda-1)^3\Lambda^3\mu+2\right)\right)/D,\\
\mathcal{M}_{c,1} &= -\left(\lambda_2\tau(3\lambda_2\tau+4)\left((\Lambda-1)^3\Lambda^3\mu+2\right)\right)/D,\\
\mathcal{M}_{c,2} &= \left(2\lambda_2\tau\left((\Lambda-1)^3\Lambda^3\mu+2\right)\right)/D,\\
\mathcal{M}_s &= \left((\Lambda-1)\Lambda^2\mu\left(3\lambda_2^2\tau(\Lambda(3\tau+2)-3\tau-4)+8\lambda_2(3(\Lambda-1)\tau+\Lambda-2)+12(\Lambda-1)\right)\right)/D,\\
\mathcal{M}_m &= -\left(2\lambda_2\left((\Lambda-1)^3\Lambda^3\mu+2\right)\right)/D,
\end{aligned}
$$

where denominator D is defined as

$$D = 3\lambda_2^2\tau\left((\Lambda-1)^2\Lambda^3\mu(3(\Lambda-1)\tau+\Lambda-4)-3\tau-4\right) + 4\lambda_2\left((\Lambda-1)^2\Lambda^3\mu(6(\Lambda-1)\tau+\Lambda-4)-6\tau-4\right)+12(\Lambda-1)^3\Lambda^3\mu-12.$$

Special Case $\tau = 0$ and $\mu = 0$

$$\begin{aligned}
\mathcal{F}_b &= -\frac{4\lambda_2+6}{4\lambda_2+3},\\
\mathcal{F}_{w,1} &= \frac{5\lambda_2+3}{8\lambda_2+6},\\
\mathcal{F}_{w,2} &= -\frac{3\lambda_2^3}{16\lambda_2+12},\\
\mathcal{F}_r &= \frac{-2(\lambda_2+3)\Lambda^3+(6\lambda_2+9)\Lambda^2-4\lambda_2-3}{4\lambda_2+3},\\
\mathcal{F}_{k,1} &= \frac{6}{4\lambda_2+3},\\
\mathcal{F}_m &= -\frac{3\lambda_2}{4\lambda_2+3},\\
\mathcal{M}_b &= \frac{4(\lambda_2+1)}{4\lambda_2+3},\\
\mathcal{M}_{w,1} &= -\frac{2\lambda_2+1}{16\lambda_2+12},\\
\mathcal{M}_{w,2} &= \frac{\lambda_2^3}{16\lambda_2+12},\\
\mathcal{M}_r &= \frac{(\Lambda-1)\Lambda((2\lambda_2+3)\Lambda-4\lambda_2-3)}{4\lambda_2+3},\\
\mathcal{M}_{k,1} &= -\frac{2}{4\lambda_2+3},\\
\mathcal{M}_m &= \frac{\lambda_2}{4\lambda_2+3}.
\end{aligned}$$

Appendix C

Coefficients of the Equations of Propagation

Equations of propagation are obtained by combining three sets of expressions: the force and the moment at the bit computed from the BHA model, those computed from the bit/rock interaction law, and the kinematic relationships. In two dimensions, only one equation is required for the borehole inclination while in three dimensions, two coupled DDEs are needed: one for the borehole inclination and one for its azimuth. The coupling is due to bit walk ϖ and bit flip ς, while the evolution of the azimuth is related to the borehole inclination as it need to be projected in inclined plane ($\boldsymbol{I}_1$, $\boldsymbol{I}_3$).

Two-dimensional Equations

Expression for the Equation of propagation

The coefficients of equation (4.2) are given here for BHAs equipped with one or two stabilizers. Only coefficients A, B, and C directly depend on the number of stabilizers. The other coefficients read

$$\mathcal{B}_0 = \frac{\mathcal{F}_s \varepsilon}{\eta \Pi \Lambda},$$

$$\mathcal{C}_0 = -\frac{-\mathcal{F}_b\mathcal{M}_s + \mathcal{F}_s\mathcal{M}_b + \eta\Pi\mathcal{M}_s}{(\eta\Pi)^2},$$
$$\mathcal{D}_i = -\frac{-\mathcal{F}_b\mathcal{M}_{w,i} + \mathcal{F}_{w,i}\mathcal{M}_b + \eta\Pi\mathcal{M}_{w,i}}{(\eta\Pi)^2},$$
$$\mathcal{E}_i = -\frac{\mathcal{F}_{w,i}\varepsilon}{\eta\Pi},$$
$$\mathcal{F} = -\frac{-\mathcal{F}_b\mathcal{M}_r + \mathcal{F}_r\mathcal{M}_b + \eta\Pi\mathcal{M}_r}{(\eta\Pi)^2},$$
$$\mathcal{G} = -\frac{-\mathcal{F}_b\mathcal{M}_m + \mathcal{F}_m\mathcal{M}_b + \eta\Pi\mathcal{M}_m}{(\eta\Pi)^2},$$
$$\mathcal{H}_i = -\frac{\mathcal{F}_{c,i}\varepsilon}{\eta\Pi}.$$

One-Stabilizer BHA

$$\mathcal{A} = \frac{\mathcal{F}_b\Lambda\varepsilon + \mathcal{F}_{c,1}\Lambda\varepsilon + \mathcal{F}_s\Lambda\varepsilon - \mathcal{F}_s\varepsilon - \Lambda\mathcal{M}_b}{\eta\Pi\Lambda},$$
$$\mathcal{B}_1 = -\frac{-\mathcal{F}_b\mathcal{M}_{c,1} + \mathcal{F}_b\eta\Pi\varepsilon + \mathcal{F}_{c,1}\mathcal{M}_b + \mathcal{F}_{c,1}\eta\Pi\varepsilon + \mathcal{F}_s\eta\Pi\varepsilon + \eta\Pi\mathcal{M}_{c,1}}{(\eta\Pi)^2},$$
$$\mathcal{C}_1 = \frac{-\mathcal{F}_b\mathcal{M}_{c,1} - \mathcal{F}_b\mathcal{M}_s + \mathcal{F}_{c,1}\mathcal{M}_b + \mathcal{F}_s\mathcal{M}_b + \eta\Pi\mathcal{M}_b + \eta\Pi\mathcal{M}_{c,1} + \eta\Pi\mathcal{M}_s}{(\eta\Pi)^2}.$$

Two-Stabilizer BHA

$$\mathcal{A} = \frac{\mathcal{F}_b\Lambda\varepsilon - \mathcal{F}_{k,1}\Lambda\varepsilon + \mathcal{F}_{c,1}\Lambda\varepsilon + \mathcal{F}_s\Lambda\varepsilon - \mathcal{F}_s\varepsilon - \Lambda\mathcal{M}_b}{\eta\Pi\Lambda},$$
$$\mathcal{B}_1 = -\frac{-\mathcal{F}_b\lambda_2\mathcal{M}_{c,1} + \mathcal{F}_{c,1}\lambda_2\mathcal{M}_b + \eta\Pi(\mathcal{F}_b\lambda_2\varepsilon - \mathcal{F}_{k,1}\lambda_2\varepsilon - \mathcal{F}_{k,1}\varepsilon + \mathcal{F}_{c,1}\lambda_2\varepsilon - \mathcal{F}_{c,2}\varepsilon + \mathcal{F}_s\lambda_2\varepsilon + \lambda_2\mathcal{M}_{c,1})}{(\eta\Pi)^2\lambda_2},$$
$$\mathcal{B}_2 = -\frac{-\mathcal{F}_b\lambda_2\mathcal{M}_{c,2} + \mathcal{F}_{k,1}\eta\Pi\varepsilon + \mathcal{F}_{c,2}\lambda_2\mathcal{M}_b + \mathcal{F}_{c,2}\eta\Pi\varepsilon + \eta\Pi\lambda_2\mathcal{M}_{c,2}}{(\eta\Pi)^2\lambda_2},$$
$$\mathcal{C}_1 = \frac{\mathcal{F}_b\mathcal{M}_{k,1} - \mathcal{F}_b\mathcal{M}_{c,1} - \mathcal{F}_b\mathcal{M}_s - \mathcal{F}_{k,1}\mathcal{M}_b + \mathcal{F}_{c,1}\mathcal{M}_b + \mathcal{F}_s\mathcal{M}_b + \eta\Pi\mathcal{M}_b - \eta\Pi\mathcal{M}_{k,1} + \eta\Pi\mathcal{M}_{c,1} + \eta\Pi\mathcal{M}_s}{(\eta\Pi)^2},$$
$$\mathcal{C}_2 = \frac{-\mathcal{F}_b\mathcal{M}_{k,1} - \mathcal{F}_b\mathcal{M}_{c,2} + \mathcal{F}_{k,1}\mathcal{M}_b + \mathcal{F}_{c,2}\mathcal{M}_b + \eta\Pi\mathcal{M}_{k,1} + \eta\Pi\mathcal{M}_{c,2}}{(\eta\Pi)^2}.$$

Expression for the Bit Inclination

The coefficients for the bit inclination when $\varepsilon = 0$, $\tau = 0$, and $\mu = 0$ are given by

$$\mathcal{C}_{\theta,1} = \frac{\mathcal{M}_b - \mathcal{M}_{k,1}}{\mathcal{M}_b},$$

$$\mathcal{C}_{\theta,i} = \frac{\mathcal{M}_{k,i-1} - \mathcal{M}_{k,i}}{\mathcal{M}_b},$$
$$\mathcal{D}_{\theta,i} = -\frac{\mathcal{M}_{w,i}}{\mathcal{M}_b},$$
$$\mathcal{F}_{\theta} = -\frac{\mathcal{M}_r}{\mathcal{M}_b},$$
$$\mathcal{G}_{\theta} = -\frac{\mathcal{M}_m}{\mathcal{M}_b}.$$

Expression for the Lateral Force at the Bit

The coefficients for the lateral force at the bit when $\varepsilon = 0$, $\tau = 0$, and $\mu = 0$ are given by

$$\mathcal{C}_{F_2,1} = \frac{\mathcal{F}_{k,1}\mathcal{M}_b - \mathcal{F}_b\mathcal{M}_{k,1}}{\mathcal{M}_b},$$
$$\mathcal{C}_{F_2,i} = -\frac{-\mathcal{F}_b\mathcal{M}_{k,i-1} + \mathcal{F}_b\mathcal{M}_{k,i} + \mathcal{F}_{k,i-1}\mathcal{M}_b - \mathcal{F}_{k,i}\mathcal{M}_b}{\mathcal{M}_b},$$
$$\mathcal{D}_{F_2,i} = \frac{\mathcal{F}_{w,i}\mathcal{M}_b - \mathcal{F}_b\mathcal{M}_{w,i}}{\mathcal{M}_b},$$
$$\mathcal{F}_{F_2} = \mathcal{F}_r - \frac{\mathcal{F}_b\mathcal{M}_r}{\mathcal{M}_b},$$
$$\mathcal{G}_{F_2} = \mathcal{F}_m - \frac{\mathcal{F}_b\mathcal{M}_m}{\mathcal{M}_b}.$$

Equation of Propagation When $\varepsilon = 0$

The coefficients for the borehole inclination when $\varepsilon = 0$, $\tau = 0$, and $\mu = 0$ and when the tilt has not saturated are given by

$$\mathcal{C}_{\Theta,i} = \mathcal{C}_i/\mathcal{A},$$
$$\mathcal{D}_{\Theta,i} = \mathcal{D}_i/\mathcal{A},$$
$$\mathcal{F}_{\Theta} = \mathcal{F}/\mathcal{A},$$
$$\mathcal{G}_{\Theta} = \mathcal{G}/\mathcal{A}.$$

If the tilt has saturated, they become

$$\mathcal{C}_{\Theta,i} = \mathcal{C}_{\theta,i},$$
$$\mathcal{D}_{\Theta,i} = \mathcal{D}_{\theta,i},$$
$$\mathcal{F}_{\Theta} = \mathcal{F}_{\theta},$$

$$\mathcal{G}_\Theta = \mathcal{G}_\theta.$$

Finally the coefficients for the DDE, obtained by deriving once the delay algebraic equation, are obtained as follows:

$$\begin{aligned}
\mathcal{A}_\Theta &= \mathcal{C}_1, \\
\mathcal{B}_{\Theta,i} &= \frac{-\mathcal{C}_i + \mathcal{C}_{i+1}}{\lambda_i}, \\
\mathcal{E}_\Theta &= \frac{\mathcal{D}_i}{\lambda_i}.
\end{aligned}$$

Three-dimensional Equations

Expression for the Pseudo-Equation of Propagation

The coefficients for the two equations of propagation for the borehole inclination and pseudo-azimuth are given below. It is assumed that the stabilizers are free to tilt and that the RSS pads do no constrain the deflection of the BHA. Following relation

$$\mathcal{I}_{\Theta\Theta} = \mathcal{I}_{\Delta\Delta},\ \mathcal{I}_{\Theta\Delta} = -\mathcal{I}_{\Delta\Theta},\ \mathcal{I} = \mathcal{A}, \mathcal{B}, \mathcal{C}, \mathcal{F}, \mathcal{G}, \tag{C.1}$$

only the coefficients pertaining to the DDE for the inclination are given. As for the two-dimensional case, only coefficients A, B, and C directly depend on the number of stabilizers. The other coefficients read

$$\begin{aligned}
\mathcal{D}_{\Theta\Theta,i} &= -\frac{-\mathcal{F}_b\mathcal{M}_{w,i}\cos(\varsigma+\varpi) + \mathcal{F}_{w,i}\mathcal{M}_b\cos(\varsigma+\varpi) + \eta\Pi\mathcal{M}_{w,i}\cos\varsigma}{(\eta\Pi)^2}, \\
\mathcal{E}_{\Theta\Theta,i} &= -\frac{\mathcal{F}_{w,i}\varepsilon\cos\varpi}{\eta\Pi}, \\
\mathcal{F}_{\Theta\Theta,i} &= \frac{\cos(\varsigma+\varpi)(\mathcal{F}_b\mathcal{M}_r - \mathcal{F}_r\mathcal{M}_b) - \eta\Pi\mathcal{M}_r\cos\varsigma}{(\eta\Pi)^2}, \\
\mathcal{F}_{\Theta\Delta,i} &= \frac{\sin(\varsigma+\varpi)(\mathcal{F}_r\mathcal{M}_b - \mathcal{F}_b\mathcal{M}_r) + \eta\Pi\mathcal{M}_r\sin\varsigma}{(\eta\Pi)^2}, \\
\mathcal{D}_{\Delta\Theta,i} &= -\frac{-\mathcal{F}_b\mathcal{M}_{w,i}\sin(\varsigma+\varpi) + \mathcal{F}_{w,i}\mathcal{M}_b\sin(\varsigma+\varpi) + \eta\Pi\mathcal{M}_{w,i}\sin\varsigma}{(\eta\Pi)^2}, \\
\mathcal{E}_{\Delta\Theta,i} &= -\frac{\mathcal{F}_{w,i}\varepsilon\sin\varpi}{\eta\Pi}.
\end{aligned}$$

One-stabilizer BHA

$$
\begin{aligned}
\mathcal{A}_{\Theta\Theta} &= -\frac{\mathcal{M}_b \cos\varsigma - \mathcal{F}_b\varepsilon\cos\varpi}{\eta\Pi},\\
\mathcal{B}_{\Theta\Theta,1} &= -\frac{\mathcal{F}_b\varepsilon\cos\varpi}{\eta\Pi},\\
\mathcal{C}_{\Theta\Theta,1} &= \frac{\mathcal{M}_b\cos\varsigma}{\eta\Pi},\\
\mathcal{A}_{\Theta\Delta} &= \frac{\mathcal{M}_b\sin\varsigma - \mathcal{F}_b\varepsilon\sin\varpi}{\eta\Pi},\\
\mathcal{B}_{\Theta\Delta,1} &= \frac{\mathcal{F}_b\varepsilon\sin\varpi}{\eta\Pi},\\
\mathcal{C}_{\Theta\Delta,1} &= -\frac{\mathcal{M}_b\sin\varsigma}{\eta\Pi}.
\end{aligned}
$$

Two-stabilizer BHA

$$
\begin{aligned}
\mathcal{A}_{\Theta\Theta} &= -\frac{-\mathcal{F}_b\varepsilon\cos\varpi + \mathcal{F}_{k,1}\varepsilon\cos\varpi + \mathcal{M}_b\cos\varsigma}{\eta\Pi},\\
\mathcal{B}_{\Theta\Theta,1} &= -\frac{\varepsilon\cos\varpi(\mathcal{F}_b\lambda_2 - \mathcal{F}_{k,1}\lambda_2 - \mathcal{F}_{k,1})}{\eta\Pi\lambda_2},\\
\mathcal{B}_{\Theta\Theta,2} &= -\frac{\mathcal{F}_{k,1}\varepsilon\cos\varpi}{\eta\Pi\lambda_2},\\
\mathcal{C}_{\Theta\Theta,1} &= \frac{\mathcal{F}_b\mathcal{M}_{k,1}\cos(\varsigma+\varpi) - \mathcal{F}_{k,1}\mathcal{M}_b\cos(\varsigma+\varpi) + \eta\Pi\mathcal{M}_b\cos\varsigma - \eta\Pi\mathcal{M}_{k,1}\cos\varsigma}{(\eta\Pi)^2},\\
\mathcal{C}_{\Theta\Theta,2} &= \frac{-\mathcal{F}_b\mathcal{M}_{k,1}\cos(\varsigma+\varpi) + \mathcal{F}_{k,1}\mathcal{M}_b\cos(\varsigma+\varpi) + \eta\Pi\mathcal{M}_{k,1}\cos\varsigma}{(\eta\Pi)^2},\\
\mathcal{A}_{\Theta\Delta} &= \frac{-\mathcal{F}_b\varepsilon\sin\varpi + \mathcal{F}_{k,1}\varepsilon\sin\varpi + \mathcal{M}_b\sin\varsigma}{\eta\Pi},\\
\mathcal{B}_{\Theta\Delta,1} &= \frac{\varepsilon\sin\varpi(\mathcal{F}_b\lambda_2 - \mathcal{F}_{k,1}\lambda_2 - \mathcal{F}_{k,1})}{\eta\Pi\lambda_2},\\
\mathcal{B}_{\Theta\Delta,2} &= \frac{\mathcal{F}_{k,1}\varepsilon\sin\varpi}{\eta\Pi\lambda_2},\\
\mathcal{C}_{\Theta\Delta,1} &= -\frac{\mathcal{F}_b\mathcal{M}_{k,1}\sin(\varsigma+\varpi) - \mathcal{F}_{k,1}\mathcal{M}_b\sin(\varsigma+\varpi) + \eta\Pi\mathcal{M}_b\sin\varsigma - \eta\Pi\mathcal{M}_{k,1}\sin\varsigma}{(\eta\Pi)^2},\\
\mathcal{C}_{\Theta\Delta,2} &= -\frac{-\mathcal{F}_b\mathcal{M}_{k,1}\sin(\varsigma+\varpi) + \mathcal{F}_{k,1}\mathcal{M}_b\sin(\varsigma+\varpi) + \eta\Pi\mathcal{M}_{k,1}\sin\varsigma}{(\eta\Pi)^2}.
\end{aligned}
$$

Coefficients for the Propagation Equation when $\varepsilon = 0$

When the bit is free to tilt, the coefficients of the coupled delay algebraic equations are given hereafter. Relation (C.1) is still valid, so that only part of the coefficients needs to be explicitly

given. If the tilt has saturated, they become

$$\mathcal{C}_{\Theta,i} = \mathcal{C}_{\theta,i},$$
$$\mathcal{D}_{\Theta,i} = \mathcal{D}_{\theta,i},$$
$$\mathcal{F}_{\Theta} = \mathcal{F}_{\theta},$$
$$\mathcal{G}_{\Theta} = \mathcal{G}_{\theta}.$$

One-stabilizer BHA

$$\begin{aligned}
\mathcal{C}_{\Theta\Theta,1} &= 1,\\
\mathcal{D}_{\Theta\Theta,1} &= -\frac{-\mathcal{F}_b\mathcal{M}_{w,i}\cos\varpi + \mathcal{F}_{w,i}\mathcal{M}_b\cos\varpi + \eta\Pi\mathcal{M}_{w,i}}{\eta\Pi\mathcal{M}_b},\\
\mathcal{F}_{\Theta\Theta} &= -\frac{-\mathcal{F}_b\mathcal{M}_r\cos\varpi + \mathcal{F}_r\mathcal{M}_b\cos\varpi + \eta\Pi\mathcal{M}_r}{\eta\Pi\mathcal{M}_b},\\
\mathcal{C}_{\Theta\Phi,1} &= 0,\\
\mathcal{F}_{\Theta\Phi} &= \frac{\sin\varpi(\mathcal{F}_r\mathcal{M}_b - \mathcal{F}_b\mathcal{M}_r)}{\eta\Pi\mathcal{M}_b},\\
\mathcal{D}_{\Phi\Theta,1} &= -\frac{\sin\varpi(\mathcal{F}_{w,i}\mathcal{M}_b - \mathcal{F}_b\mathcal{M}_{w,i})}{\eta\Pi\mathcal{M}_b}.
\end{aligned}$$

Two-stabilizer BHA

$$\begin{aligned}
\mathcal{C}_{\Theta\Theta,1} &= \frac{\mathcal{F}_b\mathcal{M}_{k,1}\cos\varpi - \mathcal{F}_{k,1}\mathcal{M}_b\cos\varpi + \eta\Pi\mathcal{M}_b - \eta\Pi\mathcal{M}_{k,1}}{\eta\Pi\mathcal{M}_b},\\
\mathcal{C}_{\Theta\Theta,2} &= \frac{-\mathcal{F}_b\mathcal{M}_{k,1}\cos\varpi + \mathcal{F}_{k,1}\mathcal{M}_b\cos\varpi + \eta\Pi\mathcal{M}_{k,1}}{\eta\Pi\mathcal{M}_b},\\
\mathcal{D}_{\Theta\Theta,i} &= -\frac{-\mathcal{F}_b\mathcal{M}_{w,i}\cos\varpi + \mathcal{F}_{w,i}\mathcal{M}_b\cos\varpi + \eta\Pi\mathcal{M}_{w,i}}{\eta\Pi\mathcal{M}_b},\\
\mathcal{F}_{\Theta\Theta} &= -\frac{-\mathcal{F}_b\mathcal{M}_r\cos\varpi + \mathcal{F}_r\mathcal{M}_b\cos\varpi + \eta\Pi\mathcal{M}_r}{\eta\Pi\mathcal{M}_b},\\
\mathcal{C}_{\Theta\Phi,1} &= \frac{\sin\varpi(\mathcal{F}_{k,1}\mathcal{M}_b - \mathcal{F}_b\mathcal{M}_{k,1})}{\eta\Pi\mathcal{M}_b},\\
\mathcal{C}_{\Theta\Phi,2} &= -\frac{\sin\varpi(\mathcal{F}_{k,1}\mathcal{M}_b - \mathcal{F}_b\mathcal{M}_{k,1})}{\eta\Pi\mathcal{M}_b},\\
\mathcal{F}_{\Theta\Phi} &= \frac{\sin\varpi(\mathcal{F}_r\mathcal{M}_b - \mathcal{F}_b\mathcal{M}_r)}{\eta\Pi\mathcal{M}_b},\\
\mathcal{D}_{\Phi\Theta,i} &= -\frac{\sin\varpi(\mathcal{F}_{w,i}\mathcal{M}_b - \mathcal{F}_b\mathcal{M}_{w,i})}{\eta\Pi\mathcal{M}_b}.
\end{aligned}$$

Stationary Solutions

$$\mathcal{S}^{\psi_2}_{\Gamma_2} = (\mathcal{F}_r\mathcal{M}_\kappa - \mathcal{F}_\kappa\mathcal{M}_r)(-\mathcal{F}_b\mathcal{M}_\kappa + \mathcal{F}_\kappa\mathcal{M}_b + \eta\Pi\mathcal{M}_\kappa\cos\varpi)/D,$$

$$\mathcal{S}^{\psi_2}_{\Gamma_3} = \eta\Pi\mathcal{M}_\kappa\sin\varpi(\mathcal{F}_\kappa\mathcal{M}_r - \mathcal{F}_r\mathcal{M}_\kappa)/D,$$

$$\mathcal{S}^{\psi_2}_{\Upsilon} = (\mathcal{F}_\kappa\mathcal{M}_w - \mathcal{F}_w\mathcal{M}_\kappa)(\mathcal{F}_b\mathcal{M}_\kappa - \mathcal{F}_\kappa\mathcal{M}_b - \eta\Pi\mathcal{M}_\kappa\cos\varpi)/D,$$

$$\begin{aligned}\mathcal{S}^{\kappa_2}_{\Gamma_2} = (&-\eta\Pi\cos\varpi(-2\mathcal{F}_b\mathcal{M}_\kappa\mathcal{M}_r + \mathcal{F}_\kappa\mathcal{M}_b\mathcal{M}_r + \mathcal{F}_r\mathcal{M}_b\mathcal{M}_\kappa)\\ &-(\mathcal{F}_\kappa\mathcal{M}_b - \mathcal{F}_b\mathcal{M}_\kappa)(\mathcal{F}_r\mathcal{M}_b - \mathcal{F}_b\mathcal{M}_r) - (\eta\Pi)^2\mathcal{M}_\kappa\mathcal{M}_r\Big)/D,\end{aligned}$$

$$\mathcal{S}^{\kappa_2}_{\Gamma_3} = \eta\Pi\mathcal{M}_b\sin\varpi(\mathcal{F}_r\mathcal{M}_\kappa - \mathcal{F}_\kappa\mathcal{M}_r)/D,$$

$$\mathcal{S}^{\kappa_2}_{\Upsilon} = (-\mathcal{M}_w D + \mathcal{M}_b(\mathcal{F}_\kappa\mathcal{M}_w - \mathcal{F}_w\mathcal{M}_\kappa)(-\mathcal{F}_b\mathcal{M}_\kappa + \mathcal{F}_\kappa\mathcal{M}_b + \eta\Pi\mathcal{M}_\kappa\cos\varpi))/M_\kappa D,$$

$$\mathcal{S}^{\psi_3}_{\Gamma_2} = \eta\Pi\mathcal{M}_\kappa\sin\varpi(\mathcal{F}_r\mathcal{M}_\kappa - \mathcal{F}_\kappa\mathcal{M}_r)/D,$$

$$\mathcal{S}^{\psi_3}_{\Gamma_3} = -(\mathcal{F}_\kappa\mathcal{M}_r - \mathcal{F}_r\mathcal{M}_\kappa)(-\mathcal{F}_b\mathcal{M}_\kappa + \mathcal{F}_\kappa\mathcal{M}_b + \eta\Pi\mathcal{M}_\kappa\cos\varpi)/D,$$

$$\mathcal{S}^{\psi_3}_{\Upsilon} = \eta\Pi\mathcal{M}_\kappa\sin\varpi(\mathcal{F}_w\mathcal{M}_\kappa - \mathcal{F}_\kappa\mathcal{M}_w)/D,$$

$$\mathcal{S}^{\kappa_3}_{\Gamma_2} = \eta\Pi\mathcal{M}_b\sin\varpi(\mathcal{F}_\kappa\mathcal{M}_r - \mathcal{F}_r\mathcal{M}_\kappa)/D,$$

$$\begin{aligned}\mathcal{S}^{\kappa_3}_{\Gamma_3} = (&-\eta\Pi\cos\varpi(-2\mathcal{F}_b\mathcal{M}_\kappa\mathcal{M}_r + \mathcal{F}_\kappa\mathcal{M}_b\mathcal{M}_r + \mathcal{F}_r\mathcal{M}_b\mathcal{M}_\kappa)\\ &-(\mathcal{F}_\kappa\mathcal{M}_b - \mathcal{F}_b\mathcal{M}_\kappa)(\mathcal{F}_r\mathcal{M}_b - \mathcal{F}_b\mathcal{M}_r) - (\eta\Pi)^2\mathcal{M}_\kappa\mathcal{M}_r\Big)/D,\end{aligned}$$

$$\mathcal{S}^{\kappa_3}_{\Upsilon} = \eta\Pi\mathcal{M}_b\sin\varpi(\mathcal{F}_\kappa\mathcal{M}_w - \mathcal{F}_w\mathcal{M}_\kappa)/D,$$

where denominator D reads

$$D = 2\eta\Pi\mathcal{M}_\kappa\cos\varpi(\mathcal{F}_\kappa\mathcal{M}_b - \mathcal{F}_b\mathcal{M}_\kappa) + (\mathcal{F}_\kappa\mathcal{M}_b - \mathcal{F}_b\mathcal{M}_\kappa)^2 + (\eta\Pi)^2\mathcal{M}_\kappa^2.$$

Appendix D

Discontinuities in the Propagation Equations

Anytime the loading on the BHA is modified instantaneously, *e.g.*, when the active weight or the RSS force changes, the borehole inclination and azimuth exhibit discontinuities. Depending on whether the bit is assumed to be free to tilt or not, the bit orientation may also sustain such discontinuities. Analytical expressions for theses jumps are here given in the three-dimensional case, both when $\varepsilon = 0$ or not ($\varsigma = 0$). These are exposed for sudden changes in the RSS force, in dimensionless group $\eta\Pi$, and in the exterior moment at the last stabilizer.

Equations (5.1)-(5.4) are used to drive the relationships between the bit and borehole inclinations and azimuths before and after the discontinuity in the loading has occurred. At these points, the right- and left-handed limits (in terms of ξ) of the bit and borehole orientation are related according to

$$\Theta^+ = \Theta^- + [\![\Theta]\!]\,, \quad \theta^+ = \theta^- + [\![\theta]\!]\,,$$

$$\Phi^+ = \Phi^- + [\![\Phi]\!]\,, \quad \phi^+ = \phi^- + [\![\phi]\!]\,.$$

The values in brackets are the magnitudes of the jumps. They may be limited by the saturation of the tilt. Its magnitude must then be compared to ψ_c and the state of the system updated if necessary.

Discontinuities for $\varepsilon \neq 0$

When the bit is not free to tilt, its orientation varies continuously; however an *internal* boundary layer is created, which in the limit case $\varepsilon \to 0$ tends to jumps given by the case $\varepsilon = 0$ (see Section 4.4.1). For jumps $[\![\Gamma_2]\!]$ and $[\![\Gamma_3]\!]$ in the RSS force, discontinuities in the borehole orientation are given by

$$[\![\Theta]\!] = \mathcal{F}_r \frac{\sin\varpi\,[\![\Gamma_3]\!] - \cos\varpi\,[\![\Gamma_2]\!]}{\eta\Pi},$$
$$[\![\Phi]\!] = -\frac{\mathcal{F}_r\cos\varpi\,[\![\Gamma_3]\!] + \mathcal{F}_r\sin\varpi\,[\![\Gamma_2]\!] + \eta\Pi\,(\phi-\Phi^-)\,(\sin\Theta^- - \sin\Theta^+)}{\eta\Pi\sin\Theta^+}.$$

Similar expressions can be derived for jumps $\left[\!\left[\tilde{M}_2^e\right]\!\right]$ and $\left[\!\left[\tilde{M}_3^e\right]\!\right]$ in the moment at the last stabilizer:

$$[\![\Theta]\!] = -\mathcal{F}_m \frac{\sin\varpi\,[\![\tilde{M}_2^e]\!] + \cos\varpi\,[\![\tilde{M}_3^e]\!]}{\eta\Pi},$$
$$[\![\Phi]\!] = -\frac{-\mathcal{F}_m\cos\varpi\,[\![\tilde{M}_2^e]\!] + \mathcal{F}_m\sin\varpi\,[\![\tilde{M}_3^e]\!] + \eta\Pi\,(\phi-\Phi^-)\,(\sin\Theta^- - \sin\Theta^+)}{\eta\Pi\sin\Theta^+}.$$

Finally for a jump $[\![\eta\Pi]\!]$, the discontinuities are given by

$$[\![\Theta]\!] = \left(\theta - \Theta^-\right)\frac{[\![\eta\Pi]\!]}{\eta\Pi^+},$$
$$[\![\Phi]\!] = \left(\phi - \Phi^-\right)\left[1 - \frac{\eta\Pi^-\sin\Theta^-}{\eta\Pi^+\sin\Theta^+}\right].$$

Discontinuities for $\varepsilon = 0$

When the bit is free to tilt, both the bit and borehole inclinations and azimuths exhibit a discontinuity. The computation of the magnitude of these jumps is straightforward, and can be extracted readily from equations (5.15), (5.16), (5.24), and (5.25). In the case of a jump in the RSS force, they are given by

$$[\![\Theta]\!] = \mathcal{F}_{\Theta\Theta}\,[\![\Gamma_2]\!] + \mathcal{F}_{\Theta\Phi}\,[\![\Gamma_3]\!],$$
$$[\![\Phi]\!] = \frac{-\mathcal{F}_{\Theta\Phi}\,[\![\Gamma_2]\!] + \mathcal{F}_{\Theta\Theta}\,[\![\Gamma_3]\!] + (\sin\Theta^- - \sin\Theta^+)\,\Phi^-}{\sin\Theta^+},$$
$$[\![\theta]\!] = \mathcal{F}_\theta\,[\![\Gamma_2]\!],$$
$$[\![\phi]\!] = \frac{\mathcal{F}_\theta\,[\![\Gamma_3]\!] + (\sin\Theta^- - \sin\Theta^+)\,\phi^-}{\sin\Theta^+}.$$

For a jump in the exterior moment, they become

$$
\begin{aligned}
[\![\Theta]\!] &= -\frac{-\mathcal{F}_b\mathcal{M}_m\cos\varpi + \mathcal{F}_m\mathcal{M}_b\cos\varpi + \eta\Pi\mathcal{M}_r}{\eta\Pi\mathcal{M}_b}\left[\!\left[\tilde{M}_3^e\right]\!\right] - \frac{\sin\varpi(\mathcal{F}_m\mathcal{M}_b - \mathcal{F}_b\mathcal{M}_m)}{\eta\Pi\mathcal{M}_b}\left[\!\left[\tilde{M}_2^e\right]\!\right], \\
[\![\Phi]\!] &= \frac{\sin\varpi(\mathcal{F}_m\mathcal{M}_b - \mathcal{F}_b\mathcal{M}_m)\left[\!\left[\tilde{M}_3^e\right]\!\right] + (-\mathcal{F}_b\mathcal{M}_m\cos\varpi + \mathcal{F}_r\mathcal{M}_b\cos\varpi + \eta\Pi\mathcal{M}_m)\left[\!\left[\tilde{M}_2^e\right]\!\right]}{\eta\Pi\mathcal{M}_b\sin\Theta^+} \\
&\quad + \frac{(\sin\Theta^- - \sin\Theta^+)\,\Phi^-}{\sin\Theta^+}, \\
[\![\theta]\!] &= -\frac{\mathcal{M}_m}{\mathcal{M}_b}\left[\!\left[\tilde{M}_3^e\right]\!\right], \\
[\![\phi]\!] &= \frac{\mathcal{M}_m\left[\!\left[\tilde{M}_2^e\right]\!\right] + \mathcal{M}_b\,(\sin\Theta^- - \sin\Theta^+)\,\phi^-}{\mathcal{M}_b\sin\Theta^+}.
\end{aligned}
$$

Finally the case of a jump in $\eta\Pi$ is similar to the case $\varepsilon \neq 0$ as it does not induce any change in the transversal BHA loading and $[\![\theta]\!] = [\![\phi]\!] = 0$.